The rational design and synthesis of novel Kv1 inhibitors and their application to neurological diseases

Ph.D.

Declan Daly B.Sc.

Supervisor

Dr. Kieran Nolan

School of Chemical Sciences

Dublin City University

Dublin 9

Ireland

Dedicated to my Mother……

Great spirits have often encountered violent opposition from weak minds

Albert Einstein

Declaration

I hereby certify that this material, which I now submit for assessment on the programme of study leading to the award of Doctor of Philosophy is entirely my own work, that I have exercised reasonable care to ensure that the work is original, and does not to the best of my knowledge breach any law of copyright, and has not been taken from the work of others save and to the extent that such work has been cited and acknowledged within the text of my work.

Signed: _____ ID No.: 56363334

Date: 05.08.2014

Abstract

The work detailed in this thesis involves the synthesis, computational analysis and biological evaluation of a series of macrocycles against Kv1 channels that could lead to a novel therapeutic for the neurological disorder multiple sclerosis (MS). The initial SAR study focuses on porphyrin derivatives possessing various alkyl ammonium substituents. The results obtained from the initial SAR study with the porphyrins was used to design a new non-conjugated scaffold based on the calix[4]pyrroles. However, the synthesis of the target calix[4]pyrroles was not achieved. Alternatively, a comparative model of rat Kv1.1 was constructed and the results of the porphyrin SAR study were modelled. This computational work led to the identification of a new dipyrromethane small molecule inhibitor which was successfully prepared. The new lead dipyrromethane **DDAAKN01** proved to be selective and potent for the target potassium channel Kv1.1 which is believed to be associated with MS. The obtained IC50 value for **DDAAKN01** was 14 μM, which is 40 times more potent than the current therapeutic 4-aminopyridine that is currently used for the treatment of MS. **DDAAKN01** also showed high selectivity toward the $Kv(1.1)_4$ channel whilst not interacting with normalised Kv(1.1)x(1.2)y channels. Further investigation into the mechanism of binding of **DDAAKN01** using a comparative model of Kv1.1 led to the preparation of a new tetrapyrrole derivative **DDAAKN02**. **DDAAKN02** was synthesised and biologically evaluated. The results for **DDAAKN02** were superior to **DDAAKN01** in both selectivity and potency. **DDAAKN02** has a preliminary IC50 value of 8 μM. Both **DDAAKN01** and **DDAAKN02** have excellent potential as new candidates to alleviate the symptoms of MS and are presently being evaluated with MS in vivo models.   .

Acknowledgements

Firstly, I would like to thank my project supervisor Dr. Kieran Nolan. Kieran's support and guidance throughout my PhD will forever stand with me. He allowed me to pursue avenues and direct myself towards where the project went from start to finish. My innovation is due to his teachings.

Dr Ahmed-Al-Sabi, was my closest contact on the biological aspect of the project, he performed all the screening on all of the channels. It was an absolute pleasure to work as closely as I did with Ahmed. Our persistence, especially on the early stages really allowed this project to develop. I would also like to thank Prof Oliver Dolly for providing the platform of the project on the biological side.

Dr Gemma Kinsella, basically taught me computational chemistry. I will be forever grateful for her time and patience. Together, we developed the models that are present in this thesis. Without her the computational component of the project would not exist.

The team we had on this project was exceptional; everyone had such a massive role and I would like to thank them once again.

I would like to thank my best friend Dr Mark Byrne, myself and mark started and finished our undergraduate and PhD together. I believe that one of the reasons we both excelled was the support we gave each other. The rest of the guys in the PRG, also Alex, Oksana, Zahra Andy, Eoin, Mags, Aaron, Chris, Monika, Andy, Hannah and Rohit .

My family that have always been extremely supportive and inquisitive.

Lastly, I would like to thank the technical staff Damien, Vinny, Ambrose, Mary and Veronica. I would like to thank John in particular for all of his help on the NMR machine. Micheal for the MALDI samples.

Table of Contents

Abbreviations:

PDT: Photodynamic therapy

E: Glutamic acid

A: Alanine

S: Serine

H: Histidine

F: Phenylalanine

G: Glycine

Y: Tyrosine

D: Aspartic acid

TCPP: 5,10,15,20 tetrakis(4-carboxyphenyl) porphyrin

DMF: Dimethylformamide

CH_2Cl_2: Dichloromethane

TEA: Triethylamine

DIPEA: Diisopropylethylamine

$CHCl_3$: Chloroform

TLC: Thin Layer Chromatography

HCl: Hydrochloric acid

CO_2: Carbon dioxide

MALDI MS: Matrix-assisted laser desorption/ionisation

TFA: Triflouroacetic acid

DCC: N,N'-Dicyclohexylcarbodiimide

NHS: N-Hydroxysuccinimide

EDCI: 1-Ethyl-3-(3-dimethylaminopropyl) carbodiimide

DMAP: 4-Dimethylaminopyride

HOBt: Hydroxybenzotriazole

HOPcp: Pentachlorophenol

HOPfp: Pentaflourophenol

HOSu: N-Hydroxysuccinimide

DMSO: Dimethylsulfoxide

EtOH: Ethanol

CH_2: Methylene

Kv: Voltage potassium channel

^{1}H NMR: Proton Nuclear Magnetic Resonance

API: Active pharmaceutical ingredient

MS: Multiple Sclerosis

SAR: Structure activity relationship

$MeSO_3H$: Methanesulfonic acid

H_2SO_4: Sulfuric acid

TOSMIC: Toluenesulfonylmethyl isocyanide

$KMnO_4$: Potassium permanganate

$Na_2Cr_2O_7$: Sodium dichromate

SBDD: Structural based drug design

LBDD: Ligand based drug design

VS: Virtual screening

QM: Quantum mechanics

MM: Molecular mechanics

CHARMm: Chemistry at Harvard Molecular mechanics

Pdf: Probability density function

DTX: Dendrotoxin

TFAA: Trifluoroacetic anhydride

TClAA: Trichloroacetic anhydride

Chapter 1: Kv channels and their association to multiple sclerosis

1.1 Multiple sclerosis

Multiple sclerosis is a progressive neurological disease that results in long term disability. Worldwide approximately 2.5 million people are affected by the condition. People that develop MS experience conditions such as ambulatory impairment, visual loss, bowel and bladder urgency, fatigue and excruciating pain. The areas affected are mainly the brain and spinal cord. The disease state can be categorised into four subtypes. These are relapsing remitting (RR), primary progressive (PP), secondary progressive (SP), and progressive relapsing (PR). Based upon these four subtypes prognosis can be made and a therapeutic course of action undertaken. Relapse remission is defined as, the individual will experience disease relapses with full recovery. RR-MS shows periods between the disease relapses characterised by a lack of progression by the disease itself.[1] Primary progressive multiple sclerosis, the sufferer will experience disease progression from the onset with occasional plateaus showing slight temporary improvements shown in PP-MS. The fundamental aspect of PP-MS is there is a steady, gradual deterioration of the disease state with minor fluctuations, however there is no real distinct relapses associated with this subtype. SP-MS is a general combination of the initial RR disease state followed by progression. The progression for SP-MS can occur with the individual experiencing or not experiencing relapses, minor remissions and plateaus.[1] Finally PP-MS, the suffer skips the relapse remitting phase and is diagnosed with the progressive disease state from the beginning. Because 80% of suffers experience RR-MS, PP-MS is the least common.[2] Clear acute relapses, with or without full recovery between the relapses with accordance with continuing progression.

1.2 Potassium channels in myelinated and demyelinated axons

Concerning MS the axon is the main species of interest as it acts as the transmission wire for any electrical stimulus from the cell body to the axon termini which in turn feeds into muscle tissue. Motor neurons are composed of a cell body, dendrites, axon, nodes of ranvier, myelin sheath and axon termini.

Myelin sheath that surrounds the axon acts as an insulator. Characteristics of this insulating property are, it provides high resistance and low capacitance, thus a greater impulse conduction velocity is achieved in the axon.[3,4] Regarding the axon it can be stated that demyelination is the pathologic hallmark of MS. When this occurs the lesions as a result delay or block the action potential.[5] As the disease progresses, further axonal and neurologic degeneration contributes to the disease process.[6,7]

The pathogenesis is not fully resolved but it is believed that MS is a T-cell dependent autoimmune disease.[8] Acute inflammatory lesions result from the breakdown of the blood brain barrier. The degree of damage that the myelin sheath and axons encounter could be directly related to immunological resistance [9] or genetic susceptibility.[10,11] Figure 1.1 shows the exposure of potassium channels as a result of demyelination. The exposure of potassium channels cause an increase in the outward flow of K^+ and prevents depolarisation, which is essential for proper axon functioning.
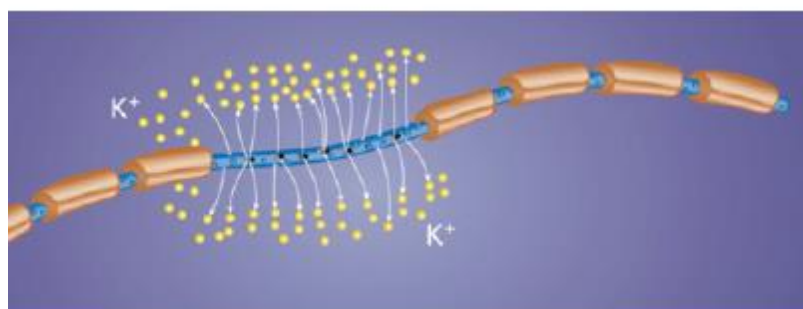
Figure 1.1: Illustrates K^+ ion dissipation into the exterior of the cell as a result of demyelination.[12]

1.2.1 Potassium channels

Potassium channels are proteins that mediate the flow of potassium ions across nerve membranes, identified in virtually all living organisms, bacterial, archeal and eukaryotic existing in both plant and animal.[13] In mammals the channels consist of four α or pore forming subunits spatially arranged around a central ion conducting pore as homotetramers or heterotetramers.[14,15] Their role is fundamental to the physiological function of the cell as they regulate the electrical potential essential for stimulus.

Potassium channels contain 78 known members and are divided into four structural types based on their various mode of action. These include 2-pore 4-transmembrane K^+ channels (K_{2p}), Ca^{2+} activated K^+ channels (K_{Ca}), inwardly-rectifying K^+ channels (K_{ir}) and voltage gated K^+ channels (K_v).[16] For the focus of this work, the emphasis will be on the voltage-gated potassium channels.

1.2.2 K_v channel molecular structure and functionality.

Voltage-gated potassium channels contribute to just over half of the K^+ channels known (40 genes), these 40 Kv channels have been studied in great detail as they have all been successfully cloned and biophysical properties characterized. They can be divided into 12 subfamilies, Kv1-Kv12. In mammalian entities Kv channels consist of four α-subunits, these proteins share a common structural configuration, they contain six transmembrane α-helical regions, S1-S6, and a membrane re-entering P-loop which is highly conserved, circumferentially around a central pore as a heterotetramer. The ion conduction pore of the selectivity filter constitutes the fifth and sixth α helical region S5-P-S6. The four S1-S4 moieties each contain positively charged arginine residues in the S4 helix. The purpose that they serve is they act as voltage sensor domains and 'gate' the pore exerting a pulling action on the S4 linker [14,17,18] as shown in figure 1.2.

The structure of the Kv channel can undergo an induced structural rearrangement due to changes in the electrical field across the transmembrane, sensed by the S4 segment. The channels when open conduct and whilst closed are non-conducting. The non-conducting channels undergo further rearrangements to open which activates or closes, deactivates the ion translocation pore.[19] For inactivating channels, N-type inactivation occurs; this is when the ion translocation pore is hindered by the binding of the N-terminal segment to the cytoplasmic vestibule of the pore [20] this can be visualised in figure 1.3 C. After a period of

binding to the pore the N terminus segment that was causing inactivation dissociates in a process called recovery from inactivation. Another form of inactivation that occurs is from the opposite C terminus region and as a result bears the name C-type inactivation shown in figure 1.3 D. This occurs with prolonged depolarization as a result of Na^+ channel opening. The prolonged depolarization leads to a dramatic decrease in the flow of current due to structural changes thus inhibiting the extracellular end of the ion pore.[21-23] Other agents that can modulate the Kv channels are small organic molecules and various venom peptides. These inhibit the regular functionality of the channels by blocking the ion translocation pore from the inner, external turret region or binding to the voltage sensor domain hence modifying the channel gating; these are shown as figure 1.3 (E), (F) and (G) respectively. The turret region being the most extracellular region in the protein tetramer.
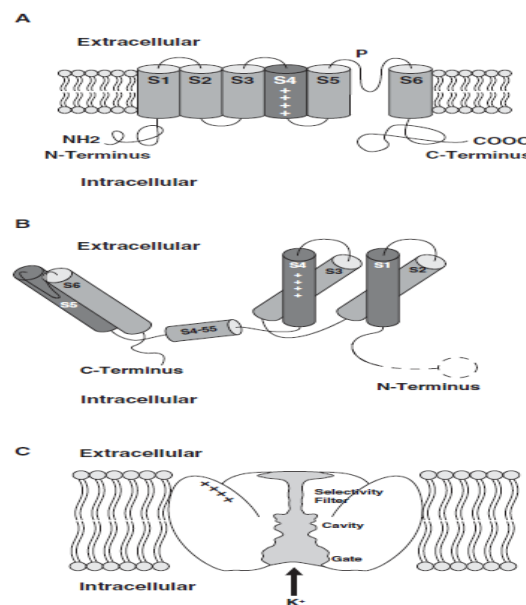
Figure 1.2: Schematic diagrams depictive of a generic Kv Channel. Each of the diagrams shows the extracellular surface (exterior) on top and the intracellular surface (Cytosol) on the bottom. In diagram (A) it is a representation of the 6 transmembrane segments (6TM) as a single Kv subunit. In (B) the intracellular C-terminus and N-terminus involved with inactivating mechanism via N/C type. In (C) this diagram illustrates the Kv channel in its open state in the vicinity of the transmembrane lipid bilayer.[15]
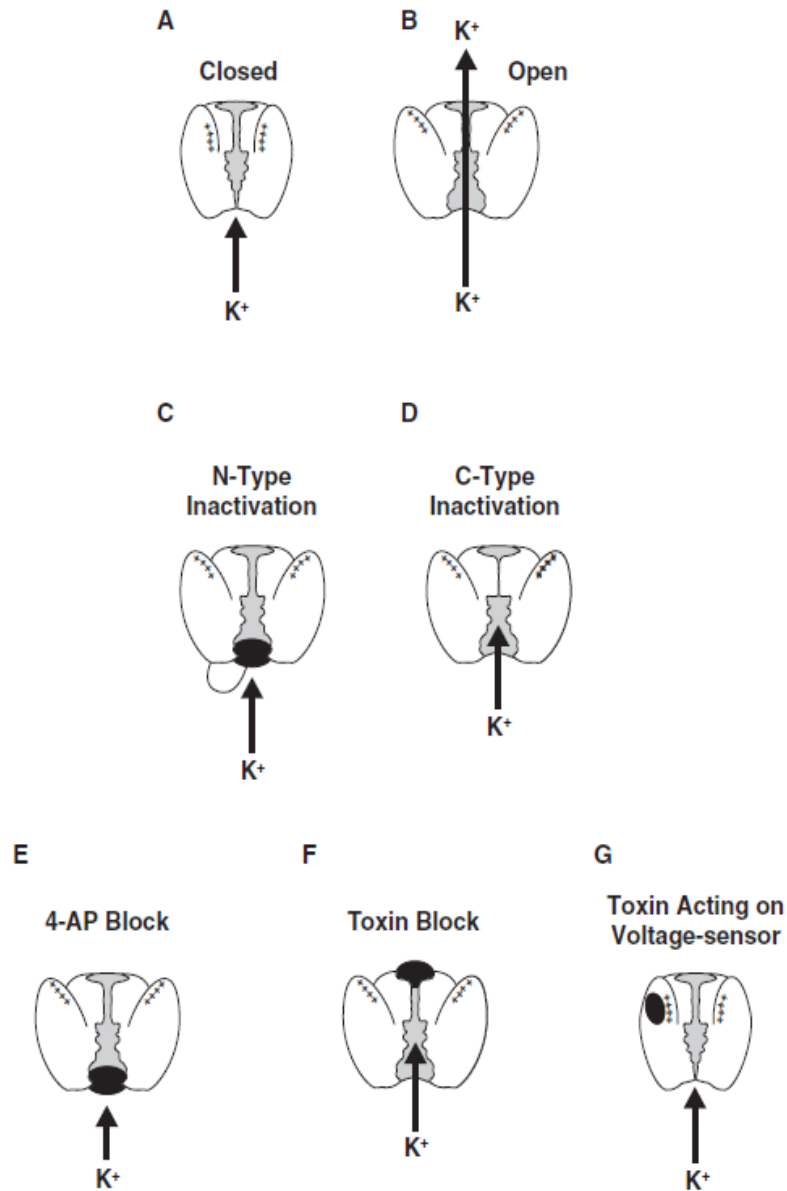
Figure 1.3: A list of schematic diagrams illustrating the various conducting and non-conducting conformations the Kv channel. (A) Shows a closed channel with non-conducting potential. (B) Open, conducting channel. (C) Open channel but non-conducting due to the N-type inactivation mechanism occurring. (D) Open, non-conducting channel to which the selectivity filter has closed due to C-type inactivation. (E) Open, non-conducting channel as a result of the inner turret binding of the small molecule 4-aminopyridine (4-AP). (F) Open, non-conducting channel inhibited by the binding of a toxin molecule at the outer turret region. (G) Closed, non- conducting channel in which a voltage-sensor modifying toxin has administered itself into the membrane lipid bylayer binding to the voltage sensor region and as a result inducing channel closure.[15]

1.3 Properties and therapeutic feasibility of Kv channels.

K^+ channels are important regulators of membrane excitability which, in turn, determine signal transmission between neurons or other effector cells (e.g. muscles). Voltage-gated K^+ channel of Shaker subfamily (Kv1) are involved in human diseases[24], where their functions are altered by mutation (e.g. certain forms of epilepsy) or truncation (e.g. Episodic ataxia type I). Also, the appearance of a new K^+ channel upon demyelination of axons in patients suffering from multiple sclerosis (MS) culminates in abnormal propagation of nerve signals, underlying muscle weakness and debilitation.

Immunohistochemical studies revealed that $K_V1.1$ and $K_V1.2$ α subunits are mainly coalesced at the juxta-paranode of myelinated nerve axons.[25-27] These subunits form hetero-multimeric channels with limited possible combination.[28] Null-mutation has also confirmed the importance of the Kv1.1 channel in the functioning of the nervous system. Deletion of the channel underlies a form of rodent temporal lobe epilepsy.[29] In demyelination lesions of the rat sciatic nerve,[26] observed a redistribution of Kv1.1 and Kv1.2. Some demyelinated axons had diffused staining at nodes, where other axons were devoid of Kv1 channel staining, but none had paranodal localization of these channels. During remyelination, Kv1.1 expression was found at the node and over time redistributed to the paranodal/juxtaparanodal sites but were never completely contained in their original juxtaparanodal sites. This alteration in Kv1 surface expression along the demyelinated axons shows the possible formation of new population of Kv1 channels associated with MS, such as homomeric Kv1.1 channel. The exposure of these newly formed channels lead to massive efflux of K^+ currents from axons which disturb nerve conduction.

To date, attempts to correct neuro-transmission abnormality associated with neuronal demeylination have relied on inhibiting these K^+ channels with aminopyridines; although that therapy is effective in the short-term, their use is limited by narrow toxic-to-therapeutic ratio and blockade of unrelated K^+ channels results in severe side effects, especially seizures.[15] This unmet medical need has led to a search for small molecules which could act extracellularly as specific inhibitors of the disease-related Kv1 channels. It should be possible to normalise neuronal communication in MS patients using a blocking drug selective for the channel uniquely associated with this disease.

Kv 1.1 is over-expressed in MS patient autopsies (Dolly, unpublished results) An ideal molecular candidate for the application of this strategy would be to inhibit the Kv 1.1 channel whilst have little or no interaction with other Kv1 channels, especially Kv1.2 which is the most expressed potassium channel in the cerebrum.

1.3.1 Treatments for multiple sclerosis.

In 2010 there was massive progress made in the treatment of multiple sclerosis, the potassium channel blocker *Dalfampridine* was released to the market. The significance of this treatment was that it was the first oral medication to engender any functional improvement in patient suffering with MS. Dalfampridine is the formulated, extended release form of fampridine. The API is 4-aminopyridine shown in figure 1.4.
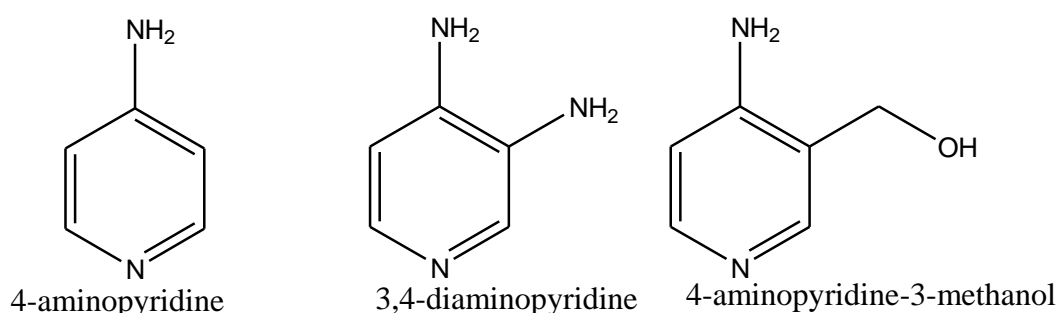
Figure 1.4: Trialled aminopyridine derivatives

1.3.2 Mechanism of action

There are a number of factors which leads to the confusion in which a plausible mechanism of action can be determined for 4-aminopyridine inhibiting Kv channels. Firstly, confusion arises because the response of the molecule is concentration dependent; this means that the doses that can be used clinically produce only very low concentrations of the drug in the cerebrospinal fluid and blood. These don't relate when compared to typical concentrations investigated in laboratory studies. Other factors include the frequency of stimulation and the kinetic environment of the potassium channel.[15,30,31,32] The various gating processes that include activation, deactivation and inactivation are all known to illustrate modulation of 4-aminopyridine blockage. For example, in particular Kv channels, 4AP can display resting

block or frequency-dependent block. Dating back to the initial electrophysiological work performed with 4-AP block in native delayed rectifier type Kv channels, in the axonal membrane of squid, frequency-dependent relief of block portrayed that 4 AP bound to closed channels[30] or closed channels just prior to opening.[31]

Table 1.1: IC$_{50}$ values of 4-AP between the various Kv1-4 channels.[15]

Kv gene subfamily	4-AP IC$_{50}$ range (µM)	4-AP IC$_{50}$ by IUPHAR (µM)
Kv1.1	89-1100	290
Kv1.2	200-800	590
Kv1.3	200-1500	195
Kv1.4	647-13000	13000
Kv1.5	50-400	270
Kv1.6	300-1500	1500
Kv1.7	150-245	150
Kv1.8	68-1500	1500
Kv2.1	500-18000	18000
Kv2.2	890-1500	1500
Kv3.1	20-600	29
Kv3.2	100-900	100
Kv3.3	100-1200	1200
Kv4.1	9000-20000	9000
Kv4.2	1005-5000	5000
Kv4.3	1540-10000	N/a

In table 1.1 it is important to take into account the differences in the state dependence of 4-AP binding and the kinetics of the channel gating. The 4-AP binding affinity is dependent on the voltage clamp protocol. It is possible that the 4-AP binding site and the activation gate correspond with each other in potassium channels. In Kv1.1 it is an open channel blocker, i.e the drug is trapped within the pore on channel closure. Kinetic comparison studies were preformed based upon the highly selective Kv3.1 channel and the low sensitivity Kv2.1. Results from this suggested the 4-AP binding site was in the 3' S6 segment and that a region in the 5' S5 segment traps bound 4-AP.[32] Another study directly related to this work demonstrated that channel activation accelerated 4-AP dissociation from a Kv1.1 channel confirming that the charged form of 4-AP was the principal cause for channel block[33]. Thus K^+ channel sensitivity to dalfampridine depends on the activation state of the channel, with open channels being more accessible to blockage compared to closed channels. The drug will enter an open ion channel more readily than a closed channel. The theory behind how 4-AP works from a simplistic view is illustrated in figure 1.5. Putative theory suggests that dalfampridine blocks the potassium channels and as a result only a fraction of the K^+ ions are lost across the axon to the exterior as a result of demyelination experienced. Damfampridine has been experimentally proven to overcome conduction block in a variety of animal modes. Using this drug restoration of axonal conduction in demyelinated rat sensory nerve fibers of the dorsal root as it effected demyelinated axons. It had no effect on the action potential of normal myelinated nerve fibers in the rat.[34]
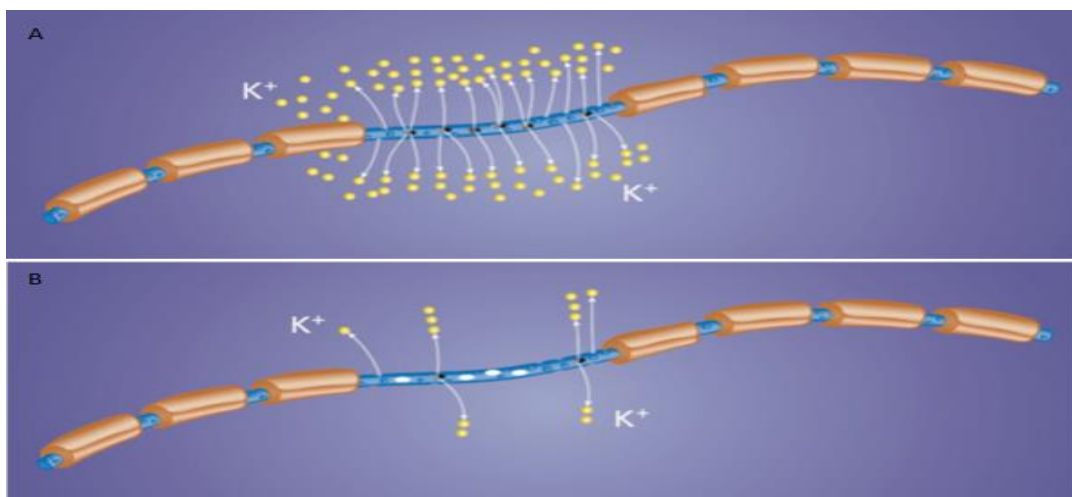
Figure 1.5: Illustrates (A) K^+ ion efflux of a normal demyelinated axon against (B) a demyelinated axon with dalfampridine acting as a K^+ channel blocker.[12]

1.3.3 Kv1.3 and immunosuppressant's as treatments

In the previous sections the neurodegenerative phase of multiple sclerosis was discussed, however, it is widely believed that MS is a two stage disease. The first phase revolves around autoimmunity.[8,9] It is widely accepted that autoimmune T cells mediate the initial steps of multiple sclerosis lesions, with particular focus on myelin antigens. Kv1.3 potassium channels were first discovered in human T cells in 1984.[35,36] T cell investigation as an immunosuppressant target arose due to studies involving 4-AP. 4-AP can inhibit T cell proliferation and interleukin-2 secretion.[36] The mechanism how immunosuppression is achieved with Kv1.3 blockers is that the T cell membrane is depolarized[37] and this reduces the driving force for calcium ion entry through the calcium released-activated calcium (CRAC) channel.[35] T cells are small on the normal cellular size and have no substantial intracellular Ca^{2+} stores, this Ca^{2+} influx through the inward rectifier CRAC is necessary for the translocation of nuclear factor of activated T cells to the nucleus and the ultimately resulting cytokine secretion and T cell proliferation.[14] The following therapeutic pipeline as a result of this work directly reflects on immunosuppression and Kv1.3 channels to treat the disease in the initial autoimmune stage rather than neurodegenerative phase. As of 2011 there are a number of drugs under clinical trials to treat MS, these include:

Fingolimod: This drug is a Sphinosine-1-phosphate inhibitor, it blocks lymphocyte egress from lymph nodes.[38] It is delivered orally and once daily. It is FDA approved on the basis of two published phase 3 trials.[39,40] Additional phase 3 trials are further evaluating safety and efficiency against placebo for RRMS and PPMS.

Cladribine: Purine nucleoside analogue; causes durable reduction in lymphocyte counts.[41]

It is delivered orally, daily for short course administration. Patients were treated for 16 or 30 days over 52 weeks in clinical trials. Currently under review by the FDA, one published phase 3 trial[42] with 2 additional phase 3 trials ongoing. There is significant reduction in relapse rates and disability compared with placebo. Long term immune suppression may increase the risk of infection and developing malignancies.

Terifluomide: Antiproliferative agent with effects on T and B cells.[41] It is an oral therapeutic taken once daily. One phase 3 trial is complete and the results are published. This is currently undergoing further phase 3 clinical trials to prove efficiency.

Alemtuzumab: Monoclonal antibody targeting CD52, produces rapid and durable depletion of T and B cells.[43] This treatment is administered intravenously for 5 consecutive days followed by yearly dosing for 3 consecutive days. Phase 2 results have been published[44], carried out over a 5 year period. There is two phase 3 currently ongoing for RRMS.[45]

Daclizumab: Monoclonal antibody targeting CD25 T cell immune modulator. Intravenously administered once monthly. Phase 2 trial completed, phase 3 currently ongoing for RRMS.[43]

Rituximab: Monoclonal antibodies targeting CD20, these produce sustained suppression of B cells.[46] This is also intravenously administered, the dosing strategy however is still under investigation. There was positive phase 2 results in RRMS patients[47], however negative phase 2/3 results for PPMS.

1.4 Venom peptide toxins targeting Kv channels.

The biodiversity in plants, animals and marina that stretch across land and ocean worldwide results in massive diversity of venoms and poisons. These moieties contain potent active toxins that range from small organic molecules to large polypeptides. The flora or fauna carrying or administering toxins acquire these as secondary metabolites as an attack/defence mechanism. The method of synthesis of these toxins can be broke down into two systems, the first is via gene expression/ complex metabolic pathway where a number of chemical reactions are catalyzed by specific enzymes leading to the secondary metabolites. Another means to acquire toxicity is by the accumulation and storage of compounds that are toxic or have the potential to become toxic.[48]
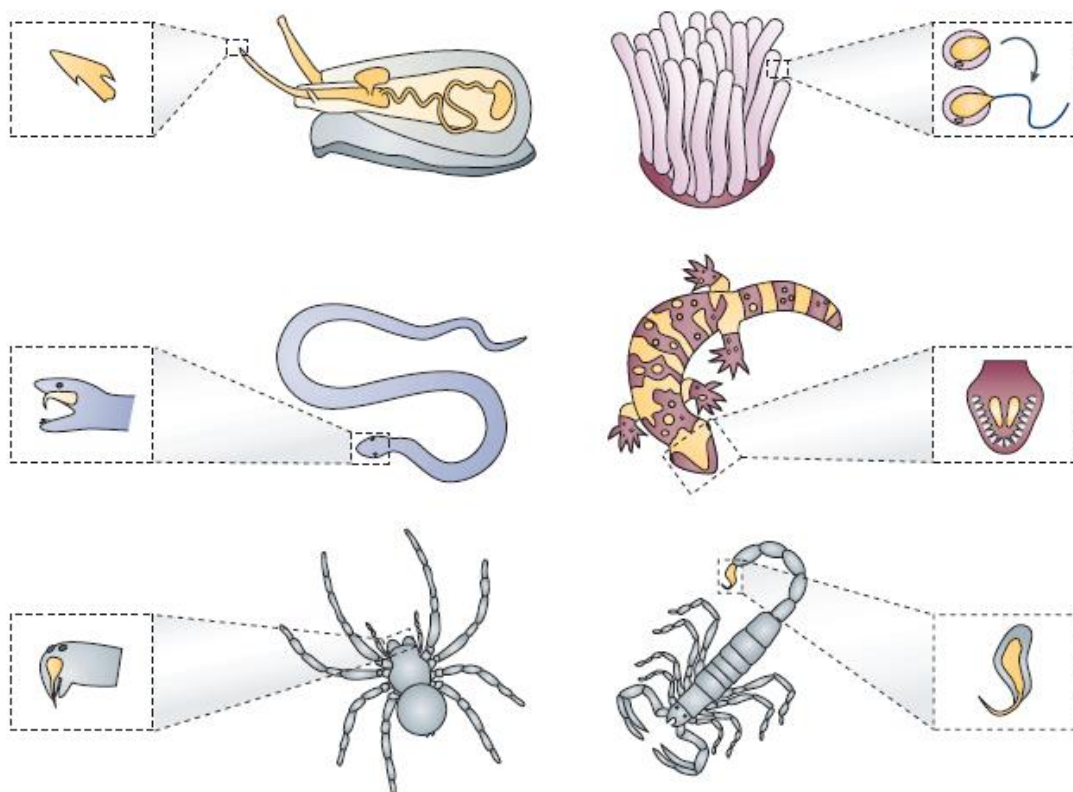
Figure 1.6: Sources of venom therapy and means of administration.

To date there has been extensive research concerning the venoms of spiders, snakes, scorpions, sea anemones and marine cone snails that produce peptide toxins that are highly potent and highly selective blockers of K+ ion channels.[49, 50-51] The features that these peptide toxins exhibit are their impeccable specificity and high sensitivity for the ion channels that have allowed the isolation and sufficient purification of the channel proteins. The use of these toxins have allowed massive advancements in the field of ion channel research mainly because they have unravelled important data concerning the structure and function of the proteins.

1.4.1 Mechanism of peptide toxin blockade in Kv channels.

K^+ channel studies and the possibility to investigate mechanistic properties of Kv channels began with the use of venom-derived peptide toxins as probes. The initial studies began with the identification and purification of the snake derived peptide toxin, dendrotoxin (DTX)[52, 53], and two scorpion-derived toxins, noxiustoxin (NxTX)[54] and charybdotoxin (ChTX).[55, 56] The two general mechanisms of how venom-derived peptide toxins interact with K^+ channels are as follows, they either bind to the extracellular mouth of the ion translocation pore inserting a

lysine side chain into the pore, as a result blocking the pore. The second mechanism involves binding to and modulating the voltage sensor region of the K$^+$ channel after dispersing into the lipid bilayer.
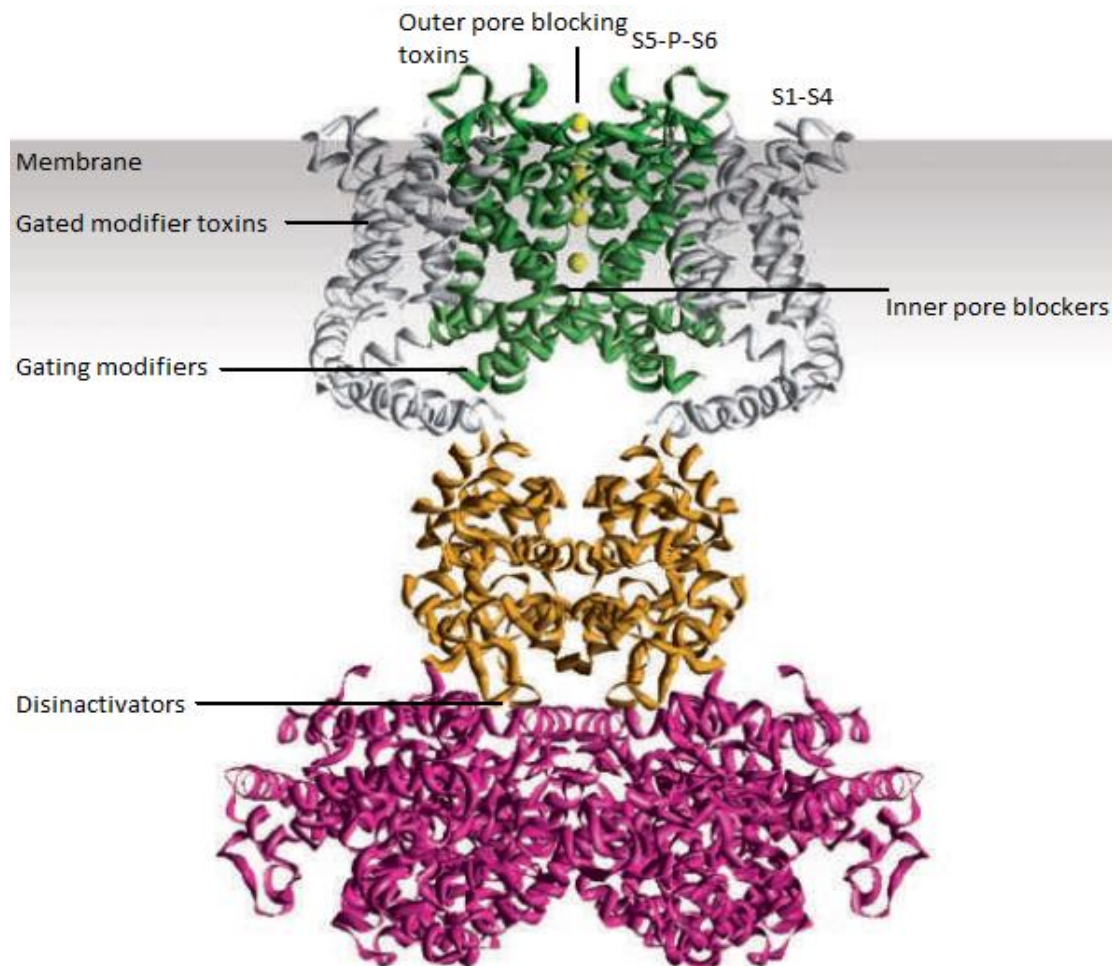
Figure 1.7: Tetrameric protein showing the main regions of interest.[14]

The binding of ChTX and DTX has been studied in tremendous detail.[57,58] Site-directed mutagenesis in combination with mutant cycle analysis techniques, deductions were made assessing the critical amino acids involved in the structural surface between dendrotoxins and their binding site at the extracellular region of the ion pore in certain Kv channels.[59,60] The initial investigation into ChTX and DTX binding in Kv1 channels acted as a platform that lead to the current functional dyad model still in practice.[61, 62] This model shows how scorpion and sea anemone peptide toxins that have vastly different tertiary structures exert very similar blockage due to critical residues that are conserved.[63, 64] The functional dyad is composed of a critical lysine residue and an aromatic hydrophobic residue separated by 6.6 Å.[61] The snail cone conotoxin does not appear to follow this functional diad.[62] From the early studies for

ChTX and DTX, our understanding is there are commonly reoccurring features of the functional amino acid dyad. These, located on the surfaces of folded scorpion, snake or sea anemone toxins can anchor into the S5-S6 loop in the pore region of the Kv channel.[65]

Unlike the peptide toxins such as scorpion, snake, marine cone snail and sea anemone that bind in the S5-P-S6 region, spider venoms act differently. Spider derived peptide toxins have shown experimentally to inhibit Kv channels by interacting with the voltage sensory region (S3-S4), as opposed to binding to the extracellular pore region like the other toxin sources discussed.

These spider venoms that have been isolated and purified from species of tarantula include the hanatoxins[66, 67], phrixtoxins[68], heteropodatoxins[69] and the venoms from the Chilean rose tarantula.[70,71] Voltage sensor modifying toxins are characteristically associated with changes that increase the stability of the channel closed state. Spider venoms produce depolarizing shifts in the voltage dependence of current activation, as mentioned in section 1.2.2, this refers to more depolarization of the membrane potential required to open the channel, hence inhibiting it. Another effect spider venoms exert is, the increase in acceleration of current deactivation kinetics thus the channel closes faster.[67,69,70] Hanatoxin was the founding member of the toxin family that bound to the voltage sensing domains, inhibiting the channels. HaTX1 and HaTX2 showed localisation in the S3-S4 linker.[72-74]

1.4.2 Venom therapy in the treatment of multiple sclerosis.

Above it has been stated the specificity, selectivity and potency of venom derived peptide toxins makes it possible to investigate and possibly treat complex diseases as they have a great affinity to bind to molecular targets. Compared to small molecule therapeutics it may seem negligible, however, there are six FDA-approved drugs derived from venom peptides or proteins and these include captopril, eptifibatide, tirofiban, bivalirudin, ziconitide and exenatide.[75]

Bee venoms

The honeybee *Apis mellifera* has venom that contains various small molecules, peptides and proteins that range from low molecular weight to high molecular weight compounds. The

larger species include melittin, apamin, adolapin and phospholipase A2.[76-78] The lower molecular weight compounds are biologically active amines, histamine and epinephrine. The use of bee venom as an effective treatment for MS has been reported.[79] This research included a body of 9 patients that had progressive forms of the disease. In this trial no serious adverse allergic reactions were witnessed in any of the subjects, but 4 patients experienced a deteriation of neurological symptoms, this could not be denounced as a side effect. From the other 5 patients administered the bee venom, 3 felt that the therapy has subjective amelioration of symptoms and the final 2 showed objective improvement.[79] This trial was only to show safety, no major conclusions could be made referring to the efficiency of using BV as a therapeutic. Another trial, a randomised crossover study based on 24 weeks of treatment with 26 patients with relapse remitting or relapse secondary progressive MS, no serious side effects were witnessed. The number of new gadolinium-enhancing lesions could not be reduced, this being one of the primary determinants for evaluating disease progression. Also there was no significant reduction in relapse rate or fatigue.[80] The results collectively obtained showed immunostimulant properties that could limit the efficiency of BV as a viable therapeutic option for the treatment of MS.[81]

Sea anemone and scorpion toxins

The sea anemone (Stichodactyk helianthus) found along the Cuban coast has been used as a source of K+ channel blockers. Sticholysins I and II are the most characterized cytolysins from this particular anemone.[82, 83] The sea anemone toxin ShK blocks K+ channels Kv1.1 and Kv1.3 in low picomolar range.[15] A synthetic derivative of ShK, ShK-Dap(22) has been synthesised, this peptide has replaced a lysine with a diaminopropionic acid residue and this has been investigated with Kv1.3.[83-85] The activity against T-cells and their immunosuppressant properties have propelled themselves into a position of evaluation for MS however no formal clinical trial has started yet. The scorpion toxin OSK1 as an immunosuppressant entity against Kv1.3 is even more potent than the sea anemone ShK.[15] There has been a synthetic derivative of OSK1, [K16,D20]-OSK1 made, both scorpion toxins have been tested in mice. Intracerebroventicular injections into the mice produced toxic epileptogenic tremors effects comparable with inoculation.[86]

Snake venom

In MS lesions, fibrinogen escapes from the blood into the brain tissue, which then permates a broken down blood brain barrier (BBB). Increased fibrin deposition has been observed experimentally at the site of lesions in patients with MS.[87] It has been shown that the absence of fibrin, the rate of regeneration of myelin sheath is improved. This was proven in mice models lacking fibrin. In the absence of fibrin, sheath cells are able to mature more quickly and can remyelinate damaged nerves. The results from this work lead to the hypothesis that, preventing fibrin deposition could be a method to help stimulate the nervous systems regenerative capacity thus having potential for MS. This hypothesis has been tested using the venom batroxobin isolated from the American pit viper. Batroxobin converts circulating fibrinogen into an insoluble material and causes afibrinogenemia. Plasma fibrogen concentration decreases significantly in bactroxobin treated rats.[88, 89]

The only current venom derived toxin undergoing clinical trials is alpha-cobratoxin, its code name is RPI-78M.[90] It is administered orally as opposed to the toxins discussed previously. It has the same immunosuppressant properties of other venoms.

With regard to the systematic administration of various peptide toxins, proteolytic degradation of toxins in the blood brain barrier has really handicapped their further development as a feasible therapeutic in MS or any neurodegenerative disease. The other concerns include the appearance of side effects following the use of the biological agents. Side effects of venom therapy could be seen as a result of their non-self polypeptide structure. Administration of these foreign entities can sensitize the subject and cause various hypersensitivity reactions.

1.5 Calixarene and porphyrins as K+ channel inhibitors

Discussed in section 1.3.1, the possibility of probing potassium channels with small molecules to inhibit multiple sclerosis is already at advanced stages of clinical trials. The mechanism to which these all adhere by is based upon Kv1.3 and immunosuppression. There are two major synthetic papers in the literature that uses macrocycles to probe the Kv1.3 channel, these are porphyrin[91] and calixerene[92]. Firstly, water soluble porphyrin derivatives were synthesised and screened against transfected HEK293 cell with the Kv1.3 channel. Results showed that inhibition as low as 13nM could be obtained with the screening

technique employed when cationic porphyrins were used. Calix[4]arenes, another macrocycle was used to probe these Kv1.3 channels, cationic calix[4]arenes gave inhibition at 50 µM which is substantially less than the results witnessed with the porphyrins. The concepts with spatial geometries by Martos *et al*, are valid however there are a number of questions that arise in the molecular modelling aspect of the work. Their work on the molecular modelling is based upon the potassium channel Kv1.2, the cell screening is based upon Kv1.3. The molecular modelling was a key aid for the argument of the paper, predicting the best candidates for optimal binding. However, the amino acid sequence in the turret regions, both inner and outer of these two channels Kv1.2 and Kv1.3 are substantially different and the plausibility of the concepts promoted by this paper has to be questioned. Comparing both pieces of work, the ideal scaffold to begin any investigation into the Kv1.1 channel associated with the neuron, porphyrins seem to be the ideal candidate. Further studies were conducted by Ader *et al*[93] using porphyrins as a probe to understand the mechanism to which these Kv channels gate in the presence of an inhibitor. Using solid state NMR techniques and an isotopically enriched ^{15}N porphyrin it was shown that the deviance of the selectivity filter residues carbonyl backbone, from its natural arrangement had a direct relationship with conductance within the channel. The similarity between the Kv1.3 channel and the Kv1.1 channel allows this work to be a platform for studies into the diseased state Kv1.1 channel.

1.5.1 Screening technologies for target molecules

Due to the complexity of the target, the biological screening to measure ion channel inhibition is difficult. There are two main methods to which this can be performed; these are conventional patch clamp and QPatch testing. Conventional patch clamp methodology measures the ion channel function directly. The system to which testing consists of a whole-cell voltage clamp, a specialized amplifier that accurately clamps the membrane potential and measures the current flow across the membrane of the cell. The high level of accuracy that this method has for measurement of the current has gave it the accolade of the gold standard for studying ion channel function and pharmacology. It is only used for testing a small number of samples. The QPatch system is however an automated method that combines high throughput screening with conventional patch clamp systems. The distinct advantage that the QPatch method offers is the ability to screen a library of compounds rather than a few, this benefits the pharmaceutical industry.[94]

Figure 1.8: QPatch screening chip

Shown in figure 1.9 is the whole-cell patch-clamp recording apparatus used.
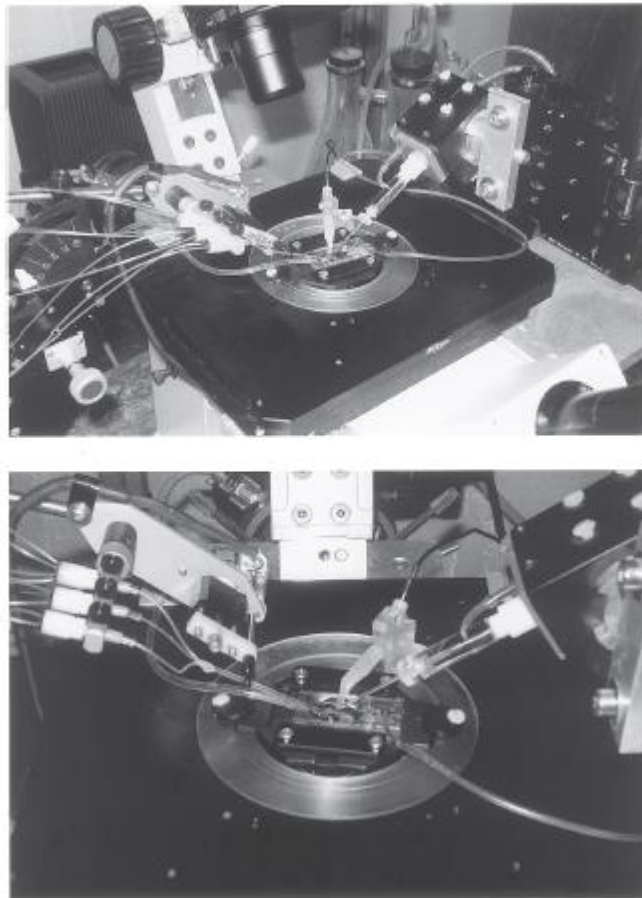
Figure 1.9: Whole-cell patch-clamp setup.

The apparatus consists of an electrically grounded microscope on an isolation table together with a recording chamber mounted to the stage of the microscope. The 'chip' which the studies are conducted on contains the cell line of interest. An electrode pierces the membrane and measures a current across the cells. Electrode resistance is monitored continuously by the application of a small voltage pulse. The application of the inhibitor to the cell is monitored by the electrode. There is also an outlet valve that allows the wash out of the inhibitor upon administration. The 'chip' is grounded and the whole system protected in a Faraday cage preventing external electromagnetic interference. The measured data is collected and represented as a function of amplitude against time.

The importance of this technology has now become an essential FDA guideline if a drug is to go to market. All potential candidates must be screened against the hERG K channels by the patch clamp method. The reasoning for this was, in the 1990's certain pharmaceuticals, thapsigargin caused potentially fatal arrhythmias amongst patients.

Shown in figure 1.10 is a typical biophysical recording of the measure of current across the membrane of a rat subject. The application of this technology is most commonly used to monitor potassium, sodium and calcium ion channels. Anionic ions such as chloride channels also use this technique. The use of these towards chloride channels is, these are related to cystic fibrosis transmembrane regulators (CFTR), mutations in the CFTR gene is studied using these ion channel apparatus.

Other channels such as P2X3 and γ-amino-butyric acid (GABA) ion channels have been studied in detail using the patch clamp and QPatch methods.[94]
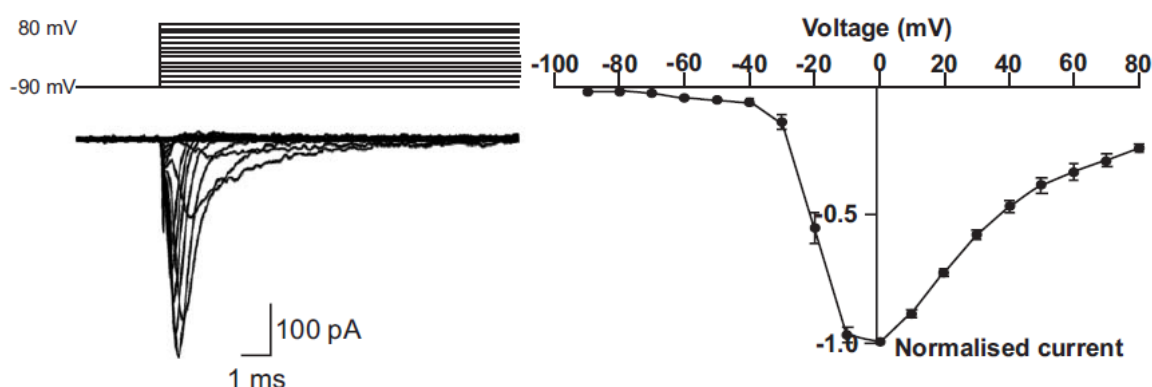
Figure 1.10: Biophysical characterisation of Rat Nav1.2 currents measured with QPatch 16.

1.6 References

1. Lublin FD, Reingold SC. Defining the clinical course of multiple sclerosis: Results of an international survey. Neurology 1996;46(4):907-11.

2. Antel J, Antel S, Caramanos Z, Arnold DL, Kuhlmann T. Primary progressive multiple sclerosis: Part of the MS disease spectrum or separate disease entity Acta Neuropathol 2012;123(5):627-38.

3. Huxley A, Stampfli R. Evidence for saltatory conduction in peripheral myelinated nerve fibres. Journal of Physiology-London 1949;108(3):315-39.

4. Waxman S. Current concepts in neurology - membranes, myelin, and the patho-physiology of multiple-sclerosis. N Engl J Med 1982;306(25):1529-32.

5. Waxman S. Conduction in myelinated, unmyelinated, and demyelinated fibers. Arch Neurol 1977;34(10):585-9.

6. Trapp B, Ransohoff R, Rudick R. Axonal pathology in multiple sclerosis: Relationship to neurologic disability. Curr Opin Neurol 1999 ;12(3):295-302.

7. De Stefano N, Narayanan S, Francis G, Arnaoutelis R, Tartaglia M, Antel J, Matthews P, Arnold D. Evidence of axonal damage in the early stages of multiple sclerosis and its relevance to disability. Arch Neurol 2001 ;58(1):65-70.

8. McFarland HF, Martin R. Multiple sclerosis: A complicated picture of autoimmunity. Nat Immunol 2007;8(9):913-9.

9. Steinman L. Multiple sclerosis: A two-stage disease. Nat Immunol 2001;2(9):762-4.

10. Dyment D, Ebers G, Sadovnick A. Genetics of multiple sclerosis. Lancet Neurology 2004;3(2):104-10.

11. Hillert J. Multiple sclerosis: Postlinkage genetics. Clin Neurol Neurosurg 2006;108(3):220-2.

12. Dunn J, Blight A. Dalfampridine: A brief review of its mechanism of action and efficacy as a treatment to improve walking in patients with multiple sclerosis. Curr Med Res Opin 2011 ;27(7):1415-23.

13. Littleton J, Ganetzky B. Ion channels and synaptic organization: Analysis of the drosophila genome. Neuron 2000;26(1):35-43.

14. Wulff H, Castle NA, Pardo LA. Voltage-gated potassium channels as therapeutic targets. Nature Reviews Drug Discovery 2009;8(12):982-1001.

15. Judge S, Bever C. Potassium channel blockers in multiple sclerosis: Neuronal K-V channels and effects of symptomatic treatment. Pharmacol Ther 2006;111(1):224-59.

16. Lujan R. Organisation of potassium channels on the neuronal surface. J Chem Neuroanat 2010 ;40(1):1-20.

17. Long S, Campbell E, MacKinnon R. Voltage sensor of kv1.2: Structural basis of electromechanical coupling. Science 2005 5;309(5736):903-8.

18. Long S, Campbell E, MacKinnon R. Crystal structure of a mammalian voltage-dependent shaker family K+ channel. Science 2005 5;309(5736):897-903.

19. McCormack K, Joiner W, Heinemann S. A characterization of the activating structural rearrangements in voltage-dependent shaker K+ channels. Neuron 1994 ;12(2):301-15.

20. Isacoff E, Jan Y, Jan L. Putative receptor for the cytoplasmic inactivation gate in the shaker K+ channel. Nature 1991 5;353(6339):86-90.

21. Grissmer S, Cahalan M. Tea prevents inactivation while blocking open K+ channels in human lymphocytes-T. Biophys J 1989 ;55(1):203-6.

22. Liu Y, Jurman M, Yellen G. Dynamic rearrangement of the outer mouth of a K+ channel during gating. Neuron 1996 ;16(4):859-67.

23. Kiss L, Korn S. Modulation of C-type inactivation by K+ at the potassium channel selectivity filter. Biophys J 1998 ;74(4):1840-9.

24. Kullmann DM. The neuronal channelopathies.. Brain 2002;125(6):1177-95.

25. Wang H, Kunkel D, Martin T, Schwartkkroin P, Tempel B. Heteromultimeric K+ channels in terminal and juxtaparanodal regions of neurons. Nature 1993 2;365(6441):75-9.

26. Rasband MN, Trimmer JS, Schwarz TL, Levinson SR, Shrager P. Potassium channel distribution, clustering, and function in remyelinating rat axons. J. Neurosci 1998;18:36-47.

27. Rasband MN, Trimmer JS. Developmental clustering of ion channels at and near the node of ranvier. Developmental Biology 2001;236(1):5-16.

28. Shamotienko O. Subunit combinations defined for K+ channel Kv1 subtypes in synaptic membranes from bovine brain. Biochemistry 1997;36:8195-201.

29. Wenzel HJ, Vacher H, Clark E, Trimmer JS, Schwartzkroin PA. Structural concsequences of Kcna1 gene deletion and transfer in mouse hippocampus. Epilepsia 2007;48:2023-46.

30. YEH J, OXFORD G, WU C, NARAHASHI T. Dynamics of aminopyridine block of potassium channels in squid axon membrane. J Gen Physiol 1976;68(5):519-35.

31. KIRSCH G, YEH J, OXFORD G. Modulation of aminopyridine block of potassium currents in squid axon. Biophys J 1986 ;50(4):637-44.

32. KIRSCH G, SHIEH C, DREWE J, VENER D, BROWN A. Segmental exchanges define 4-aminopyridine binding and the inner mouth of K+ pores. Neuron 1993 ;11(3):503-12.

33. Castle NA, Fadous S, Logothetis DE, Wang GK. Aminopyridine block of Kv1.1 potassium channels expressed in mammalian-cells and xenopus-oocytes. Mol Pharmacol 1994;45(6):1242-52.

34. Sherratt RM, Bostock H, Sears TA. Effects of 4-aminopyridine on normal and demyelinated mammalian nerve-fibers. Nature 1980;283(5747):570-2.

35. Chandy KG, Wulff H, Beeton C, Pennington M, Gutman GA, Cahalan MD. K+ channels as targets for specific immunomodulation. Trends Pharmacol Sci 2004;25(5):280-9.

36. Decoursey TE, Chandy KG, Gupta S, Cahalan MD. Voltage-gated K+ channels in human lymphocyte-T - a role in mitogenesis. Nature 1984;307(5950):465-8.

37. Lin CS, Boltz RC, Blake JT, Nguyen M, Talento A, Fischer PA, Springer MS, Sigal NH, Slaughter RS, Garcia ML, et al. Voltage-gated potassium channels regulate calcium-dependent pathways involved in human lymphocyte-T activation. J Exp Med 1 1993;177(3):637-45.

38. Horga A, Castillo J, Montalban X. Fingolimod for relapsing multiple sclerosis: An update. Expert Opin Pharmacother 2010;11(7):1183-96.

39. Kappos L, Radue E, O'Connor P, Polman C, Hohlfeld R, Calabresi P, Selmaj K, Agoropoulou C, Leyk M, Zhang-Auberson L, et al. A placebo-controlled trial of oral fingolimod in relapsing multiple sclerosis. N Engl J Med 4 2010;362(5):387-401.

40. Cohen JA, Barkhof F, Comi G, Hartung H, Khatri BO, Montalban X, Pelletier J, Capra R, Gallo P, Izquierdo G, et al. Oral fingolimod or intramuscular interferon for relapsing multiple sclerosis. N Engl J Med 4 2010;362(5):402-15.

41. Conway D, Cohen JA. Emerging oral therapies in multiple sclerosis. Current Neurology and Neuroscience Reports 2010;10(5):381-8.

42. Giovannoni G, Comi G, Cook S, Rammohan K, Rieckmann P, Sorensen PS, Vermersch P, Chang P, Hamlett A, Musch B, et al. A placebo-controlled trial of oral cladribine for relapsing multiple sclerosis. N Engl J Med 4 2010;362(5):416-26.

43. Buttmann M. Treating multiple sclerosis with monoclonal antibodies: A 2010 update. Expert Review of Neurotherapeutics 2010;10(5):791-809.

44. Coles AJ, Compston DAS, Selmaj KW, Lake SL, Moran S, Margolin DH, Norris K, Tandon PK, CAMMS223 Trial Investigators. Alemtuzumab vs. interferon beta-1a in early multiple sclerosis. N Engl J Med 2008;359(17):1786-1801.

45. Cohen JA, Coles AJ, Arnold DL, Confavreux C, Fox EJ, Hartung H, Havrdova E, Selmaj KW, Weiner HL, Fisher E, et al. Alemtuzumab versus interferon beta 1a as first-line treatment for patients with relapsing-remitting multiple sclerosis: A randomised controlled phase 3 trial. Lancet 2012 2012;380(9856):1819-28.

46. Aktas O, Kieseier B, Hartung H. Neuroprotection, regeneration and immunomodulation: Broadening the therapeutic repertoire in multiple sclerosis. Trends Neurosci 2010;33(3):140-52.

47. Hauser SL, Waubant E, Arnold DL, Vollmer T, Antel J, Fox RJ, Bar-Or A, Panzara M, Sarkar N, Agarwal S, et al. B-cell depletion with rituximab in relapsing-remitting multiple sclerosis. N Engl J Med 2008;358(7):676-88.

48. Mebs D. Toxicity in animals trends in evolution? Toxicon 2001;39(1):87-96.

49. Fletcher JI, Wang XH, Connor M, Christie MJ, King GF, Nicholson GM. Spider toxins: A new group of potassium channel modulators. Perspect Drug Discov Des 1999;16:86-91.

50. Possani LD, Selisko B, Gurrola GB. Structure and function of scorpion toxins affecting K+-channels. Perspect Drug Discov Des 1999;16:103-110.

51. Gazarian KG, Gazarian T, Hernandez R, Possani LD. Immunology of scorpion toxins and perspectives for generation of anti-venom vaccines. Vaccine 2005;23(26):3357-68.

52. Harvey AL, Karlsson E. Dendrotoxin from the venom of the green mamba, dendroaspis-angusticeps - a neurotoxin that enhances acetylcholine-release at neuromuscular-junctions. Naunyn-Schmiedeberg's Arch Pharmacol 1980;312(1):1-6.

53. Harvey AL, Karlsson E. Protease inhibitor homologs from mamba venoms - facilitation of acetylcholine-release and interactions with prejunctional blocking toxins. Br J Pharmacol 1982;77(1):153-61.

54. Possani LD, Martin BM, Svendsen IB. The primary structure of noxiustoxin - a K+-channel blocking peptide, purified from the venom of the scorpion centruroides-noxius hoffmann. Carlsberg Res Commun 1982;47(5).

55. Miller C, Moczydlowski E, Latorre R, Phillips M. Charybdotoxin, a protein inhibitor of single ca-2(+)-activated K+ channels from mammalian skeletal-muscle. Nature 1985;313(6000):316-318.

56. Gimenezgallego G, Navia MA, Reuben JP, Katz GM, Kaczorowski GJ, Garcia ML. Purification, sequence, and model structure of charybdotoxin, a potent selective inhibitor of calcium-activated potassium channels. Proc Natl Acad Sci U S A 1988;85(10):3329-33.

57. Garcia ML, Hanner M, Kaczorowski GJ. Scorpion toxins: Tools for studying K+ channels. Toxicon 1998;36(11):324-39.

58. Tenenholz TC, Klenk KC, Matteson DR, Blaustein MP, Weber DJ. Structural determinants of scorpion toxin affinity: The charybdotoxin (alpha-KTX) family of K+-channel blocking peptides. Reviews of Physiology Biochemistry and Pharmacology 2000;140:135-85.

59. Hidalgo P, Mackinnon R. Revealing the architecture of a K+ channel pore through mutant cycles with a peptide inhibitor. Science 1995;268(5208):307-10.

60. Imredy JP, MacKinnon R. Energetic and structural interactions between delta-dendrotoxin and a voltage-gated potassium channel. J Mol Biol 2000;296(5):1283-94.

61. Dauplais M, Lecoq A, Song JX, Cotton J, Jamin N, Gilquin B, Roumestand C, Vita C, deMedeiros CLC, Rowan EG, et al. On the convergent evolution of animal toxins - conservation of a diad of functional residues in potassium channel-blocking toxins with unrelated structures. J Biol Chem 1997;272(7):4302-9.

62. Savarin P, Guenneugues M, Gilquin B, Lamthanh H, Gasparini S, Zinn-Justin S, Menez A. Three-dimensional structure of kappa-conotoxin PVIIA, a novel potassium channel-blocking toxin from cone snails. Biochemistry (N Y) 1998;37(16):5407-16.

63. Gasparini S, Gilquin B, Menez A. Comparison of sea anemone and scorpion toxins binding to Kv1 channels: An example of convergent evolution. Toxicon 2004;43(8):901-8.

64. Mouhat S, Mosbah A, Visan V, Wulff H, Delepierre M, Darbon H, Grissmer S, De Waard M, Sabatier JM. The 'functional' dyad of scorpion toxin Pi1 is not itself a prerequisite for toxin binding to the voltage-gated Kv1.2 potassium channels. Biochem J 2004;377:25-36.

65. Gilquin B, Braud S, Eriksson MAL, Roux B, Bailey TD, Priest BT, Garcia ML, Menez A, Gasparini S. A variable residue in the pore of Kv1 channels is critical for the high affinity of blockers from sea anemones and scorpions. J Biol Chem 2005;280(29):27093-27102.

66. Swartz KJ, Mackinnon R. An inhibitor of the Kv2.1 potassium channel isolated from the venom of a chilean tarantula. Neuron 1995;15(4):941-9.

67. Swartz KJ. Tarantula toxins interacting with voltage sensors in potassium channels. Toxicon 2007;49(2):213-30.

68. Diochot S, Drici MD, Moinier D, Fink M, Lazdunski M. Effects of phrixotoxins on the Kv4 family of potassium channels and implications for the role of I-to1 in cardiac electrogenesis. Br J Pharmacol 1999;126(1):251-63.

69. Sanguinetti MC, Johnson JH, Hammerland LG, Kelbaugh PR, Volkmann RA, Saccomano NA, Mueller AL. Heteropodatoxins: Peptides isolated from spider venom that block Kv4.2 potassium channels. Mol Pharmacol 1997;51(3):491-8.

70. Ruta V, Jiang YX, Lee A, Chen JY, MacKinnon R. Functional analysis of an archaebacterial voltage-dependent K+ channel. Nature 2003;422(6928):180-5.

71. Ruta V, MacKinnon R. Localization of the voltage-sensor toxin receptor on KvAP. Biochemistry (N Y) 2004;43(31):10071-9.

72. Swartz KJ, MacKinnon R. Hanatoxin modifies the gating of a voltage-dependent K+ channel through multiple binding sites. Neuron 1997;18(4):665-73.

73. Swartz KJ, MacKinnon R. Mapping the receptor site for hanatoxin, a gating modifier of voltage-dependent K+ channels. Neuron 1997;18(4):675-82.

74. Li-Smerin Y, Swartz KJ. Gating modifier toxins reveal a conserved structural motif in voltage-gated Ca2+ and K+ channels. Proc Natl Acad Sci U S A 1998;95(15):8585-9.

75. King GF. Venoms as a platform for human drugs: Translating toxins into therapeutics. Expert Opinion on Biological Therapy 2011;(11):1469-84.

76. Eiseman JL, Vonbredow J, Alvares AP. Effect of honeybee (apis-mellifera) venom on the course of adjuvant-induced arthritis and depression of drug-metabolism in the rat. Biochem Pharmacol 1982;31(6):1139-46.

77. Kwon YB, Lee HJ, Han HJ, Mar WC, Kang SK, Yoon OB, Beitz AJ, Lee JH. The water-soluble fraction of bee venom produces antinociceptive and anti-inflammatory effects on rheumatoid arthritis in rats. Life Sci 2002;71(2):191-204.

78. Schmidt JO. Biochemistry of insect venoms. Annu Rev Entomol 1982;27:339-68.

79. Castro HJ, Mendez-Inocencio JI, Omidvar B, Omidvar J, Santilli J, Nielsen HS, Pavot AP, Richert JR, Bellanti JA. A phase I study of the safety of honeybee venom extract as a possible treatment for patients with progressive forms of multiple sclerosis. Allergy and Asthma Proceedings 2005;26(6):470-6.

80. Wesselius T, Heersema DJ, Mostert JP, Heerings M, Admiraal-Behloul F, Talebian A, van Buchem MA, De Keyser J. A randomized crossover study of bee sting therapy for multiple sclerosis. Neurology 2005;65(11):1764-8.

81. Hamedani M, Vatanpour H, Saadat F, Khorramizaheh MR, Mirshafiey A. Bee venom, immunostimulant or immunosuppressor? insight into the effect on matrix metalloproteinases and interferons. Immunopharmacol Immunotoxicol 2005;27(4):671-81.

82. Martinez D, Morera V, Alvarez C, Tejuca M, Pazos F, Garcia Y, Raida M, Padron G, Lanio ME. Identity between cytolysins purified from two morphos of the caribbean sea anemone stichodactyla helianthus. Toxicon 2002;40(8):1219-21.

83. Middleton RE, Sanchez M, Linde AR, Bugianesi RM, Dai G, Felix JP, Koprak SL, Staruch MJ, Bruguera M, Cox R, et al. Substitution of a single residue in stichodactyla helianthus peptide, ShK-dap(22), reveals a novel pharmacological profile. Biochemistry (N Y) 2003;42(46):13698-13707.

84. Norton RS, Pennington MW, Wulff H. Potassium channel blockade by the sea anemone toxin ShK for the treatment of multiple sclerosis and other autoimmune diseases. Curr Med Chem 2004;11(23):3041-52.

85. Wulff H, Calabresi PA, Allie R, Yun S, Pennington M, Beeton C, Chandy KG. The voltage-gated Kv1.3 K+ channel in effector memory T cells as new target for MS. J Clin Invest 2003;112(2): 1703-13.

86. Mouhat S, Visan V, Ananthakrishnan S, Wulff H, Andreotti N, Grissmer S, Darbon H, De Waard M, Sabatier J. K+ channel types targeted by synthetic OSK1, a toxin from orthochirus scrobiculosus scorpion venom. Biochem J 2005;385:95-104.

87. Akassoglou K, Strickland S. Nervous system pathology: The fibrin perspective. Biol Chem 2002;383(1):37-45.

88. Inoue A, Koh CS, Shimada K, Yanagisawa N, Yoshimura K. Suppression of cell-transferred experimental autoimmune encephalomyelitis in defibrinated lewis rats. J Neuroimmunol 1996;71(1-2):131-37.

89. Iwai S, Okazaki M, Kiuchi Y, Oguchi K. Changes in mRNA levels of fibrinogen subunit polypeptides in rats defibrinogenated with batroxobin. Thromb Res 1999;96(6):421-26.

90. Reid PF. Alpha-cobratoxin as a possible therapy for multiple sclerosis: A review of the literature leading to its development for this application. Crit Rev Immunol 2007;27(4):292-301.

91. Gradl SN, Felix JP, Isacoff EY, Garcia ML, Trauner D. Protein surface recognition by rational design: Nanomolar ligands for potassium channels. J Am Chem Soc 2003;125(42):12668-69.

92. Martos V, Bell SC, Santos E, Isacoff EY, Trauner D, de Mendoza J. Calix[4]arene-based conical-shaped ligands for voltage-dependent potassium channels. Proc Natl Acad Sci U S A 2009;106(26):10482-6.

93. Ader C, Schneider R, Hornig S, Velisetty P, Wilson EM, Lange A, Giller K, Ohmert I, Martin-Eauclaire M, Trauner D, et al. A structural link between inactivation and block of a K+ channel. Nature Structural & Molecular Biology 2008;15(6):605-12.

94. Mathes C, Friis S, Finley M, Liu Y. QPatch: The missing link between HTS and ion channel drug discovery. Comb Chem High Throughput Screen 2009;12(1):78-95.

Chapter 2: The synthesis and biological evaluation of porphyrins against Kv1 channels

2.1 Introduction

Porphyrins

The porphyrin is derived from its basic skeleton known as a porphine. The molecular composition of porphine comprises of four pyrrole rings covalently linked in the α position by four methine bridges and consists of 26 pi electrons (figure 2.1). Kuster first proposed the structure in 1912 but porphyrins were not isolated or structurally characterised until 1928 by Fischer who originally discredited the work of Kuster stating that a ring structure of such size was intrinsically too unstable.[1] Ironically Fischer a critic of this work would later be renouned as the father of modern porphyrin chemistry.
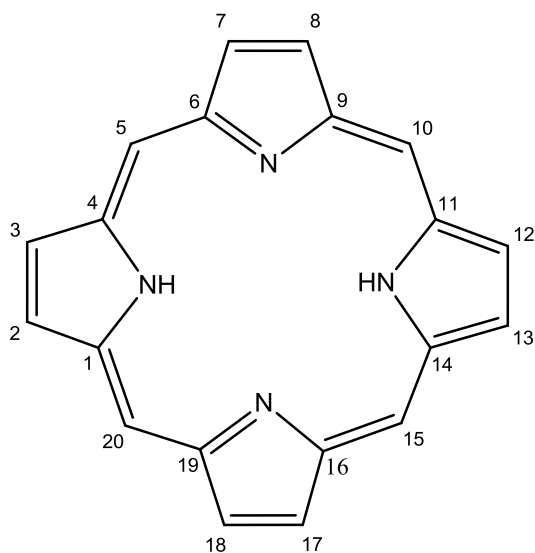

Figure 2.1 : General structure of porphine.

Porphyrins can be prepared by either an acid catalysed condensation between pyrrole and an aldehyde in refluxing propionic acid[2] or condensation of pyrrole and aldehyde via a Lewis acid e.g. $BF_3.OEt_2$ (scheme 2.1), forming porphyrinogen followed by oxidation to give the porphyrin macrocycle[3]. There are two types of substituted porphyrin: β substituted porphyrins, which have one or more substituents on the pyrrole rings. All naturally occurring porphyrins are of this type and heme belongs to this class also. The other type *meso* substituted porphyrins, which have substituents attached to the methine bridge (the *meso* position). The majority of synthetically produced porphyrins are the latter type and for the scope of the work presented here it is *meso* modifications that will be considered.
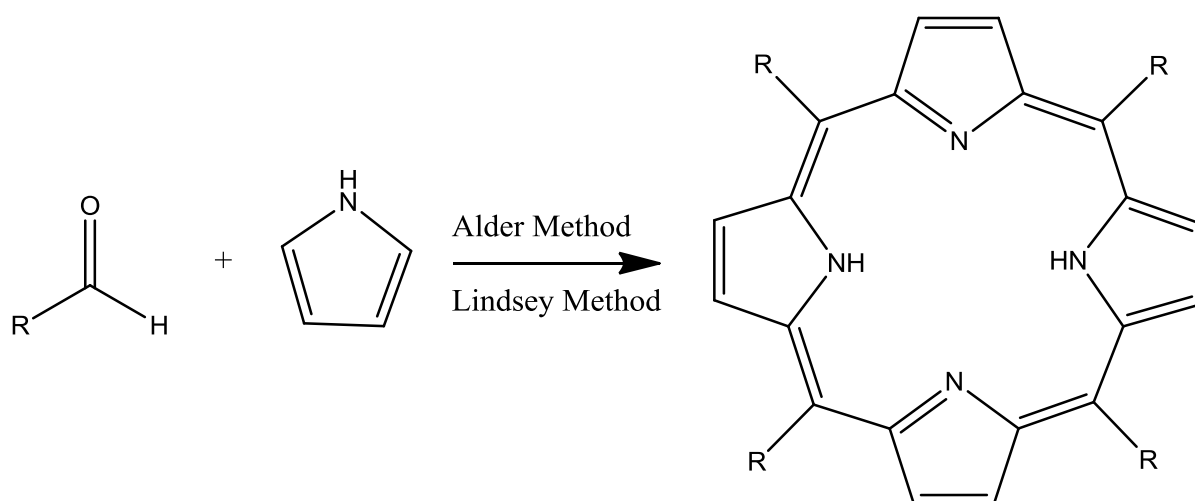
Scheme 2.1: Preparation of porphyrins, (where R= Ar). Alder Method, refluxing propionic acid, Lindsey method, $BF_3.OEt_2$, DDQ, CH_2Cl_2 at room temperature.

2.1.1 Symmetry and point group

Porphyrins are not ideal species for direct translation from research to our therapeutic application due to their photoactive properties. Their high conjugation is what makes them so appealing for singlet oxygen production and photodynamic therapy[4]. However it is the four fold symmetrical properties it possesses which makes the porphyrins attractive as a model compound to target the tetramer Kv channels.

Group theory can be used to characterise the various symmetry elements of a lead compound. Free base Porphyrins belong to the point group D_{2h}[5]. They have a C_2 principal axis of rotation, two C_2 axes in the plane of the molecule and a horizontal plane. Observing through a cartesian plane, the C2 axis in the z-plane cuts through the centre of the macrocycle, this is the principal axis. There is a C2 axis in the x-plane and a C2 axis in the y-plane. The centre of inversion is observed through the centre of the macrocycle and a series of symmetry planes defined in the yz-/ xz- and xy- planes. Rotational axes and the various planes of symmetry are shown in Figure 2.1(b).
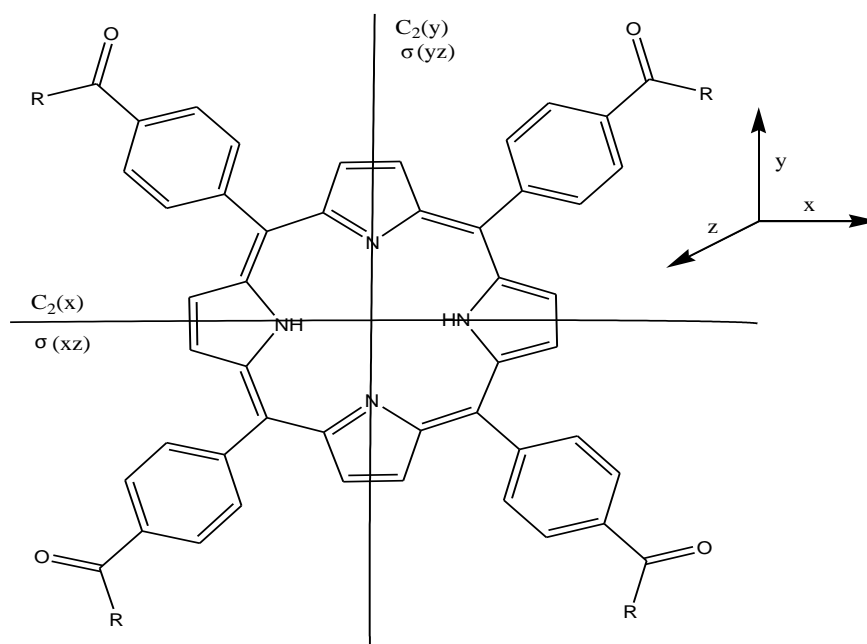
Figure 2.1(b): Symmetry elements of D_{2h} point group for TCPP **1**.

Macrocycles such as porphyrins have been investigated with the *Shaker* channel[6]. The K^+ channel, Kv1.3 was also studied in this line of research by Gradl.[6] This particular channel is highly associated with autoimmunity. Porphyrins are useful scaffolds to use for the probing of Kv channels because of their fourfold symmetries. The target channels are tetrameric proteins, thus symmetry and spacial orientation are key fundamental characteristics for this medicinal/biological investigation. Metal-free porphyrins (D_{2h}) fit this model. The application of porphyrins for this work is to determine their inhibition effectiveness and selectivity against the target neuronal channel Kv1.1. It is desirable, for an MS treatment, that the inhibitor *act selectively against the Kv1.1 channels*, leaving the remainder of the Kv1 family (eg. Kv1.2, Kv1.3, Kv1.4 and Kv1.6) unaffected. It should be noted that the existing marketed therapies do not show this selectivity, which results in severe side-effects.

As shown in figure 2.2(a) the porphyrins that were made consisted of a porphyrin scaffold, phenyl ring system, amide bond, alkyl chain and protonated amine. As mentioned the amino acid residues that are under investigation in the Kv1.1 channel consist of residues that have potential ionic, pi-pi and hydrogen bonding interactions. The selectivity filter of Kv1.1 consists of two glycine, a tyrosine and an aspartic acid residue. The inner turret region consists of a tyrosine residue unique to the channel[7]. The potential ionic interaction between the porphyrin and the channel residues can be investigated by replacing the protonated primary amine with a protonated tertiary methylated amine, steric hindrance and H-bonding at the binding site can also be investigated via this modification of the porphyrin. Glycine, present in the selectivity filter, is an interesting residue as this side group consists of only a hydrogen but the carbonyl moiety of the peptide chain has hydrogen bond donating potential. Thus the amide bond in the porphyrin can be modified to an ester eliminating the amide proton that could possibly contribute to hydrogen bonding to the glycine. We proposed to prepare a series of porphyrins that would allow for the development of a structure activity relationship (SAR); to determine the essential functional groups and their spacial arrangements for biological activity. Of particular interest, with respect to the prophyrin, are the following:

1. Fourfold symmetrical plane
2. π electron rich scaffold
3. Hydrogen bond donating and accepting sites
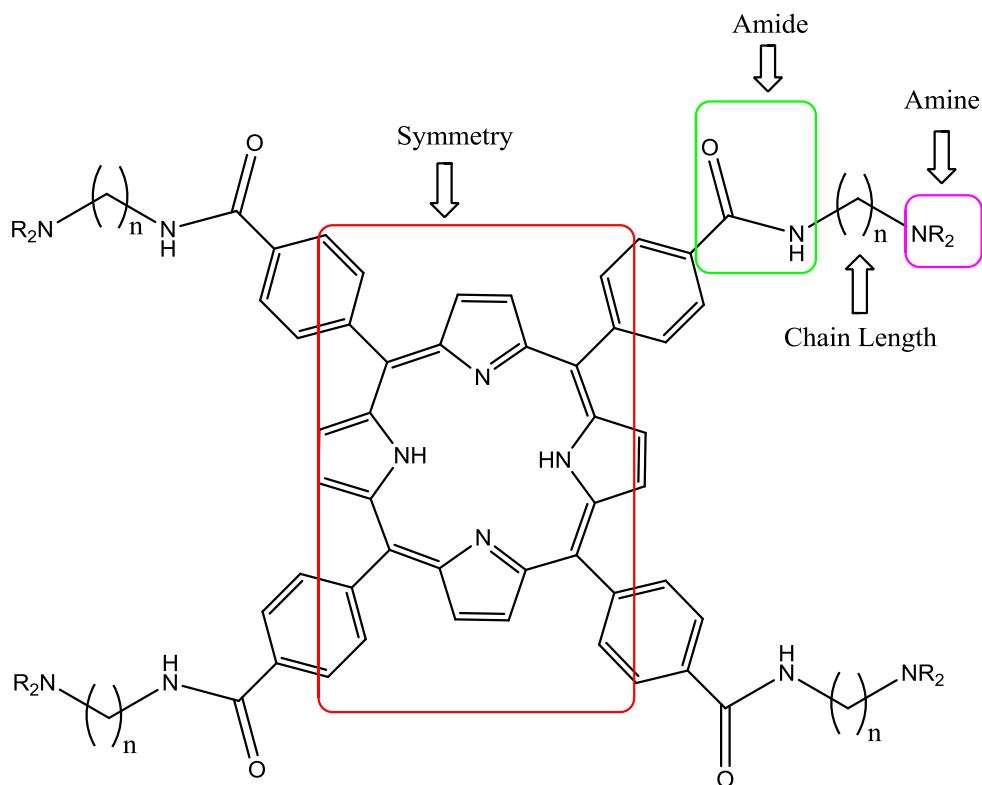4. Alkyl chain lenght
5. Ionic interactions

Figure 2.2(a): General structure of the target sites of the porphyrin to be manipulated in the SAR study.

The compounds that are shown in figure 2.2(b) allows for a full SAR study based upon the porphyrin scaffold. The hydrogen bonding donor/acceptor interaction has been planned to be investigated by substituting the secondary amide bond with an ester or tertiary amide, keeping the chain length and terminal amine constant. Chain length of the alkyl ammonium side groups will be examined by introducing a series of different spacers ranging from two to six carbons. The results of this study will reveal the effect of chain length on the inhibition of the Kv1 channels.. Lastly, in this SAR study the side groups will contain terminal amines that are methylated and the alkyl chain extended from two to three. By performing this last modification the effect of ionic interaction with the protonated primary amine can be probed with respect to steric constraints with the binding site.
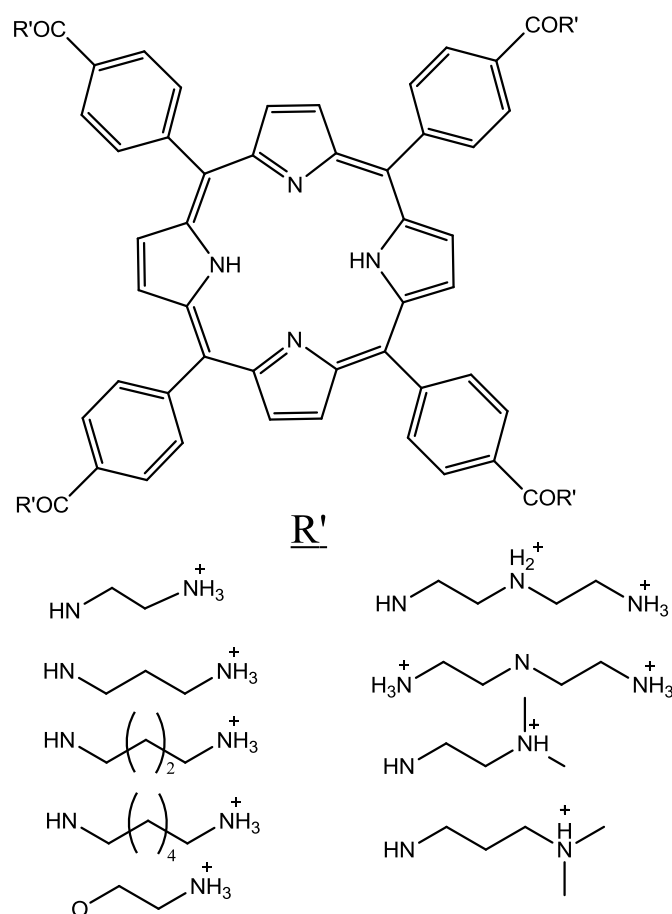
Figure 2.2(b): Proposed compounds to perform SAR study.

The region of interest within the complex assembly of the protein are the turret regions, pore helix and selectivity filter (S5-S6). This has widely been explored in the past by using large venom peptide toxins of the snake, scorpion and sea anemone. The amino acid residue of interest in the turret region is highlighted in figure 2.3(a). This sequence occurs in the Kv (348-386) region of the neuronal Kv 1.1 channel. The previous work detailed by Gradl *et al*[6] illustrated how their porphyrin derivatives with cationic alkyl ammonium bearing side arms can be used to inhibit potassium channels. The potassium channel that was the focus of their research was Kv1.3 which is related to the immune system. The amino acid residue they focused on as outlined in figure 2.3(b). It should be noted that both rat Kv1.1 and Kv1.3 channels are similar in residue sequence with only minor variations.

E A E E A E S H F S S I P D A F W W A V V S M T T V G Y G D M Y P V
T I G G K.

Figure 2.3(a) : Rat Kv1.1 amino acid sequence.

E A D D P S S G F N S I P D A F W W A V V T M T T V G Y G D M H P V
T I G G K.

Figure 2.3(b) : Rat Kv1.3 amino acid sequence.

## 2.2 The synthesis of amino functionalised porphyrins by acid chloride coupling

For the synthesis of these amino derivative porphyrins, the methodology of acid chloride chemistry was investigated first. The starting material 5,10,15,20- tetrakis (4-carboxyphenyl) porphyrin (TCPP) was synthesised via the Alder method[2]. Pyrrole and 4-formylbenzoic acid were condensed at reflux using propionic acid as both the solvent and acid catalyst. The porphyrin TCPP was then treated with oxalyl chloride in the presence of catalytic quantities of DMF in CH_2Cl_2 at room temperature to yield the acid chloride porphyrin as per the method used by Gradl *et al*[6] (scheme 2.2). Once formed, the acid chloride porphyrin was treated with the corresponding alkyl diamine in the presence of a number of organic bases such as pyridine, TEA and DIPEA. The material obtained from these reactions were tar-like and highly insoluble in any solvent making any characterisation difficult. The isolated material was suspected to be polymerised macrocycle as a result of the diamine substrate having the potential to react at both amine sites with the highly reactive acid chloride. To prevent polymerisation it was decided to selectively protect one of the amine groups of the alkyl diamine prior to coupling.
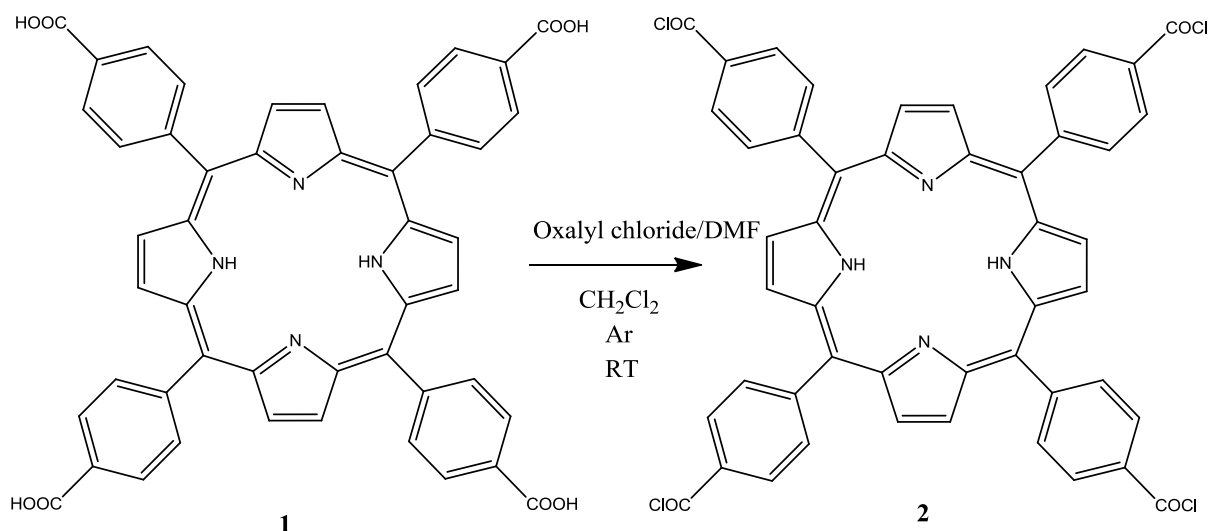
Scheme 2.2: The synthesis of the acid chloride porphyrin from TCPP.

2.2.1 Synthesis of mono N-Boc alkyldiamines.

The preparation of the N-Boc protected alkylene diamines were prepared as per the protocol Muller *et al*[8] (scheme 2.3). Di-tert-butyl bicarbonate (0.1 mol eq) was dissolved in $CHCl_3$ and added dropwise over a period of 3 hours to the alkyldiamine (1 mol eq) dissolved in $CHCl_3$ at $0\ ^{o}C$. The reaction was allowed stir for a further 16 hours at room temperature. The reaction was worked up and TLC analysis with ninhydrin stain showed one spot. This was observed with all N-Boc alkyldiamines except with N-Boc-1,6-diaminohexane. N-Boc diaminohexane required column chromatography for purification. The synthesis of these mono-protected amine derivatives are conducted under stoichiometric controlled conditions and the order of addition is essential to prevent double Boc addition.

x=1, 1,2 diaminoethane
x=2, 1,3 diaminopropane
x=3, 1,4 diaminobutane
x=4, 1,6 diaminohexane
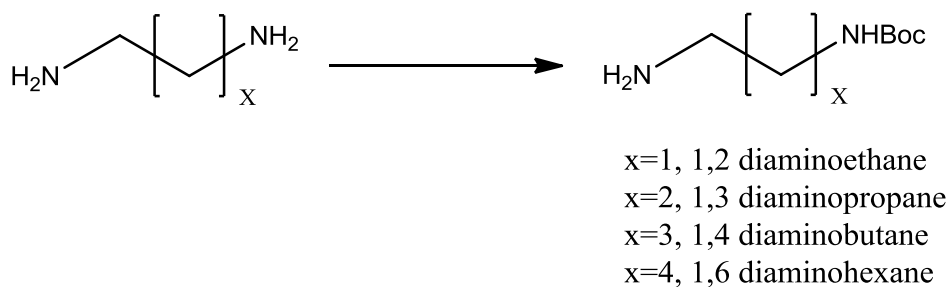
Scheme 2.3: Synthesis of monoprotected diamines.

## 2.2.2 Application of N-Boc alkyldiamines to the acid chloride system.

The porphyrin acid chloride was prepared via the method described in scheme 2.2 by Gradl *et al*. The formation of the acid chloride is observed by effervescence and the reaction colour changing to green. To ensure reaction completion occurred the mixture was stirred for 24 hours under an argon atmosphere. The crude acid chloride intermediate was concentrated under a stream of argon and then the excess oxalyl chloride removed via vacuum pump at room temperature. The acid chloride was redissolved in anhydrous CH_2Cl_2, treated with diisopropylethylamine and the mono-Boc protected diamine and allowed stir for a further 24 hours at room temperature. Evolution of a white gas was observed with the addition of the base. Analysis of the reaction was performed by TLC. Due to the nature of the intermediate molecule being an acid chloride, concentrated HCl formed in solution can potentially react with the acid liable Boc protecting group on each of the alkyldiamine moieties. TLC analysis showed multiple spots. Problems were encountered in the work up, extremely difficult emulsions formed and were challenging to separate into two phases.

The optimisation of the method was carried out to obtain the desired derivatives, this included changing the equivancies and organic bases. The objective was to obtain an analytical pure set of samples for bio-analysis however, reasonable yields were also desired. The side arm amine derivatives that this method was applied to was N-Boc ethylenediamine, N-Boc-1,3-diaminopropane, N-Boc-1,4-diaminobutane and N-Boc-1,6-diaminohexane. Using 4 eq of amine (1eq per COCl) a large amount of starting material (TCPP) remained when the work up was performed. This problem was eliminated by using a slight excess of N-Boc alkyldiamine. There was no difference in yield or conversion rates when 8 eq (2 per COCl), 12eq (3 per COCl) and 16 eq (4 per COCl) were used. For this reason 8eq-per reaction was sufficient. Negligible differences in conversions were observed when either DIPEA or TEA were used as catalysts. The yields dropped however as the alkyl chain length increased. Yields ranged between 3-35%. The N-Boc-1,6-diaminohexane derivative was obtained as low as 3%. Yields are shown in table 2.1.

Table 2.1: Yields of isolated porphyrins obtained by using acid chloride coupling methods.

Substrate	Ligand	% Yield
TCPP	N-Boc ethylenediamine	35%
TCPP	N-Boc 1,3 diaminopropane	28%
TCPP	N-Boc 1,4 diaminobutane	10-15%
TCPP	N-Boc 1,6 diaminohexane	3-6%

To prevent cleavage of the N-Boc groups, N-Boc ethylenediamine was treated with the acid chloride porphyrin in the presence of diisopropylethylamine (DIPEA) which is shown in scheme 2.4. DIPEA was used to help neutralise the acid formed during the reaction however the rate of cleavage seemed to exceed the rate of amide bond formation. Carpino *et al*[9] details the problems with acid chloride coupling with N-Boc protected species.
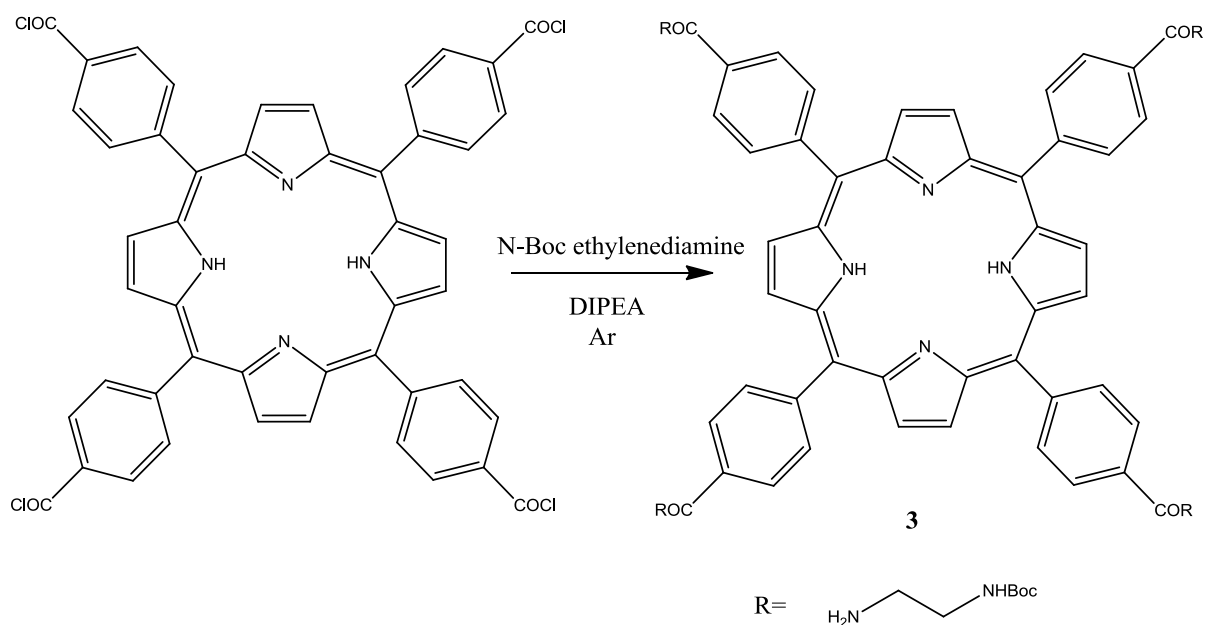

Scheme 2.4: The expected reaction between the porphyrin acid chloride and the N-Boc protected ethylene diamine.

The fractions that were cleaved in situ by HCl were observed by TLC and were combined together. Attempts to purify these mixtures failed since the free amines become charged (ionised) and become extremely difficult to move on silica gel.

2.2.3 Cleavage of N-Boc protected porphyrins via TFA acid

All isolated fractions containing mono to tetra Boc protected porphyrins were combined and treated with trifluoroacetic acid (TFA). The fractions were dissolved in anhydrous CH_2Cl_2 and the TFA added and stirred overnight under an argon atmosphere (scheme 2.5). The solvent and TFA were removed and the final product was triturated using diethyl ether. Regardless of how many triturations were performed a pure sample could not be obtained. A purple/green oil for each product was obtained. Ideally, these compounds should be crystalline.
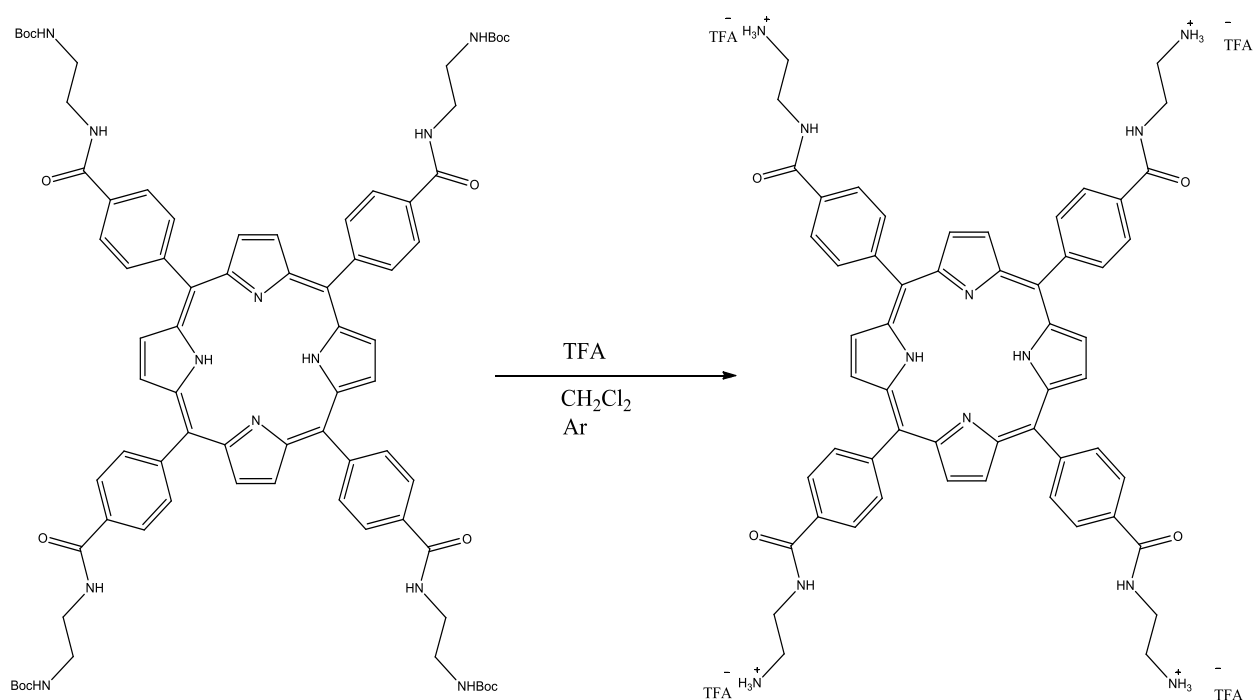
Scheme 2.5: TFA cleavage of N-Boc ethylenediamine porphyrin.

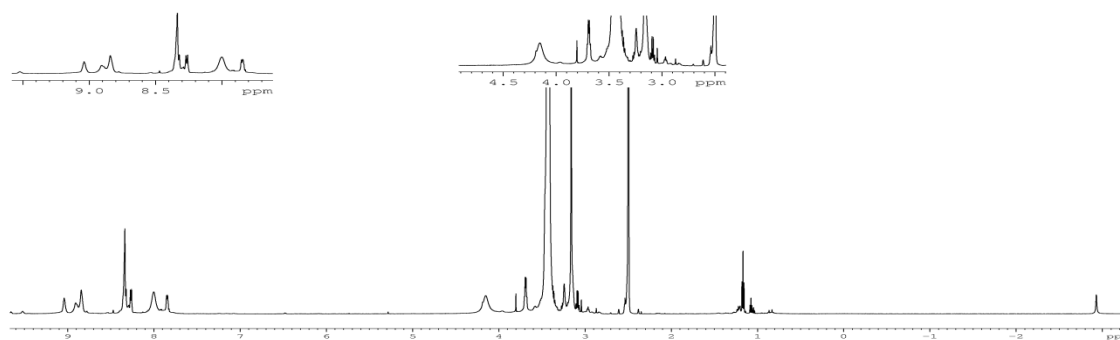The ^{1}H NMR that was obtained for the product is shown in Figure 2.4:

Figure 2.4: ^{1}H NMR of compound **13** obtained from TFA cleavage.

The ^{1}H NMR obtained for compound **13** contains extra peaks (excluding solvent) that are impurities. The aromatic region in particular shows the presence of unwanted impurities, even after the compound has been purified by column chromatography and a number of triturations performed. It would appear that a clean intermediate Boc protected porphyrin is essential to obtain a final cleaved product with acceptable purity. The preparation of these compounds under the described acid chloride conditions does not yield high purity products for bio-analysis. Thus, an alternative method using carbodiimide coupling was explored as an alternative.

2.3 The synthesis of amino functionalised porphyrins by carbodiimide coupling

It is apparent that the amines must be introduced under softer methods and not harsh acidic transformations. To isolate clean, pure Boc protected intermediates would be a more logical route to undergo and this method can be achieved by carbodiimide coupling.

Coupling reagents that are used for coupling carboxylic acids with amines are detailed extensively in the literature.[10, 11] For the synthesis of the target porphyrins N-Boc amino derivatives and two carbodiimide reagents were chosen. Initially the reaction with N-Boc ethylenediamine and TCPP was trialled with N,N'-dicyclohexylcarbodiimide (DCC) and N-hydroxysuccinimide (NHS) shown in (scheme 2.6), the conversion to the target product was excellent however there were problems removing large quantities of the by-product associated with the carbodiimide DCC. The by-product dicyclohexylurea (DCU), eluted strongly with the porphyrin product on silica gel columns. To overcome this purification
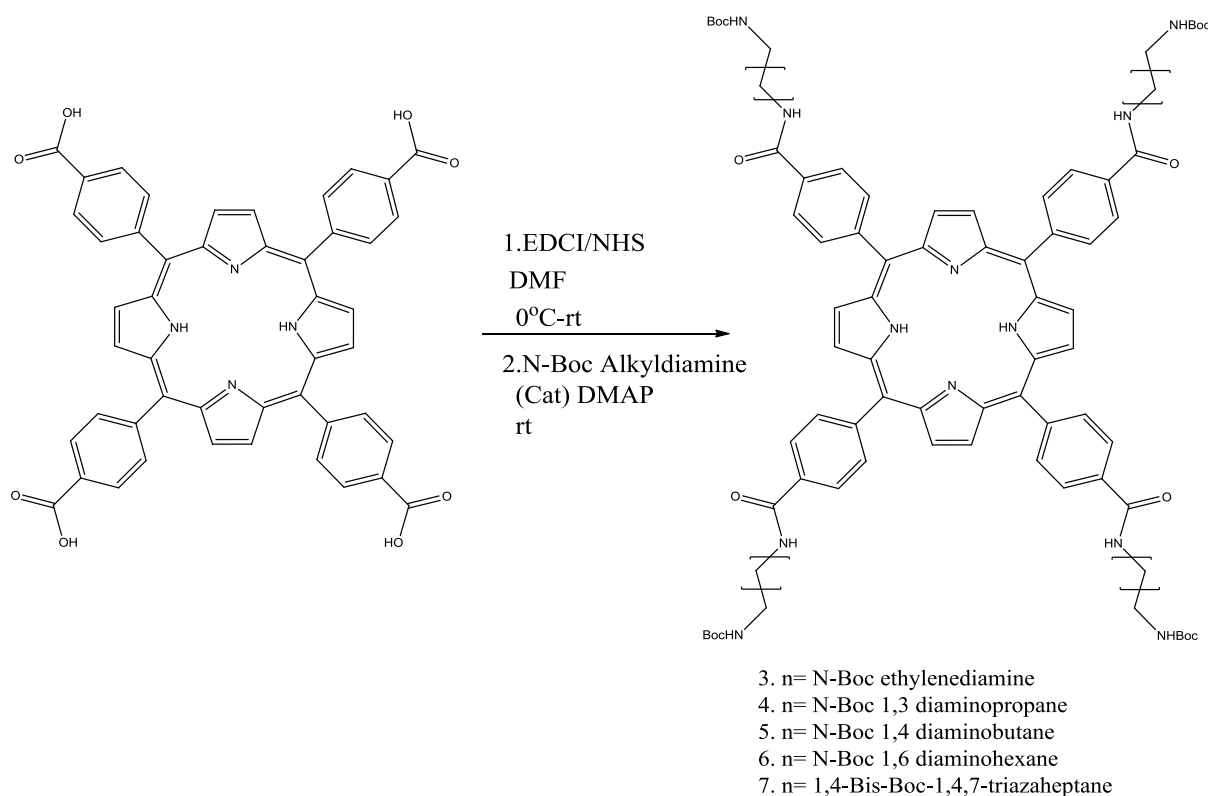
problem DCC was replaced with 1-ethyl-3-(3-dimethylaminopropyl)carbodiimide hydrochloride (EDCI). EDCI forms water soluble by-products that can be removed with greater ease.
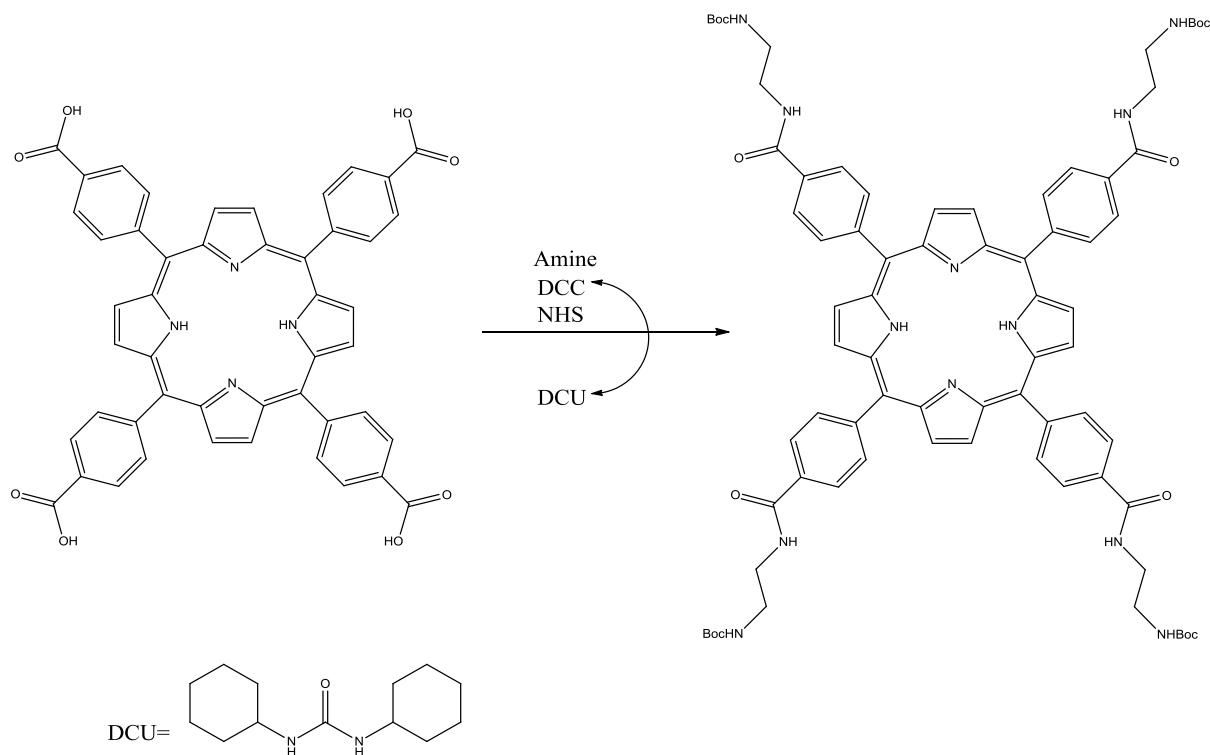
Scheme 2.6: DCC/NHS coupling of TCPP and N-Boc ethylenediamine to give compound **3**.

2.3.1 Application of EDCI

The carbodiimide EDCI has shown it can successfully couple TCPP with N-Boc alkyldiamines.[12] This procedure was used with slight modification from the literature and applied to synthesize the target N-Boc alkyldiamines from EDCI, NHS and DMAP as shown in scheme 2.7

1.EDCI/NHS
DMF
0°C-rt

2.N-Boc Alkyldiamine
(Cat) DMAP
rt

3. n= N-Boc ethylenediamine
4. n= N-Boc 1,3 diaminopropane
5. n= N-Boc 1,4 diaminobutane
6. n= N-Boc 1,6 diaminohexane
7. n= 1,4-Bis-Boc-1,4,7-triazaheptane

Scheme 2.7: Synthesis of the coupled amino porphyrin.

The initial step to the formation of the amide involved the addition of the carbodiimide to the porphyrin (TCPP) to form four O-acylisourea ester intermediates. This intermediate is extremely reactive and experiences intramolecular acyl transfer forming an N-acylurea by-product shown in scheme 2.8. The formation of this by-product is believed to contribute to the reduction in yields when using these coupling reagents. The fact that these porphyrin compounds are fourfold substituted increases the probability for the rate of formation of the by-product which can compete with the rate of formation of the product as amide bond formation can be sluggish. There are a number of co-additives that are used to suppress the intramolecular acyl transfer to the corresponding N-acylurea. The co-additive used throughtout this work was NHS. Others additives include HOBt, HOPip, HOPcp and HOPfp

but for the purpose of this work were not used. Addition of NHS interacts with the O-acylisourea ester, before high levels of the N-acylurea can be formed, and the resulting active ester is formed. The active ester reacts with the amine thus forming the amide bond.
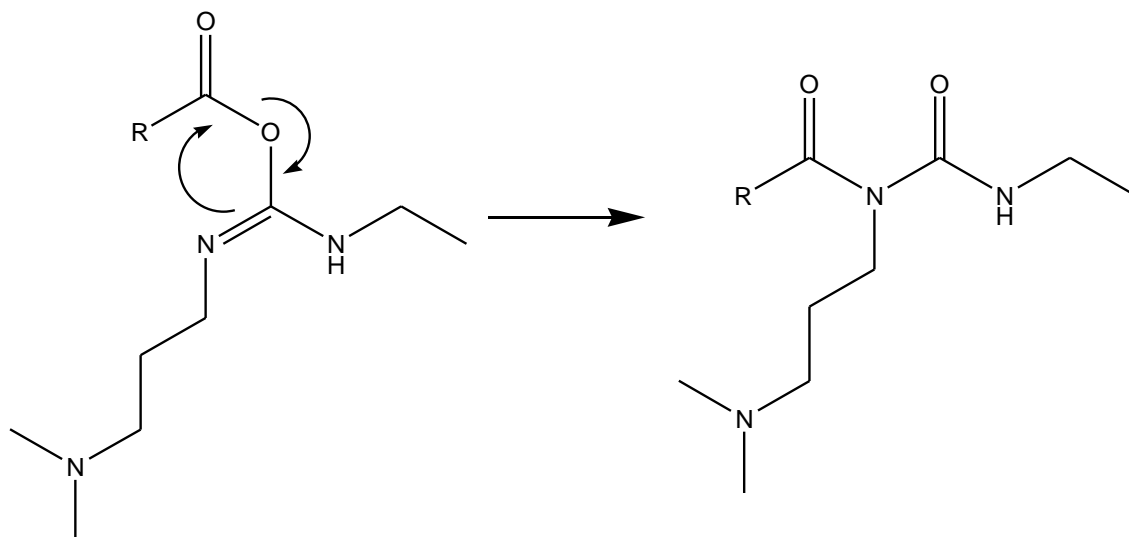
Scheme 2.8: Intramolecular acyl transfer of the O-acylisourea to the corresponding N-acylurea.

The synthesis of the N-Boc protected porphyrins using the N-Boc protected diamines in scheme 2.7 gave isolated yields ranging from 14-70%. The results are shown in table 2.2.

Table 2.2: Conversion of TCPP to corresponding porphyrin.

Substrate	Ligand	% Yield
TCPP	N-Boc ethylenediamine	70%
TCPP	N-Boc 1,3 diaminopropane	68%
TCPP	N-Boc 1,4 diaminobutane	65%
TCPP	N-Boc 1,6 diaminohexane	14%
TCPP	1,4-Bis-Boc 1,4,7-triazaheptane	35%

These compounds when isolated were not fully soluble in chlorinated solvents such as CH_2Cl_2 and $CHCl_3$. It was only with the addition of 5% MeOH or 5% EtOH to the chlorinated solvent that full solubility was achieved. In the case of the amine derivative N-Boc-1,6-diaminohexane, the isolated porphyrin was 100% soluble in chlorinated solvents, no alcohol was required to aid solubility. When the substrate N-Boc-1,6-diaminohexane was synthesized the yield for the final porphyrin dropped to 14%. A high number of impurities were shown by TLC in this reaction.

All compounds were purified using silica gel chromatography with CH_2Cl_2 and EtOH as the eluting mobile phase in the ratio (90:10) for the compounds **3**, **4** and **5**. Purification of the N-Boc-1,6-diaminohexane derivative was tedious, required a much less polar solvent system (20:1) CH_2Cl_2 and EtOH. There was an impurity that eluted with the target compound and the only way to separate it was using a slow flow rate to elute the compound pure from the silica column.

2.4 ^{1}H NMR Spectroscopic studies of N-Boc alkyl amino porphyrins

All the ^{1}H NMR experiments were performed in DMSO-d_6 as the amide alkyldiamine Boc protected porphyrins showed limited solubility in the other common deuterated solvents. For all the ^{1}H NMR experiments performed on compounds **3**, **4**, **5** and **6**, it was observed that the splitting patterns for all amides and CH_2 signals were broad, not sharp peaks. This was due to the broadening effect that is associated with adjacent amino functionalization. Apparent triplet, quartet and pentets are observed depending on the chemical environment.

2.4.1 ^{1}H NMR and ^{13}C spectroscopic study of 5,10,15,20 tetra[4-benzoamido(*tert*-butyl *N*-(2-amino-*n*-butyl)carbamate)] porphyrin.

The ^{1}H NMR spectrum of the porphyrin derivative **5** is shown in figure 2.5. The β-pyrrole protons and the amide adjacent to the phenyl ring appear as an overlapping multiplet at δ 8.9 ppm with an intergration of 12 (sum of the 8 protons from the β-pyrrole and 4 protons from the amide). The phenyl hydrogens at 8.3 ppm integrate as 16. The multiplicity these protons show are a broad overlap of a doublet of doublets as a result of para substitution on the phenyl ring. The Boc carbamate amide is seen as a triplet at δ 6.9 ppm and integrates as 4 protons. The methylene peaks from the alkyl chain adjacent to the amide bond (CH$_2$NHPh) is observed at δ 3.4 ppm as a broad quartet. The integration for these protons is 8. The

methylene peak that is adjacent to the carbamate (CH$_2$NHCO) is observed as a quartet at δ 3.0 ppm intergrating to 8. The methylene protons that are observed at δ 1.7 ppm and δ 1.6 ppm show as pentets, these protons correspond to the two inner methylene groups on the four carbon chain side arm. The Boc protons are observed at δ 1.4 as a singlet and intergrate as 36 protons. The internal protons on the nitrogen can be seen at δ -2.9 as a broad singlet with an intergration of 2.

The ^{13}C of the porphyrin is shown in figure 2.5b, the carbonyl carbons for both the amide and the carbamate were found at 166.1 ppm and 155.7 ppm. The β-pyrrole carbon is located at 143.8 ppm. It must be noted that the two quaternary carbons on the porphyrin ring do not show for any of the samples ran, even at 10000 scans. The two aryl C-H carbons are shown at 134.3 ppm and 125.9 ppm. The two associated aryl quaternary carbons are found at 134.1 ppm and 119.5 ppm. The quaternary Boc carbon is found at 77.4 ppm, the two aliphatic carbons that are adjacent to the amide and carbamate are located underneath the DMSO peak, DEPT-135 verified this. The terminal methyl groups on the Boc group is located at 28.6 ppm. Lastly, the remaining methylene carbons are found at 27.2 ppm and 26.7 ppm.
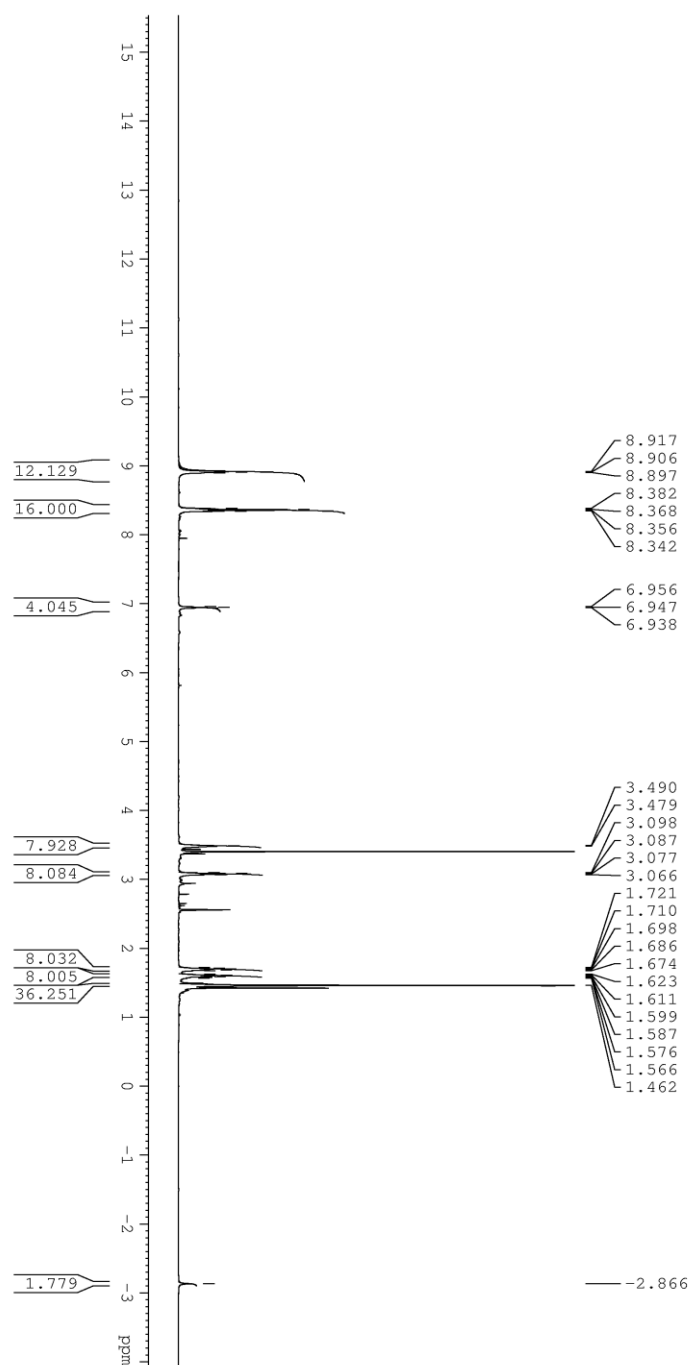
Figure 2.5a: ^{1}H NMR of 5,10,15,20 tetra[4-benzoamido(*tert*-butyl *N*-(2-amino-*n*-butyl)carbamate)] porphyrin **5**.
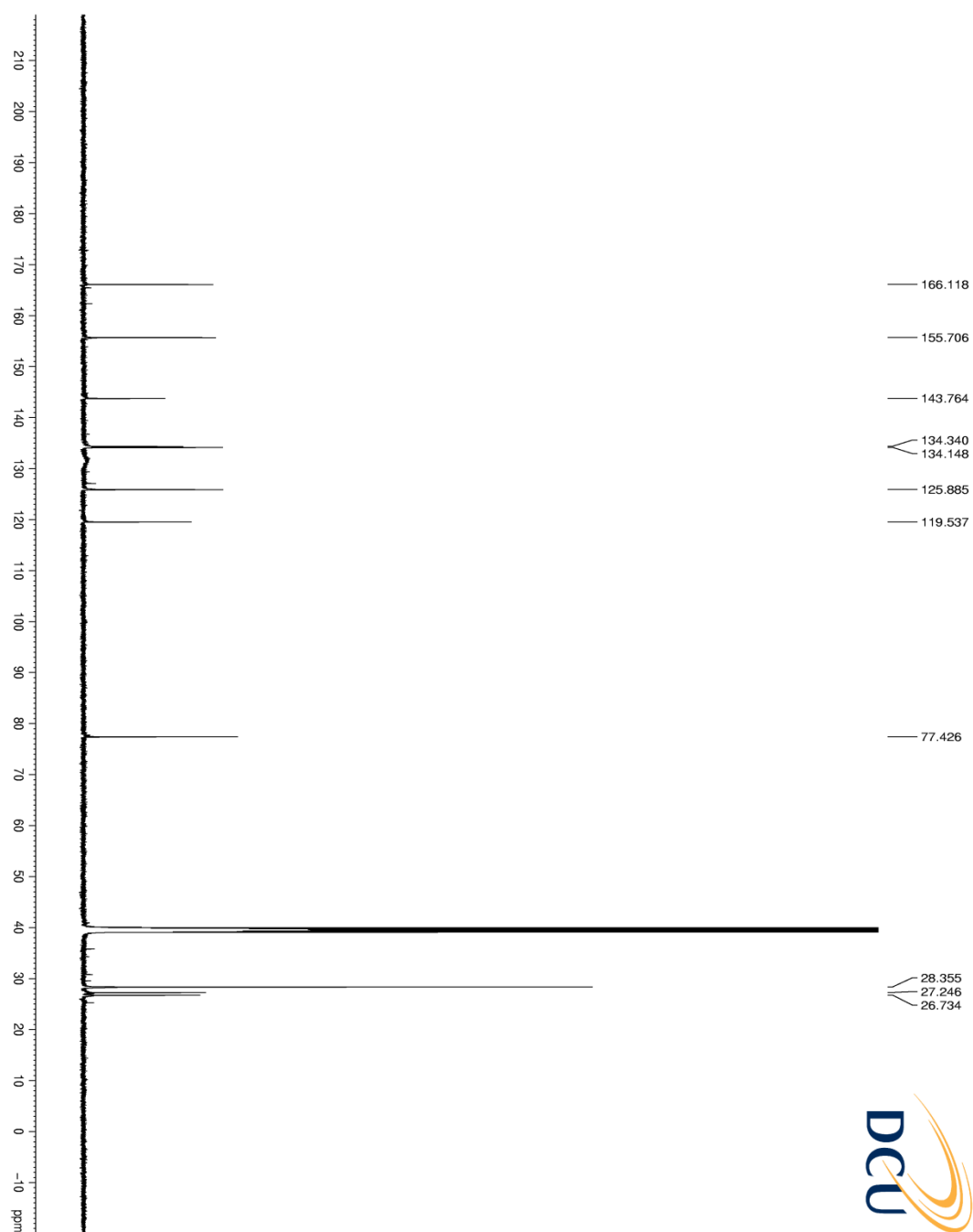
Figure 2.5b: ^{13}C NMR of 5,10,15,20 tetra[4-benzoamido(*tert*-butyl *N*-(2-amino-*n*-butyl)carbamate)] porphyrin **5**.

2.5 Synthesis of modified porphyrins for SAR investigation.

### 2.5.1 Synthesis of ester functionalised porphyrins

The N-Boc protected ester porphyrin **8** shown in scheme 2.9 was synthesised via a modified Steglich esterification method replacing DCC with EDCI. The porphyrin was prepared by reacting N-Boc aminoethanol with TCPP in the presence of the coupling reagent EDCI, DMAP as a catalyst and DMF as the reaction solvent. After 24h the material was isolated by pouring the reaction mixture onto water, the precipitate filtered to give a red/purple solid. This was purified by column chromography on silica, eluting with a mobile phase of CH_2Cl_2 and EtOH in the ratio (90:10) to give compound **8** in 80% yield.
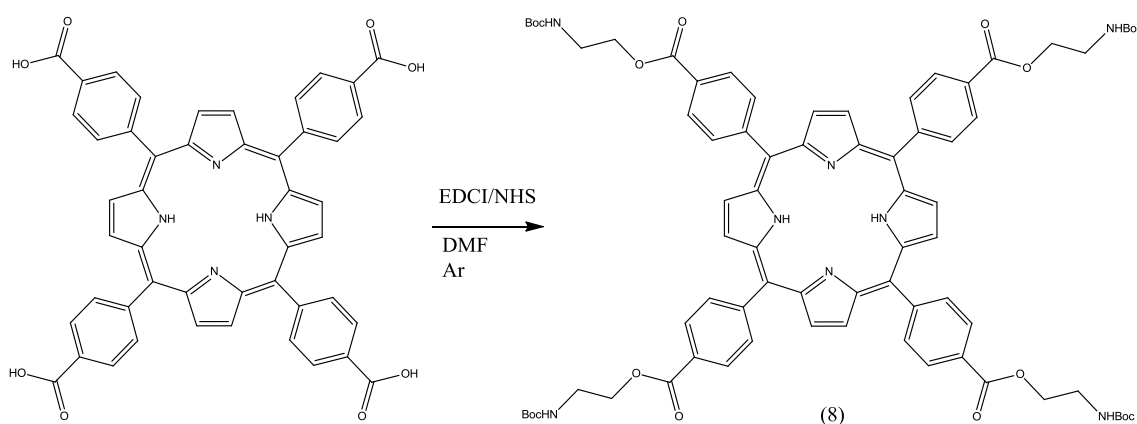
Scheme 2.9: Conversion of TCPP to the ester derivative aminoporphyrin **8**.

2.5.2 Synthesis of tertiary amide functionalised porphyrin as another lead to probe the hydrogen bonding effect.

Secondary amines are more reactive than primary amines due to the inductive effect and the lone pair of electrons are more reactive. This poses a problem with the protection of the starting material diethylenetriamine that is required to prepare porphyrin **19** (scheme 2.10). The primary amines required protection, leaving the secondary amine free to couple and form the corresponding tertiary amide bond. The problem arose that Boc anhydride is selective for secondary amine protection over primary amines and is not a viable method of protection.
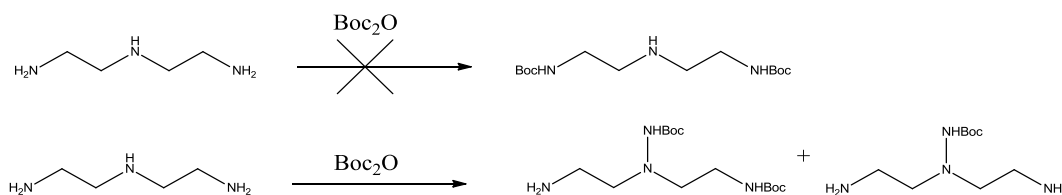

Scheme 2.10: Problems that arise when Boc_2O is used to try protect the primary amines.

48

However the use of an alternative protection group, phthalic anhydride which is selective for primary amines was attempted. Diethylenetriamine was selectively protected with phthalimide groups[13] (scheme 2.11).
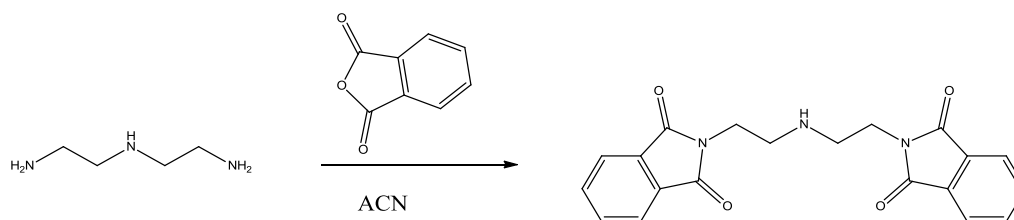
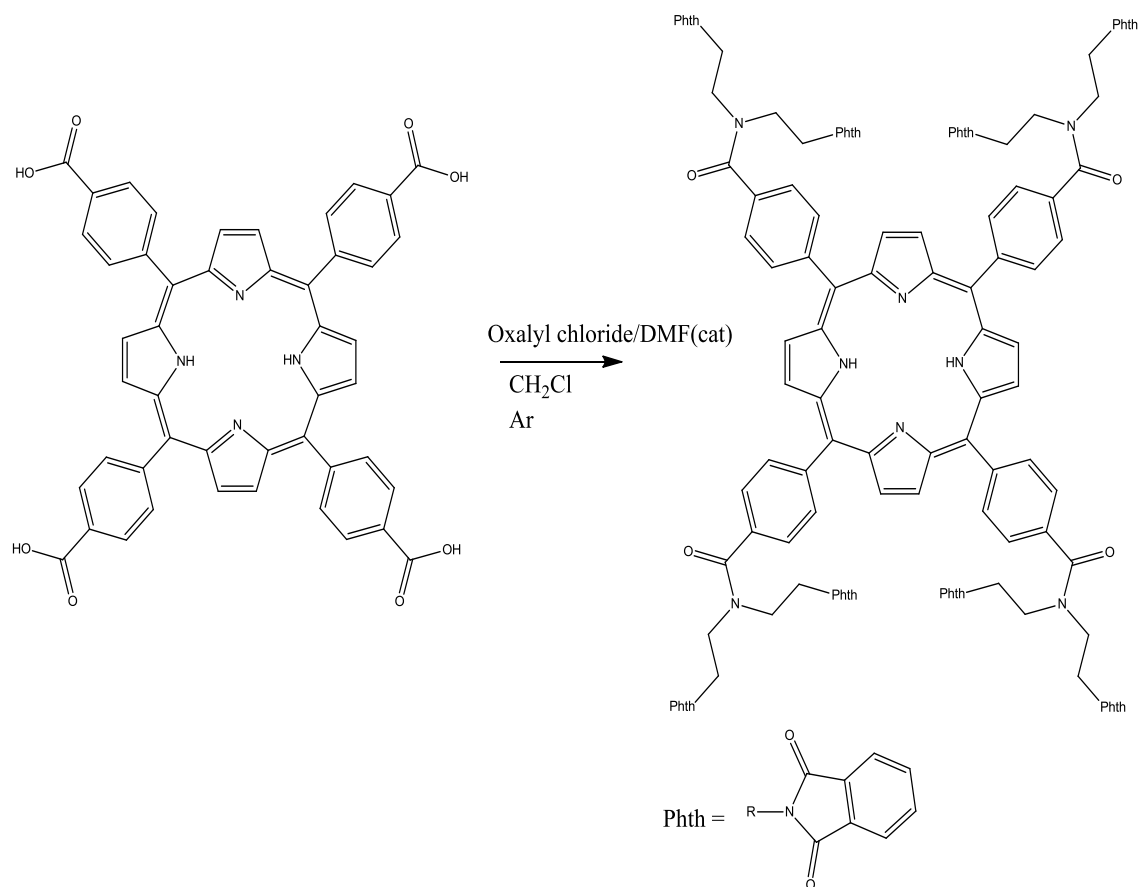Scheme 2.11: Primary amine selectively protected with phthalimide groups.

Two methods were then employed to prepare the porphyrins; coupling via carbodiimide and acid chloride coupling. Carbodiimide coupling was not successful using the phthalimide protected amine and TCPP, the ligand was highly insoluble in DMF (scheme 2.12).
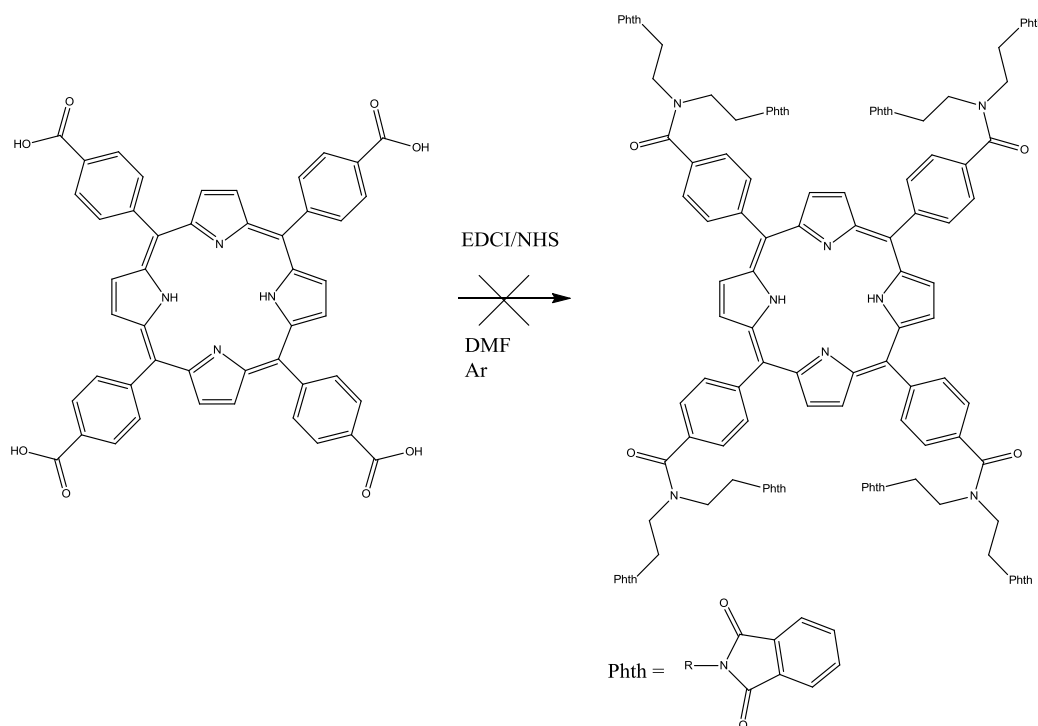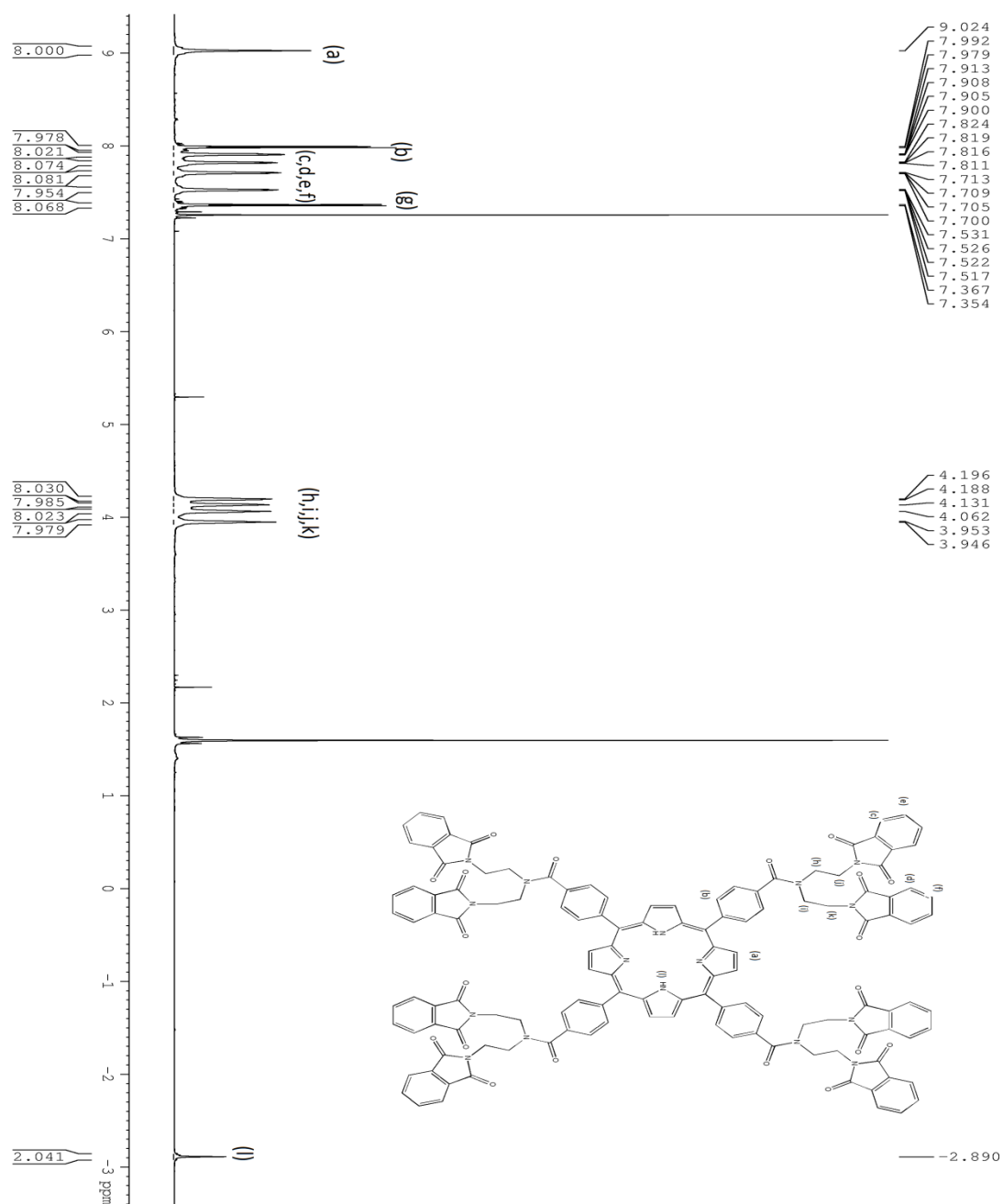

Scheme 2.12: Failed conversion of TCPP to phthalimide protected porphyrin **10**.

However, acid chloride activation of TCPP followed by amine coupling was successful for this specific compound. The conditions that were described in section 2.1 shown in scheme 2.13 were used with the phthalimide protected amine. Purification of the crude reaction mixture by column chromography on silica, eluting with a mobile phase of CH$_2$Cl$_2$ and

acetone in the gradient ratio (90:10)-(80-20) gave compound **10** in 53% yield. Figure 2.9 and 2.10 shows ^{1}H NMR and MALDI MS characterisation for **10**.

Oxalyl chloride/DMF(cat)

CH_2Cl

Ar

Phth =

Scheme 2.13: Conversion of TCPP to the phthalimide protected porphyrin **10**.

Figure 2.6: ^{1}H NMR of **10**.

The ^{1}H NMR spectrum shown in figure 2.6 represents compound **10**. Although this compound is symmetrical, however, on analysis of the side arm phthalimide protected diethylene triamine, the phthalimide protons and the alkyl protons are in different environments. On examining the phthalimide protons, if this compound was symmetrical

there would be only two peaks observed, however this isn't the case as four are observed for the phthalimide substituents. It is the same in the alkyl region, four peaks are observed where two would be expected. The reasoning for this could be due to the size of the molecule and the axis orientation of side arms due to rotation. An argument could be presented that there could be intra-molecular pi-pi stacking occurring with the phthalimides.
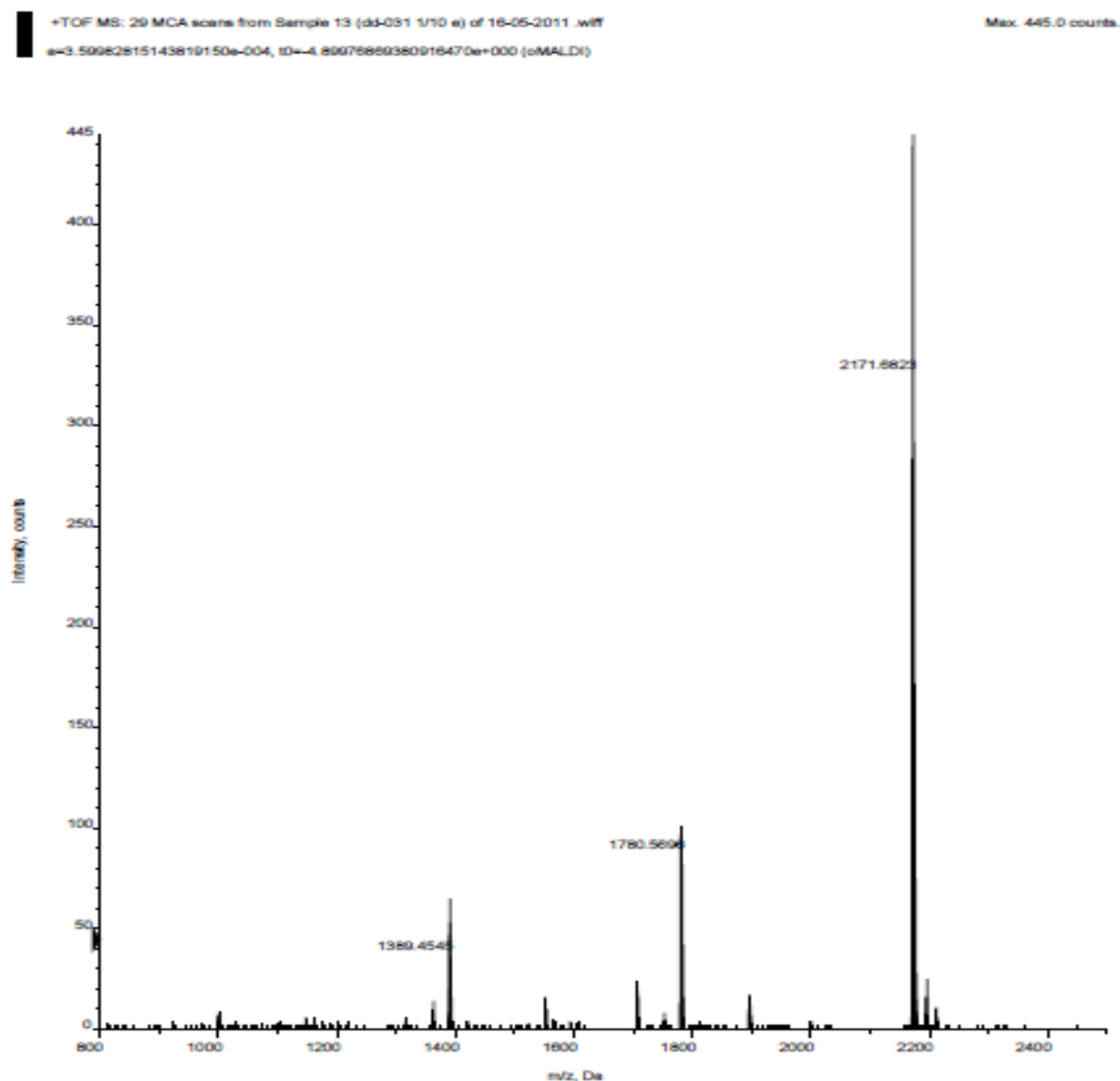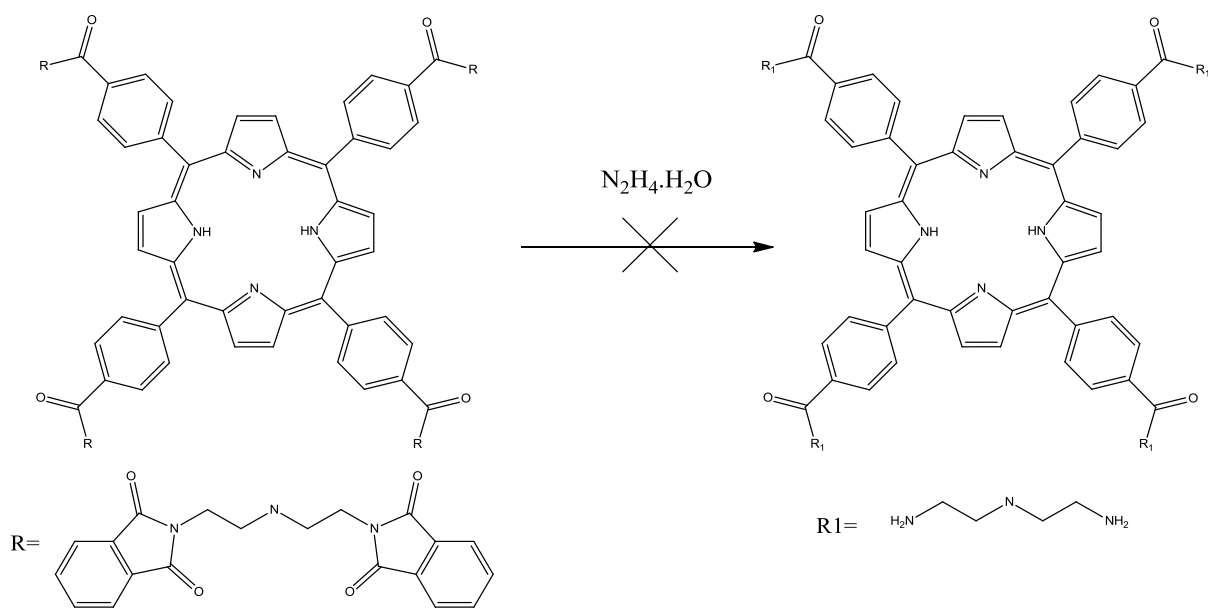

Figure 2.7: MALDI MS of the compound **10**.

The presence of **10** is confirmed by MALDI MS (figure 2.7) shows the M+1 peak of **10** at 2171.6823 m/z. The peak shown at 1780.5696 m/z corresponds to the fragmentation of three phthalimide groups and at 1389.4545 m/z with six groups fragmented.

Scheme 2.14: The failed attempt at hydrazine induced cleavage of the phthalimide protecting group.

Before synthesising **10** it was always suspected that there could be competitive cleavage with the hydrazine and the tertiary amide bonds that are bound to the phenyl rings of the porphyrin along with the phthalimide group. Experimentally this was shown as the cleaved product using this method was never obtained (scheme 2.14). ^{1}H NMR for this experiment showed the phthalimide groups never fully cleaved and also there was a number of impurities throughout the spectrum. MALDI MS confirmed the product was not present as the peak at 1131 m/z was not observed.

As an alternative to phthalimide protecting groups, an attempted synthesis of the diethylenetriamine amino porphyrin with trifluoroacetimide protecting groups was tried (scheme 2.15+2.16). The trifluoroacetimide protecting group method proved to be highly unstable to mild carbodiimide coupling conditions and all that was obtained was a purple material insoluble in all deuterated solvents, and suspected to be a polymeric mixture.
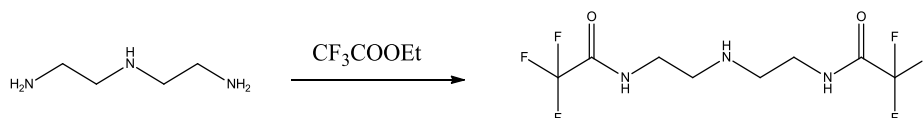

Scheme 2.15: Trifluoroacetimide protection of diethylenetriamine.
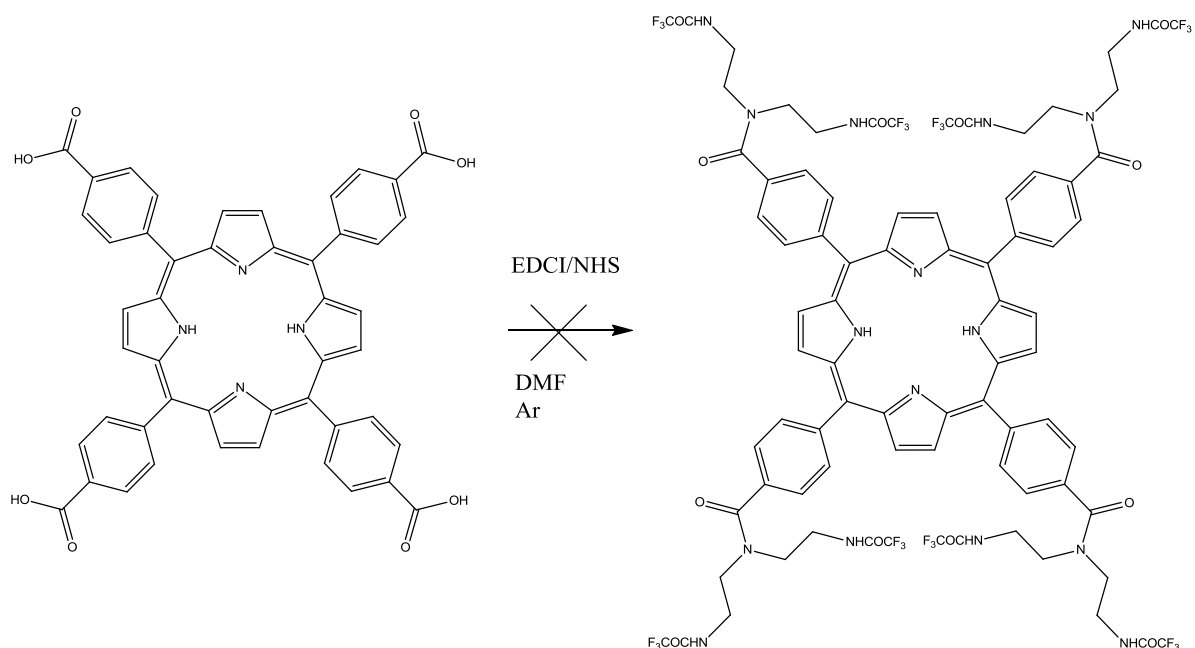
Scheme 2.16: Failed conversion of TCPP to trifluoroacetimide protected diethylenetriamine porphyrin.

An alternative protection strategy had to be found. Common methods such as Boc anhydride and Boc-OSu couldn't be employed however Boc-ON (2-(*tert*-butoxycarbonyloxyimino)-2-phenylacetonitrile) allows for the selective protection of primary over secondary amines to be obtained in excellent yield.[14] The difference between conventional Boc protection using Boc anhydride and Boc-ON is that Boc-ON provides a highly steric hindered addition that favours primary amines rather than secondary amine addition. Coupling the target protected amine shown in scheme 2.17 with TCPP via carbodiimide conditions gave the Bis-Boc diethylene porphyrin **9** which was purified via silica column chromatography, (95:5) CH$_2$Cl$_2$: EtOH with an isolated yield of 66% (scheme 2.18).
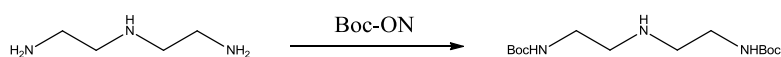
Scheme 2.17: Selective primary amine protection of diethylenetriamine.
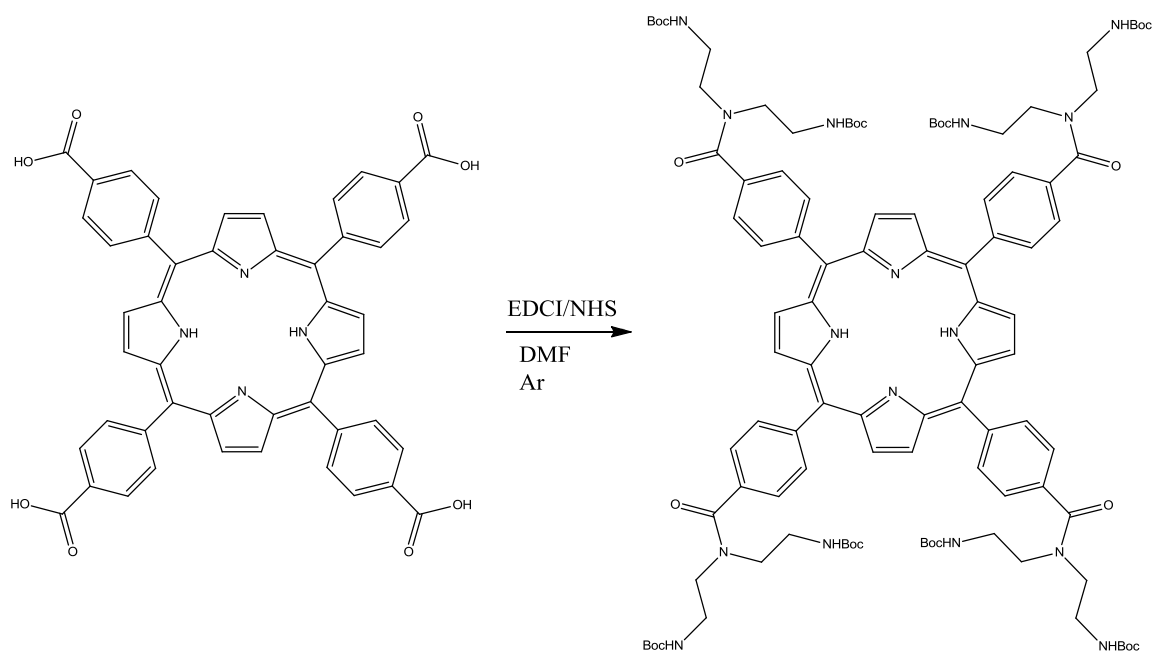
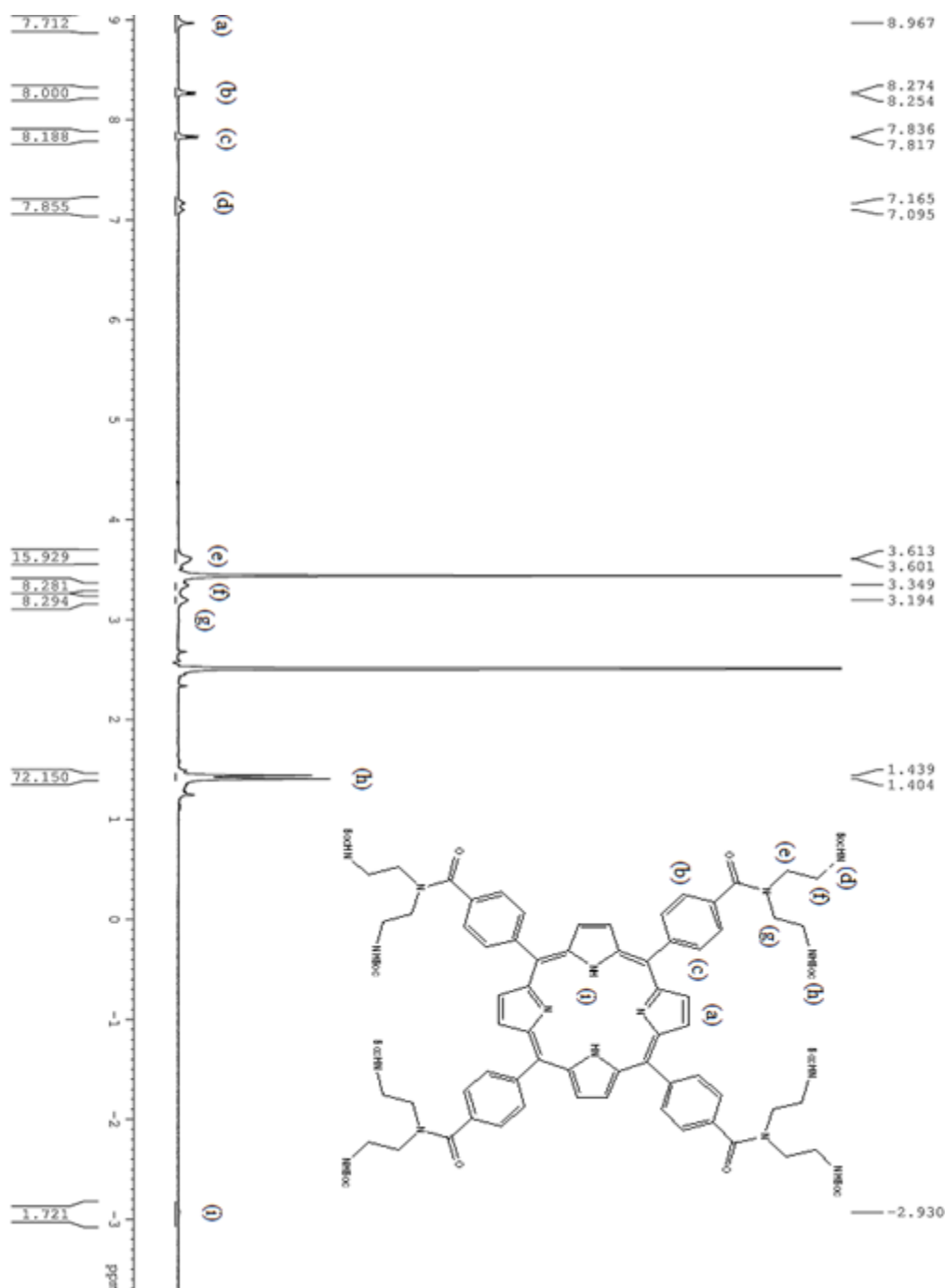Scheme 2.18: Synthesis of Boc protected diethylenetriamine porphyrin.

Figure 2.8: ^{1}H NMR of the Bis-Boc protected diethylenetriamine porphyrin **9**.

Similar to compound **10**, there is evidence that **9** is not symmetrical by ^{1}H NMR (figure 2.8). The amide bond associated with the carbamate Boc group shows two close overlapping triplets. The alkyl region shows three peaks; one that intergrates to sixteen and the other two methylene peaks intergrating to eight protons each. The Boc groups should intergrate to seventy-two with a singlet mutiplicity, however a doublet is observed indicating the Boc groups are in different environments. As mentioned with compound **10** there was a proposed

theory that the observed lower symmetry for **10** could occur as a result of intramolecular pi-pi stacking, however with the removal of the aromatic phthalimide groups, as is the case with **19**, this phenomena is still observed. This conformational phenomena will be discussed in more detail later.

2.5.3 Synthesis of tertiary amine porphyrins

As opposed to the literature method of synthesising porphyrins with ammonium side chains via acid chloride chemistry[15], the more milder carbodiimide approach was used shown in scheme 2.19. Both porphyrins **11** and **12** were synthesised from TCPP and their corresponding amine side arms, N,N-ethylenediamine and N,N-dimethyl-1,3-diaminopropane. The coupling conditions that were used were the same as previously described EDCI/NHS methodology, purified by column chromatography 5:5:1. CH_3Cl: EtOH: NH_3OH. The respective yields were 62% **11** and 59% **12**.
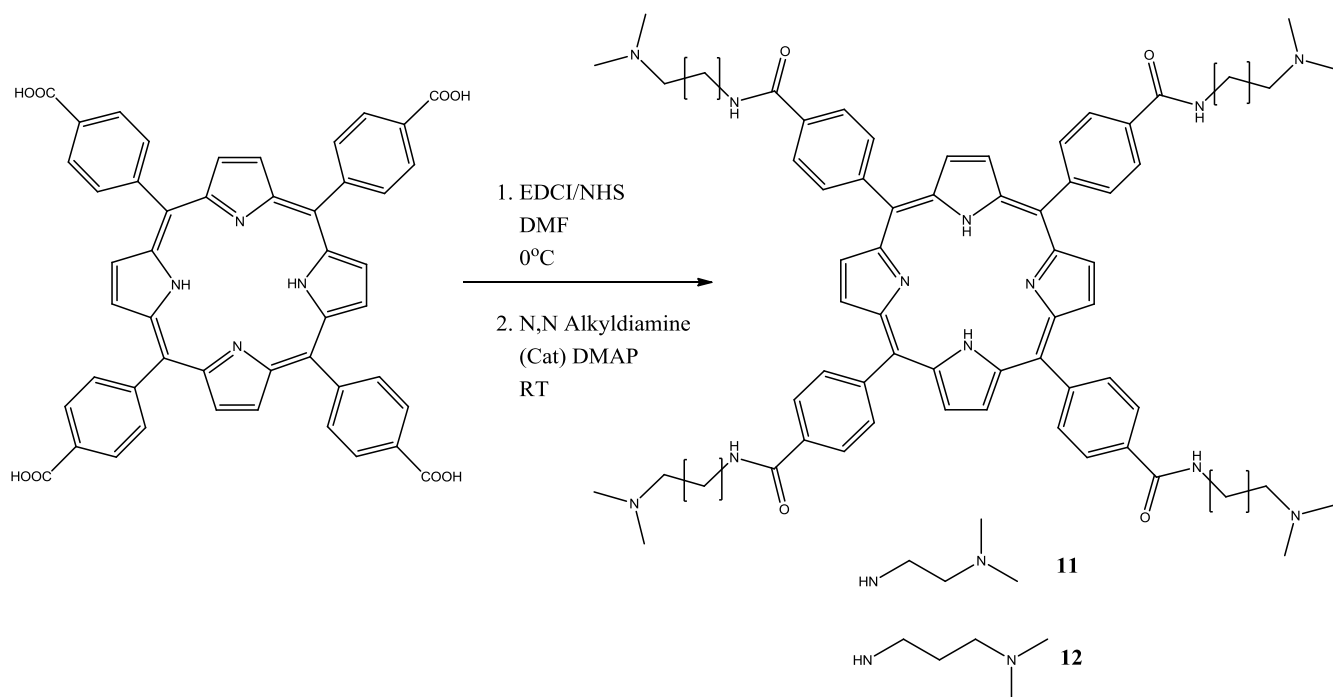
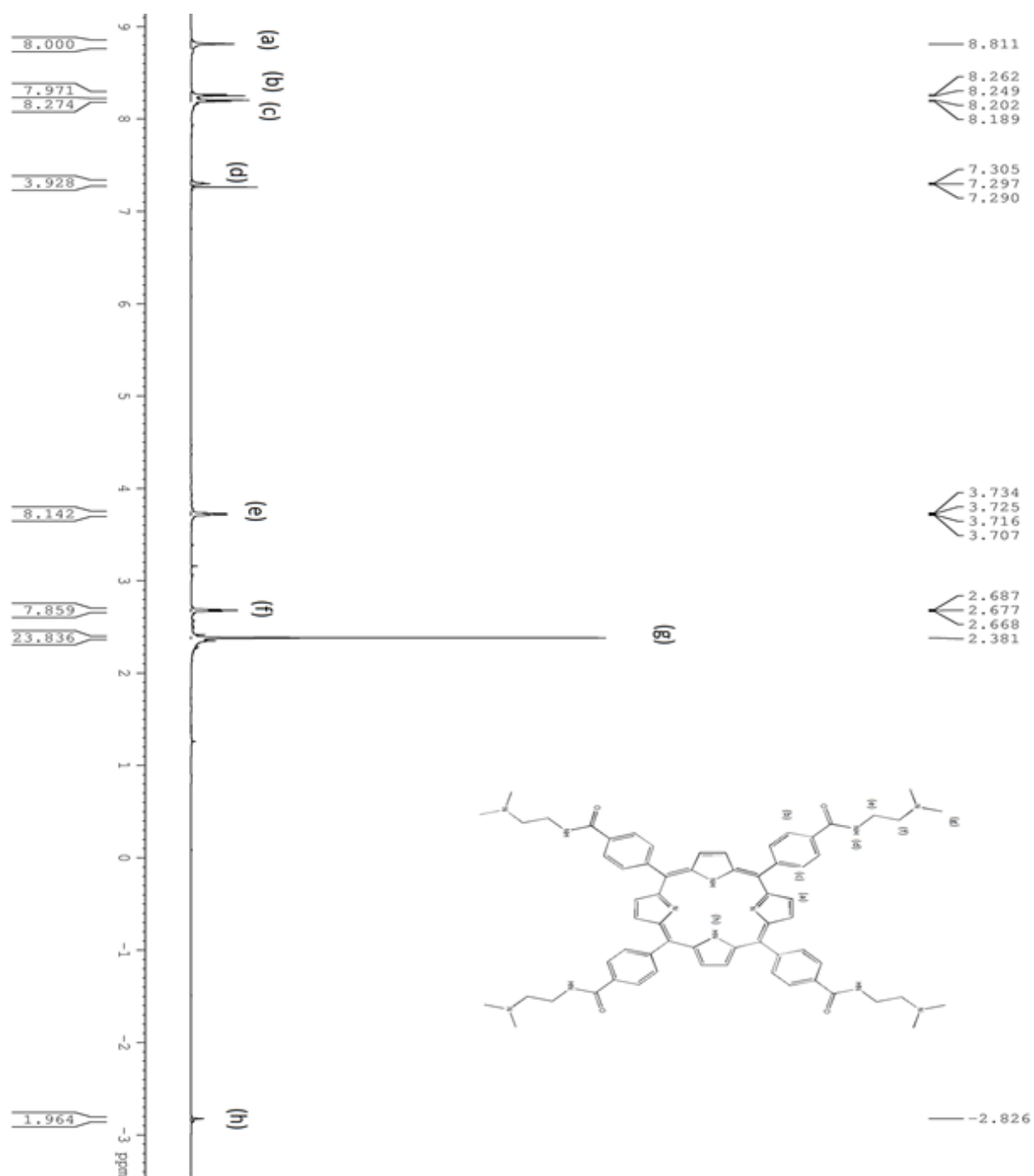Scheme 2.19: Synthesis of tertiary amine porphyrins **11** and **12**.

Figure 2.9: ^{1}H NMR of compound **11**.

2.6 Cleavage of the N-Boc aminoporphyrins

As discussed previously in section 2.2.2, the TFA cleavage gave impure ^{1}H NMR spectra and the solubility of these TFA salts in water was not 100%, and a slight precipitate observed. The alternative to TFA was to use 4M HCl in dioxane solution. All of the Boc protected porphyrins were suspended/dissolved in CH_2Cl_2 and a 20 fold molar excess of the 4M HCl in dioxane was added dropwise at 0 ^{o}C under an argon atmosphere. After addition, the solution was allowed stir at room temperature for 24 hr. The reaction work-up involved pouring the reaction solution into diethyl ether, the precipitate formed was collected by filtration through a glass frit and washed with diethyl ether, CH_2Cl_2 and allowed dry under vacuum overnight at room temperature. This gave pure porphyrin derivatives as HCl salts in quantitative yields.

2.6.1 ^{1}H NMR studies of cleaved amino porphyrins
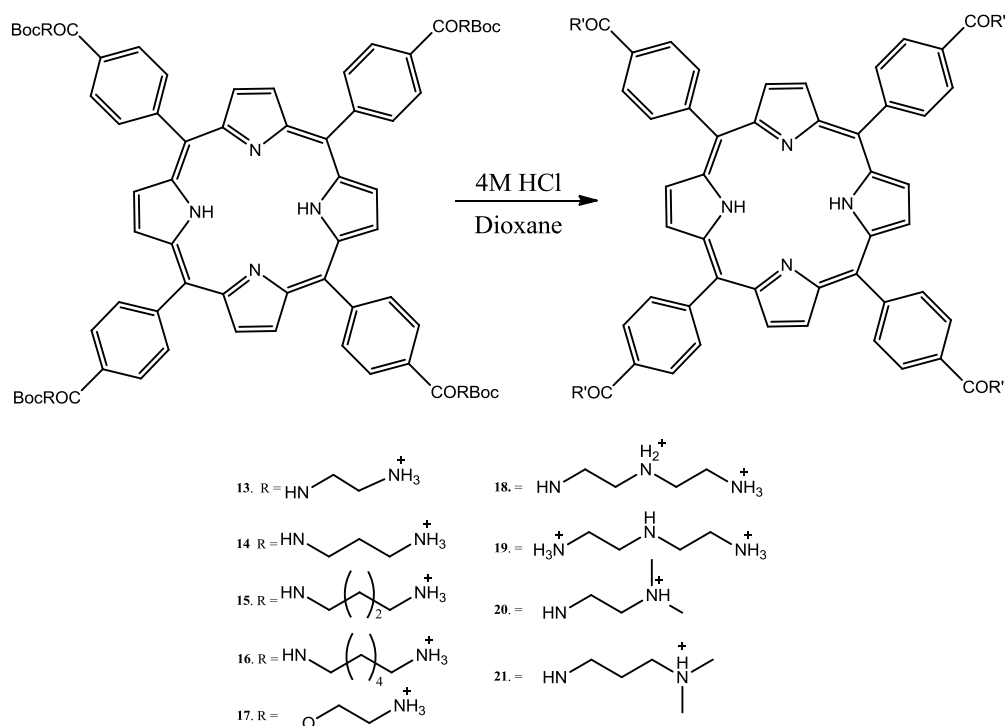
Scheme 2.20: Cleavage of the Boc protecting groups, and preparation of tertiary amine salts.

2.6.2 ^{1}H NMR spectroscopic study of 5,10,15,20 tetra[4-benzoamido(*N*-(2-amino-*n*-butyl hydrochloride] porphyrin.

The ^{1}H NMR spectrum of the porphyrin derivative **15** is shown in figure 2.10. The peak at 8.99 ppm is observed as a apparent triplet, this peak is the amide bond that is bound to the phenyl ring and intergrates as 4 hydrogens. The β-pyrrole protons at 8.85 ppm are observed

as a singlet, and integrates at 8H. The phenyl hydrogen's show as a singlet (as described in section 2.6.1). The protonated amine hydrogen's, as a result of the acid cleavage of the Boc protection groups, are observed as a broad singlet at 7.97 ppm that integrates as 12 hydrogens. The alkyl region shows a peak at 2.89ppm with an integration of 8 and can be assigned to the carbon adjacent to the $NH3^+$ Cl^-, a second peak at 1.72 with an intergration of 16 can be assigned to the remaining methylene protons in the alkyl chain. As observed in the spectrum in figure 2.9, there are only 24 methylene hydrogens however there are four methylene carbon protons (8 protons) missing. These are under the water peak which cannot be avoided with working with the hydroscopic solvent DMSO-d$_6$. COSY NMR was used to confirm that the 'missing' methylene peaks are indeed under the water peak. An alternative method to prove this point was a temperature NMR study on the porphyrin. At 70-80 ^{o}C the alkyl peaks shift from under the water peak and are observed at 3.51 ppm. The final protons are the highly shielded internal hydrogen protons of the porphyrin at -2.9 ppm as a broad singlet.
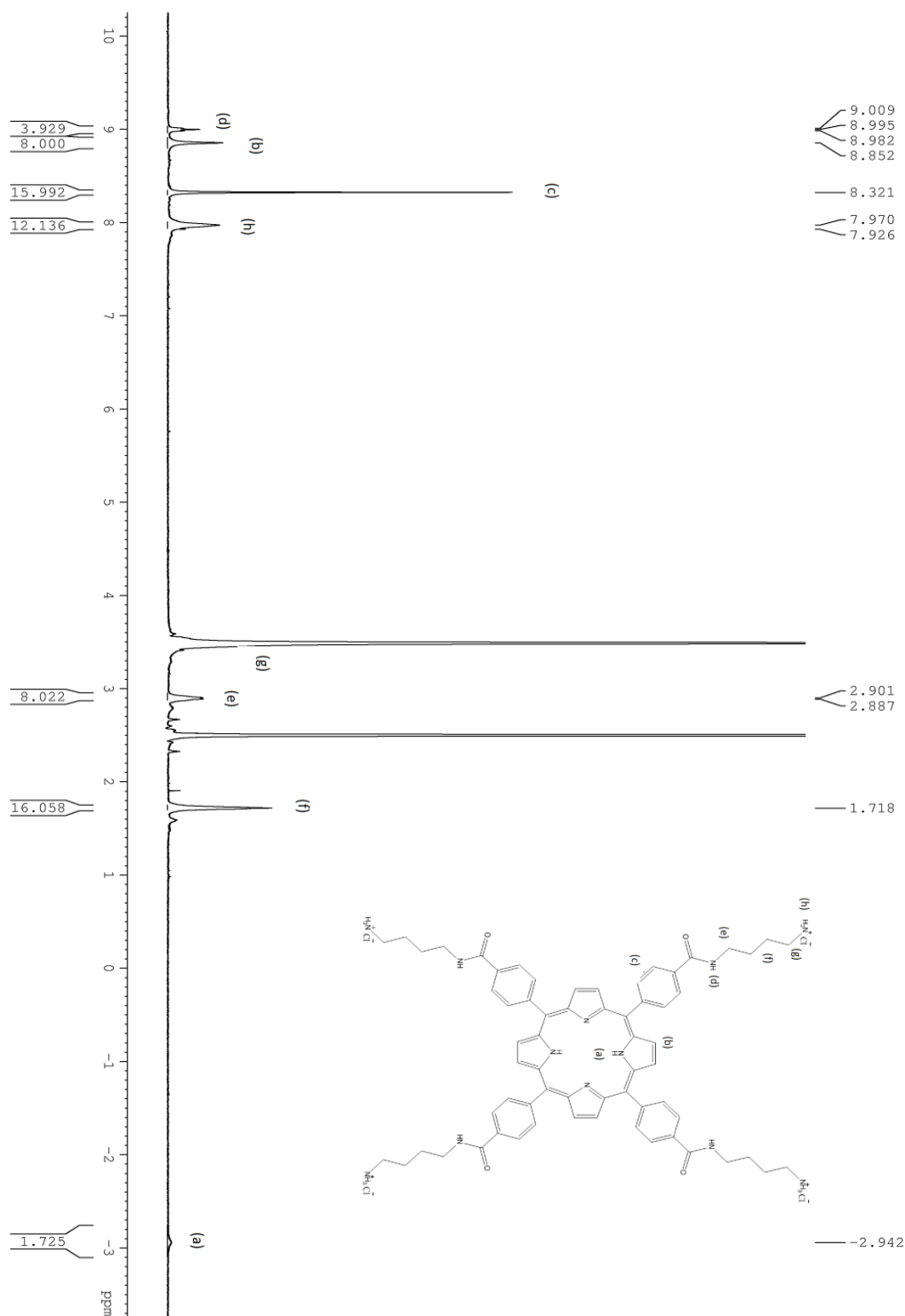
Figure 2.10: ^{1}H NMR of 5,10,15,20 tetra[4-benzoamido(*N*-(2-amino-*n*-butyl hydrochloride] porphyrin **15.**

Mentioned previously, when we synthesised compounds **9** and **10** it was observed that both contained spectral features that were irregular (figure 2.6 and figure 2.8). When analysed by ^{1}H NMR, peaks that should be symmetrical appeared as unsymmetrical. Using the acid

methods detailed in section 2.6.1 for the cleavage of the Boc groups, compound **9** was converted to **19** and analysed by ^{1}H NMR (figure 2.11). Upon cleavage the spectrum of **19** simplifies in the alkyl region to two broad singlets that intergrate as 16 each. The protonated NH$_3^{+}$ species does not simplify into a singlet, instead two broad singlets are observed at 8.4 ppm and 8.3 ppm. It would appear that the terminal amines of **19** are inequivalent as was also observed with both the phthalimide and Boc protected porphyrins **9** and **10**.
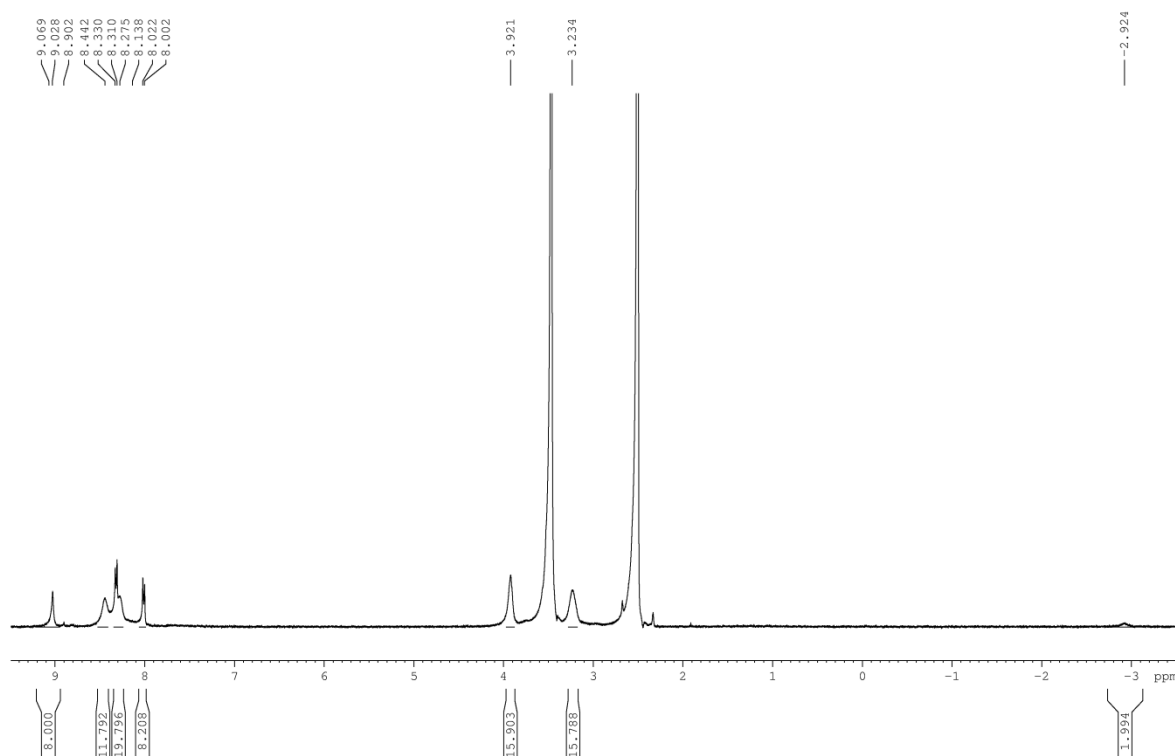

Figure 2.11: 1H NMR of compound **19**.

2.7 SAR study evaluation of porphyrin moieties with biological screen against Kv1 channels.

As stated previously the purpose of the SAR study was to evaluate previous work reported on the interaction of macrocycle moieties against potassium channels. The work reported in the literature is based upon the massive multi-million investment research project undertook by Merck. Their work was highly focused on the autoimmunity potassium channel Kv1.3. Our work is focused upon the neurological Kv1.1 channel. Table 2.4 lists the porphyrin derivatives tested against not only Kv1.1 but Kv1.1-Kv1.6.

Table 2.4: Associated bioactivity with the porphyrin derivatives and Kv1 channels (10μM).

Compound number	% Block Kv1.1	% Block Kv1.2	% Block Kv1.4	% Block Kv1.6
13	45	22	Insensitive	42
14	22	34	32	15
15	62	Insensitive	44	57
16	Insensitive	Insensitive	Insensitive	Insensitive
17	Insensitive	Insensitive	Insensitive	Insensitive
18	Insensitive	50	Insensitive	Insensitive
19	Insensitive	Insensitive	Insensitive	Insensitive
20	Insensitive	Insensitive	Insensitive	Insensitive
21	Insensitive	Insensitive	Insensitive	Insensitive
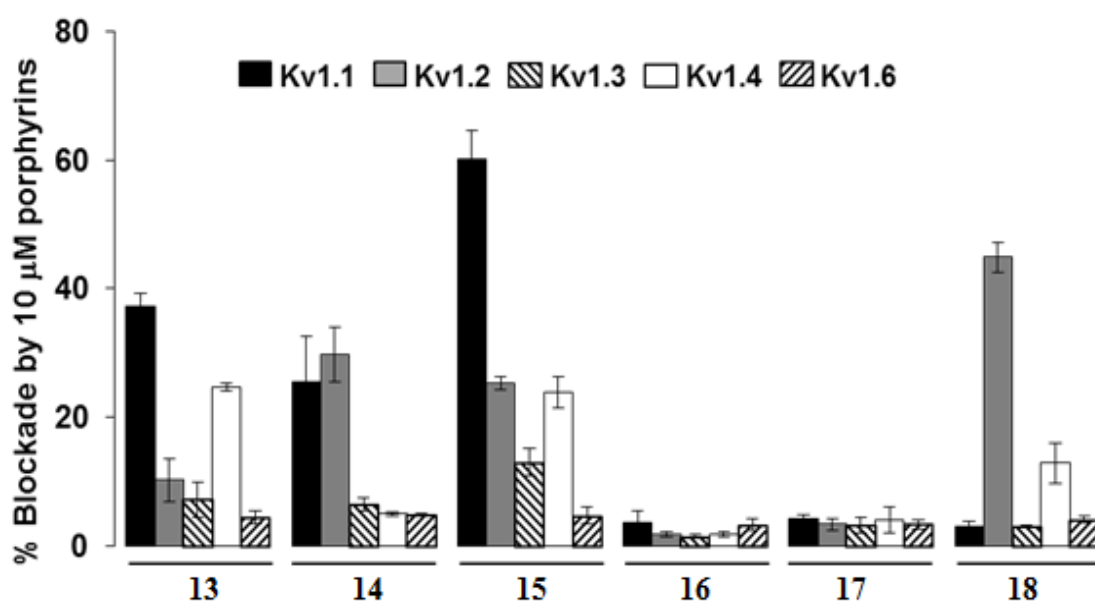
Correlating the SAR study to the biological results obtained from the screening there are fundamental features that arose. Surprisingly the majority of derivatives are insensitive and do not cause an inhibition at the concentration of 10 μM to the Kv1 channels. Looking at the channel we believe to be directly involved with MS (Kv1.1) the porphyrins that exhibited inhibition at 10 μM were, derivatives **13**, **14** and **15** all containing amide bonds, and primary amines protonated as the HCl salt. The inhibition values were 45, 22 and 62% respectively. There was no visual correlative trend observed with alkyl chain extension, compound **15**

docks into the protein to administer the highest inhibition effect. Derivative **16** gave no inhibition effect, the reasoning for this is that the carbon chain of **16** could be too long and the amine cannot dock into the turret region.

Changing the amide bond to an ester has a significant effect on the biological activity of these compounds. As shown in table 2.4, **13** inhibits the potassium channel at 45% at a 10 μM concentration. The same compound with the amide converted to an ester **17** has no observed inhibition. This phenomenon can be deduced to the fact that the hydrogen bond donor has been removed (figure 2.12). It is apparent that this hydrogen bonding interaction is important.
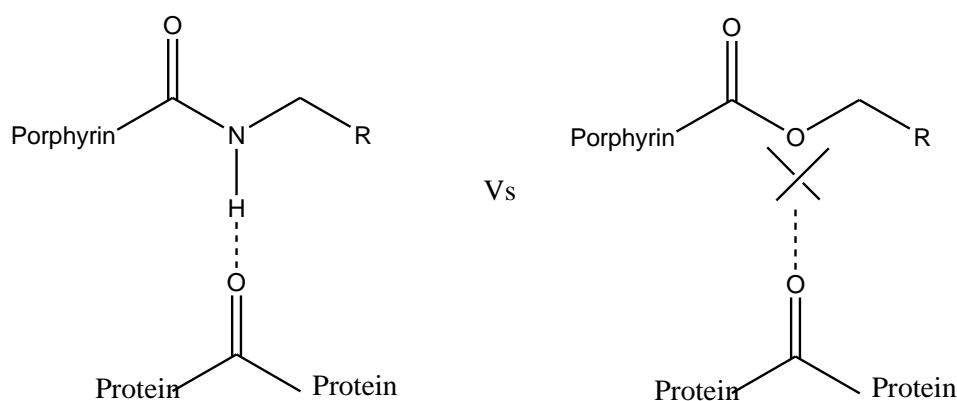

Figure 2.12: Bonding effect of amide vs ester with the protein.

On comparison of the bioactivities of the primary (**13**, **14**) and tertiary amine porphyrins (**20**, **21**) it is evident that replacing the terminal hydrogens with methyl groups the number of free hydrogens has been significantly reduced, thereby reducing hydrogen bonding potential between the inhibitor and the amino acid residue Asp377 as shown in figure 2.13. It should also be noted that steric hindrance, caused by the introduction of two methyl groups into **20** and **21** could also have an effect in the binding between the amino side arm and the protein binding site. Both the derivatives **20** and **21** of the tertiary amine series had no inhibitory effect.
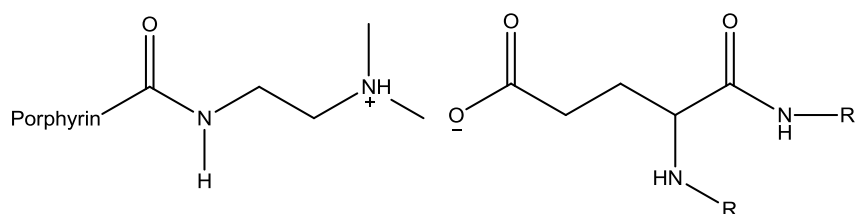

Figure 2.13: Weak bond formation could be due to the sterics of methyl groups of the porphyrin **20** and Asp377 in rat Kv1.1.

Comparison of the biological activity of **19** with **13** again demonstrates the importance of the secondary amide proton since **19** shows no activity.

The problems with porphyrins **13-15** is that inhibition is observed, however they are not selective to any specific potassium channel. Similar to 4-aminopyridine the porphyrin induces inhibition in other members of the Kv1 family (Kv1.1-Kv1.6). The porphyrin **13**, inhibits Kv1.1, 1.2 and 1.6 and is insensitive to Kv1.4 whereas **14** inhibits all the channels tested and finally **15** inhibits Kv1.1,1.4 and 1.6 but is insensitive to Kv 1.2. These results are all detailed in table 2.4. The final compound tested was **18**. This compound was designed to mimic porphyrin **16**. The interesting result for **18** is it has specific activity for Kv1.2 at 50%, and showed no inhibition of the other channels. Although not useful for our research, **18** could possibly be used as a starting point for other diseases related to Kv1.2. Thus, for inhibition it has been experimentally shown that (i) amide bonds are essential to the inhibition of these tertameric proteins (ii) free primary amines are also essential for the inhibition of these Kv1.1 channels. However the two must complement each other. Both amide and amines are essential to inhibit with hydrogen bonding contributing immensely (figure 2.14).
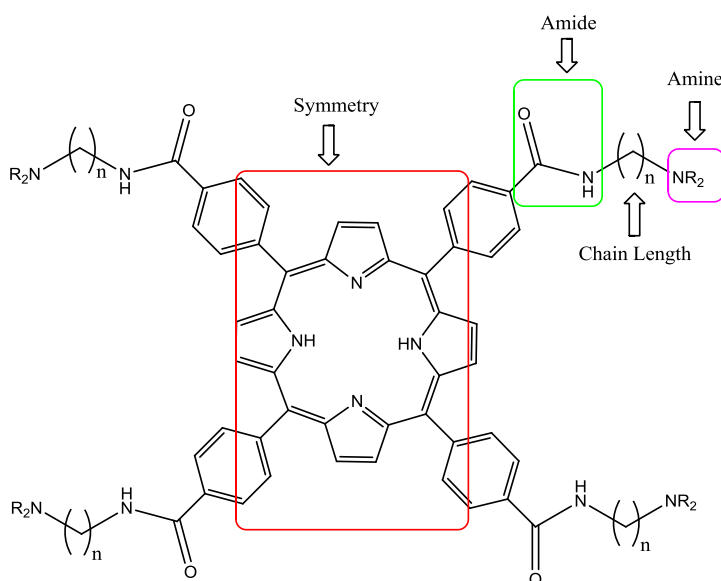

Figure 2.14: Key pharmacophore regions from porphyrin interactions with Kv1 channels.

2.8 Effect of hydrogen bonding on the protonated porphyrins

The chemistry of these amino porphyrins has been shown to exhibit interesting properties based on their ^{1}H NMR. Upon cleavage, the free amines exist in the protonated state as chloride salts. It was observed that the ^{1}H NMR splitting pattern of the phenyl hydrogens of

the porphyrins, was dependant on the ester or amide linkage and alkyl chain length. The effect observed can give an insight into the conformation of these compounds in solution.
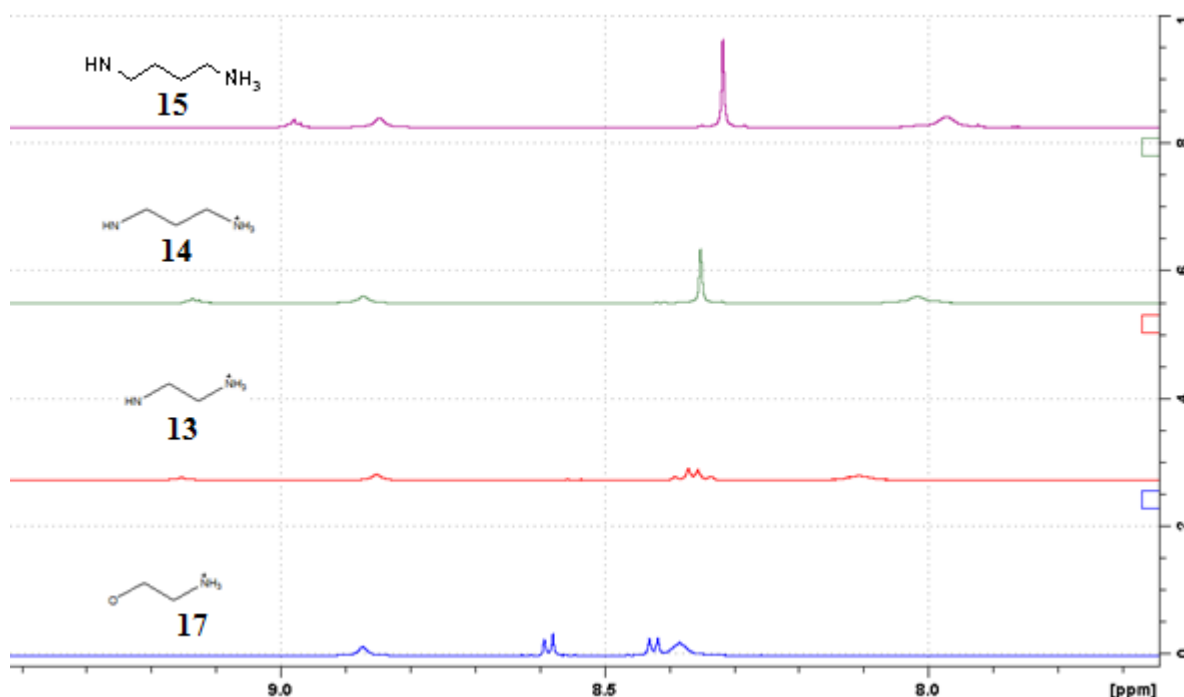

Figure 2.15: ^{1}H NMR of Aromatic region of the porphyrins **13** ,**14**, **15** and **17** at room temperature.

Shown in Figure 2.15 is the aromatic region in the ^{1}H NMR spectra of **13**, **14**, **15** and **17** in DMSO-d$_6$. The ester functionality gives a doublet of doublets as a result of the para substitution. The phenyl hydrogens are separated by 0.2 ppm. Replacing the ester functionality with an amide bond the same doublet of doublets is affected drastically. The splitting pattern for the protons converge together and are seen as an overlapping multiplet. The ester porphyrin **17** resembles a pseudo AX system, when the ester is replaced by an amide **13** the splitting pattern becomes an AB system. The electronegativity of the adjacent protons are influenced significantly by the resonance delocalisation of the amide.

With the alkyl chain increasing from a two carbon chained system to a three and four carbon moiety (**13** − **15**), the splitting pattern of the changes from an AB pattern to a singlet.. To better understand what is occurring a number of temperature ^{1}H NMR experiments were carried out. The spectra of **15** at 20 ^{o}C, 70 ^{o}C and 80 ^{o}C are shown in figure 2.16. The splitting pattern of the phenyl protons of **15** changes from a 'singlet' to an AB pattern with increasing temperature. Also the β- pyrrole hydrogens at 8.83 ppm also resolve to a sharper singlet and slightly shift downfield (which is to be expected since aggregation between the

porphyrins is reduced with increased temperature), the amide hydrogens move downfield with increasing temperature. The protons related to the amide bond are shifted from 8.99 ppm to 8.79ppm on going from 20 $^{\circ}$C to 80 $^{\circ}$C.
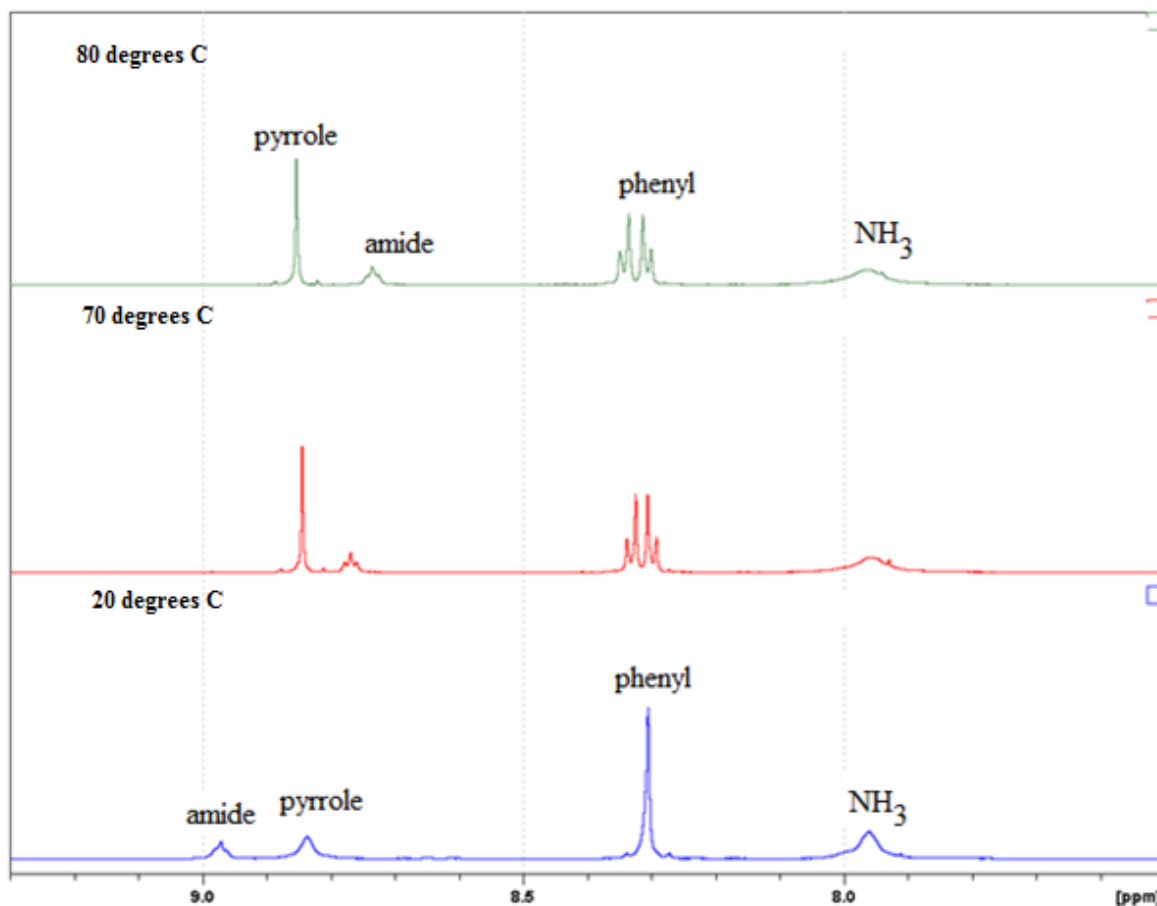

Figure 2.16: The observed change in chemical shifts and resolution seen from the porphyrin 5,10,15,20 tetra[4-benzoamido(*N*-(2-amino-*n*-butyl hydrochloride] porphyrin **15**.

The observed temperature effect on the 1H NMR of the phenyl protons of **15** could be explained as follows: The AB system is observed as a singlet at room temperature wheree Aυ = Bυ, at room temperature a ring conformation, as shown in figure 2.17, can likely form via intramolecular hydrogen bonding. As a result of this intramolecular hydrogen bonding, the amide bond bound to the phenyl ring will have a change in electron density thereby affecting the amount of electron density that it is withdrawing from the phenyl ring. As a consequence of this effect the chemical shift for protons A changes and becomes equivalent to the chemical shift of protons B, thereby resulting in a classic AB singlet (Aυ = Bυ). The application of heat disrupts this hydrogen bonding and the peaks resolve to the expected AB

doublet of doublet pattern as shown in figure 2.16. It should be noted that this phenomena was not observed for **14** which has only a two cabon spacer between the amide and terminal amino group.
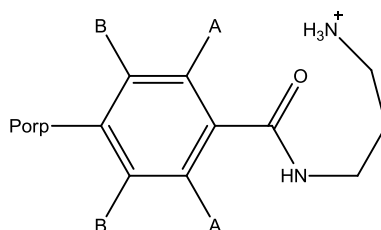

Figure 2.17a: Effect of H-Bonding on the AB phenyl system.

This effect is dependant on the primary amines being in their protonated salt forms. Similar effects were witnessed when the protonated tertiary amines **20** and **21** were analysed by ^{1}H NMR (figure 2.18). The two carbon chained quaternary dimethylated amine salt **20** shows a broad doublet of doublets due to para substitution similar to that observed with the protonated two carbon chained amine **13**. When the chain length is further extended by 1 methylene group, as is the case with **21**, a singlet is observed just as is the case with porphyrin **14** It seems when comparing the two sets of porphyrins, regardless of replacing the terminal hydrogens with methyl groups, the hydrogen bonding will still occur. The factors that affect the resolution of these peaks is chain length and temperature in which the spectra is run at as shown in figure 2.18.

Another plausible reason for the effect on the AB system could be due to rotamers on amide, this is shown in figure 2.17b. Depending on the position of the NH with the carbonyl it could be directly affecting the AB system.
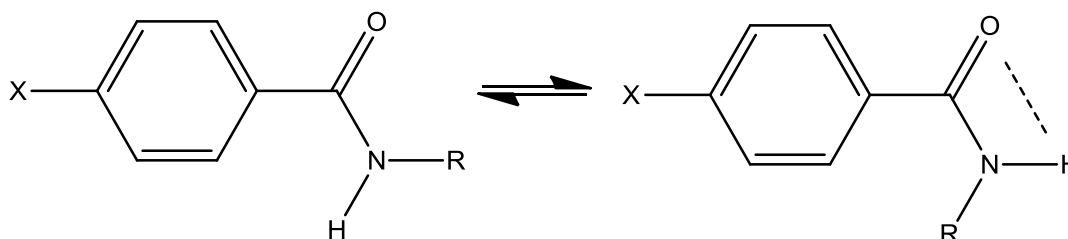

Figure 2.17b: Effect of H-Bonding on the AB phenyl system due to rotamers.
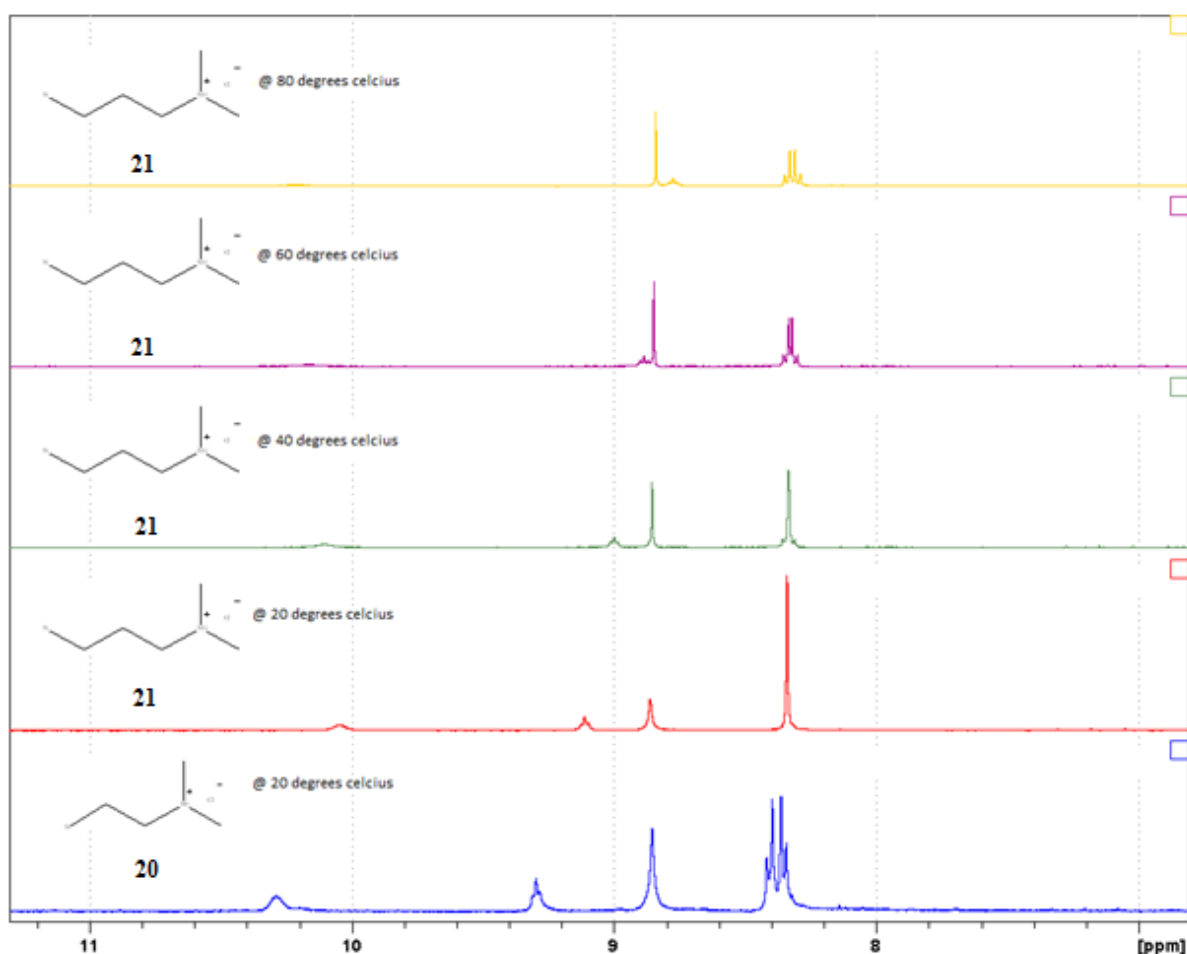
Figure 2.18: ^{1}H NMR of compounds **20** and **21** in the aromatic region. How chain length and temperature effects the hydrogen bonding between each molecule

Further evidence of the intramolecular hydrogen bonding phenomena proposed above is supported by ^{1}H NMR concentration studies (30-25 mg - 0.7 mg). Shown in figure 2.19 is a concentration study of **15**. At high concentrations a complicated spectrum is observed as a consequence of increased aggregation between the porphyrin rings in solution (π-π stacking). However, on dilution toward a unimolecular species (reduced aggregation) the spectrum simplifies to that observed in figure 2.16 at room temperature. If intermolecular hydrogen bonding was causing the observed effect with **15** (aromatic protons being a singlet) then the spectrum should have resolved into a doublet of doublets upon dilution, but it does not, therefore it is reasonable that it is intramolecular hydrogen bonding causing the observed singlet.
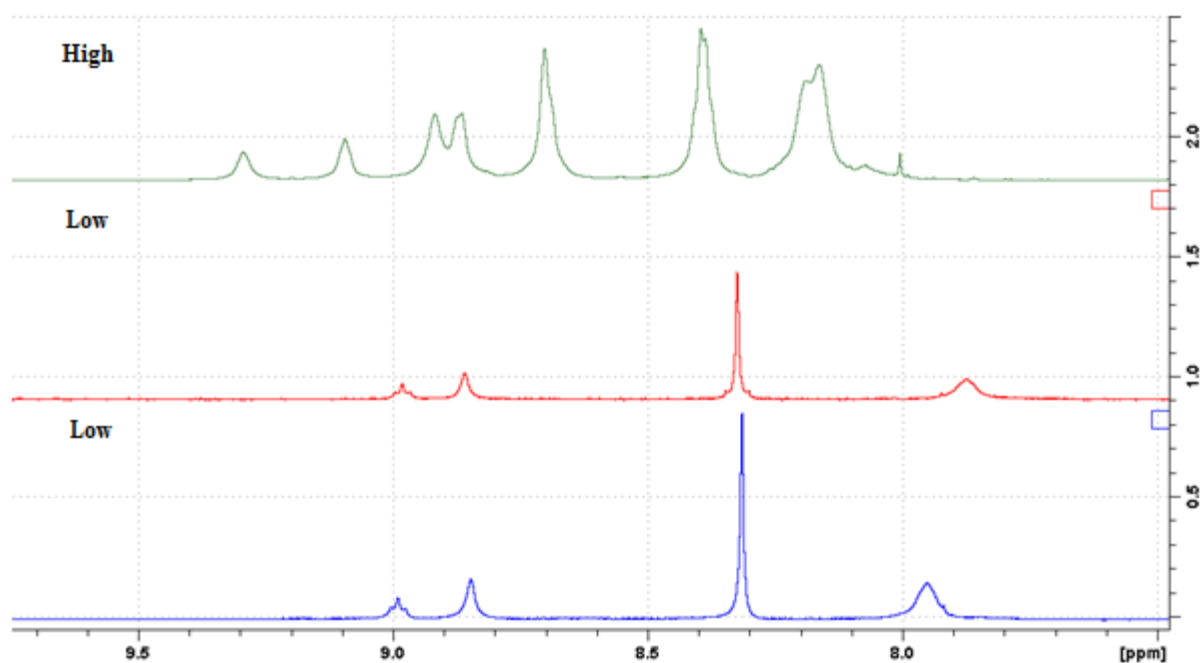
Figure 2.19: ^{1}H NMR of compound **15** (spectral effects high concentration (30-25 mg/0.7 ml) vs low concentration (5mg/0.7 mL).

2.9 Conclusion

Using porphyrins as a suitable scaffold gave invaluable SAR information with the range of potassium channels studied. The hydrogen bonding, alkyl chain length and ability to ionic bond provided to be essential characteristics needed to cause any inhibition of the channels investigated. There was no single selectivity witnessed for any of the porphyrin derivatives tested amongst the channel of interest. This was not expected and was not an objective of the SAR work. The objective was to determine if the compounds would interact with Kv 1.1, (the previous work is solely based *shaker* and Kv 1.3 channels). Once the basic interactions were established the key elements that caused inhibition could be explored.

^{1}H NMR identified interesting phenomena concerning the manner in which the compounds in their protonated form behave in solution. The main variables that surround the observations are concentration, temperature, type of bond (ester/amide) and chain length. The latter two, type of bond and chain length could be related to the biological activity but this has yet to be determined

2.10 Experimental

Materials

All operations were carried out under an atmosphere of argon or nitrogen using standard Schlenk techniques. All solvents were supplied by the Aldrich Chemical Company and TCI. Dichloromethane was dried over MgSO4 prior to use. Methanol was distilled over magnesium turnings and iodine before use. All organic reagents were purchased from the Aldrich Chemical Company. Pyrrole was freshly distilled over potassium hydroxide before use. Anhydrous triethylamine, propionic acid, borontrifluoride diethyletherate and were all used without further purification.

Column chromatography was carried out using neutral silica gel (Merck, used as received). All mobile phases for column chromatography were dried over $MgSO_4$ prior to use. All solvents were deoxygenated by purging withargon or nitrogen for ~10 minutes

Equipment

All syntheses involving air- and moisture-sensitive reagents were performed in oven or flame dried glassware. NMR spectra were recorded on a Bruker model AC 400 MHz spectrometer and Bruker model ANC 600 MHz spectrometer using $CDCl_3$ as solvent. All NMR spectra were calibrated according to the residual solvent peak, i.e. $CHCl_3$ at 7.26 ppm DMSO-d_6 2.50 ppm for all ^1H spectra and 77.16 ppm and 39.52 ppm for all ^{13}C spectra. Chemical shifts are given in parts per million (ppm). All UV vis spectra were measured on an Agilent Technologies 8453 photodiode array spectrometer using a 1 cm^3 quartz cell. Melting points were measured on a Stuart Scientific SMP1 melting point apparatus.

aq= apparent quartet, at = apparent triplet, ap = apparent pentet

All Melting points of the porphyrins were measured to >350 ^{o}C

λmax for the porphyrins was 418 nm
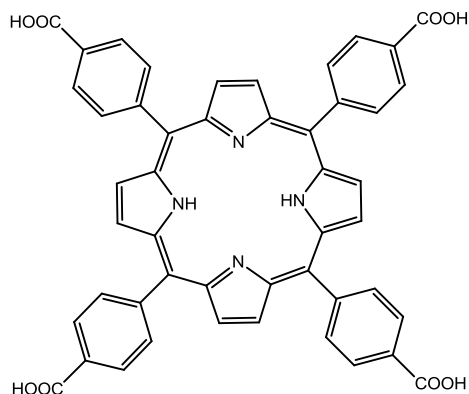
5,10,15,20-tetrakis (4-carboxyphenyl) porphyrin 1

To a 250 mL round bottom flask 1.5 g (10 mmol) of 4-formylbenzoic acid and 50 mL of propanoic acid were added and the reaction mixture was magnetically stirred. To completely dissolve 4-formylbenzoic acid the reaction mixture had to be heated to 80 ^{o}C at this point the aldehyde fully dissolved. Freshly distilled pyrrole (0.7 mL; 10 mmol) was then added to the mixture and the temperature was then brought to reflux and allowed stir for 2 h at reflux. After 2 hours the reaction mixture was let cool to room temperature and the reaction flask was placed in the freezer overnight, to aid precipitation of the porphyrin. The reaction mixture was then vacuum filtered using a glass frit and a dark purple solid was collected and washed with 5x50 mL aliquots of CH_2Cl_2 and was then dried overnight in vacco to give 1.1 g, of. 5,10,15,20-tetrakis (4-carboxyphenyl) porphyrin (55% yield).

^{1}H NMR (600 MHz) δ (DMSO- d$_6$) 13.33 (4H, s, -COOH), 8.87 (8H, s, β-H), 8.31 (16H, dd, o+m aryl-H), -2.92 (2H, s, NH) ; ^{13}C NMR (150 MHz) δ 167.1, 145.6, 134.4, 130.2, 127.3, 119.9.Mass Spec: (MALDI MS) Calculated (M+1) C$_{48}$H$_{30}$N$_4$O$_8$: 791.2097 , Observed (M+1) 791.0887 UV (EtOH): 418, 513, 546, 590 and 647 nm

**General procedure 1: Preparation of N-Boc protected porphyrins**

To a 25mL two necked round bottom flask, 235 mg (0.297 mmol) of TCPP was dissolved in 4 mL of anhydrous DMF. To this mixture was added 357 mg (1.96 mmol) of EDCI and 226 (1.96 mmol) NHS and the reaction mixture was stirred at room temperature for 1 h under nitrogen. After this time, a solution containing 376 µL (2.36 mmol) of N-boc ethylenediamine and 295 mg (2.36 mmol) of DMAP both dissolved in 1 mL of anhydrous DMF was added dropwise to the reaction mixture. After addition was completed the reaction mixture was allowed to stir for 24 h at room temperature. After this time the reaction mixture was poured into 80 mL distilled H_2O and filtered through a glass frit. The collected crude residue was then subjected to column chromatography and separated using a mobile phase of 90:10 CH_2Cl_2: ethanol on silica gel to give the protected porphyrins.
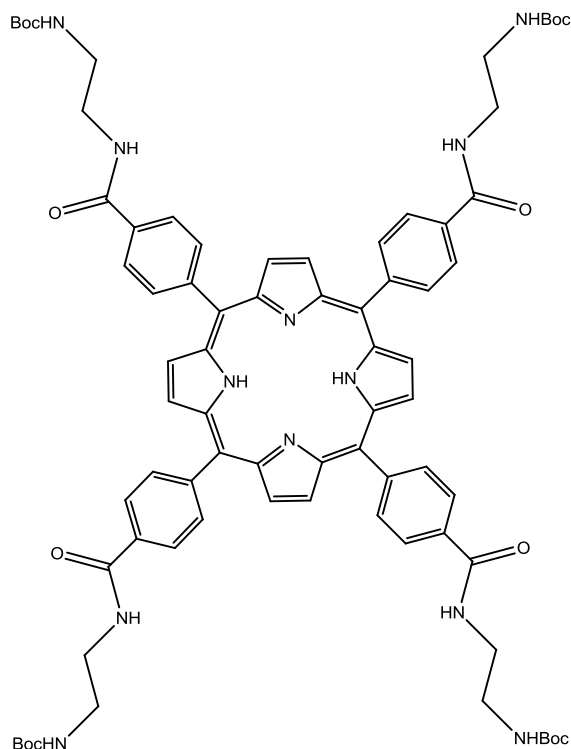
5,10,15,20-tetrakis 2-([4-*tert*-butyl benzamido]ethyl carbamate) porphyrin (3)

General procedure 1 was followed using 235 mg (0.297 mmol) of TCPP and 376 μL; (2.36 mmol) of N-boc 1,2-diaminoethane. The isolated crude residue was subjected to column chromatography and separated using a mobile phase 90:10 CH_2Cl_2: ethanol on silica to give 282 mg of 5,10,15,20-tetrakis 2-([4-*tert*-butyl benzamido] ethyl carbamate) porphyrin (70% yield)

^{1}H NMR: (600MHz) δ (DMSO-d$_6$) 8.89 (12H, s, β-H+ NH Amide) 8.32 (16H, dd, J= 5.2 Hz, aryl-H) 7.01 (4H, at, NH-Amide) 3.51 (8H, aq, CH_2) 3.33 (8H, aq, CH_2) 1.42 (36H, s, Boc-H) -2.92 (2H, s, NH). ^{13}C NMR (150 MHz): 166.1, 155.6, 143.5, 134.1, 134.1, 125.9, 119.1, 77.7, 39.5, 39.3, 28.2. UV (CH_2Cl_2): 418 nm, 513 nm, 546 nm, 590 nm, 647 nm Mass Spec: (MALDI MS) Calculated (M+1) $C_{76}H_{86}N_{12}O_{12}$ 1359.6522; Observed (M+1) 1359.6915.
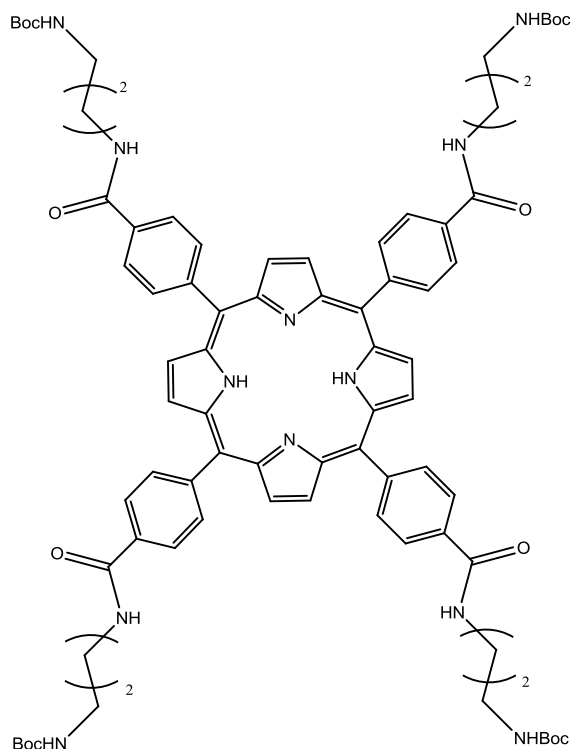
5,10,15,20-tetrakis 3-([4-*tert*-butyl benzamido] propyl carbamate) porphyrin (4)

General procedure 1 was followed using 235 mg (0.297 mmol) of TCPP and 412 μL; (2.36 mmol) of N-boc 1,3-diaminopropane. The isolated crude residue was subjected to column chromatography and separated using a mobile phase 90:10 CH_2Cl_2: ethanol on silica gel to give 286 mg of 5,10,15,20-tetrakis 3-([4-*tert*-butyl benzamido] propyl carbamate) porphyrin (68% yield).

^{1}H NMR: (600MHz) δ (DMSO-d_6) 8.87 (12H, s, β-H+ NH Amide) 8.33 (16H, dd, J= 5.6 Hz, aryl-H) 6.91 (4H, at, NH-Amide) 3.41 (8H, aq, CH_2) 3.13 (8H, aq, CH_2) 1.85 (8H, ap, CH_2) 1.42 (36H, s, Boc-H) -2.92 (2H, s, NH). ^{13}C NMR (150 MHz) 166.1, 156.5, 143.3, 134.8, 125.5, 119.2, 77.6, 37.8, 37.1, 29.6, 28.2 UV (CH_2Cl_2): 418 nm, 513 nm, 547 nm, 591 nm, 647 nm Mass Spec: (MALDI MS) Calculated (M+1) $C_{80}H_{94}N_{12}O_{12}$ 1415.7148, Observed (M+1) 1415.7576

.
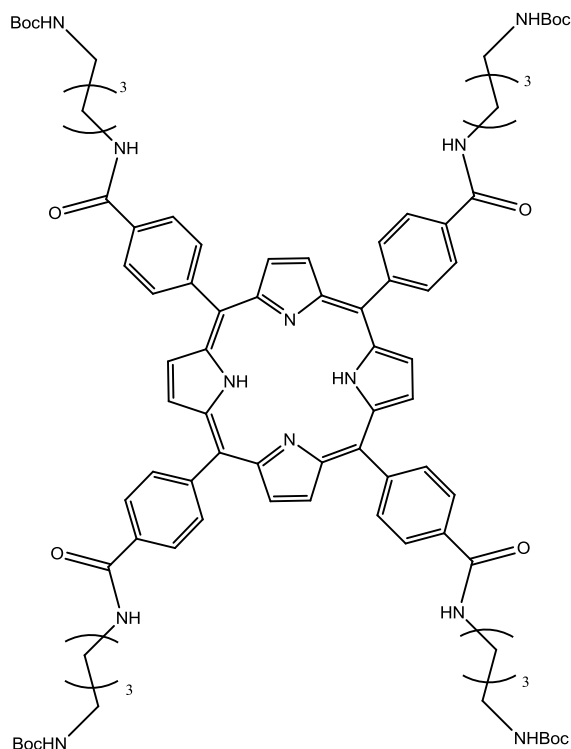
5,10,15,20-tetrakis- 4-([4-*tert*-butyl benzamido] butyl carbamate) porphyrin (5)

General procedure 1 was followed using 235 mg (0.297 mmol) of TCPP and 452 μL (2.36 mmol) of N-boc 1,4-diaminobutane. The crude residue was subjected to column chromatography and separated using a with a mobile phase 90:10 CH_2Cl_2: ethanol on silica to give 286 mg of 5,10,15,20-tetrakis- 4-([4-*tert*-butyl benzamido] butyl carbamate) porphyrin (65% yield).

^{1}H NMR: (600MHz) δ (DMSO-d_6) 8.98 (12H, m, β-H + NH Amide), 8.30 (16H, dd, J=5.6 Hz, aryl-H) 6.94 (4H, aq, NH Amide) 3.42 (8H, aq, CH_2) 3.19 (8H, aq, CH_2) 1.74 (8H, ap, CH_2) 1.66 (8H, ap, CH_2) 1.42 (36H, s, Boc-H) -2.92 (2H, s, NH) ^{13}C NMR (150 MHz) 166.5, 155.5, 143.8, 134.3, 134.1, 125.4, 119.2, 77.7, 39.8, 39.4, 28.3, 27.2, 26.6. UV (CH_2Cl_2): 419 nm, 513 nm, 546 nm, 590 nm, 647 nm Mass Spec: (MALDI MS) Calculated (M+1) $C_{84}H_{102}N_{12}O_{12}$ 1471.7774, Observed (M+1) 1471.8192.
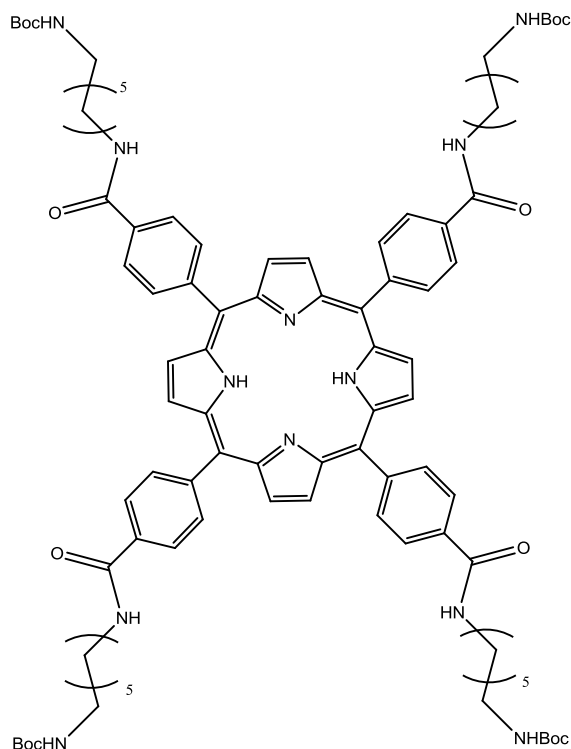
5,10,15,20-tetrakis 2-([4-*tert*-butyl benzamido] hexyl carbamate) porphyrin (6)

General procedure 1 was followed with 235 mg (0.297 mmol) of TCPP and N-boc 1,6-diaminohexane (530 µL; 2.36 mmol). The collected crude residue was subjected to column chromatography using a mobile phase of (20:1) CH_2Cl_2: ethanol to give 66 mg of 5,10,15,20-tetrakis 2-([4-*tert*-butyl benzamido] hexyl carbamate) porphyrin (14% yield)

^{1}H NMR: 8.88 (12H, m, β-H + NH Amide), 8.31-8.28 (16H, dd, J=5.6, aryl-H), 6.84 (4H, at, NH Amide), 3.44 (8H, aq, CH_2), 2.96 (8H, aq, CH_2), 1.61 (8H, ap, CH_2), 1.41 (24H, m, CH_2), 1.35 (36H, s, Boc-H), -2.92 (-2.9, s, NH) ^{13}C NMR (150 MHz) 166.6, 156.5, 144.4, 134.3, 134.1, 126.8, 119.7, 77.8, 39.7, 39.4, 30.2, 29.8, 28.6, 26.3, 26.1 UV (CH_2Cl_2): 418 nm, 513 nm, 546 nm, 590 nm, 647 nm Mass Spec (MALDI-HR): Calculated: (M+1) $C_{92}H_{118}N_{12}O_{12}$: 1583.9026, Observed (M+1) 1182.97 (Boc cleaved, free NH_2 observed).
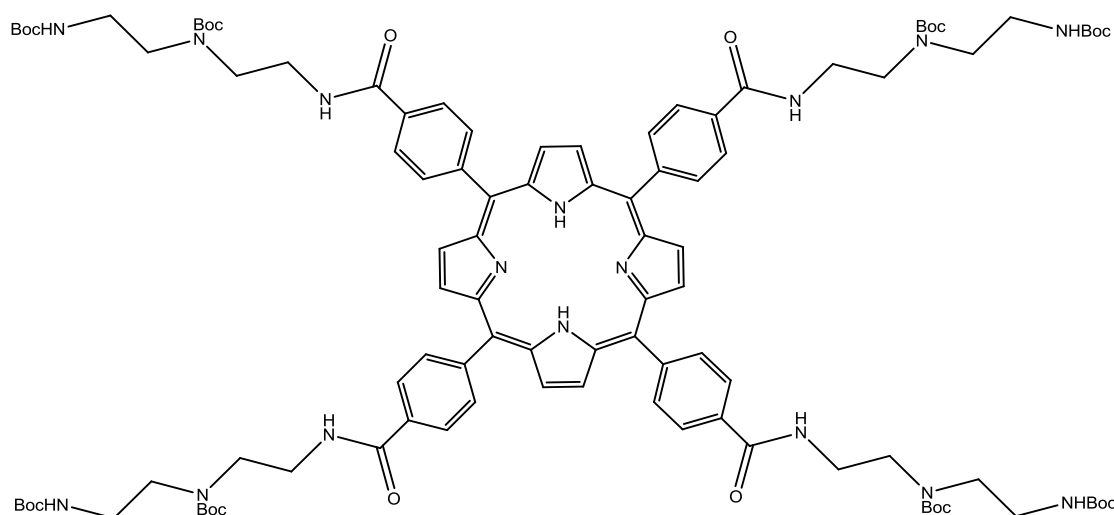
5,10,15,20-tetrakis-2-([tert-butyl-(2-benzamidoethyl) (2-((tert-butoxycarbonyl) amino)ethyl) carbamate porphyrin. (7)

To a two neck 25 mL round bottom flask 250 mg (0.313 mmol) of TCPP was charged, to this 4mL of anhydrous DMF was added and stirred at 0 $^{\circ}$C for 10 mins under an argon atmosphere. To this 360 mg (1.88 mmol) EDCI was added. Once the EDCI was added 320 mg; (2.5 mmol) of DMAP dissolved in 1 mL of anhydrous DMF was added. The EDCI and DMAP addition is done simultaneously. The reaction mixture was allowed stir for 1 h at 0 $^{\circ}$C. 0.760 g (2.5 mmol) of tert-butyl (2-aminoethyl)(2-((tert-butoxycarbonyl) amino) ethyl) carbamate was slowly added to the reaction flask dropwise, this was allowed stir for a further half an hour at 0 $^{\circ}$C and then at room temperature overnight. The reaction was poured into 100mL of water and filtered. The material was columned with 95:5 CH_2Cl_2: ethanol as eluant to give 212mg of 5,10,15,20-tetrakis-2-([tert-butyl-(2-benzamidoethyl) (2-((tert-butoxycarbonyl) amino) ethyl) carbamate porphyrin. (35% yield).

^{1}H NMR: (600MHz) δ (DMSO-d_6) 8.94 (12H, m, β-H + NH amide) 8.32 (16H, m, aryl-H) 7.01 (4H, m, NH-amide) 3.53 (16H, m, CH_2) 3.31 (8H, m, CH_2) 3.11 (8H, m, CH_2) 1.42 (72H, d, Boc-H) -2.92 (2H, s, NH). ^{13}C NMR (150 MHz) 166.6, 156.5, 155.5, 144.6, 134.4, 134.2, 127.8, 120.1, 77.9, 77.4, 39.6, 39.5, 30.2, 29.8, 28.6, 26.3, UV (CH_2Cl_2): 418 nm, 513 nm, 546 nm, 590 nm, 647 nm Mass Spec: (MALDI-HR) $C_{106}H_{142}N_{16}O_{20}$ Calculated (M+1) 1959.0586: Observed (M+1) 1959.0888.
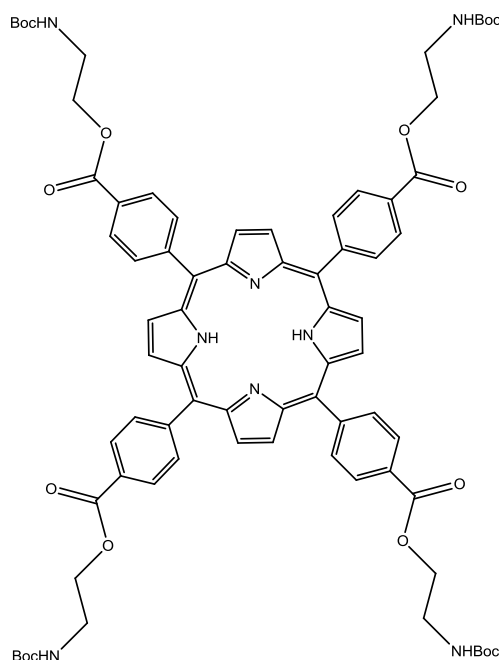
5,10,15,20-tetrakis 2-([4-*tert*-butyl benzester] ethyl carbamate) porphyrin (8)

To a two neck 25 mL round bottom flask was added TCPP (200 mg; 0.254 mmol) and 4 mL of anhydrous DMF and the mixture was stirred under an argon atmosphere and cooled to 0°C on an ice bath. After ten minutes of stirring at 0 ^{o}C both EDCI (285 mg; 1.47 mmol) and DMAP (245 mg; 1.97 mmol dissolved in 1 mL of anhydrous DMF) were added simultaneously to the reaction mixture at 0°C.. The reaction mixture was allowed stir for an additional 1 hr at 0°C, after this time N-boc ethanolamine (320 µL; 2.04 mmol) was then added dropwise to the reaction flask. The reaction mixture was then allowed to stir for a further 30 mins at 0 ^{o}C , after which time the reaction was allowed to warm to room temperature and left to stir for 36 h. The reaction mixture was then poured into 80 mL of water and filtered. The collected precipitate was further purified by column chromatographed using silica gel with 90:10 CH_2Cl_2: ethanol as eluant. the isolated product was further purified by reprecipitation from a $CHCl_3$: hexane mixture (1:1) to give 277 mg of 5,10,15,20-tetrakis 2-([4-*tert*-butyl benzester] ethyl carbamate) porphyrin (80% yield).

^{1}H NMR: (600MHz) δ (CDCl$_3$) 8.86 (8H, s, β-H) 8.51 (8H, d, aryl-H) 8.30 (8H, d, aryl-H) 5.04 (4H, t, NH-carbamate) 4.62 (8H, t, CH$_2$) 3.73 (8H, q, CH$_2$) 1.55 (36H, s, Boc-H) -2.89 (2H, s, NH). ^{13}C NMR (150 MHz): 155.7, 144.1, 134.6, 134.2, 125.7, 119.4, 78.0, 39.8, 39.4, 28.3. UV (CH$_2$Cl$_2$): 418 nm, 514 nm, 546 nm, 590 nm, 647 nm Mass Spec: (MALDI MS) Calculated (M+1) C$_{76}$H$_{82}$N$_8$O$_{16}$ 1363.5882: Observed (M+1) 1363.6461.
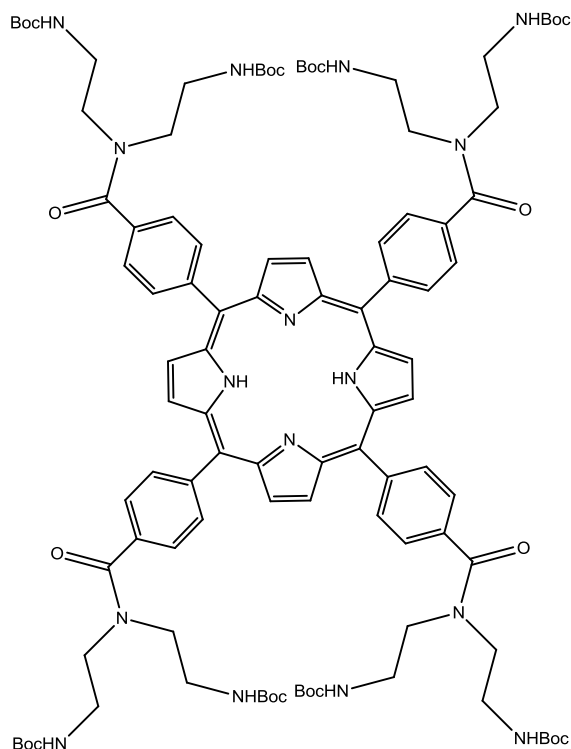
5,10,15,20-tetrakis 2-([di-tert-butyl ((benzoylazanediyl)bis(ethane-2,1-diyl))dicarbamate porphyrin (9)

To a two neck 25 mL round bottom flask 250 mg (0.313 mmol) of TCPP was charged, to this 4mL of anhydrous DMF was added and stirred at 0 ^{o}C for 10 min under an argon atmosphere. To this 360 mg (1.88 mmol) EDCI was added. Once the EDCI was added 320 mg (2.5 mmol) of DMAP dissolved in 1 mL of anhydrous DMF was added. The EDCI and DMAP addition is done simultaneously. The reaction mixture was allowed stir for 1 hour at 0 ^{o}C. 0.760 g (2.5 mmol) of di-tert-butyl (azanediylbis(ethane-2,1-diyl))dicarbamate was slowly added to the reaction flask dropwise, this was allowed stir for a further half an hour at 0 ^{o}C and then at room temperature overnight. The reaction was poured into 100mL of water and filtered. The material was columned with 95:5 CH_2Cl_2: ethanol as eluent to give 399mg of 5,10,15,20-tetrakis 2-([di-tert-butyl ((benzoylazanediyl)bis(ethane-2,1-diyl))dicarbamate porphyrin (66% yield).

^{1}H NMR: (600MHz) δ (DMSO-d$_6$) 8.89 (8H, s, β-H) 8.34 (8H, d, aryl-H) 7.83 (8H, d, aryl-H) 7.16 (8H, m, NH-amide) 3.59 (16H, m, CH_2) 3.28 (8H, m, CH_2) 3.23 (8H, m, CH_2) 1.42 (72H, d, Boc-H) -2.93 (2H, s, NH). UV (CH_2Cl_2): 418 nm, 513 nm, 546 nm, 590 nm, 647 nm Mass Spec: (MALDI-HR) $C_{106}H_{142}N_{16}O_{20}$ Calculated (M+1) 1959.0586: Observed (M+1) 1959.0986.
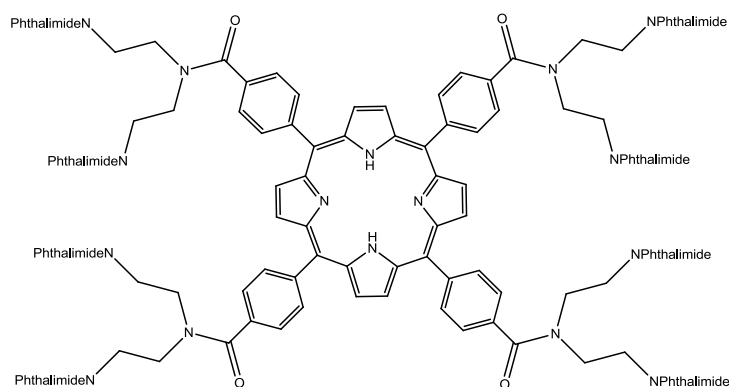
5,10,15,20-tetrakis(4-carboxphenyl-N,N''-bis(phthalimido)diethylenetriamine) porphyrin 10.

To a 100 mL two neck round bottom flask 200 mg (0.255 mmol) of TCPP was charged. A volume of 20 mL of anhydrous CH_2Cl_2 was added and the reaction was stirred for 10 min under nitrogen at room temperature. Through a SUBA seal port 3 mL (6 mmol) of a 2M oxalyl chloride solution in methylene chloride was added simultaneously with 2 drops of catalytic DMF. This was allowed stir overnight to effectively form the acid chloride. A stream of nitrogen was placed over the reaction at room temperature to remove the solvent, once the solvent was removed the flask was subjected to a high vaccum pump to remove excess oxalyl chloride. After this the reaction contents were redissolved in 20 mL CH_2Cl_2 and stirred. A mass of 0.741 g (2.04 mmol) of N,N''-bis(phthalimido)diethylenetriamine was dissolved in 10 mL CH_2Cl_2 along with 136 mg; DMAP and added to the reaction mix simultaneously with 2.5 mL (14.35 mmol), diisopropylethylamine and the reaction mixture was let stir overnight at room temperature. The reaction mixture was diluted with 200 mL CH_2Cl_2 to dilute the sample and was then washed with 2x100 mL 5% HCl solution, 2x100 mL 1 M NaOH solution, 2x100 mL brine solution and dried over $MgSO_4$. Solvent removed *in vacuo*. Column chromatography was used to isolate the product on silica using a mobile phase of CH_2Cl_2: acetone (90-10)-(80:20)

^{1}H NMR: (600 MHz) δ (CDCl3) 9.04 (8H, s, β-H), 7.99 (8H, dd, aryl-H), 7.91 (8H, m, phth-H), 7.81 (8H, m, phth-H), 7.71 (8H, m, phth-H) 7.52 (8H, m, phth-H), 7.36 (8H, m, phth-H), 4.2 (8H, m, CH_2), 4.11 (8H, m, CH_2), 4.02 (8H, m, CH_2), 3.96 (8H, m, CH_2), -2.89 (2H, s, NH); ^{13}C NMR: 172.6, 169.7, 168.4. 143.5, 135.4, 134.6, 134.5, 134.5, 132.1, 132.2, 125.5, 123.9, 123.7, 119.8, 47.4, 43.6, 36.3, 35.1. UV (CH_2Cl_2): 418 nm, 513 nm, 546 nm, 590 nm, 647 nm Mass Spec: (MALDI MS) Calculated (M+1) $C_{128}H_{90}N_{16}O_{20}$ 2171.6551, Observed (M+1) 2171.6823
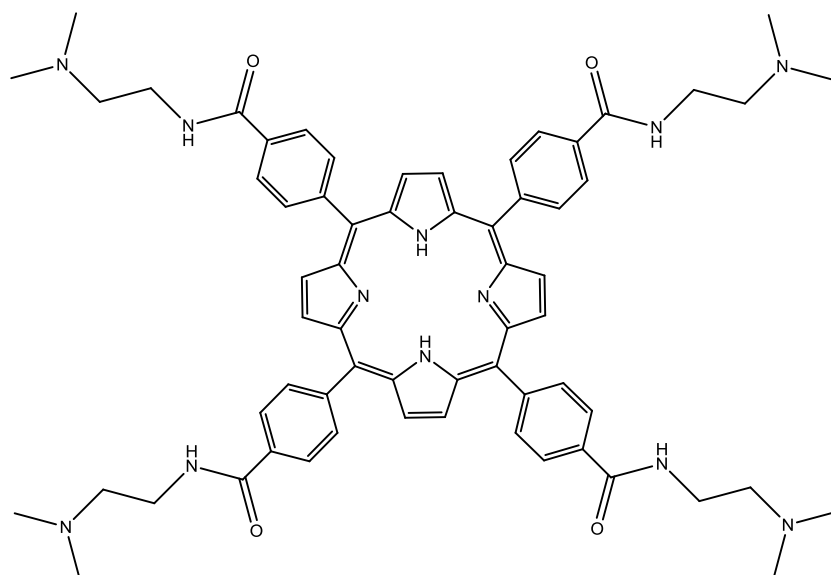
General procedure 2: N-(2-(dimethylamino)ethyl)benzamide porphyrin 11

TCPP (500 mg; 0.632 mmol) was charged into a 25 mL two neck round bottom flask. To this 10 mL anhydrous DMF was added and the reaction mixture was placed on an ice bath and allowed to stir under an argon atmosphere for 15 minutes. To this mixture both EDCI (740 mg; 3.86 mmol) and NHS (340 mg; 3.86mmol) were added and the reaction mixture was allowed to stir at 0 ^{o}C for a further hour. After this time N,N dimethylethylenediamine (552 μL; 4.38 mmol) was added to the mixture (at 0 ^{o}C) and the reaction mixture was allowed to stir at 0 ^{o}C for a further 20 minutes. After this time the reaction mixture was allowed to warm to room temperature and was then stirred overnight. The reaction mixture was then poured into 80 mL of water and filtered. The collected precipitate was further purified by column chromatography using silica gel and a mobile phase of 5:5:1 CHCl$_3$: EtOH : NH$_3$OH . The product collected after column chromatography was further purified by reprecipitation from MeOH/H$_2$O (1:1) to give 419 mg of N-(2-(dimethylamino)ethyl)benzamide porphyrin as a purple solid (62% yield).

^{1}H NMR: (600MHz) δ (CDCl$_3$) 8.82 (8H, s, β-H) 8.31 (8H, dd, J=5.2Hz, aryl-H) 8.26 (8H, dd, J=5.2Hz, aryl-H) 7.31 (4H, at, NH Amide), 3.73 (8H, aq, CH$_2$), 2.62 (8H, at, CH$_2$) 2.34 (24H, s, N-CH3) -2.88 (2H, s, NH) ^{13}C NMR (150 MHz) 168.8, 145.2, 134.6, 134.2, 126.4, 119.8, 58.7, 45.4, 34.5. UV (CH$_2$Cl$_2$): 418 nm, 513 nm, 546 nm, 590 nm, 647 nm. Mass Spec: (MALDI MS) Calculated (M+1) C$_{64}$H$_{70}$N$_{12}$O$_4$ 1071.5677, Observed (M+1) 1071.5953.
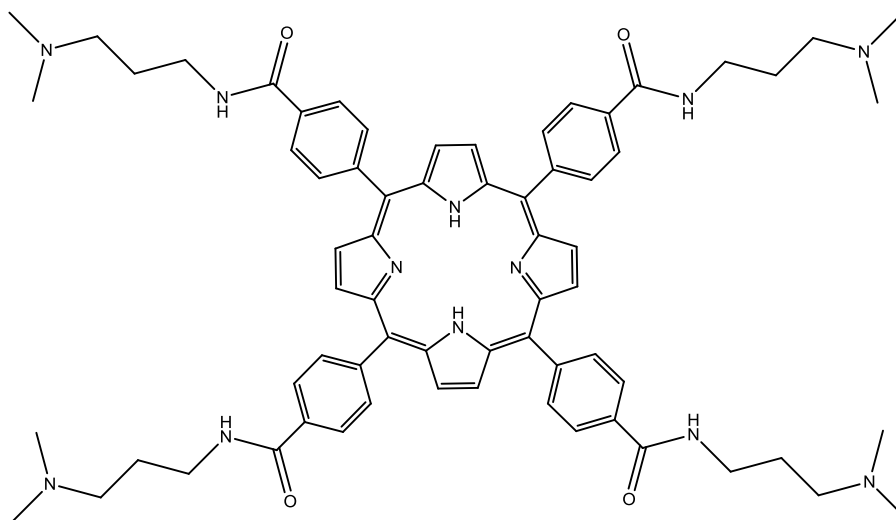
5,10,15,20-tetrakis N-(3-(dimethylamino)propyl)benzamide porphyrin 12

General procedure 2 was used to prepare **12** using TCPP (500 mg; 0.632 mmol) and N,N dimethylpropylenediamine (552 μL; 4.38 mmol) to give 413 mg of **12** (59% yield) after purification as per the general procedure 2.

^{1}H NMR: (600MHz) δ (CDCl$_3$) 8.96 (4H, at, NH Amide) 8.85 (8H, s, β-H) 8.25 (8H, dd, J=5.2Hz, aryl-H) 8.11 (8H, dd, J= 5.2, aryl-H) 3.76 (8H, aq, CH$_2$) 2.66 (8H, at, CH$_2$) 1.94 (8H, ap, CH$_2$) -2.89 (2H, s, NH) ^{13}C NMR (150 MHz) 167.9, 145.5, 135.8, 134.7, 125.9, 119.9, 60.5, 46.1, 41.2, 25.1. UV (CH$_2$Cl$_2$): 418 nm, 513 nm, 546 nm, 590 nm, 647 nm. Mass Spec: (MALDI MS) Calculated (M+1) C$_{68}$H$_{78}$N$_{12}$O$_4$: 1127.6303, Observed (M+1) 1127.6917.

General procedure 3: Deprotection of N-boc protected porphyrins.

To a 25mL round bottom flask 80 mg of boc protected porphyrin was added and placed over an argon atmosphere. Anhydrous CH_2Cl_2 (5mL) was then added and the mixture was stirred at 0 °C for 15 min at which time 1 mL of 4M HCl in dioxane was added dropwise (the reaction mixture was kept at 0 °C during the addition). The reaction was let stir overnight at room temperature, before being poured into 30 mL diethyl ether and the precipitate was collected by suction filtration. The collected precipitate was then washed with two 8 mL aliquots of diethyl ether. No ^{13}C could be obtained for any of the compounds 13-21 due to the H-Bonding phenomena mentioned previously.
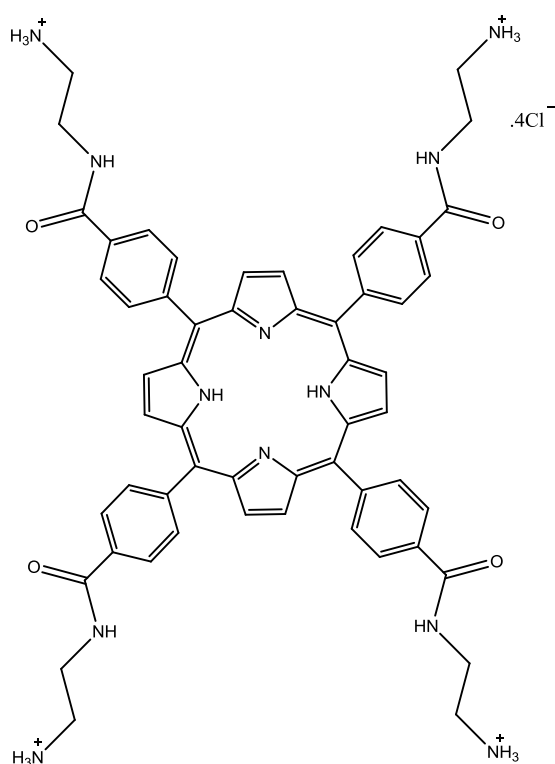
Coumpound 13:

General procedure 3 was followed using 80 mg of 5,10,15,20-tetrakis 2-([4-*tert*-butyl benzamido] ethyl carbamate) porphyrin. Compound **13** was isolated as a green solid in quantitative yield.

^1H NMR: (600MHz) δ (DMSO-d$_6$) 9.22 (4H, t, NH-amide) 8.88 (8H, s, β-H) 8.48 (16H, dd, aryl-H) 8.21 (12H, s, NH$_3$) 3.76 (8H, q, CH$_2$) 3.10 (8H, q, CH$_2$) -2.91 (2H, s, NH). UV (H$_2$O): 418 nm, 513 nm, 546 nm, 590 nm, 647 nm Mass Spec: (MALDI MS) Calculated (M+1-4HCl) $C_{56}H_{58}Cl_4N_{12}O_4$ 959.4425, Observed (M+1-4HCl) 959.4461.
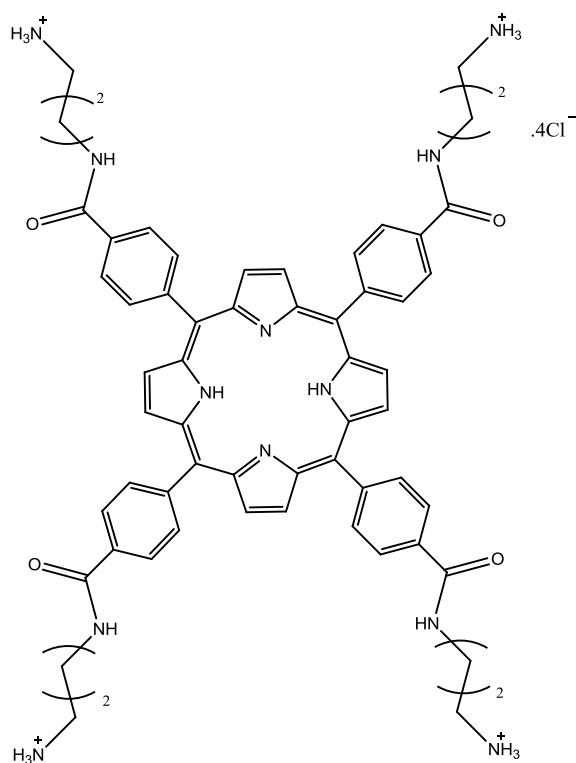
Compound 14:

General procedure 3 was followed using 80 mg of 5,10,15,20-tetrakis 3-([4-*tert*-butyl benzamido] propyl carbamate) porphyrin. Compound **14** was isolated as a green solid in quantitative yield.
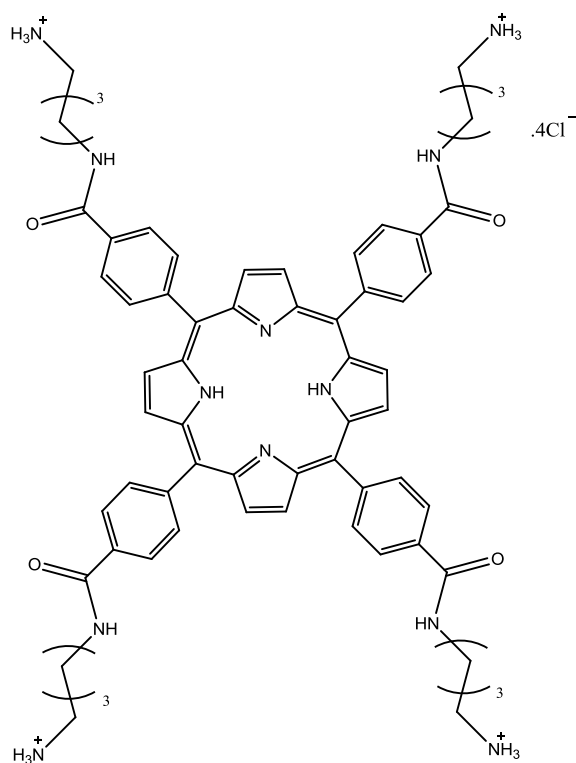
^{1}H NMR: (600MHz) δ (DMSO-d$_6$) 9.12 (4H, t, NH-amide) 8.98 (8H, s, β-H) 8.46 (16H, s, aryl-H) 8.08 (12H, s, NH$_3$) 3.52 (8H, t, CH$_2$) 3.02 (8H, q, CH$_2$) 2.01 (8H, p, CH$_2$) -2.91 (2H, s, NH) UV (H$_2$O): 418 nm, 513 nm, 546 nm, 590 nm, 647 nm Mass Spec: (MALDI MS) Calculated C$_{60}$H$_{66}$Cl$_4$N$_{12}$O$_4$ (M+1-4HCl) 1015.5051, Observed (M+1-4HCl) 1015.5107.

Compound 15:

General procedure 3 was followed using 80 mg of 5,10,15,20-tetrakis 4-([4-*tert*-butyl benzamido] butyl carbamate) porphyrin. Compound **15** was isolated as a green solid was obtained in quantitative yield.
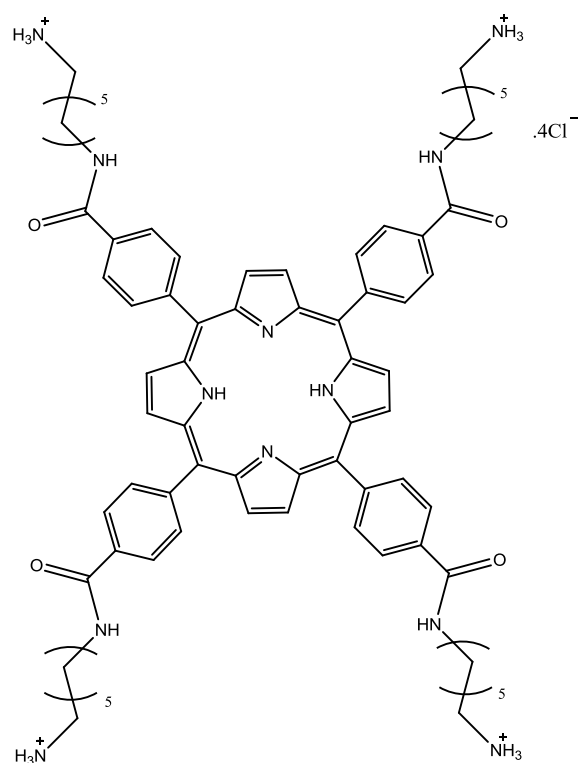
^{1}H NMR: (600MHz) δ (DMSO-d$_6$) 9.04 (4H, t, NH-amide) 8.89 (8H, s, β-H) 8.32 (16H, s, aryl-H) 7.95 (12H, s, NH$_3$) 3.56 (8H, under water peak , CH$_2$) 2.91 (8H, m, CH$_2$) 1.71 (16H, m, CH$_2$) -2.92 (2H, s, NH). UV (H$_2$O): 419 nm, 514 nm, 546 nm, 590 nm, 647 nm Mass Spec: (MALDI MS) Calculated C$_{64}$H$_{74}$Cl$_4$N$_{12}$O$_4$ (M+1-4HCl) 1071.5677, Observed (M+1-4HCl) 1071.5763.

Compound 16:

General procedure 3 was followed using 80 mg of 5,10,15,20-tetrakis 6-([4-*tert*-butyl benzamido] hexyl carbamate) porphyrin . A green solid **16** was obtained in quantitative yield..

^{1}H NMR: (600MHz) δ (DMSO-d$_6$) 9.01 (4H, t, NH-amide) 8.96 (8H, s, β-H) 8.34 (16H, s, aryl-H) 8.06 (12H, s, NH$_3$) 3.54 (8H,q , CH$_2$) 2.82 (8H, q, CH$_2$) 1.74 (16H, m, CH$_2$) 1.43 (16H, m, CH$_2$) -2.91 (2H, s, NH). UV (H$_2$O): 418 nm, 513 nm, 547 nm, 591 nm, 647 nm Mass Spec: (MALDI MS) Calculated C$_{72}$H$_{90}$Cl$_4$N$_{12}$O$_4$: (M+1-4HCl) 1183.6929, Observed (M+1-4HCl) 1183.6995.
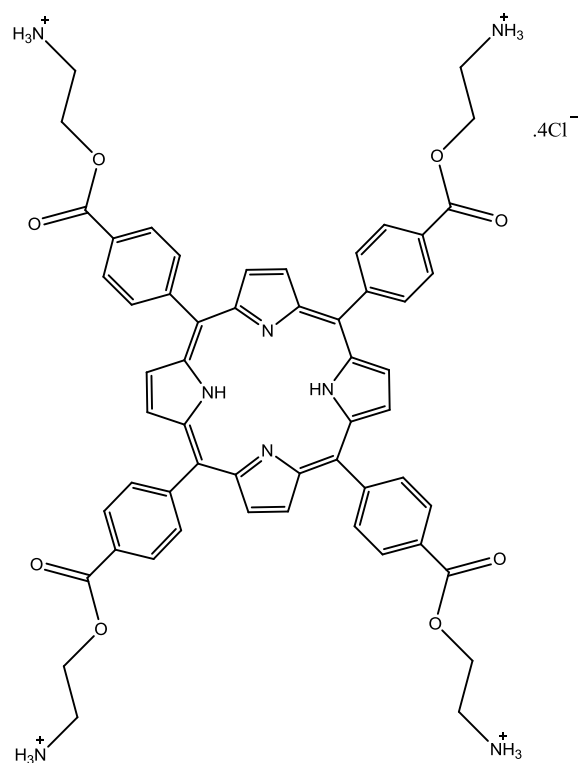
Compound 17:

General procedure 3 was followed using 80 mg of 5,10,15,20-tetrakis 2-([4-*tert*-butyl benzester] ethyl carbamate) porphyrin. A green solid was obtained in quantitative yield.

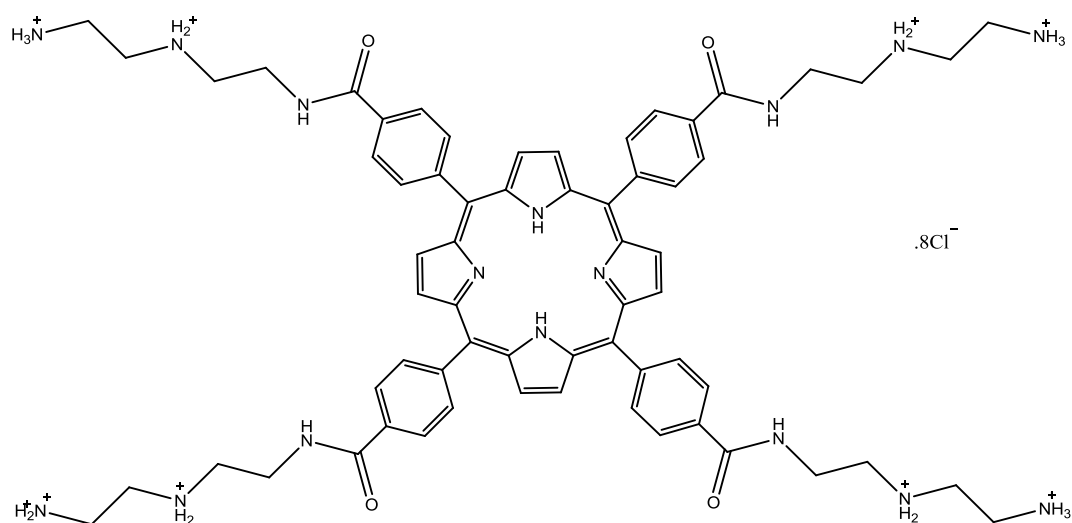^{1}H NMR: (600MHz) δ (DMSO-d$_6$) 8.90 (8H, s, β-H) 8.62 (8H, d, aryl-H) 8.46 (8H, d, aryl-H) 8.37 (12H, s, NH$_3$) 4.66 (8H, q, CH$_2$) 3.48 (8H, q, CH$_2$) -2.92 (2H, s, NH). UV (H$_2$O): 419 nm, 513 nm, 545 nm, 590 nm, 647 nm Mass Spec: (MALDI MS) Calculated C$_{56}$H$_{54}$Cl$_4$N$_8$O$_8$ (M+1-4HCl) 963.3785, Observed (M+1-4HCl) 963.3157.

Compound 18:

General procedure 3 was followed using 80 mg of.5,10,15,20-tetrakis 2-([di-tert-butyl ((benzoylazanediyl)bis(ethane-2,1-diyl))dicarbamate porphyrin A green solid was obtained in quantitative yield.

^{1}H NMR: (600MHz) δ (DMSO-d$_6$) 9.63 (8H, s, NH$_2$) 9.28 (4H, t, NH-amide) 8.81 (8H, s, β-H) 8.44 (20H, m,aryl-H + NH$_3$) 8.33 (8H,d , aryl-H) 3.82 (8H, m, CH$_2$) 3.41 (16H, m, CH$_2$) 3.34 (8H, m, CH$_2$) -2.92 (2H, s, NH). UV (H$_2$O): 418 nm, 513 nm, 546 nm, 590 nm, 647 nm Mass Spec: (MALDI MS) Calculated C$_{64}$H$_{82}$Cl$_4$N$_{16}$O$_4$: (M+1-4HCl) 1131.6112, Observed (M+1-4HCl) 1131.5670.
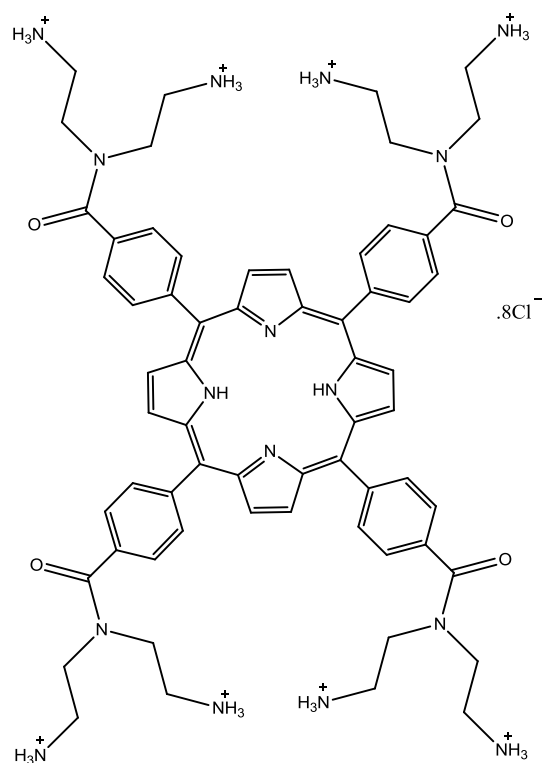
Compound 19:

General procedure 3 was followed using 80 mg of 80 mg of 5,10,15,20-tetrakis-2-([tert-butyl-(2-benzamidoethyl) (2-((tert-butoxycarbonyl) amino) ethyl) carbamate porphyrin. A green solid was obtained in quantitative yield.

^{1}H NMR: (600MHz) δ (DMSO-d_6) 9.11 (8H, s, β-H) 8.48 (12H, s, NH$_3$) 8.27 (8H, d, aryl-H) 8.18 (8H, s, NH$_2$) 8.06 (8H,d , aryl-H) 3.92 (16H, m, CH$_2$) 3.25 (16H, m, CH$_2$) -2.91 (2H, s, NH). UV (H$_2$O): 418 nm, 513 nm, 546 nm, 590 nm, 647 nm Mass Spec: (MALDI MS) Calculated C$_{64}$H$_{82}$Cl$_4$N$_{16}$O$_4$: (M+1-4HCl) 1131.6112 Observed (M+1-4HCl) 1131.6693.

.4Cl⁻
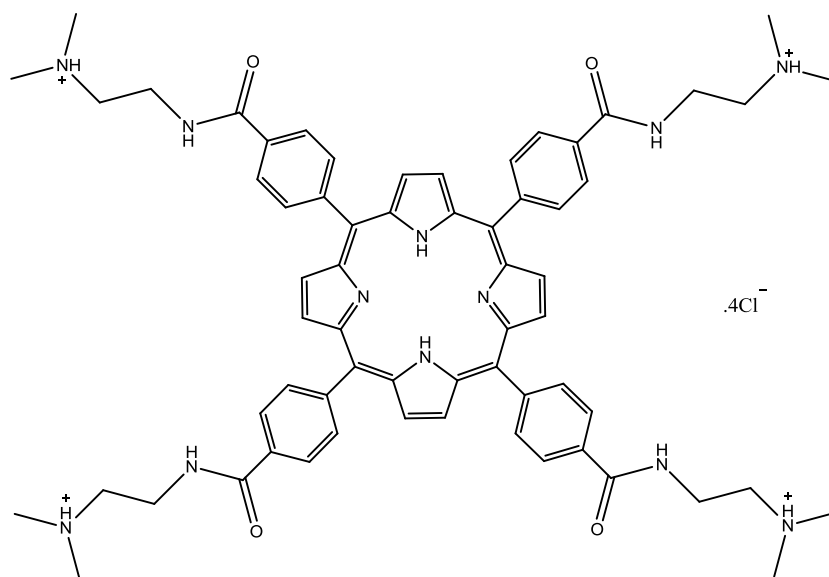
Protonation procedure to prepare 20

General procedure 3 was followed using 80 mg of 5,10,15,20-tetrakis N-(2-(dimethylamino)ethyl)benzamide porphyrin. A green solid was obtained in quantitative yield..

^{1}H NMR: (600MHz) δ (DMSO-d_6) 8.32 (4H, s,,NH(CH$_3$)$_2$) 9.33 (4H, t, NH-amide) 8.51 (8H, s, β-H) 8.45 (16H, s, phenyl-H) 3.88 (8H, m, CH$_2$) 3.41 (8H, m, CH$_2$) 2.92 (24H, d, (CH$_3$)$_2$) -2.91 (2H, s, NH). UV (H$_2$O): 418 nm, 513 nm, 546 nm, 590 nm, 647 nm Mass Spec: (MALDI MS) Calculated C$_{64}$H$_{74}$Cl$_4$N$_{12}$O$_4$: (M+1-4HCl) 1071.5677, Observed (M+1-4HCl) 1071.5673.
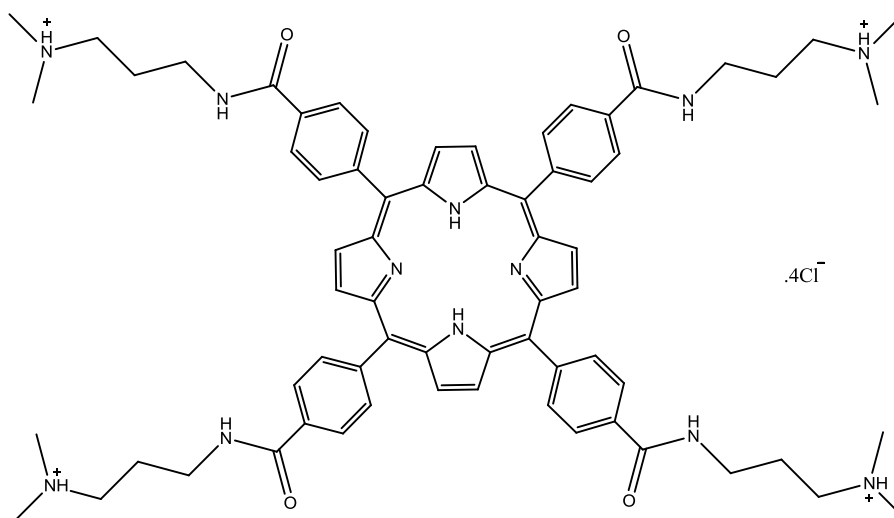
Protonation procedure to prepare 21:

The general procedure was followed using 80 mg of 5,10,15,20-tetrakis N-(3-(dimethylamino)propyl)benzamide porphyrin. A green solid was obtained in quantitative yield

^{1}H NMR: (600MHz) δ (DMSO-d$_6$) 8.01 (4H, s,NH(CH$_3$)$_2$) 9.12 (4H, t, NH-amide) 8.89 (8H, s, β-H) 8.31 (16H, s, phenyl-H) 3.52 (8H, m, CH$_2$) 3.28 (8H, m, CH$_2$) 2.89 (24H, d, (CH$_3$)$_2$) 2.12 (8H, p, CH$_2$) -2.91 (2H, s, NH). UV (H$_2$O): 418 nm, 513 nm, 546 nm, 590 nm, 647 nm Mass Spec: (MALDI MS) Calculated C$_{68}$H$_{82}$Cl$_4$N$_{12}$O$_4$: (M+1-4HCl) 1127.6303, Observed (M+1-4HCl) 1127.6328.

2.11 References

1. Milgrom LR. The colours of life: An introduction to the chemistry of porphyrins and related compounds. Oxford University Press; 1997.

2. Adler A, Longo F, Finarell.JD, Goldmach.J, Assour J, Korsakof.L. A simplified synthesis for meso-tetraphenylporphin. J Org Chem 1967;32(2):476.

3. Lindsey J, Schreiman I, Hsu H, Kearney P, Marguerettaz A. Rothemund and adler-longo reactions revisited - synthesis of tetraphenylporphyrins under equilibrium conditions. J Org Chem 1987 6;52(5):827-36.

4. Dichtel W, Serin J, Edder C, Frechet J, Matuszewski M, Tan L, Ohulchanskyy T, Prasad P. Singlet oxygen generation via two-photon excited FRET. J Am Chem Soc 2004 5;126(17):5380-1.

5. Gandini S, Gelamo E, Itri R, Tabak M. Small angle X-ray scattering study of meso-tetrakis (4-sulfonatophenyl) porphyrin in aqueous solution: A self-aggregation model. Biophys J 2003;85(2):1259-68.

6. Gradl SN, Felix JP, Isacoff EY, Garcia ML, Trauner D. Protein surface recognition by rational design: Nanomolar ligands for potassium channels. J Am Chem Soc 2003;125(42).

7. Ader C, Schneider R, Hornig S, Velisetty P, Wilson EM, Lange A, Giller K, Ohmert I, Martin-Eauclaire M, Trauner D, et al. A structural link between inactivation and block of a K+ channel. Nature Structural & Molecular Biology 2008;15(6):605-12.

8. Muller D, Zeltser I, Bitan G, Gilon C. Building units for N-backbone cyclic peptides .3. synthesis of protected N-alpha-(omega-aminoalkyl)amino acids and N-alpha-(omega-carboxyalkyl) amino acids. J Org Chem 1997;62(2).

9. Carpino LA, Beyermann M, Wenschuh H, Bienert M. Peptide synthesis via amino acid halides. Acc Chem Res 1996;29(6):268-74.

10. Joullie MM, Lassen KM. Evolution of amide bond formation. Arkivoc2010:189-250.

11. Matsumori N, Yamaji N, Matsuoka S, Oishi T, Murata M. Amphotericin B covalent dimers forming sterol-dependent ion-permeable membrane channels. J Am Chem Soc 2002 24;124(16):4180-1.

12. Gianferrara T, Bergamo A, Bratsos I, Milani B, Spagnul C, Sava G, Alessio E. Ruthenium-porphyrin conjugates with cytotoxic and phototoxic antitumor activity. J Med Chem 2010;53(12).

13. Kang SO, Powell D, Day VW, Bowman-James K. Trapped bifluoride. Angewandte Chemie-International Edition 2006;45(12):1921-5.

14. Deng B, Beingessner RL, Johnson RS, Girdhar NK, Danumah C, Yamazaki T, Fenniri H. Covalent capture of self-assembled rosette nanotubes. Macromolecules 2012;45(17):7157-62.

15. Schneider HJ, Wang MX. Supramolecular chemistry .50. dna interactions with porphyrins bearing ammonium side-chains. J Org Chem1994;59(24):7473-8.

Chapter 3: The synthesis of calix[4]pyrroles

3.1 Introduction

Calix[4]pyrroles are an interesting potential replacement for porphyrins as potential inhibitors of the tetrameric Kv1 channels since they possess a similar fourfold scaffold to porphyrins and are not photocytotoxic.

Calix[4]pyrroles, previously named meso-octaalkylporphyrinogens, are macrocycles bearing four pyrrole entities linked via four dialkylsubstituted sp^3 hybridised carbons. Similar to porphyrin macrocycles they are linked at the α position. The main distinction between a calix[4]pyrrole and a porphyrin is the hybridisation number at the meso position. The calix[4]pyrrole is prepared by the condensation of a ketone with pyrrole.

It was the goal of this work to translate the findings of the porphyrin SAR study to the calix[4]pyrrole scaffold, that is to introduce a series of both phenylalkylaminoamides and alkylaminoamides into the meso positions of the calix[4]pyrroles thus replicating the same substitution patterns as the porphyrin series of compounds.

3.1.1 Synthetic approaches to synthesising calix[4]pyrrole macrocycles

The general methods that have been employed for the synthesis of calix[4]pyrroles are the [1+1+1+1] condensation (scheme 3.1) and the [2+2] condensation (scheme 3.2). The one pot synthesis of a calix[4]pyrrole involves the condensation of pyrrole and ketone in a 1:1 ratio in the presence of an acid catalyst. The acid catalysts commonly used include hydrochloric acid [1], methanesulfonic acid[2], boron trifluoride diethyl etherate[3] and trifluoroacetic acid[4]. Others include ytterbium(III) triflate, bismuth nitrate and amberlyst resin.
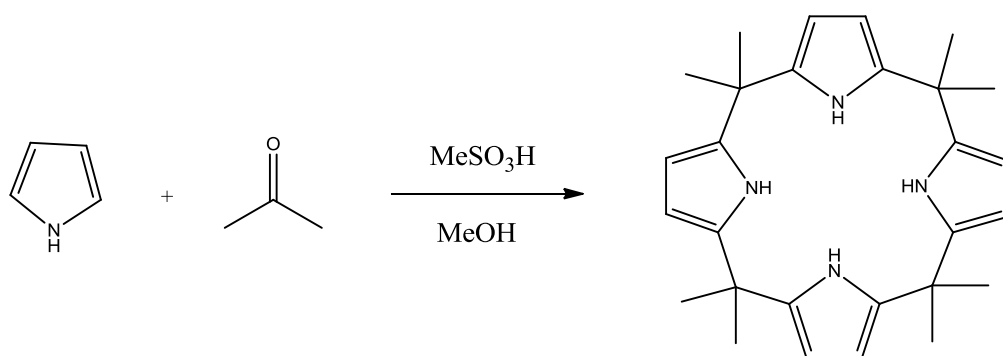
Scheme 3.1: Simple [1+1+1+1] condensation involving pyrrole and the symmetric ketone acetone[2].
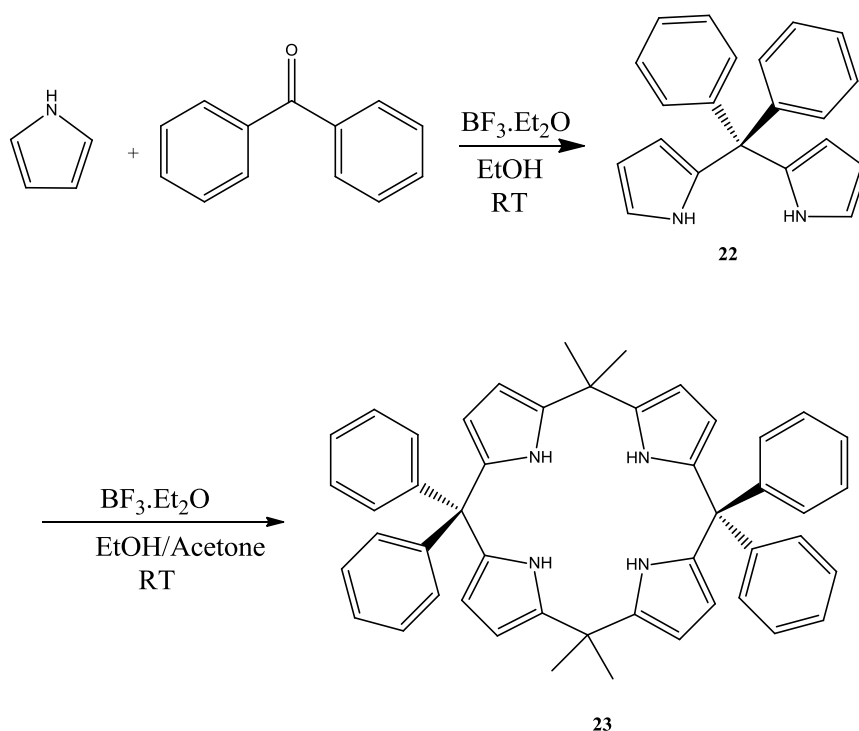
Scheme 3.2: [2+2] condensation for the preparation the asymmetric calix[4]pyrrole **23**.

3.1.2 Calix[4]pyrrole functionalization

There are two possible positions in a calix[4]pyrrole scaffold that can be potentially functionalised.[5] The meso position and the β-position (C-rim) shown in figure 3.1. The synthetic route to modifying the meso position is limited. The modification of the C-rim (β-position) has more variety as functionalization can be made via condensation or post macrocycle condensation.
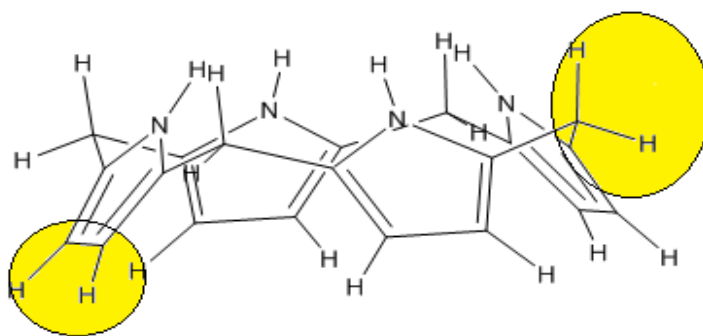
Figure 3.1: Illustration of the possible positions available for modification at the meso and C-rim positions in the calix[4]pyrrole.

Halogenation with fluorine, chlorine or bromine and the incorporation of methoxy[6] substitiuents have been used to replace the hydrogen's on the β-pyrroles. When fluorine has been the halogen of choice the method of synthesis used has been a direct condensation between 3,4-difluoro-1H-pyrrole and acetone using methanesulphonic acid as the catalyst.[7]

3.2 Objective of chapter

It was the goal of this chapter to translate the findings of the porphyrin SAR study to the calix[4]pyrrole scaffold, that is we wished to introduce a series of both phenylalkylaminoamide and alkylamino substituents into the meso positions and C-rim of the calix[4]pyrroles thus replicating the same substitution patterns as the porphyrin series of compounds (figures 3.2-3.5).

Figure 3.2: An example of one of the alkylamino targets **24.**

Figure 3.3: An example of the calix[4]pyrrole **25** required to prepare the phenylalkylaminoamide series of compounds**.**

26

Figure 3.4: Required C-rim modified starting precursor **26** for the preparation of alkylaminoamide substituted calix[4]pyrroles**.**
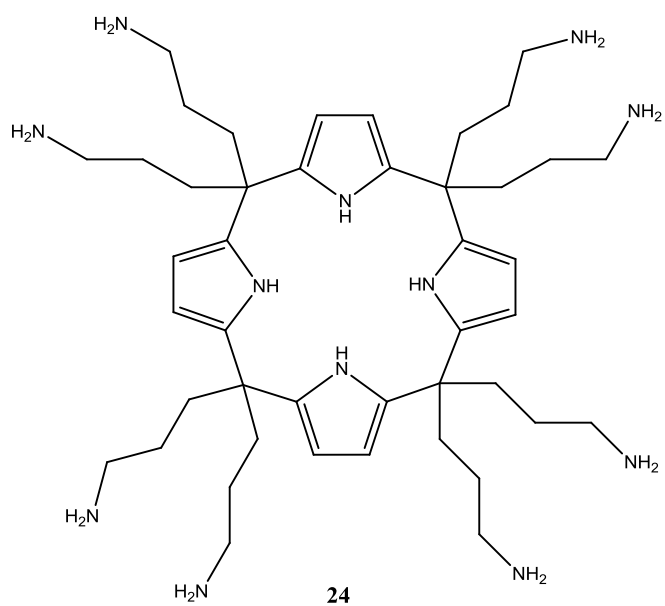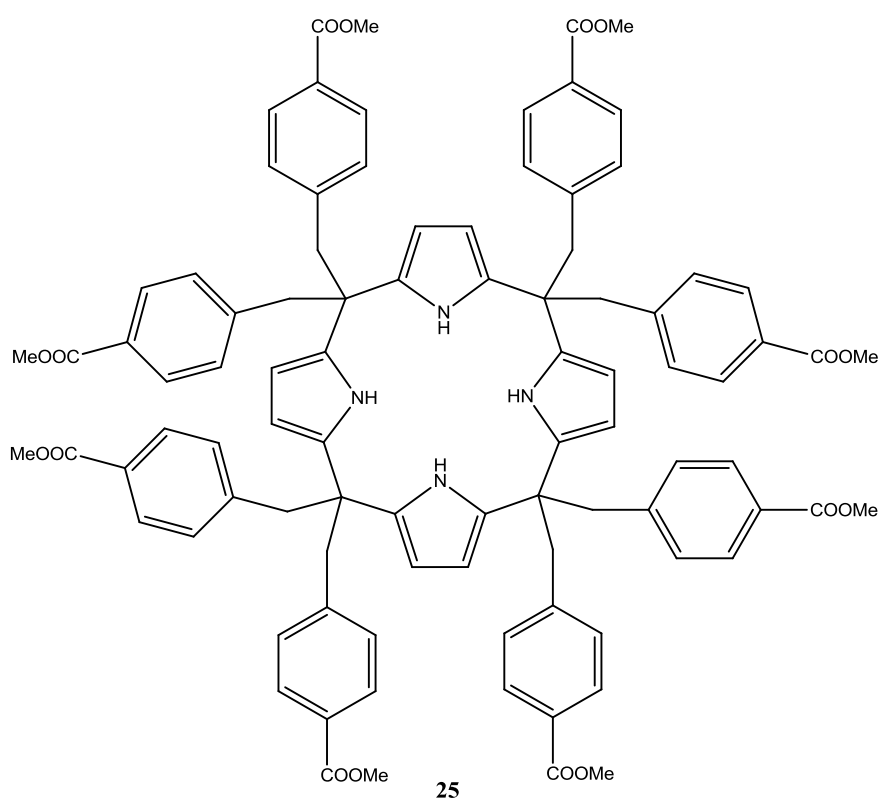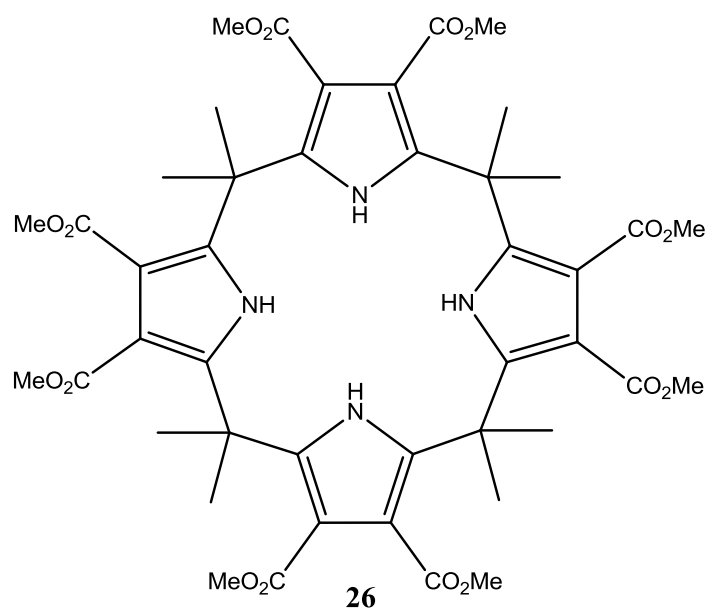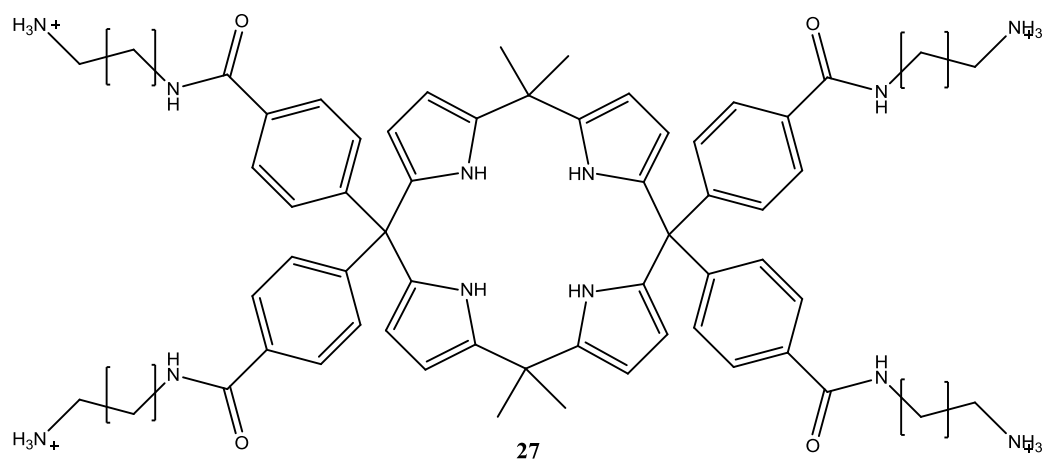

27

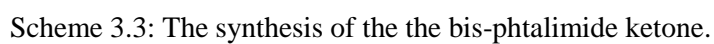Figure 3.5: Target molecule from the carboxylic acid derivative **27.**

3.3 Results and Discussion

3.3.1 Synthesis of meso-octapropylamino-calix[4]pyrrole

The synthetic strategy employed to synthesize **24** (shown in figure 3.2) required the corresponding starting ketone 1,7 diaminoheptan-4-one to be synthesised first as this ketone was not commercially available (scheme 3.3).

The preparation of 1,7 diaminoheptan-4-one involved treating dicyclopropylketone with HCl gas (HCl gas was prepared by the slow, dropwise addition of H_2SO_4 to aqueous HCl in a closed system with a cannula transferring the gas through to the neat ketone for an hour) to obtain a brown oil in quantitative yield. The reaction progression was monitored by ^{1}H NMR. It was essential to maintain a stream of HCl gas bubbling through the neat ketone to drive the reaction to completion. The product formed, 1,7-dichloroketone is extremely unstable and begins to decompose once made thus the use of this substrate for further modification must be done in-situ.

The 1,7 dichloroketone was treated with potassium phthalimide in DMF at 90 ^{o}C to obtain the bis-phthalimide ketone derivative. The reaction of the dichloroketone with potassium phthalimide produces two products. There is a competitive decomposition product formed parallel to the bis-phthalimide ketone formation due to the unstable nature of the precursor. As a result column chromatography on silica is required. The products were separated by column chromatography on silica using ethyl acetate and hexane (1:1) to yield the target ketone in 55%. It should be noted that the Gabriel synthesis approach, of using potassium phthalimide to introduce the amine functionality, was favoured over bubbling ammonia gas through the dichloroketone as the generated amine would have the potential to cyclise to the corresponding imine.

Scheme 3.3: The synthesis of the the bis-phtalimide ketone.

With the ketone obtained it was then condensed with pyrrole, with the phthalimide protection groups still present, as shown in scheme 3.4.

Scheme 3.4: Attempted synthesis of the octa-phthalimide calix[4]pyrrole.

The results of the attempted condensation, under various conditions, are shown in table 3.1. Using $BF_3.(OEt)_2$, $MeSO_3H$ and (aq) HCl as acid catalyst and $MeOH/CH_2Cl_2$ as solvent the condensations did not proceed at either room temperature or reflux. It was necessary to carry

out these reactions in a mix of solvents due to the insolublity of the ketone in methanol. Analysis of the reactions only showed unreacted **ketone**. The inability of the ketone to form calix[4]pyrrole may be a result of the steric bulk of the phthalimide groups.

Table 3.1: Reaction table of the conditions used for the condensation between the bis-phthalimide and pyrrole.

Solvent	Acid Catalyst	Temperature	Reaction progression
MeOH/CH$_2$Cl$_2$	BF$_3$.(OEt)$_2$	RT	No Rxn
MeOH/CH$_2$Cl$_2$	MeSO$_3$H	RT	No Rxn
MeOH/CH$_2$Cl$_2$	HCl	RT	No Rxn
MeOH/CH$_2$Cl$_2$	BF$_3$.(OEt)$_2$	50 $^{\circ}$C	No Rxn
MeOH/CH$_2$Cl$_2$	MeSO$_3$H	50 $^{\circ}$C	No Rxn
MeOH/CH$_2$Cl$_2$	HCl	50 $^{\circ}$C	No Rxn

3.3.2 Synthesis of octa-methlenephenylmethyl carboxylate

The proposed synthesis of compound **25** was investigated, however it has been previously reported that diarlyketones do not form calix[4]pyrroles due to steric constrains, but rather produce dipyrromethanes as shown in scheme 3.5.[15]
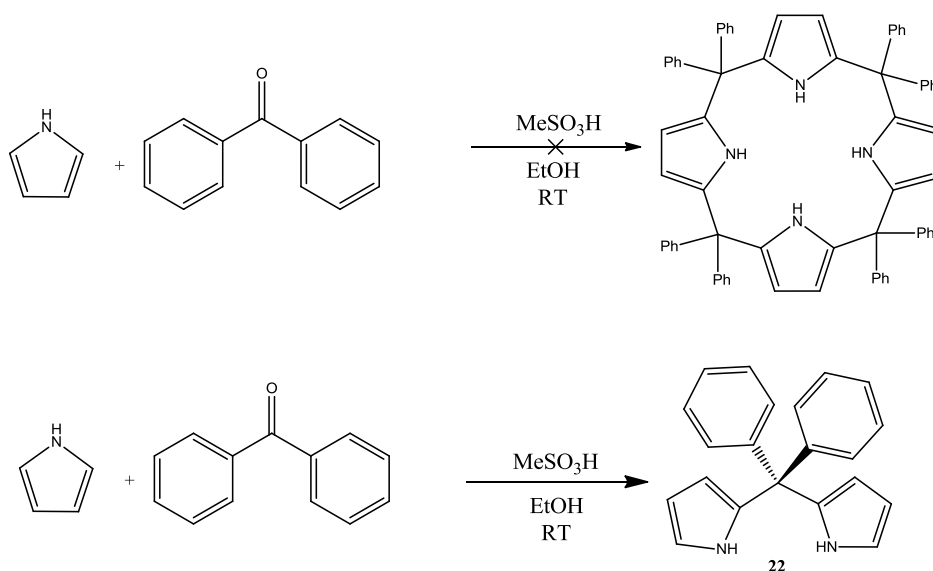
Scheme 3.5: The condensation of pyrrole with bezophenone typically yields **22** over the calyx[4]pyrrole.

An attempt to prepare the target tetra-aryl calix[4]pyrrole outlined in scheme 4.5 from benzophenone failed to give the target macrocycle however, the bispyrrole was isolated in good yields. Thus, benzophenone derivatives fail to condense to calix[4]pyrrole. An alternative to using benzophenone derivatives are dibenzylketones and it has been previously shown that calix[4]pyrrole can be prepared from dibenzylketone and pyrrole using MeSO$_3$H as an acid catalyst[8,9] (scheme 3.6) in 32% yield.
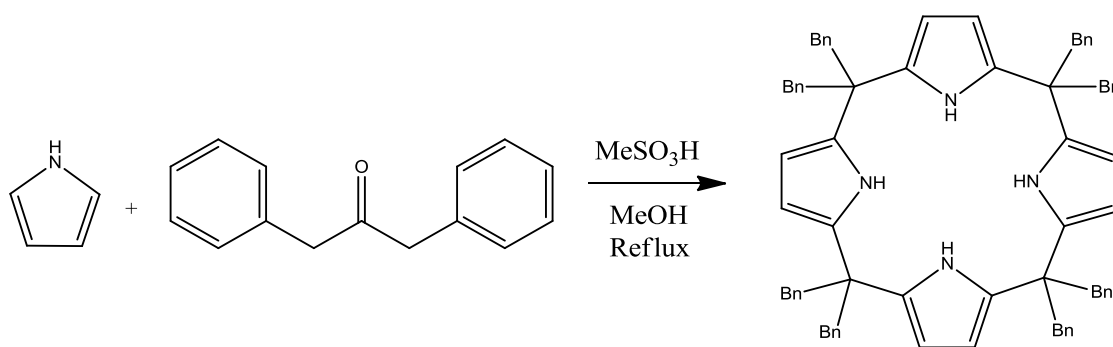
Scheme 3.6: Synthesis of meso-octabenzylcalix[4]pyrrole.[8]

The same condensation conditions were attempted with 4,4-dibenzylmethylcarboxylate ketone as outlined in scheme 3.7. 4,4-Dibenzylmethylcarboxylate was prepared using the method of Potter *et al*[10] to yield a yellow solid in 59% yield.
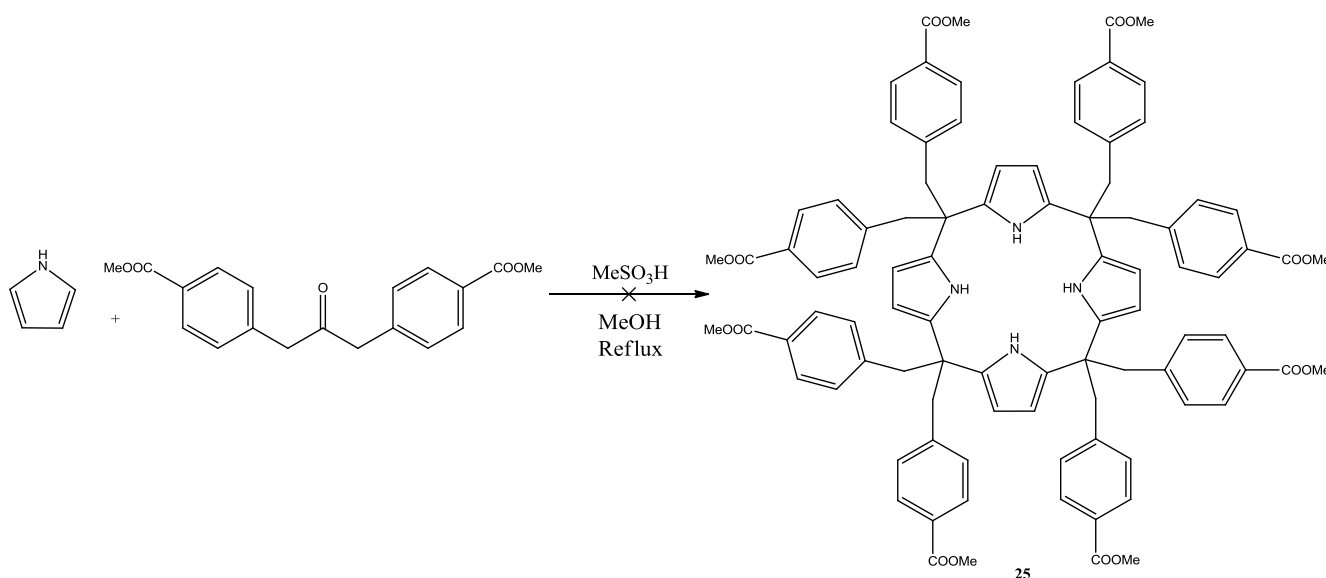
Scheme 3.7: Attempted condensation between pyrrole and 1,3-bis-(4-(methoxycarbonyl)phenyl)-propan-2-one **25**.

104

Unfortunately, these conditions failed to yield **25**. A tar-like material was obtained after the reaction was worked up. Column chromatography of the crude reaction material did not yield the target **25**.

3.4 C-rim modification

Introduction of functionality into the calix[4]pyrrole may also be achieved by C-rim modification. The Sessler group have been pioneers in calix[4]pyrrole synthesis and have developed a method for the introduction of functional groups, such as carboxylic acids and esters, involve the deprotonation of the pyrrole hydrogen of the macrocycles at low temperature with n-BuLi in hexanes followed by addition of CO_2(s) or ethyl bromoacetate.[6, 11, 12] However, octa-substitution has never been achieved using this approach. C-rim octasubstituted calix[4]pyrroles have been successfully prepared using 3,4-alkyl carboxylate pyrroles and trioxane with TFA as the acid catalyst.[14]

3.4.1 Synthesis of the C-rim condensed octa methylcarboxylate-calix[4]pyrrole

3,4-Dimethyl carboxylate pyrrole was prepared using a modified version of the method developed by Woo *et al.*[13] To a solution of dimethyl fumarate and 60% sodium hydride stirring in DMF at 0 ^{o}C, toluenesufonylmethyl isocyanide (TosMIC) was added dropwise. After stirring for 15 minutes at 0 ^{o}C the reaction mixture was poured onto ice-water. The resulting precipitate was filtered and dried to give a yellow solid in 55% yield.

.
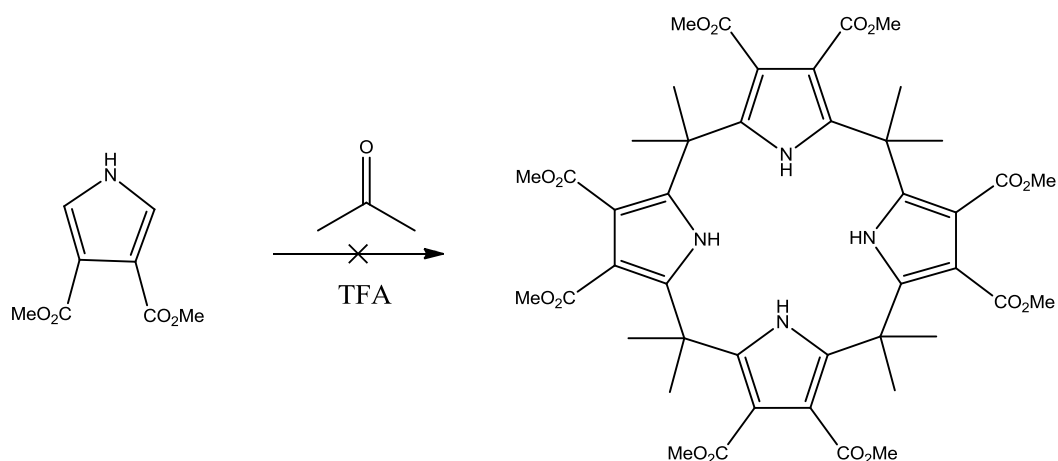
Scheme 3.8: Synthesis of octa- substitutedcalix[4]pyrroles using TFA acetone.

The application of the procedure shown in scheme 3.8 using dimethyl pyrrole-3,4-dicarboxylate and acetone was performed. The reaction was refluxed for 24 hours where full conversion of the pyrrole was consumed. Column chromatography of the crude material on silica gel and using ethyl acetate: hexane (1:6) was applied and three factions isolated. The reaction mixture again did not yield the target calix[4]arene target, however a number of linear oligomers were obtained.

3.5 Synthesis of the asymmetric calix[4]pyrrole

A possible route to the preparation of an asymmetric calix[4]pyrrole **27** is outlined in scheme 3.9 where a di-tolyldipyrromethane is condensed with dry acetone in the presence of an acid catalyst.
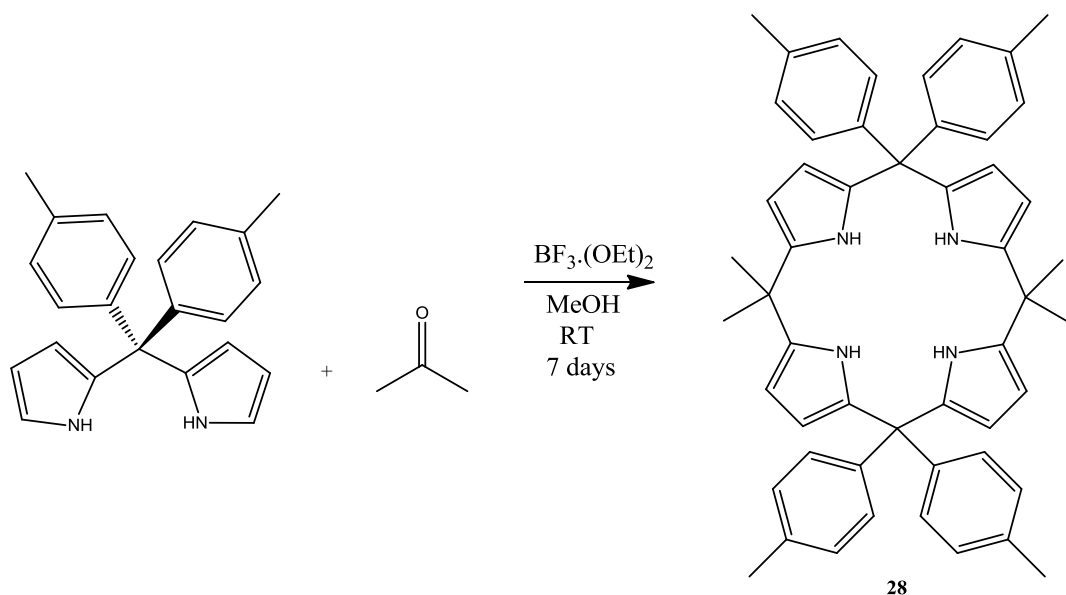
Scheme 3.9. Synthesis of meso-1,1,3,3-tetratolyl-meso-2,2,4,4-tetramethylcalix[4]pyrrole, **28**.

The di-tolyldipyrromethane was prepared, pyrrole was condensed with 4,4 dimethylbenzophenone and $BF_3.(OEt)_2$ as an acid catalyst for 5 days, after five days the precipitated material was filtered and washed with 3x10 mL aliquots of cold MeOH. The product shown in scheme 3.10 is the di-tolyldipyrromethane (**29**) obtained in 50% yield.
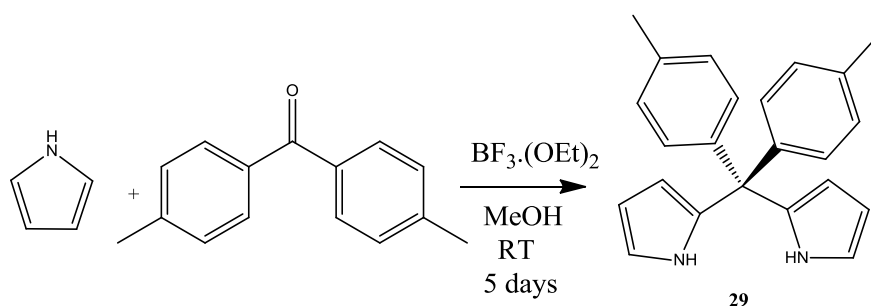
Scheme 3.10: Synthesis of di-tolyldipyrromethane **29**.

The di-tolyldipyrromethane starting material was initially insoluble in methanol (and ethanol) as reaction solvent, however, the dropwise addition of acetone started to solubilise the dipyrromethane. Both the $BF_3 \cdot (OEt)_2$ and methanesulphonic acid ($MeSO_3H$) were used as acid catalysts in separate reactions to compare yields. For both catalysts the reaction turned a lime green colour upon dropwise addition of catalyst to either reaction. The reactions were kept under an argon atmosphere and left to react for 7 days at room temperature with stirring.

The reactions turned a dark brown and a small amount of light brown coloured precipitate started to form, as the reaction progressed. The reaction was stopped after 7 days, and the solvents removed under vacuum. A mobile phase of 1:1 CH_2Cl_2: hexane was used to purify the resulting calix[4]pyrrole (scheme 3.9).

Comparison of both catalysts showed that $BF_3.(OEt)_2$ gave higher yields than $MeSO_3H$. In the literature, there are yields reported for a similar calix[4]pyrrole (with phenyl groups) at 20% for $MeSO_3H$ and 56% for $BF_3 \cdot (OEt)_2$. One of the reasons for the low yields exhibited in these reactions is the fact that they are multi-component condensations which can produce a series of different products, this was observed by TLC where multiple spots were observed during the course of both reactions.

3.5.1 ^{1}H NMR of meso-1,1,3,3-tetratolyl-meso-2,2,4,4-tetramethylcalix[4]pyrrole (28)

The ^{1}H NMR spectrum of **28** is shown in figure 3.6. The protons associated with the NH from the pyrrole are located as a broad singlet at 7.35 ppm, and integrate as 4. The phenyl hydrogens show as two doublets at 7.0 and 6.9 ppm and integrate as 8 respectively. The β-pyrrole hydrogens appear as multiplets at 5.9 and 5.7 ppm, each with an integration of four. The singlet peak at 2.3 ppm represents the methyl hydrogens of the toluyl group with an integration of 12. The final singlet peak in the spectrum is the aliphatic methyl substituents which have an integration of 12.
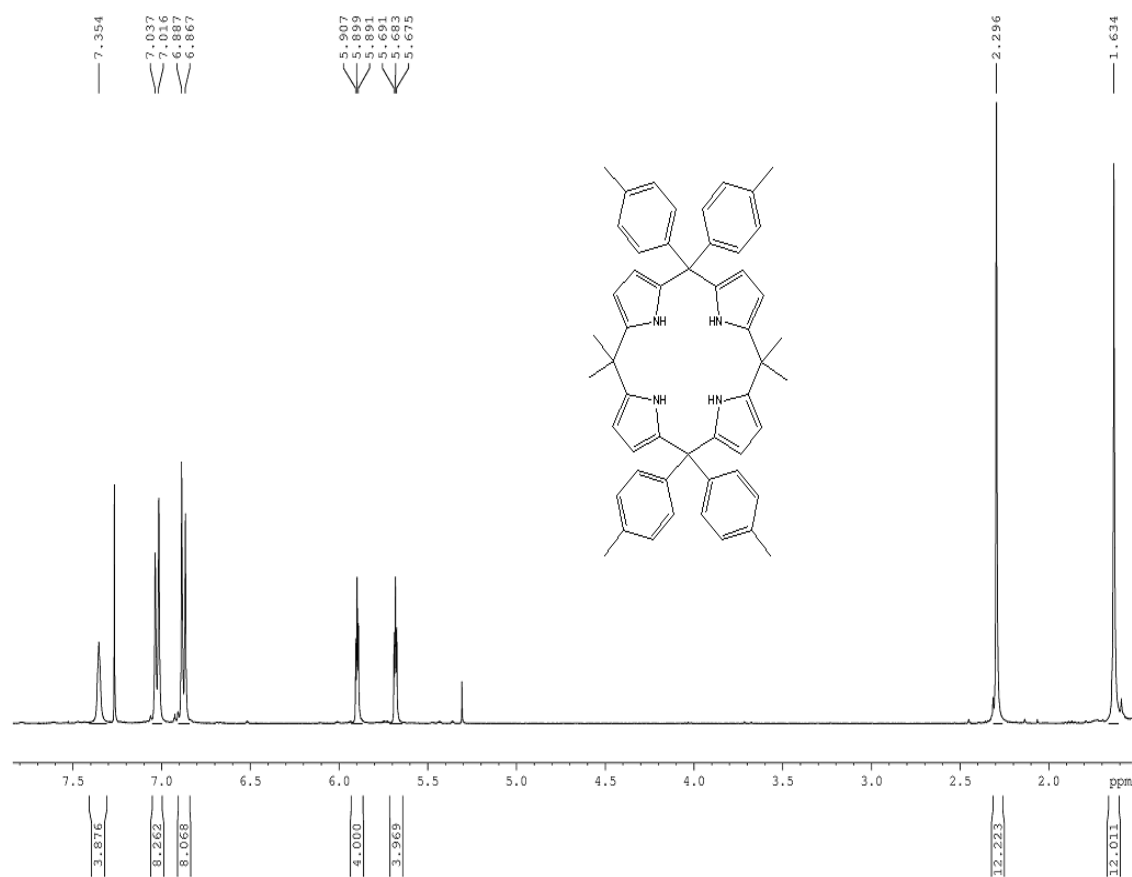
Figure 3.6: ^{1}H NMR of **28** in CDCl$_3$.

3.5.2 Oxidation of 28.

Attempts to synthesize calix[4]pyrroles with functionality have resulted in unsuccessful macrocycle condensation. The main goal was to introduce a carboxylic acid into the calix[4]pyrrole either pre or post condensation via the conventional [1+1+1+1] condensation. An alternative strategy was undertaken whereby **28,** bearing toluene substituents, would be oxidised to the corresponding acids post cyclisation (scheme 3.11).

Scheme 3.11: Oxidation of **28** to the corresponding carboxylic acid **30**.
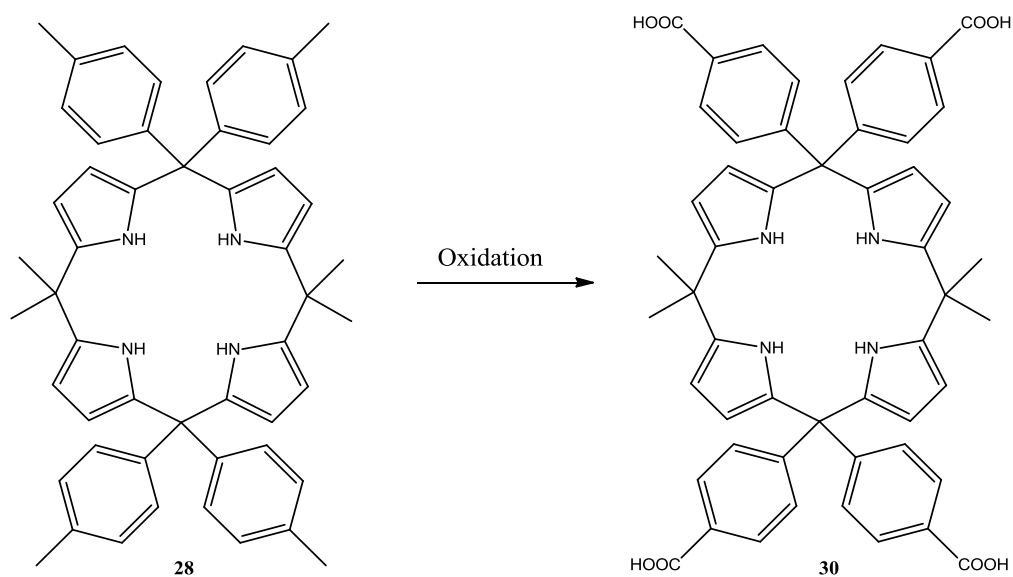
A variety of classical methods were used in the attempt to oxidise **28** to **30** the results of which are shown in Table 3.2. All reactions yielded a complex mixture.

Table 3.2: List of oxidation conditions employed on **28.**

Oxidant	Temperature	Time	Catalyst	Solvent
$KMnO_4$	Reflux	24 hours	Pyridine	H_2O
$KMnO_4$	Reflux	48 hours	Pyridine	H_2O
$KMnO_4$	Reflux	5 days	Pyridine	H_2O
$Na_2Cr_2O_7$	(250^oC) autoclave	5 hours	Pyridine	H_2O
$Na_2Cr_2O_7$	(250^oC) autoclave	10 hours	Pyridine	H_2O
$Na_2Cr_2O_7$	(250^oC) autoclave	20 hours	Pyridine	H_2O
$Mn(OAc)_2/Co(OAc)_2$ H_2O_2 O_2	RT	24 hours	NaBr	Acetic acid
O_2, hv	RT	24 hours	CBr_4	EtOH

Table 3.2 shows the failed attempts at oxidation of **28** to **30**. Analysis of the reactions by ^{1}H NMR showed consistant decomposition of the pyrrole hydrogens on the macrocycle for all reactions. FT-IR did show that partial oxidation had occurred, as characteristic peaks for COOH groups were present, however the macrocycle could not withstand any of the oxidation conditions used and as a result the target molecule **30** could not be prepared by oxidative methods. At this point the calix[4]pyrrole work was abandoned.

3.6 Conclusion

The attempts to synthesize a calix[4]pyrrole with multiple carboxylic acids or hydrolystable esters via [1+1+1+1] condensation or [2+2] condensations proved unsuccessful. Macrocycle formation proved to be extremely sensitive with carbonyl functionality in the ketone or pyrrole positions. Oxidation of the macrocycle post condensation also proved to be unsuccessful as the instability of the asymmetric calix[4]pyrroles led to unwanted side reactions on the pyrrole scaffold thus leading to decomposition of the macrocycle. It would have been valuable to the study the effect of the target calix[4]pyrroles vs the porphyrins on the Kv1 channels. Work on the calix[4]pyrroles was stopped at this point.To go to the next stage of the project, that being the development of a new non photocytotoxic small molecule inhibitor, a molecular modelling analysis was undertaken using Accelerys discovery studio. Docking simulations were performed using the results from the porphyrin SAR study to better understand the interaction of the porphyrin with the Kv1 channels. These results will then be used to aid in the design of new potential, selective inhibitors of Kv1 channels.

3.7 Experimental

Materials

All operations were carried out under an atmosphere of argon or nitrogen using standard Schlenk techniques. All solvents were supplied by the Aldrich Chemical Company and TCI. Dichloromethane was dried over $MgSO_4$ prior to use. Methanol was distilled over magnesium turnings and iodine before use. All organic reagents were purchased from the Aldrich Chemical Company. Pyrrole was freshly distilled over potassium hydroxide before use. Anhydrous triethylamine, borontrifluoride diethyletherate and were all used without further purification.

Column chromatography was carried out using neutral silica gel (Merck, used as received). All mobile phases for column chromatography were dried over $MgSO_4$ prior to use. All solvents were deoxygenated by purging withargon or nitrogen for ~10 minutes

Equipment

All syntheses involving air- and moisture-sensitive reagents were performed in oven or flame dried glassware. NMR spectra were recorded on a Bruker model AC 400 MHz spectrometer and Bruker model ANC 600 MHz spectrometer using $CDCl_3$ as solvent. All NMR spectra were calibrated according to the residual solvent peak, i.e. $CHCl_3$ at 7.26 ppm DMSO-d_6 2.50 ppm for all ^1H spectra and 77.16 ppm and 39.52 ppm for all ^{13}C spectra. Chemical shifts are given in parts per million (ppm).

General procedure for the preparation of di-(4-methyl phenyl)di-(2-pyrrolyl)methane (29)

To a clean, dry 500 mL two necked round bottom flask were added dry methanol (300 mL) and 4,4-dimethylbenzophenone (7.8224 g, 0.0372 mol, 1 eq.). Freshly distilled pyrrole (6.452 mL, 0.093 mol, 2.5 eq.) was added to the flask via syringe. $BF_3 \cdot OEt_2$ (6.4 mL, 0.0518 mol, 1.4 eq.) was then added to the reaction dropwise via syringe. The reaction was kept under an argon atmosphere and stirred for 5 days at room temperature.

The precipitated product was filtered through a frit, washed with cold methanol and dried under vacuum overnight. 5.97 g (50% yield) of the grey powder was obtained.

^{1}H NMR (600 MHz, DMSO-d_6): δ = 10.02 (br.s, 2H, N-H), 7.04 (d, 4H, aryl-H), 6.81 (d, 4H, aryl-H), 6.70 (m, 2H, pyrrole-H_α), 5.90 (m, 2H, pyrrole-H_β), 5.53 (m, 2H, pyrrole-H_β), 2.30 (s, 6H, CH_3).

^{13}C NMR (150.9 MHz, DMSO): δ = 143.6, 135.7, 135.1, 129.0, 127.9, 117.9, 108.7, 106.0, 54.6, 20.5

General procedure for the preparation of *meso*-1,1,3,3-tetramethyl,-2,2,4,4-tetra(4-methyl phenyl)calix[4]pyrrole (20):

To a clean, dry 250 mL two necked round bottom flask were added dipyrromethane (0.718 g, 2.2 mmol, 2 eq.) dry methanol (60 mL), and dry acetone (60 mL, 2 eq.) $BF_3 \cdot OEt_2$ (300 μL, 2.4 mmol, ~2 eq.) was added to the reaction dropwise via syringe. The reaction was kept under an argon atmosphere and stirred for 7 days at room temperature. Solvents were removed under vacuum. The crude solid was purified by column chromatography over silica using a 50: 50 CH_2Cl_2: Hexane mobile phase. R_f value of 0.46 were kept and combined, and the solvents removed under vacuum to yield 0.288 g (36% yield) of the calix[4]pyrrole.

^{1}H NMR (400 MHz, CDCl$_3$): δ = 7.32 (br.s, 4H, N-H), 7.03 (d, 8H, aryl-H), 6.87 (d, 8H, aryl-H), 5.90 (t, 4H, pyrrole-H_β), 5.68 (t, 4H, pyrrole-H_β), 2.30 (s, 12H, Tol-CH_3), 1.65 (s, 12H, CH_3).

^{13}C NMR (100.6 MHz, CDCl$_3$): δ = 144.0, 139.3, 135.7, 134.5, 128.7, 128.4, 109.1, 102.8, 54.7, 35.2, 29.3, 21.0.

3.8 References

1. Shao SJ, Wang AQ, Yang M, Jiang SX, Yu XD. Synthesis of meso-aryl-substituted calix[4]pyrroles. Synthetic Communications 2001;31(9):1421-6.

2. Blangy V, Heiss C, Khlebnikov V, Letondor C, Stoeckli-Evans H, Neier R. Synthesis, structure, and complexation properties of partially and completely reduced meso-octamethylporphyrinogens (calix[4]pyrroles). Angewandte Chemie-International Edition 2009;48(9):1688-91.

3. Lee CH, Lee JS, Na HK, Yoon DW, Miyaji H, Cho WS, Sessler JL. Cis- and trans-strapped calix[4]pyrroles bearing phthalamide linkers: Synthesis and anion-binding properties. J Org Chem 2005;70(6):2067-74.

4. Smithen DA, Cameron TS, Thompson A. One-pot synthesis of asymmetric annulated bis(pyrrole)s. Org Lett 2011;13(21):5846-9.

5. Sessler JL, Anzenbacher P, Jursikova K, Miyaji H, Genge JW, Tvermoes NA, Allen WE, Shriver JA, Gale PA, Kral V. Functionalized calix[4]pyrroles. Pure and Applied Chemistry 1998;70(12):2401-8.

6. Gale PA, Sessler JL, Allen WE, Tvermoes NA, Lynch V. Calix[4]pyrroles: C-rim substitution and tunability of anion binding strength. Chemical Communications 1997(7):665-6.

7. Anzenbacher P, Try AC, Miyaji H, Jursikova K, Lynch VM, Marquez M, Sessler JL. Fluorinated calix[4]pyrrole and dipyrrolylquinoxaline: Neutral anion receptors with augmented affinities and enhanced selectivities. J Am Chem Soc 2000;122(42):10268-72.

8. Bonomo L, Solari E, Scopelliti R, Floriani C. The pi complexation of alkali and alkaline earth ions by the use of meso-octaalkylporphyrinogen and aromatic hydrocarbons. Chemistry-a European Journal 2001;7(6):1322-32.

9. Allen WE, Gale PA, Brown CT, Lynch VM, Sessler JL. Binding of neutral substrates by calix[4]pyrroles. J Am Chem Soc 1996;118(49):12471-2.

10. Potter RG, Hughes TS. Synthesis of poly(para-phenylene)(2-isocyano-2-tosylpropane-1,3-diyl), poly(para-phenylene)(2-oxopropane-1,3-diyl) and oligo(cyclopentadienones) via carbonylative coupling of alpha,alpha '-dibromoxylene. Chemical Communications 2007(44):4665-7.

11. Anzenbacher P, Jursikova K, Shriver JA, Miyaji H, Lynch VM, Sessler JL, Gale PA. Lithiation of meso-octamethylcalix[4]pyrrole: A general route to C-rim monosubstituted calix[4]pyrroles. J Org Chem 2000;65(22):7641-5.

12. Miyaji H, Anzenbacher P, Sessler JL, Bleasdale ER, Gale PA. Anthracene-linked calix[4]pyrroles: Fluorescent chemosensors for anions. Chemical Communications 1999(17):1723-4.

13. Woo JS, Sigurdsson ST, Hopkins PB. Dna interstrand cross-linking reactions of pyrrole-derived, bifunctional electrophiles - evidence for a common target site in dna. J Am Chem Soc 1993;115(9):3407-15.

14. Uno H, Inoue K, Inoue T, Ono N. Oligocyclization of 2-(hydroxymethyl)pyrroles with electron-withdrawing groups at beta-positions: Formation and structural elucidation of porphyrinogens and hexaphyrinogens. Organic & Biomolecular Chemistry 2003;1(21):3857-65.

15. Turner B, Botoshansky M, Eichen Y. Extended calixpyrroles: Meso-substituted calix[6]pyrroles. Angewandte Chemie-International Edition 1998;37(18):2475-8.

16. Turner B, Shterenberg A, Kapon M, Suwinska K, Eichen Y. The role of template in the synthesis of meso-hexamethyl-meso-hexaphenyl- calix[6] pyrrole: Trihalogenated compounds as templates for the assembly of a host with a trigonal cavity. Chemical Communications 2002(5):404-5.

17. Maxwell BD. The radiolabeled syntheses of JV 485, a herbicide candidate for winter wheat. Journal of Labelled Compounds & Radiopharmaceuticals 2000;43(7):645-54.

18. Hirashima S, Nobuta T, Tada N, Miura T, Itoh A. Direct aerobic photo-oxidative synthesis of aromatic methyl esters from methyl aromatics via dimethyl acetals. Org Lett 2010;12(16):3645-7.

Chapter 4: The construction of Kv1.1 comparative model

4.1 Introduction

Drug discovery is a laborious, expensive process. The method by which therapeutics are traditionally discovered relies on clusters of interdisciplinary teams, who first identify a class of compound, by screening the target. Then by synthesizing a large library of these compounds with minor derivatives and then screening of these compounds against the biological target. The activity profile is established and the 'hit candidate' is selected and further optimised and pre-clinical/clinical trials follow.[1]

The arrival of improved computational hardware and software, united with an increase in the number of available protein 3D structures from the protein database[2] has enabled molecular modelling to contribute and be an excellent component of modern drug discovery. The pivotal benefit of introducing molecular modelling into a drug discovery pipeline is to move away from traditional "trial and error" approaches such as large synthetic library constructions, and consider moving towards rational drug design, resulting in a reduction of the cost and time.

The various rational drug design techniques can be applied across the drug discovery pipeline from the initial hit identification, to hit to lead optimization.[3] Lead optimization can be used in a synergic relationship with experiment through synthesis, modelling and testing. Computational software approaches include both structure based[4,5] and ligand based[6] drug design (SBDD and LBDD). Structure based approximations such as molecular docking utilize the available information on the protein's 3-D structure and are used to aid in the prediction of the binding pose and interactions of proposed ligands with the protein target. Ligand based methods take advantage of the available information of known active ligands e.g. pharmacophores, the steric and electronic features that are necessary to ensure the various key intermolecular interactions with a specific biological target and to administer the corresponding biological response.

Once a computational model has been developed using Accelry's Discovery Studio 3.5- 4.0 virtual screening (VS) processes can be implemented to examine large compound databases *in silico* and to identify a selected number of molecules for *in vitro* testing. Such virtual high throughput screens (vHTS) allow the key interactions that are associated with biological activity of a large number of compounds to be studied without the need to synthesize them in the laboratory which can be tedious depending on the class of organic

molecules needed for the project. The approach can be cheaper, faster, and safer than real experiments, and the data can help scientists to eliminate the uninteresting compounds that would not perform the required function.

In chapter two we built a foundation for the project based upon the results obtained for the porphyrins. Following this work in chapter three, it was suggested that the synthesis of calix[4]pyrroles with potential amide functionality could serve as a suitable replacement for a porphyrin as the elimination of conjugation and photocytotoxicity is achieved. The issue with using calix[4]pyrroles as a drug is its large molecular weight. Having a compound with large molecular weight has a number of problems; the first problem is it has little drug-like oral bioavailability as it does not fall under the Lipinski pharmacokinetic guidelines.[7,8] The second reason and probably the most important, is the number of non-specific interactions the calix[4]pyrrole would encounter due to its size. Similar to the porphyrin, the size and number of potential interactions the calix[4]pyrrole can have with residue amino acids such as H-bonding, π-π stacking can hinder the use of the scaffold. Lastly, the compounds we wish to use for the probing of the channels are synthetically challenging. The Kv1 channel sequences, shown in figure 4.1, highlights the high similarity between the channels Kv1.1-1.6. A large molecule such as a porphyrin/calix[4]pyrrole would have unwanted interactions and this is believed to be the reason for the lack of selectivity between the channels. A molecule that shows excellent inhibition is relativity ineffective without the high selectivity for the channel of interest. 4-Aminopyridine as discussed earlier has no selectivity for the channels and the patient experiences the associated side effects of the drug because of this lack of selectivity.[9]

Kv1.1 (348–386): E A E C A E S H F S S I P D A F W W A V V S M T T V G Y G D M Y P V T I G G K

Kv1.2 (350–388): E A D E R D S Q F P S I P D A F W W A V V S M T T V G Y G D M V P T T I G G K

Kv1.3 (373–411): E A D D P S S G F N S I P D A F W W A V V T M T T V G Y G D M H P V T I G G K

Kv1.4 (501–539): E A D E P T T H F Q S I P D A F W W A V V T M T T V G Y G D M K P I T V G G K

Kv1.6 (398–436): E A D D V D S Q F P S I P D A F W W A V V T M T T V G Y G D M Y P M T V G G K

Figure 4.1: The rat Kv1 channels, amino acids identical throughout all channels are shown in yellow, turret region amino acids are shown in blue, selectivity filter amino acids are shown in green and the inner turret residue shown in grey.

Molecular docking studies can aid in the design for synthesis of a new candidate by studies identifying the key interactions with important amino acid residues in the amino acid sequence shown in figure 4.1. By observing how these dock into the channel it is then possible to obtain *in silico* theoretical observations of the spatial orientation of the porphyrin

compound to the channel and the predicted binding affinity. Using this data could aid in the design of a smaller more drug-like molecule that experiences the key interactions whilst eliminating the unwanted interactions. This route could offer the required selectivity for Kv1.1 over the other channels. The main modelling approaches will now be discussed.

4.2 Molecular mechanics

There are two general approaches to computational studies; quantum mechanical (QM) calculations of the molecular electronic structure and molecular mechanical (MM) calculations.[10] The QM approach can have a high degree of accuracy due to the fact this method takes electrons into account, however it is computationally expensive and requires access to supercomputers.[11] Due to this, computational simulations of biological protein macromolecules are more favoured using classical MMs derived from Newtonian theory. This approach considers atoms as balls/spheres with an associated mass.

The force-fields that we utilized within our work for MM calculations used the Chemistry at Harvard Molecular Mechanics CHARMM program that is a component of the accelrys software. The Cdocker algorithm[12] is a grid-based molecular docking method that employs CHARMM.[13]

The total energy (E_{tot}) is a function of the nuclear coordinates. As mentioned above the atoms are considered balls/spheres (the nucleus and electrons collectively), the electrons are not categorically considered and the field they generate is not calculated. The equation that this total energy is based upon is shown where the sum of bond stretching $\upsilon_r(r)$, angle bending $\upsilon_\theta(\theta)$, torsion potentials $\upsilon_\phi(\phi)$, improper torsions $\upsilon_\chi(\chi)$ and non-bonding interactions $\upsilon_{nb}(r)$.[10, 14,15]

$$E_{tot} = \sum \upsilon_r(r) + \sum \upsilon_\theta(\theta) + \sum \upsilon_\phi(\phi) + \sum \upsilon_\chi(\chi) + \sum \upsilon_{nb}(r)$$

Or   (1)

$$E_{steric} = E_{str} + E_{bnd} + E_{tor} + E_{oop} + E_{vdW} + E_{electrostatic}$$

4.2.1 Bonded functions

Energy due to bond stretching.

The interpretation on how the potential energy of a typical bond is represented is derived from harmonic oscillation based on Hookes law. The potential energy is related to the bond state compressed or stretched. (k_r) is the bond stretching constant, the stronger the bond the larger the associated force constant to that particular bond is. The bond length is represented by (r) and the equilibrium bond length (r_0).

$$\upsilon_r(r) = \frac{k_r}{2}(r - r_0)^2$$

(2)

Energy for bond angle bending

The deviation of an angle θ between atoms from the reference angle θ_0 relates to the frequency element of Hookes law. As the angles are bent from its original state the energy increases. The related force constant (k_θ), in the harmonic angle potential are proportionately smaller than for the bonded function. Less energy is needed to distort an angle from equilibrium than to stretch or compress a bond.

$$\upsilon_\theta(\theta) = \frac{k_\theta}{2}(\theta - \theta_0)^2$$

(3)

Energy due to torsional strain

Intramolecular rotations defined as torsional or dihedral angles require energy. These describe the degrees of freedom in a molecule. The dihedral angle is expressed from 1-4 atoms. The presence of barriers to rotation around these chemical bonds is fundamental to understanding the structural properties of molecules and conformational analysis. These torsional energies are defined through cosine expansions.[14]

$$\upsilon_\phi(\phi) = \frac{V_1}{2}[1 + \cos(\phi - \gamma) + \frac{V_2}{2}[1 + \cos(2\phi - \gamma) + \frac{V_3}{2}[1 + \cos(3\phi - \gamma)$$

(4)

Φ is the torsion angle between the atoms of interest; V refers to the barrier height. This value gives qualitative information of the relative barriers to rotation. The phase factor is represented by γ, this determines exactly where the torsion angle passes through the absolute minimum value.

The improper torsion motion is sometimes alternatively shown as the equation 'out-of-plane' bending energy. This is the equation used to select the correct geometry or the chirality of atoms. This type of bonding strain is defined by four atoms i, j, k and l. The middle atom j is covalently bound to the other three atoms i, k and l. The improper angle is thus defined as the angle between jl and the plane (ijk). This is shown in figure 4.1
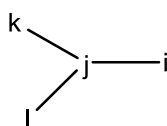
Figure 4.2: Improper torsion around a four atom species

$$\upsilon_\chi(\chi) = k_\chi(\chi - \chi_0)^2$$

(5)

4.2.2 Non bonded functions

Completing the total overall energy equation it is important to incorporate the non-bonding forces that molecules also adhere to, these are mainly van der Waal (vdw) and electrostatic potentials. The non-bonded interations (υ_{nb}) consists of the van der Waal forces defined from the short ranged separations between the atoms (υ_{sr}) the electrostatic potentials are defined from the long ranged weak attractions ($\upsilon_{coulomb}$).

$$\upsilon_{nb} = \upsilon_{sr} + \upsilon_{coulomb}$$

(6)

The short ranged, Lennard-Jones potential is a derived function based upon a non-bonding interaction approximation between a pair of atoms. This potential relates to the short ranged van der Waal forces shown in the above equation. There is a repulsive component (r^{-12}) and an attractive component (r^{-6}). The components together illustrate the behaviour of a pair of atoms that repel each other at short distances and attract each other at longer distances. In equation 7, υ_{sr} is the potential energy that exists between the two non-bonded atoms. Internuclear separation is defined as r. The coefficient A and B determine the depth and location of the energy minima. The mathamatical expression is shown as:

$$\upsilon_{nb} = \upsilon_{sr} + \upsilon_{coulomb}$$

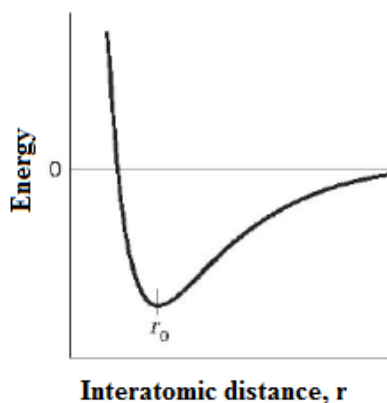$$\upsilon_{sr} = \frac{A}{r^{12}} - \frac{B}{r^6}$$

(7)

Figure 4.3: Van der Waal energy function.

The Lennard-Jones potential is highly dependent on distance. At a certain point non-bonded atom pairs are not believed to contribute to the atom pair interactions as they exceed a finite distance where the forces that govern the variables of the principle are negligible.

$$\upsilon_{nb} = \upsilon_{sr} + \upsilon_{coulomb}$$

$$\upsilon_{coulomb} = \frac{q_1\,q_2}{4\pi\varepsilon_0 r}$$

(8)

The electrostatic interaction component of the non-bonded energy equation allows the calculation of long ranged potentials that the Lennard-Jones is not feasible for. This is based upon Coulombs law. q is defined as the point charges on the atoms, ε_0 is the permittivity of free space and $(4\pi\varepsilon_0)^{-1}$ is a Coulomb constant. These force field calculations will be utilised in the later sections.

4.3 Protein sequence analysis and structure prediction

Section 4.1 discussed the theoretical basis of MM as used in the molecular modelling Accelry's software suite. These are used to determine a wide array of information from molecular conformations to the various interactions between host and guest. The application these methods will be applied during the techniques of comparative modelling and conformational analysis.

The key protein that we are working with is the tetramer of rat Kv1.1. The issue with analysis of the key interaction sites of this protein is it has not been crystallised, as membrane proteins are difficult to express in soluble form, purify and crystallise. As a result a three dimensional (3D) structure of the target Kv1.1 protein was developed from the protein sequence and the known Kv1.2 structure that has been successfully crystallised.[16,17]

4.3.1 Comparative Modelling overview

Homology modelling techniques use the templates of crystallised proteins to aid the prediction of the conformations of other proteins i.e. (Kv1.2; 2A79)[16] from the protein data bank (pdb) can be used to develop homology models[18] of Kv1.1. The resolution of the crystal structure from the pdb Kv1.2; 2A79 is 2.9 Å.[17]
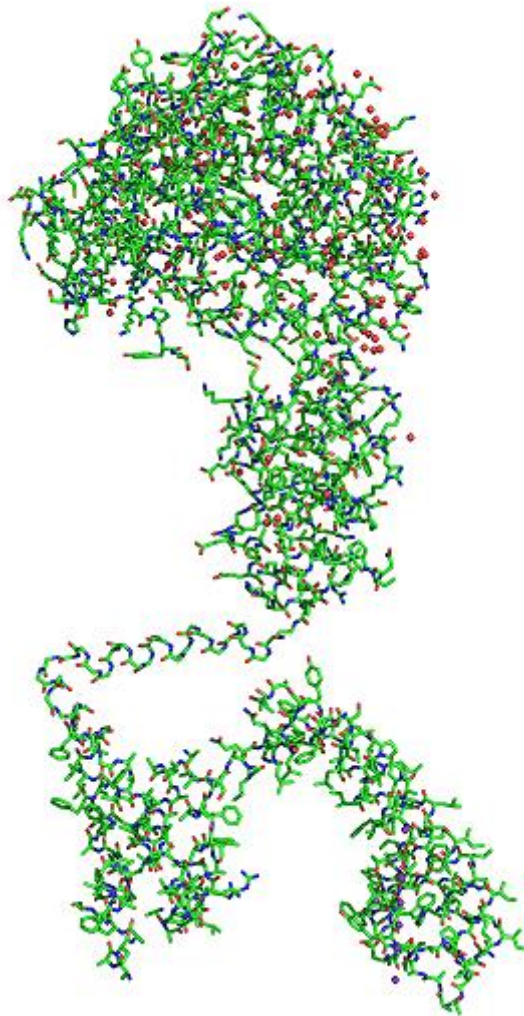

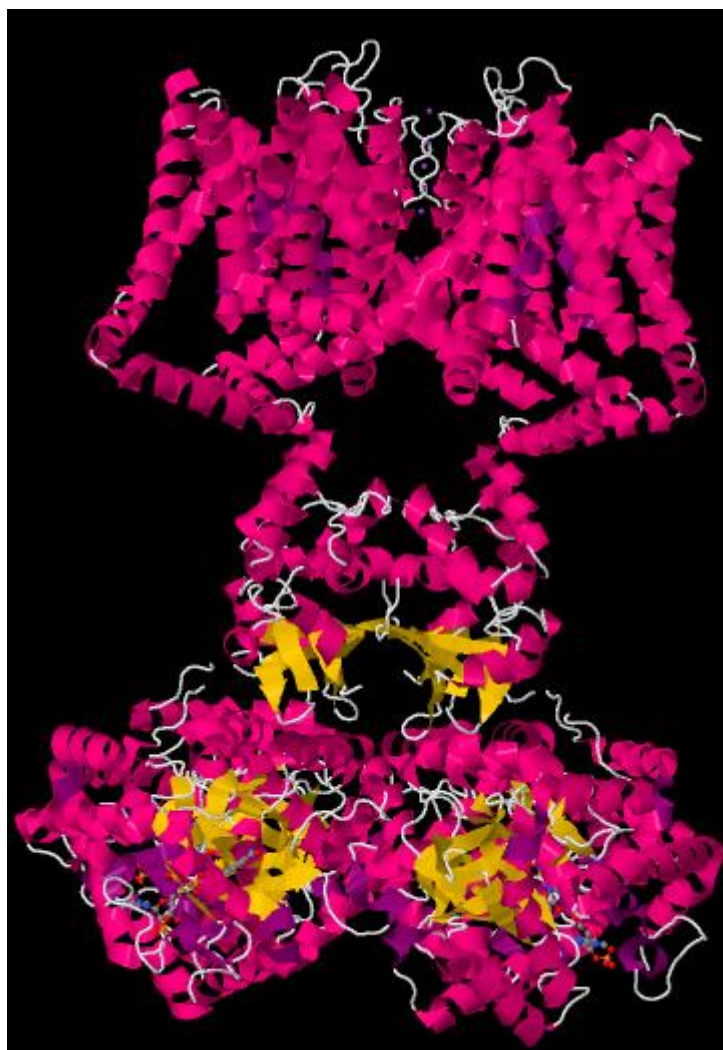Figure 4.4: Homomeric crystal structure of 2A79 from pdb, generated using pymol software.[19]

Figure 4.5: Theoretical image of 2A79 tetramer from pdb.[16]

When determining if the proteins have a high sequence identity, the target sequence from the uniprot code[20] for rat Kv1.1 was aligned against the template rat sequence Kv1.2;2A79. The percentage sequence identity was identified using the pairwise alignment function in Accelrys.

The comparative modelling undertaken followed a step by step process consisting of initial sequence alignment, the generation of spatial restraints, the construction of the homomeric model, constructing the tetramer model and evaluation of the models quality.[18,21]

Once aligned, the template coordinates and a series of spatial restraints are employed in conjunction with an optimisation procedure to derive a structure of the target protein. Typical spatial resraints involve the distribution of distances between Cα atoms, residue solvent

accessibilites or side chain torsion angles. The restraints are expressed as probability density functions (pdf) and are combined to give a molecular function, which is then optimised.[18] The ability to then separate appropriate models of protein structures from incorrect models is of great importance for protein structure prediction methods. The conformation of an amino acid can be classified according to the torsion angles of its rotatable bonds Fig.4.5. There are three backbone torsion angles labelled φ (angle about the Cα-N bond), ψ (angle about the Cα-C bond) and ω (the amide bond).
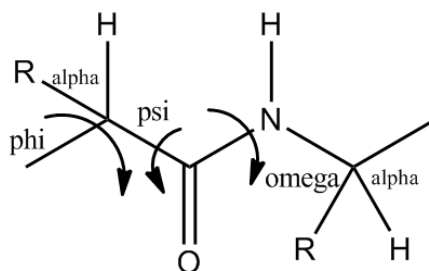
Figure 4.5: There are three backbone torsion angles labelled φ (angle about the Cα-N bond), ψ(angle about the Cα-C bond) and ω(the amide bond).[13]

A Ramachandran plot[22-24] is a contour map of angles as the backbone torsions φ and ψ are rotated. An amino acid in a sterically favourable conformation will have φ, ψ angles in set ranges if in an α helix or β strand. Ramachandran plots also indicate regions of stereochemical conflict (disallowed regions), which corresponds to conformations where atoms in the polypeptide come to close to one another. Other validation tools include ERRAT and Prosa which indicate potential problem regions in the modelled protein structure.[25,26]

4.4 Conformational searches

The properties of a molecule and the interactions it can form can be highly influenced by the conformation it possesses. The ligands are prepared first, by enumerating stereoisomers, tautomers and add hydrogens. The energetics of any given molecule may possess multiple local minima along with its global minimum. The goal of a conformational search is to sample the energy surface of the molecule and to recognize the energetically favoured conformations. There are two methods that can be used to do this and the choice of which to use is highly dependent on the number of rotatable bonds. These can be categorised into systematic and random conformational searches.

4.4.1 Systematic conformational searches

Systematic conformational searches is a technique conducted to explore the rotatable bonds in a molecule systematically through 360 $^{\circ}$ using a fixed increment i.e. 15 $^{\circ}$,30 $^{\circ}$,90 $^{\circ}$, etc. When generating the various conformations a number for factors including associated sterics[27] with the conformation and energy are considered.[28] The high energy conformations are discarded. The final step involves the minimisation of the conformations. This type of method is used for molecules that possess ligands with 4 or less rotatable bonds.

4.4.2 Random conformational searches

Random conformational searches are used for molecules that possess more than four rotatable bonds. Randomising the torsions i.e. 10 $^{\circ}$, 25 $^{\circ}$, 50 $^{\circ}$, 105 $^{\circ}$ allows the computation to be significantly reduced. Large molecules with more rotatable bonds generate a high number of conformers using a systematic approach require too much computing power. Combinatorial explosion is the term used to explain the generation of high amounts of data to the degree that the system cannot handle. Using the equation below, A is the torsion angle at 15 $^{\circ}$ increments and T is the number of rotatable bonds i.e. five. The number of conformations is **7,962,624**

$$V = (\frac{360}{A})^T$$

(9)

4.5 Molecular docking:

The turret region of Kv1.1 was defined as per the residues highlighted in Fig 4.6. All atoms within 4Å of these residues were selected and the combination was utilised to define a binding sitesphere. The CDOCKER algorithm[12] is a grid-based molecular docking method that employs CHARMm. The channel is held rigid while the ligands are allowed to flex during the refinement. Ligand placement in the active site is performed using a binding site sphere. Random ligand conformations are generated from the initial ligand structure through high temperature molecular dynamics, followed by random rotations. The random conformations are refined by grid-based (GRID 1) simulated annealing and a final grid-based or full forcefield minimization. The docked ligands were minimized in the presence of the channel (in situ). Residues with atoms inside the specified sphere were allowed to minimize.

In a subsequent flexible docking approach - a number of protein conformations were generated differing in side chain conformations in the turret region and the ligand poses rescored using the CDOCKER protocol shown in figure 4.6.
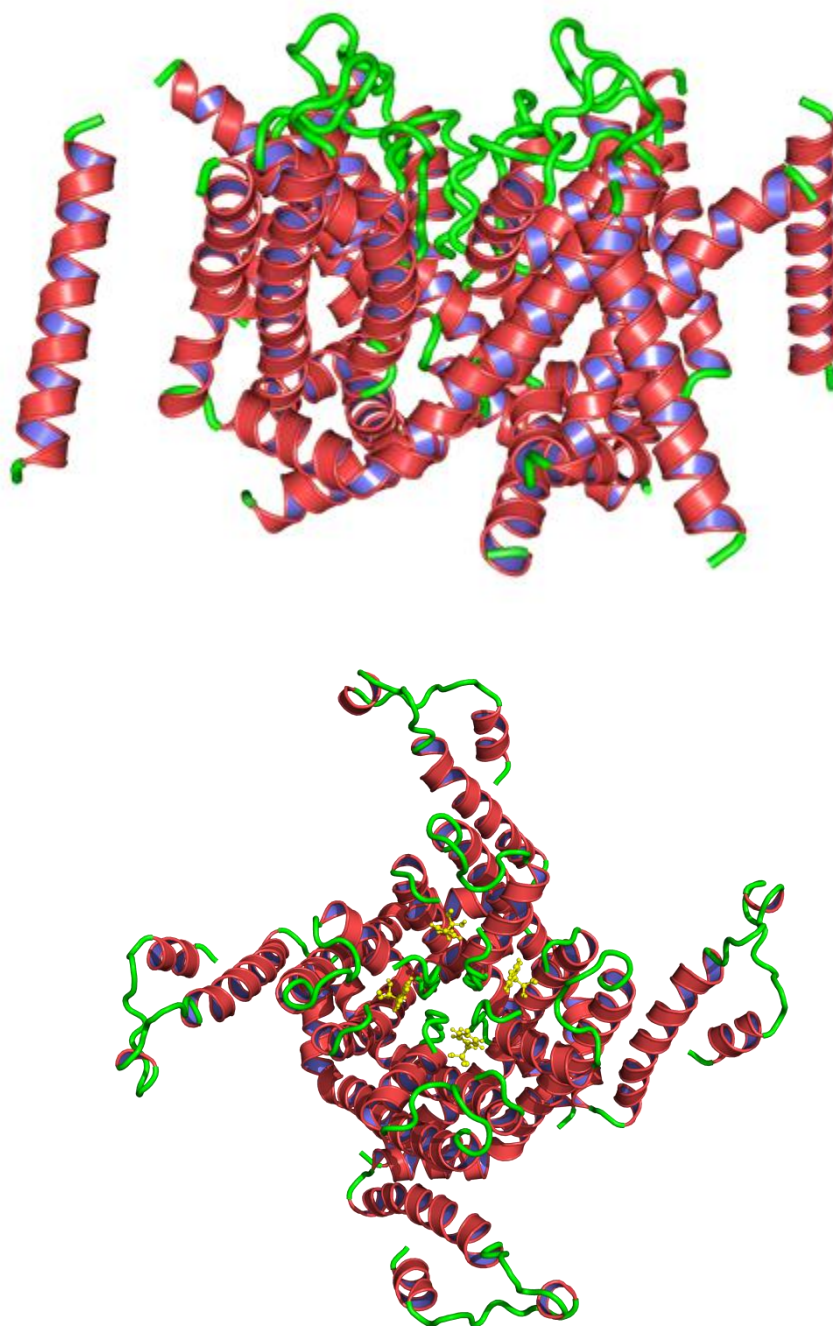

Figure 4.6: Image of comparative model for Kv1.1 Tyr379 residues in each chain are indicated (in yellow). Turret region includes residue 351-355 in each chain.

The geometric quality of the backbone conformation, the residue interaction, the residue contact and the energy profile of the structure are well within the restrictions established for reliable structures.

The compounds were allowed dock into the region shown in figure 4.7. The region ranges from residue Glu353-Lys386
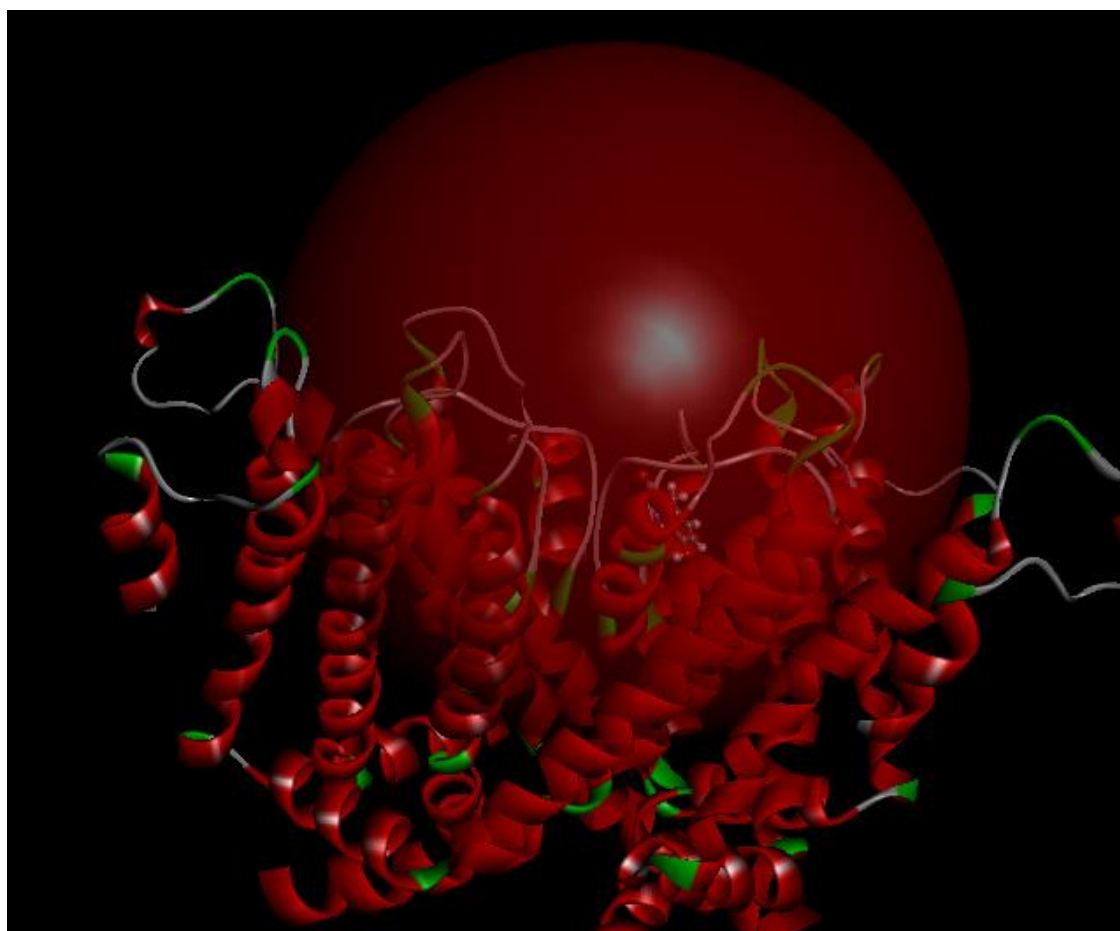
Figure 4.7: Potential binding site for molecule-protein interaction highlighted by the sphere.

4.6 Results and discussion

4.7 Application of the porphyrin series to the Kv1.1 Homology model.

All porphyrins (13-21) that were synthesized, were modelled and docked into the comparative model of Kv1.1. The porphyrin **15** was the best porphyrin derivative that inhibited the Kv1.1 channel *in vitro*.
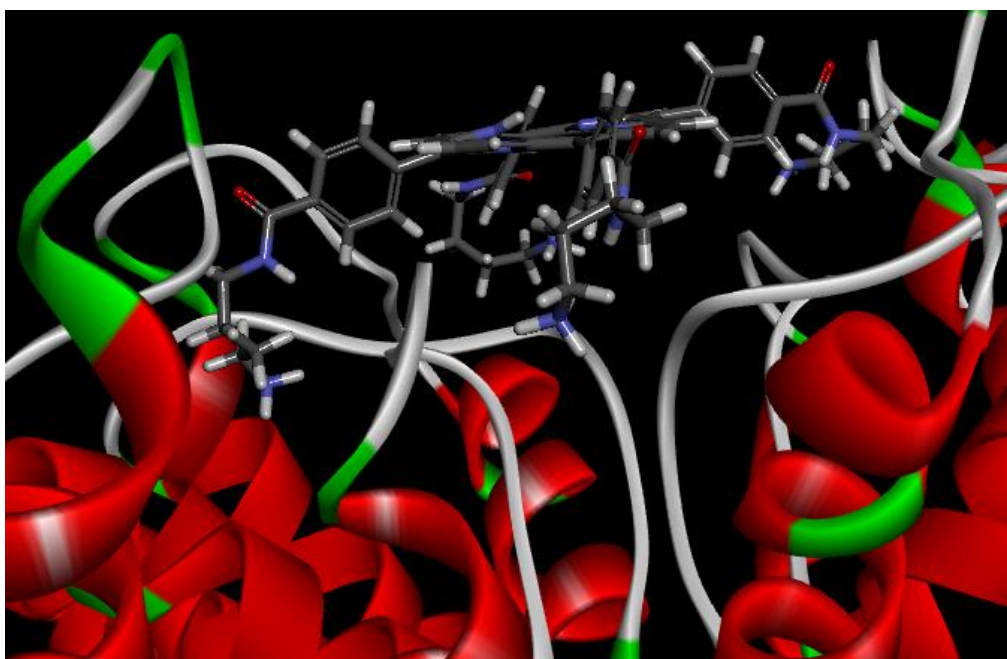
Figure 4.8: Docking model of compound **15** into the homology model of Kv1.1.

Shown in figure 4.8 is the functionalised porphyrin **15** docked into the constructed Kv1.1 homology model. The porphyrin scaffold is spatially and rigidly restricted from entering into the deep inner pore regions that small 4-aminopyridine molecules can bind into. It is because of this that these large macrocycles can be compared to toxins such as snake venom previously discussed in detail in chapter one.[29-31] There are two subsequent results that were obtained from the *in silico* interaction between the porphyrin and the channel. The binding energy (Cdocker function) and more importantly, the types of interactions occurring between the inhibitor and protein. The Cdocker energy for porphyrin **15** was the most effective amongst the compounds that were screened experimentally biologically active in Kv1.1 channels.

The Cdocker energy gives an estimate as to how efficiently the molecule binds to the protein in a particular pose. The mechanism of how these proteins inhibit is too complex for the type of docking simulations we are limited to, higher calculations such as QM can offer this but due to computational expense these were not applied.

The principal interactions observed by the docking study on porphyrin **15** included hydrogen bonding with the Asp377 residue on all chains of the tetramer protein. A strong hydrogen bonding interaction between the amide bond region of the porphyrin and the alcohol of Tyr375 were key interactions that was shown from the models. This is an important site in the selectivity filter region. Ader *et al*[32] states that a hallmark of the conductive conformation of the selectivity filter is a regular alignment of the backbone carbonyls. Strong hydrogen bonding can distort the carbonyl of specific residues thus causing nonconductive inhibition to occur. π-π interactions are also present with the inner pore amino acid residue Tyr379. It could be the combination of all these interactions collectively causing the effect on the sensitive region in the protein. The ligand-plot shown in figure 4.4 indicates these specific interactions.

Notice the large number of interactions that occur with the porphyrin **15** and protein, there are interactions from glutamic acid (Glu353) in the turret region ranging to valine (Val381) located two residues past the selectivity filter/inner pore region. This sequence of 28 amino acids, could indicate an issue. Numerous interactions over a wide array of amino acids could be the cause for the lack of selectivity in the channels when the porphyrin molecules were tested. The lack of selectivity could be due to the fact that all the Kv1 channels are highly similar in this region as shown in figure 4.1. The pore region is highly conserved throughout all of the Kv1 channels, the only variations are observed in the turret region, small variations in the pore helix and the selectivity filter/inner pore region. If the molecule covers a wide area it has the potential to interact with more residues that is common to all channels rather than interact with the minority of residues that is unique to the individual channels.
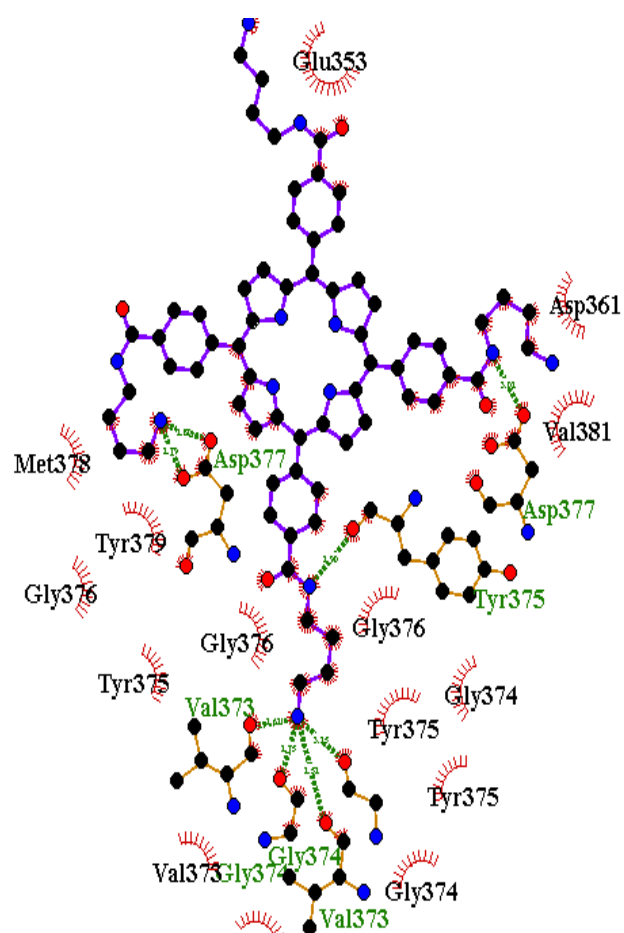
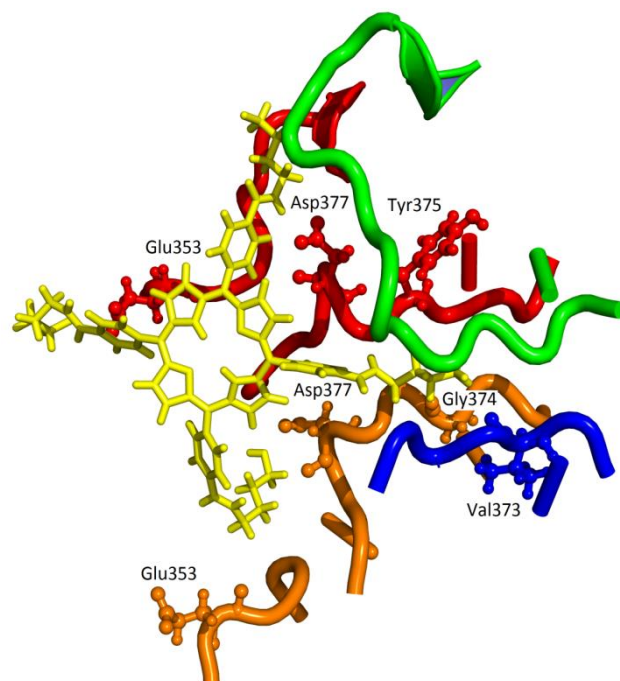Figure 4.9: Ligand-plot of **15** with Kv1.1 homology model.

Figure 4.10: 3D resolved image of the interaction between **15** and the Kv1.1 homology model generated in Pymol.[19]

Table 4.2: Table of Cdocker energy of porphyrin series.

Porphyrin	-Cdocker energy
16	40.8
20	38.8
17	38.6
15	33.5
21	32.6
13	28.3
14	26.1
18	13.6
19	12.7

In Table 4.2, the list of associated binding energies that occur between the interaction of a molecule and the Kv1.1 homology model. The modelling scores this energy based upon overall residue interaction, it fails to isolate and score the energy based upon key residue interactions such as Tyr 375, Gly376, Asp 377, Met 378 and the most important Tyr 379 and this is its major limitation. These key residue interactions would be directly related to

bioactivity.[32] The Cdocker energy should be used to indicate how the molecule has an affinity towards the region of the protein and not to predict a direct correlation between any modifications in side group to exact bioactivity.

Porphyrins **13** and **14**, the ethyl and propyl porphyrin derivatives were predicted to give similar docking energies to **15**, these three compounds were the only bioactive porphyrins that showed inhibition of the Kv1.1 channel when experimentally tested using electrophysiology methods. From the docking study we expected these three compounds to be the best as the biological studies proved these findings. This was not consistent however, porphyrins **16**, **20** and **17** were observed to computationally superior to **13**, **14** and **15**. Electrophysiologically **16**, **20** and **17** proved to be insensitive to the Kv1 channels. This was the limitation of our model.

Cdocker, the original docked poses only uses a static protein model i.e one snapshot; To refine this, the side chains of some residues were then allowed to be flexible to optimise key local interactions. This is limited flexibility of the region, it works effectively well for some systems but might not always be appropriate if large conformational changes are associated with binding.

To examine conformational changes of the protein molecular dynamics simulations would be performed. The *in silico* simulations are primarily applied to indicate how and where the molecule interacts. As discussed in chapter two when the hydrogen bonding that is experienced by the secondary amide is removed and replaced by an ester or tertiary amide the hydrogen bonding that has been shown at Tyr375 is lost. We see this in figure 4.8, the only significant interactions that occur is with porphyrin **17** which interacts with the four Asp 377 tetramer residues and one Tyr 379, the rest of the residues were shown to have negligible effects.
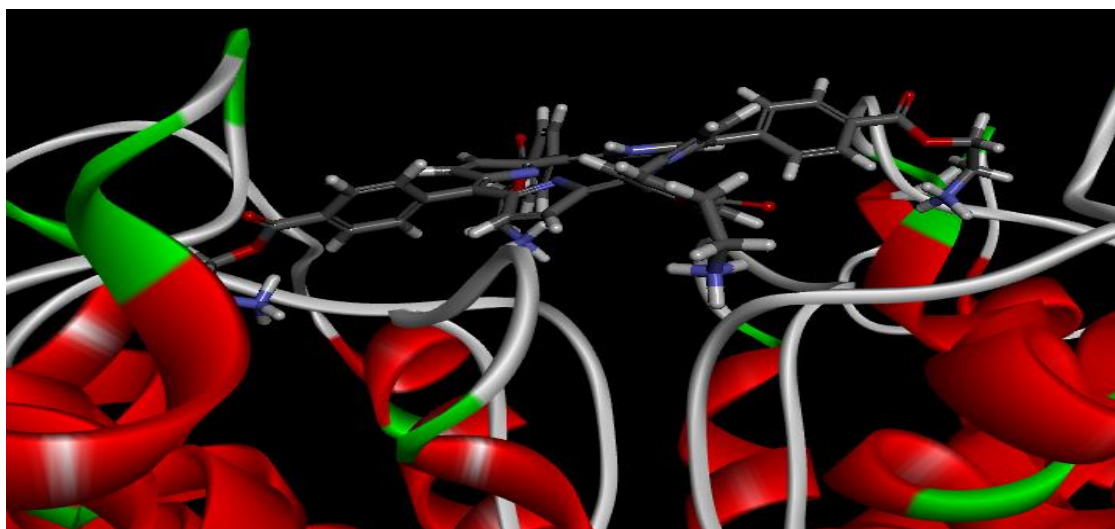
Figure 4.11: Ester functionalised porphyrin **17** docked with the rat Kv1.1 model.
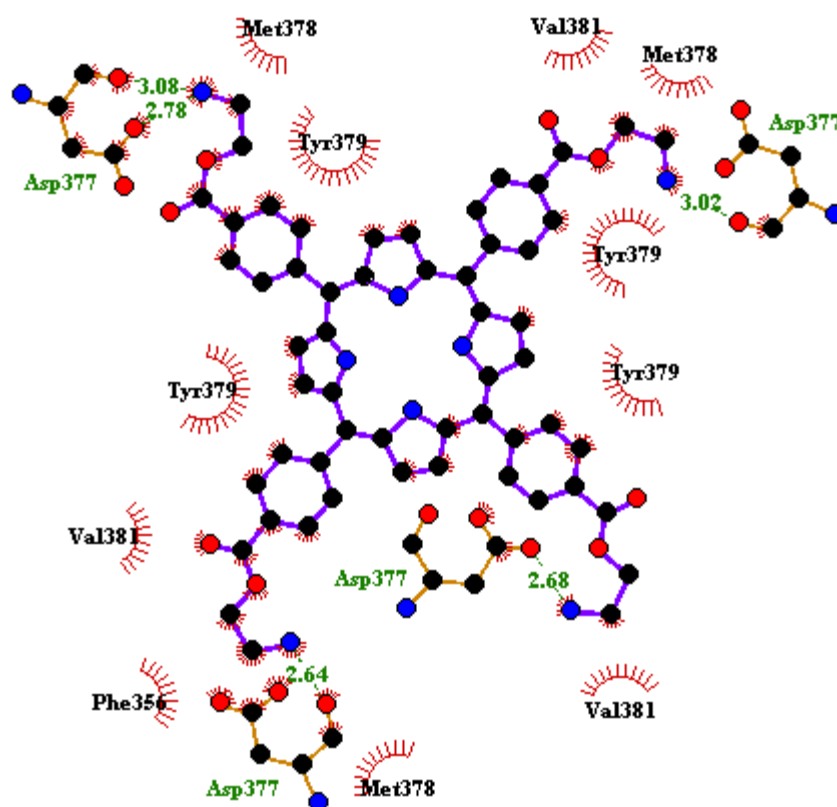

Figure 4.12: The ligand-plot between the porphyrin **17** and the Kv1.1 tetramer comparative model. Asp 377 and **17** are the primary interactions observed.

There were vast differences with porphyrin **17** and **13**. As shown in figure 4.12, the side chain alkyl ammonium group enters into the protein and has a completely different orientation as a lot of distortion is observed.
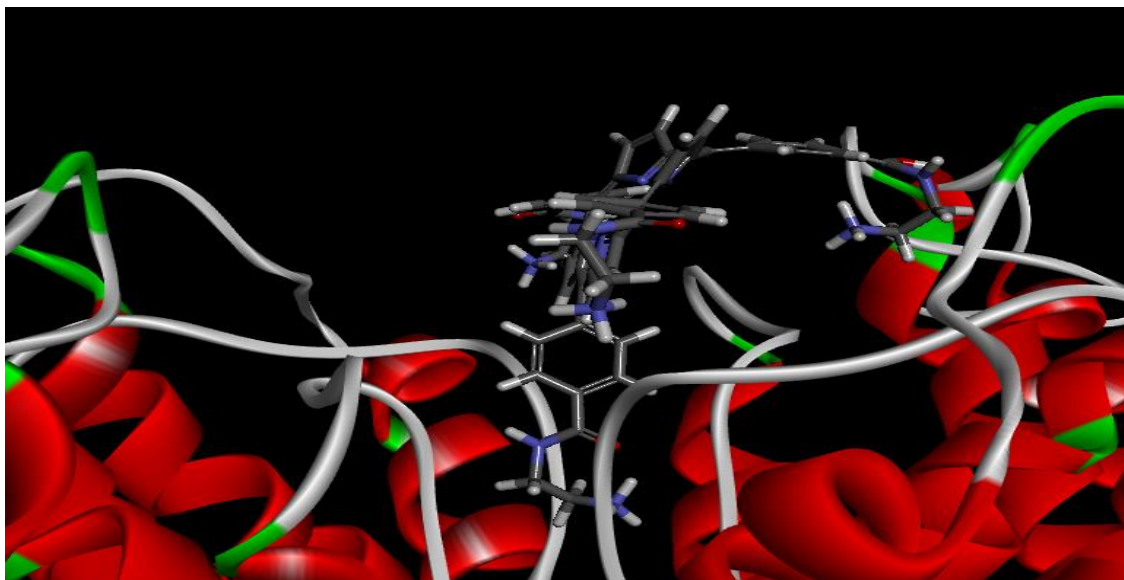

Figure 4.12: Amide functionalised porphyrin **13** docked with the rat Kv1.1 model.
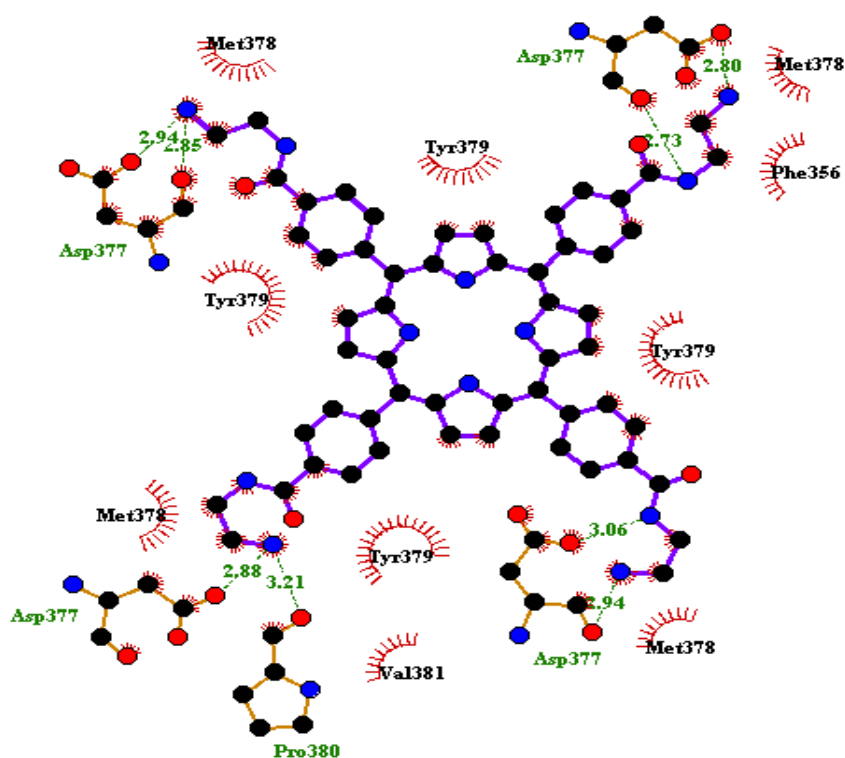
Figure 4.13: Ligand-plot of porphyrin **13.**
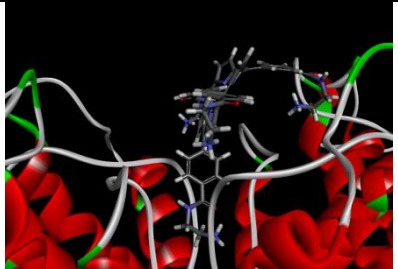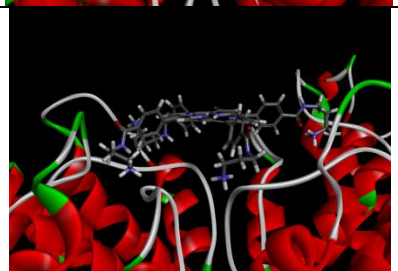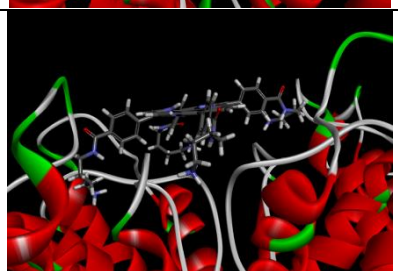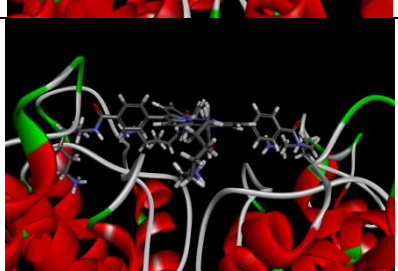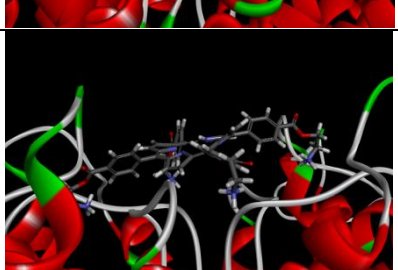
The deviance between experimental and the theoretical results could be the lack of specific HB and π-π interactions between the molecules and the proteins key selectivity filter and inner turret residues. The ester interacts with the Asp 377 residues but so does porphyrin **13**. The difference is the amide has a higher number of interactions with Tyr 379 compared to the ester derivative which is believed to be the most important residue associated with conductivity in the channel.
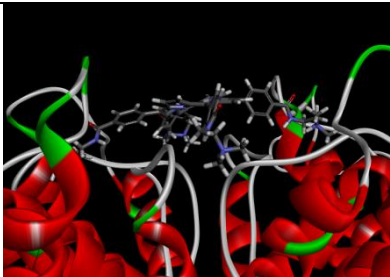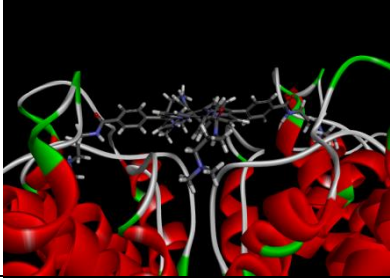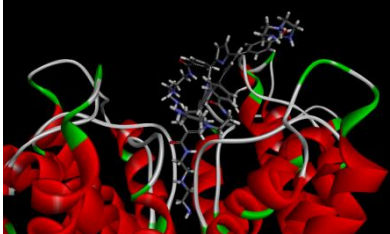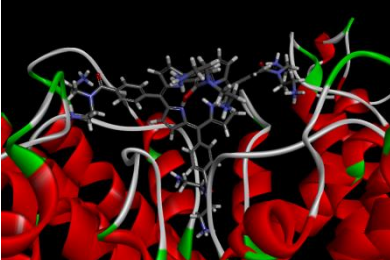
The modelling shows porphyrin **17** has a docking energy significantly better than its amide counterpart **13** however experimentally this is the opposite. Porphyrin **13** inhibits Kv1.1 at 45% at 10 μM where the ester shows negligible inhibition. The main distinction between porphyrins **15** and **13** against **17** is there is no predicted hydrogen bonding to the Tyr375 or Tyr 379 residues which is highlighted in figure 4.12. This is a significant finding as the difference in inhibition and non-inhibition between the amide/ester seems to be directly related to the HB/ π-π interactions at these residues. The ligand-plot shown in figure 4.12 of the ester porphyrin shows a high affinity to dock to Asp377. It is evident from the results that to cause inhibition requires more than just this interaction. The interaction between the alkyl ammonium and Asp377 may only serve as an anchor for the molecule and the other regions of the molecule may interact with other important residues. This again would link into the findings by Ader *et al*[32], distorting the amino acid residues in the vicinity of the selectivity filter stops the conductance of current.

Porphyrin **16**, computationally has an excellent Cdocker energy but shows negligible inhibition when biologically tested. The limitation of the software seems to be that every interaction gives a score however every interaction is not associated with biological inhibition. The high number of interactions due to the size and the space the molecule occupies is showing false potential.

Porphyrins **18** and **19**, these compounds possess tertiary terminal amines. These computationally, docked extremely poor and also had negligible bioactivity. This was expected and was shown due to the poor interactions with Asp377 due to steric restraints. This is a further indication that Asp377 is important to position the potential inhibitor in the region where key inhibition residues reside.

Table 4.3: Porphyrin binding pose and interaction with the amino acid residues of the rat Kv1.1 homology model.

Porphyrin (compound number)	Binding pose	Interaction
13		HB with Asp377 (all chains) HB with Pro 380 (1 chain) HB with Tyr 379 (1 chain) Pi interaction: Tyr379
14		HB with Asp377 (all chains) HB with Pro380 (1 chain) Pi interaction: Tyr379, Trp364
15		HB with Asp377 (all chains) HB with Pro380 (1 chain) HB with Tyr375 (1 chain) HB with Asp 361 (1 chain) Pi interaction: Tyr379, Trp364
16		HB with Asp377 (all chains) HB with Pro380, Val (1 chain) Tyr379 (1 chain) HB with Asp361 (1 chain) Glu353 (2 chains), Val 381 (1 chain) Pi interaction: Tyr379, Trp364
17		HB with Asp377 (all chains) Pi interaction: Tyr379

18		HB with Asp377 (all chains) Pi interaction: Tyr379, Phe356
19		HB with Asp377 (all chains) Pi interaction: Tyr379, Phe356, Trp364
20		HB with Asp377 (all chains) HB with Pro380 (1 chain) HB with Glu 353 (2 chain) Pi interaction: Tyr379, Trp364
21		HB with Asp377 (3 chains) HB with Glu353 (2 chains) Pi interaction with Tyr379

4.8 Molecular modelling of an alternative scaffold

The molecular modelling of the porphyrin series yielded valuable information concerning the approximate binding affinity energy the molecules had for the homology model of the Kv1.1 channel. More importantly, it showed the types of interactions that could be crucial for the inhibition of Kv1.1. The literature confirms a number of these interactions were essential for inhibition of the channel but the modelling has further aided in our understanding by the experimental SAR study performed with the compounds that were modelled. The modelling on the porphyrin series suggests that the lack of selectivity throughout the channels could be a result of the large number of interactions the porphyrin has with non-essential amino acid residues that are consistent in all Kv1 channels. Targeting selectivity amongst the channels should start by reducing the size of the scaffold to which the side arm alkyl ammonium groups are attached. The size is an issue because making it too small, the inhibitor would enter deep into the inner pore region of the potassium channel and similar to 4-aminopyridine the selectivity would be lost. The goal is to model an inhibitor which is 1) large enough to avoid entering the deep inner pore region of the protein, 2) target the essential amino acid residues in the vicinity of the selectivity filter/inner turret region 3) and abide by Lipinski's rules.

In the previous chapter we unsuccessfully attempted the synthesis of calix[4]pyrrole molecules. However, in these attempts an efficient synthesis of the corresponding dipyrromethanes was achieved. The scaffold of the dipyrromethane possesses characteristic regions that can have hydrogen bonding and π-π stacking interactions. Proposed molecules were constructed based upon the dipyrromethanes and were then modelled accordingly to the method used for the porphyrin figure 4.14.

The dipyrromethane molecules shown in figure 4.9 were modelled using the same homology model of Kv1.1 as previously used with the porphyrins. The first interesting feature that these molecules had was their higher affinity to the Kv1.1 channel as their Cdocker energy scores were almost double that of any of the porphyrin molecules modelled.
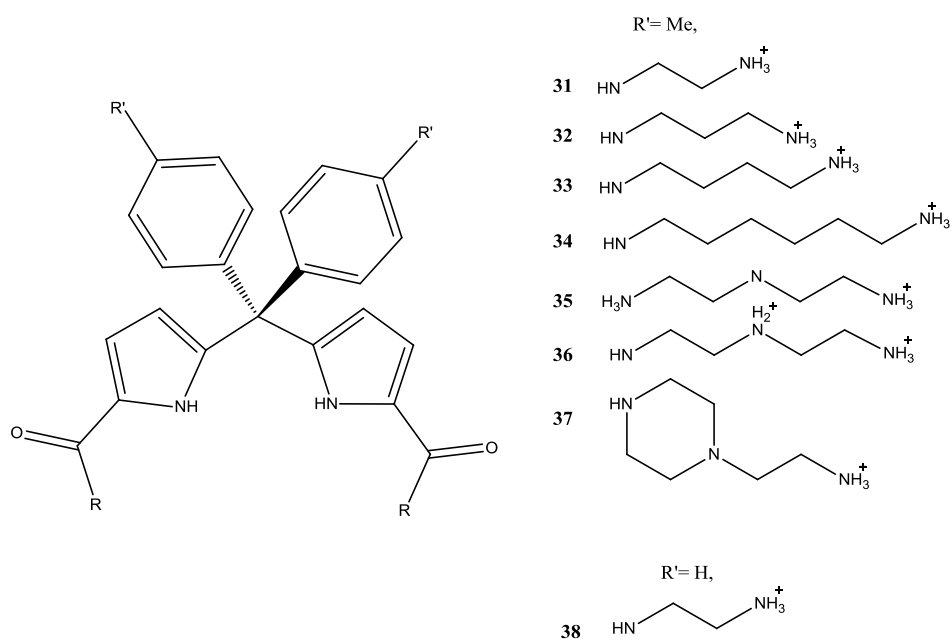
Figure 4.14: The di-tolyldipyrromethanes that were modelled **31**-**38**.

This is an interesting result solely from a binding perpective however, as observed with the porphyrins the true potential to inhibit would be related to the frequency and types of key interactions surrounding the selectivity filter region and inner turret residue, Tyr 379.

Table 4.4: Table of Cdocker energies of the dipyrromethane derivatives **31**-**38** sorted by score.

Dipyrromethane	-Cdocker energy
32	84.6
31	80.8
38	75.7
33	74.3
36	72.2
35	71.3
34	71.2
37	41.2
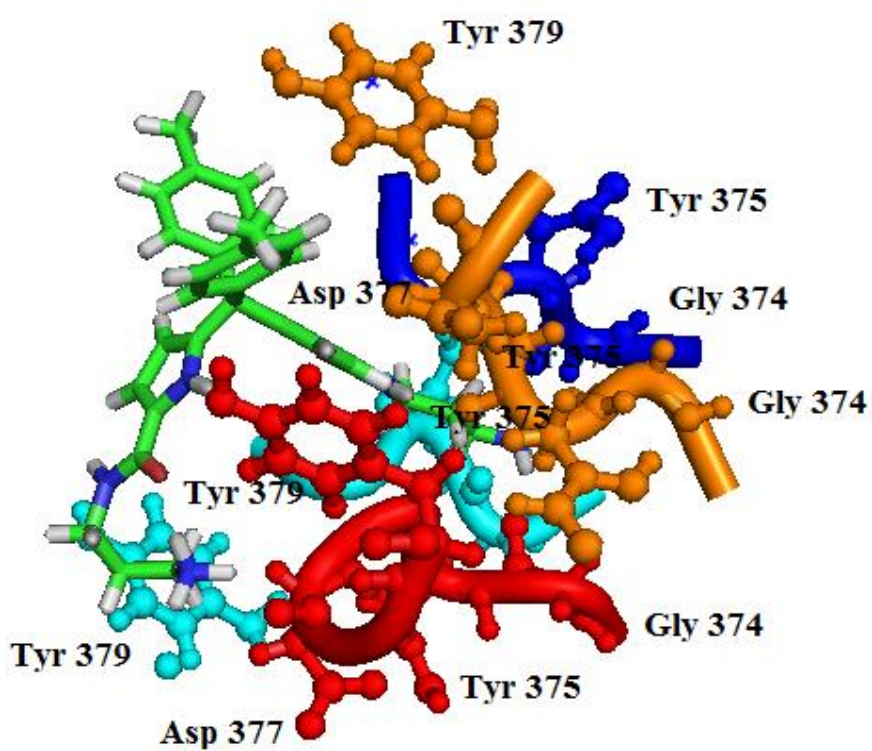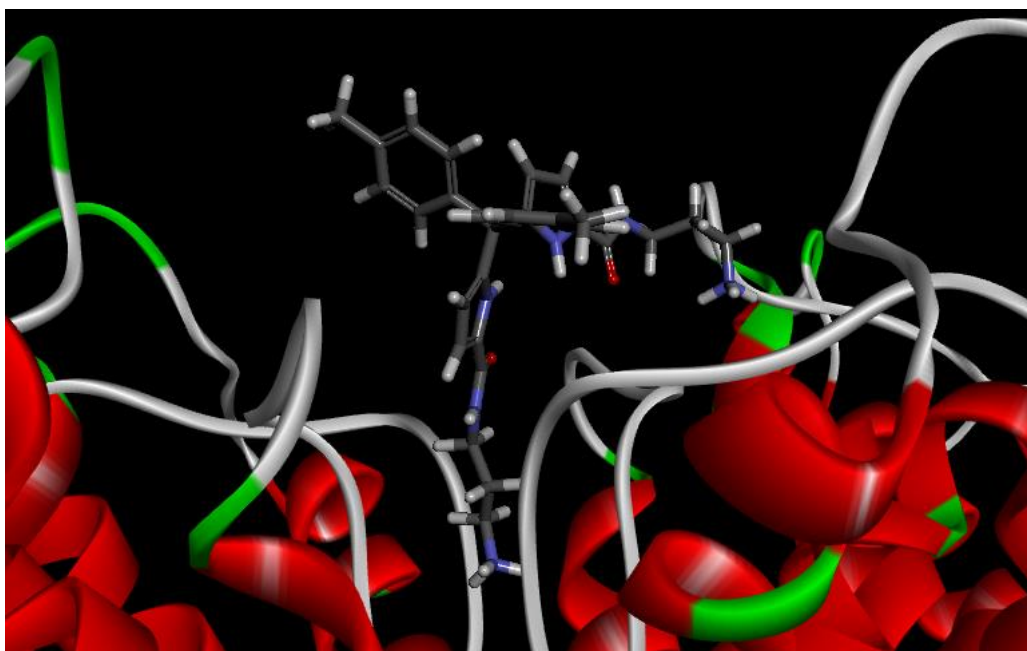
Figure 4.15: The propyl di-tolyldipyrromethane **32** docked into the rat Kv1.1 model.

The highest scoring dipyrromethane was shown to be compound **32** shown in figure 4.15. When modelled the results that were obtained were extremely interesting. The first observation is the molecule binds to the outer region of the protein. This is the type of binding that is required to mimic the venom toxins such as DTX that can inhibit these channels. By binding to the outer region and inserting reactive groups into the pore it does not possess the same characteristics of 4-aminopyridine showing that this scaffold is promising as a new lead target molecule.

The main interactions that **32** had with the homology model of Kv1.1 were the hydrogen bonding of Gly374 at all sites of the tetramer. The key interaction with Asp377 was also observed, the amide bond of the molecule showed direct hydrogen bonding with the alcohol of the amino acid residue Tyr375 and there was a π-π interaction between the inner pore residue Tyr379. A combination of all these interactions, the hypothesis proposed earlier by Ader *et al* that distortion of the selectively filter residues coupled with our theory, distorting the inner turret Tyr 379, could be plausible for **32**. Figure 4.16 highlights the interactions on the ligand-plot. Another promising feature observed is that the number of interactions of **32** with the channels is limited across 5 amino acid residues in the tetramer, these are Gly374-Tyr379. The number of interactions is greatly reduced compared to the porphyrins which showed potential interactions across 28 amino acid residues. Thus, this new proposed scaffold could improve highly on the selectivity to between channels.
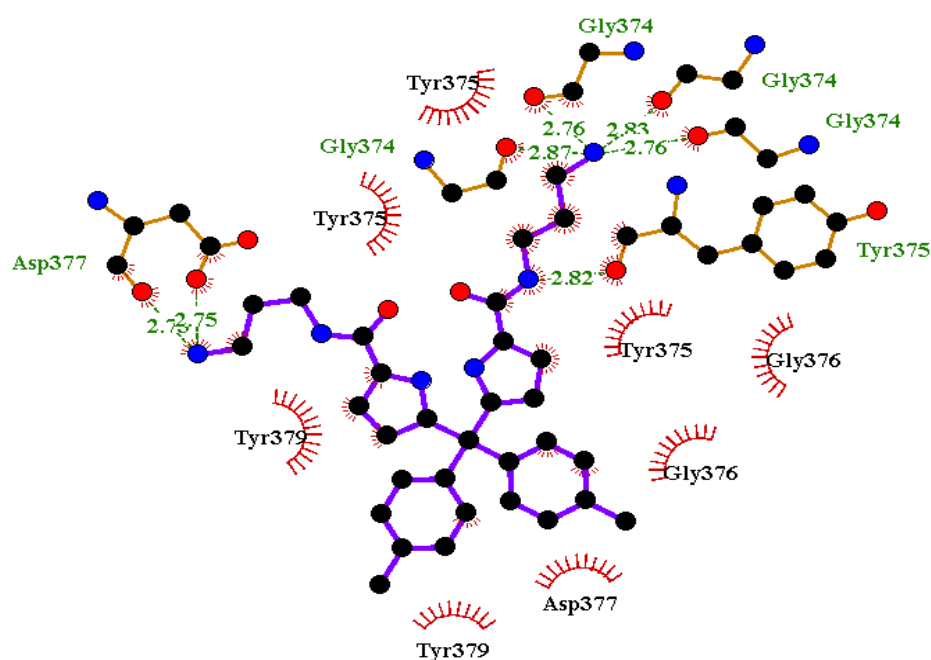

Figure 4.16: Ligand-plot of compound **32** with the rat Kv1.1 model

The next dipyrromethane in the list of energies was **31**. This dipyrromethane was the ethyl derivative to the propyl derivative **32**. The interactions of compound **31** are similar to that of **32** however it appears that the interactions with the key amino acids which we believe to be Gly374, Thy375, Asp377 and Tyr379 are greater. The four Gly374 are interacting via HB with **31** along with the Asp377 and Tyr375. Shown in figure 4.17, the ethyl side chain seems to be the correct fit to optimise maximum interaction with Asp377 as the amide and protonated amine have total interaction whilst the other side arm amide can still undergo HB with Tyr375. The π-π interaction between the compound and Tyr379 distributed throughout the tetramer appears to be highly active with both the toluene component of the molecule and the pyrrole region of the molecule. This type of finding gives enough theoretical evidence that this molecule should be targeted as a legitimate lead structure for the probing of these Kv1 channels.
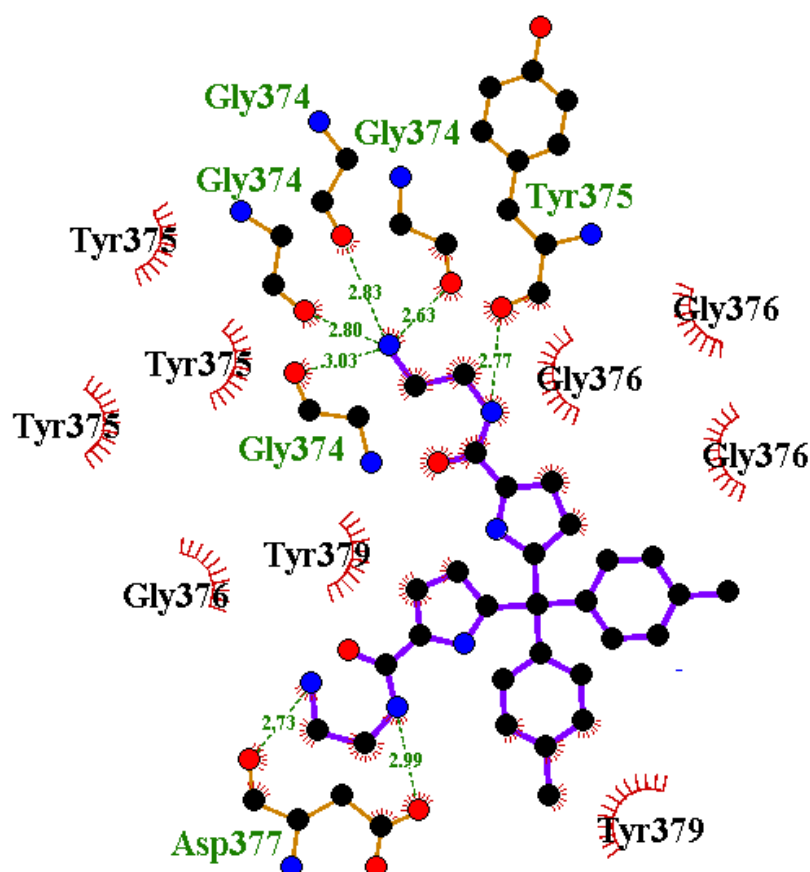

Figure 4.17: The ligand-plot of the ethyl ditolyldipyrromethane derivative **31** interacting with the rat Kv1.1 model.
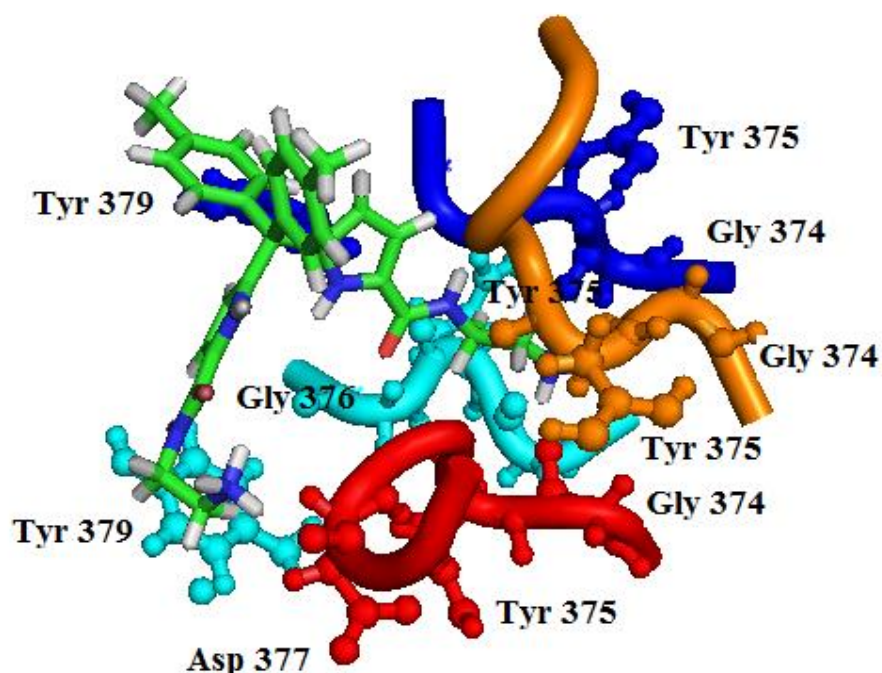
Figure 4.18: 3D model of the ethyl ditolyldipyrromethane **31** derivative interacting with the Kv1.1 homology model.

Dipyrromethane **33**, the butane derivative, gave interesting results compared to the other two derivatives **31** and **32**. The observed HB and π interactions that were so prevalent in the ethyl and propyl derivatives (**31, 32**) are not observed with **33**. Figure 4.19 and 4.20 for compound **42** does not show the HB between the amide of the dipyrromethane and that of the Tyr375 residue. This is interesting as the ester from the porphyrin did not show this interaction either; experimentally the ester was shown not to be bioactive. The ligand-plot appears to show that a large percentage of the molecule is not in any direct region where the proposed key amino acids reside. If the models are correct, these results should correlate with biological results.
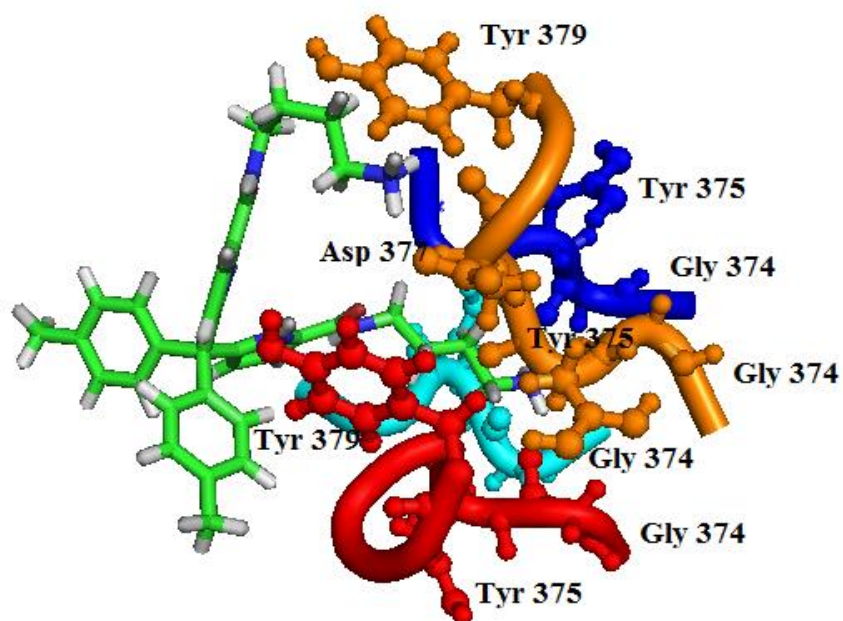
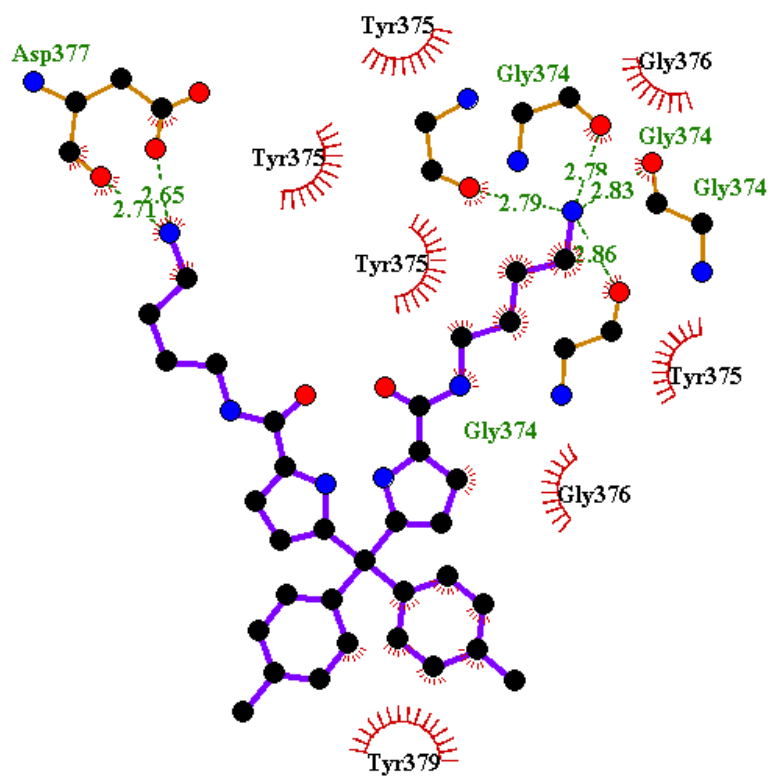Figure 4.19: 3D image of the interaction between **33** and Kv1.1 homology model.

Figure 4.20: The ligand-plot of the butane ditolyldipyrromethane **33** and the rat Kv1.1 model.

The top three molecules **(31-33)** have highlighted the types of interactions observed when the alkyl chain length is extended. The changes in interaction could also be witnessed if the toluene substituent is replaced by a phenyl group. The implications of replacing the methyl group with a hydrogen has a direct effect on the electronics of the π system in the aromatic ring and also on sterics. The sterics of the molecule has two effects when binding to the protein; 1) is the space the methyl group occupies can have a positive or negative effect and 2) removing the methyl group from the toluene substituent can change the angle on the central quaternary carbon, thus changing the overall angle to which the rest of the regions of the molecule interact.

Dipyrromethane **38** was simulated accordingly with the Kv1.1 homology model that has been shown for **31**, **32** and **33**. The binding of this molecule is similar to that of its toluene counterpart **31** except there is a negligible interaction with Tyr379. All expected interactions with Tyr375 and Asp377 are shown in figure 4.21. The main distinction between the interactions in compounds **38** and **31** is in **38** only one of the amides is utilised in HB and the π interactions are significantly weaker.
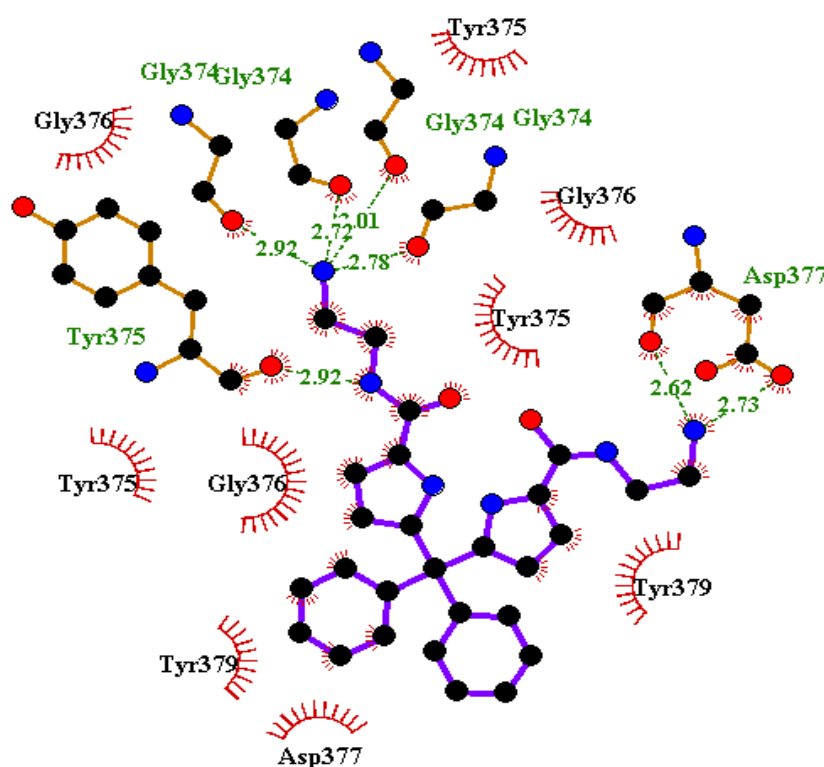

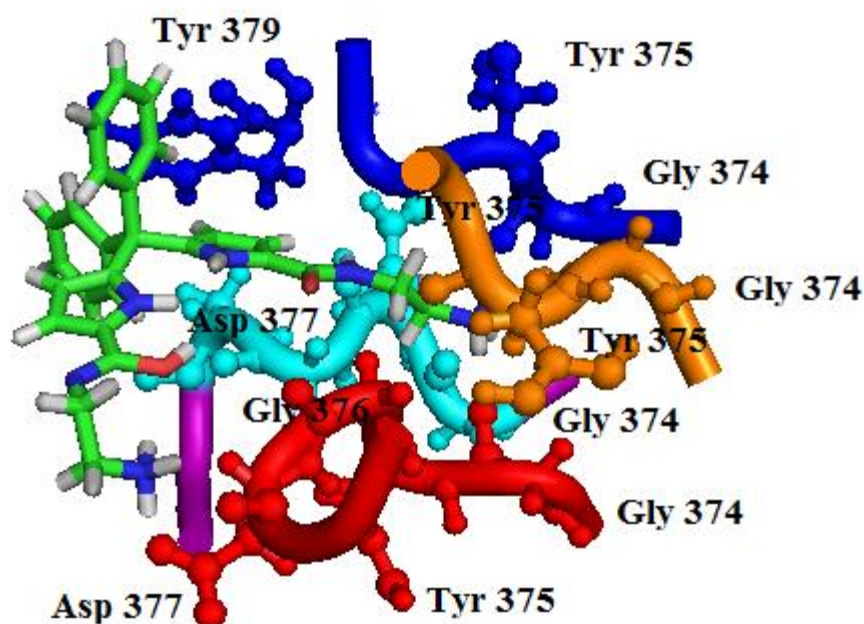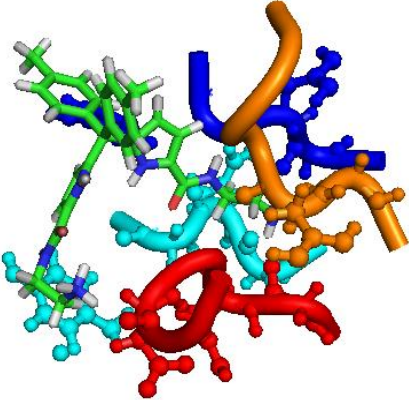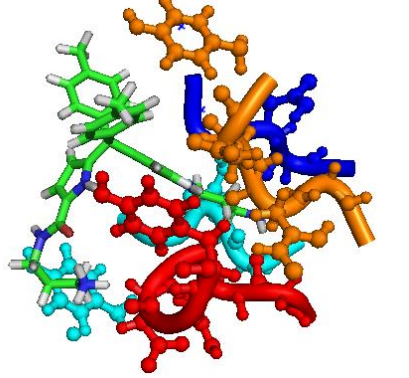Figure 4.21: The ligand-plot of the ethyl diphenyldipyrromethane **38** interacting with the rat Kv1.1 model.
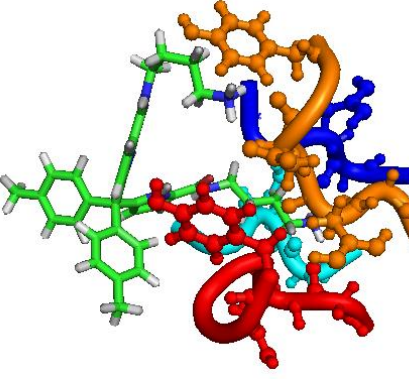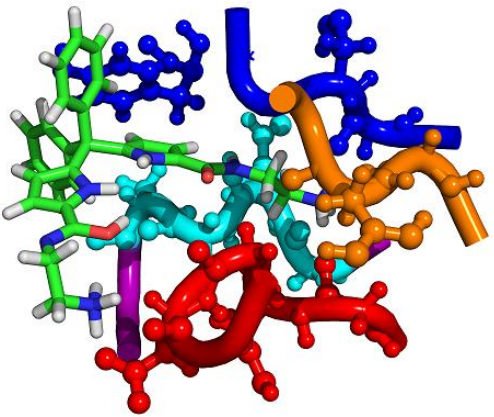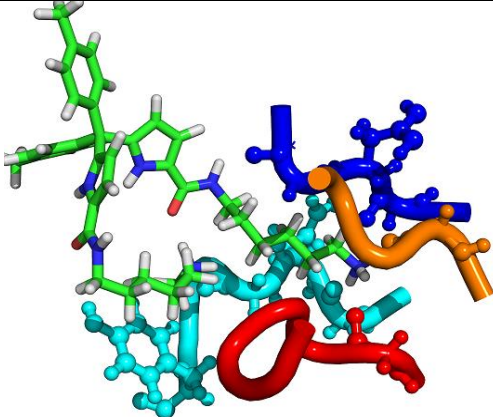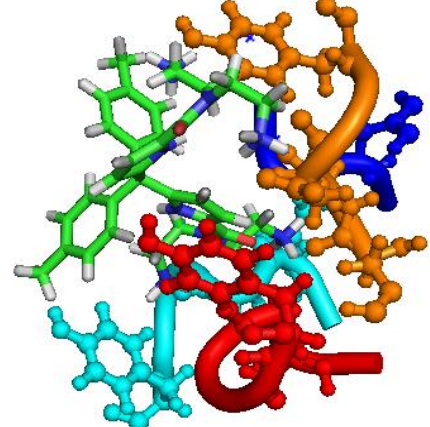
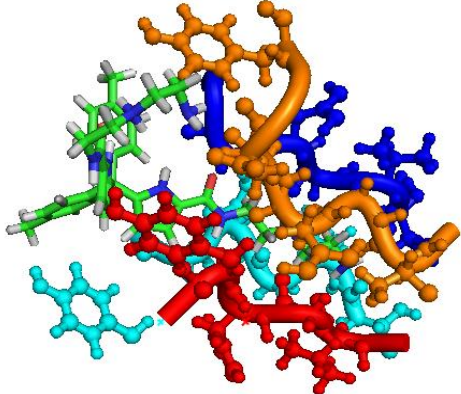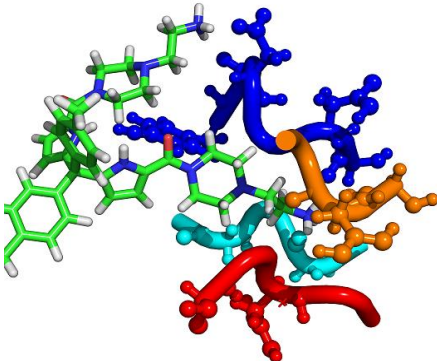Figure 4.22: 3D Pose of **38** docked into the homology model of rat Kv1.1.

It was mentioned that the π interactions between **38** and Tyr379 are weak. This interaction is shown in figure 4.22, the phenyl component of the dipyrromethane and the Tyr379 residue are perpendicular to one another. Efficient π-π interactions are optimum when the orbitals are parallel to give optimum orbital overlap.

Table 4.5: Di-tolyldipyrromethane binding poses and interaction with the amino acid residues of the rat Kv1.1 homology model.

Kv1.1	Pose description	Predicted HB and π interactions.
31		HB Gly374 x 4 chains; Tyr375 x 4 chains; Asp377 x1 chain Pi: Tyr379 x 2 chains
32		HB: Gly374 x 4 chains; Tyr375 x 4 chains; Tyr379 x 1 chain; Asp377 x1 chain; Gly376 x 1 chain Pi: Tyr379 x 2 chains
33		HB Gly374 x 4 chains; Asp377 x 1 chain Pi: Tyr379 x1 chain

38		HB Gly374 x 4 chains; Asp377 x 2 chains; Tyr375 x4 chains No π interactions
34		HB Gly374 x 4 chains; Asp377 x 2 chains; Gly 376 x 2 chains; Tyr375 x2 chains Pi: Tyr379 x 1 chain
35		HB Asp377 x 1 chain; Gly 376 x 3 chains; Tyr375 x4 chains Pi: Tyr379 x 3 chains
36		HB Thr372 x 2 chains; Val373 x 4 chains; Gly 374 x 4 chains; ; Asp377 x 1 chain; Gly 376 x 3 chains Tyr375 x4 chains Pi: Tyr379 x 3 chains

| 37 | | HB Gly374 x 3 chains; Tyr375 x 3 chains; Asp377 x2 chains

Pi: Tyr379 x 1 chain |

4.9 Modelling of a fourfold functionalised scaffold

The above di-tolyldipyrromethane derivatives showed potential to inhibit the $Kv(1.1)_4$ biological target based upon the types and number of interactions with key amino acid residues. A number of other derivatives were also modelled and are shown in figure 4.23. By incorporating alternative functional groups it may be possible to enhance HB and π interactions within the dipyrromethane scaffold.
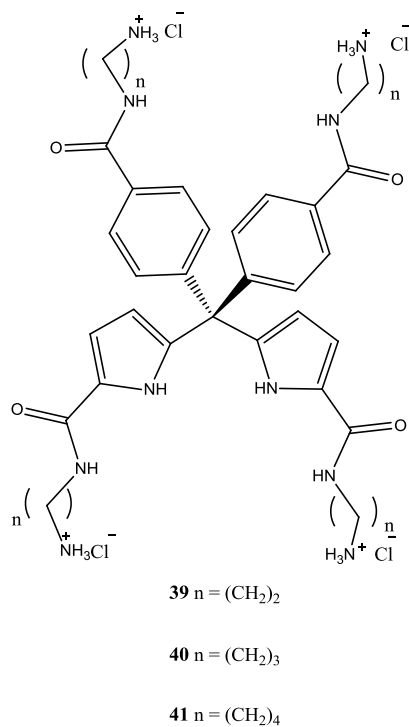

39 n = $(CH_2)_2$

40 n = $(CH_2)_3$

41 n = $(CH_2)_4$

Figure 4.23: Plausible compounds **39**-**41** for enhanced interaction.

The tetra-functionalised amino derivatives **39**-**41** (figure 4.23-4.29), when modelled in the Kv(1.1)$_4$ homology model, showed promising results with an increase in Cdocker energy, however as described previously this energy does not directly correspond to bioactivity but it does show that the molecule has a strong affinity for the region where the key amino acids reside. The energies for these tetra functionalised molecules have rose to ~120 kcal/mol from 85 kcal/mol shown for the ditolyldipyrromethanes and 40 kcal/mol for the porphyrins. Shown in figure 4.25-4.29 are the ligand-plots for **39**, **40** and **41** derivatives respectively. The key features from all of these interaction maps are that they correspond to the fundamental theory that we observe interactions in the selectivity filter region with Gly374, Tyr375, Gly376, Asp377 and inner pore Tyr379. The propane and butane derivatives also interact with the residue Glu353 in the outer turret region.
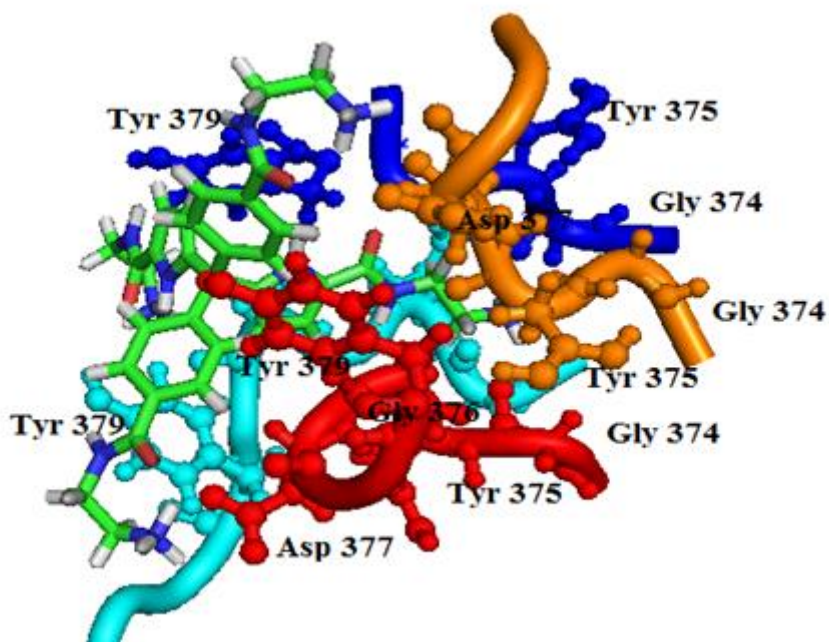

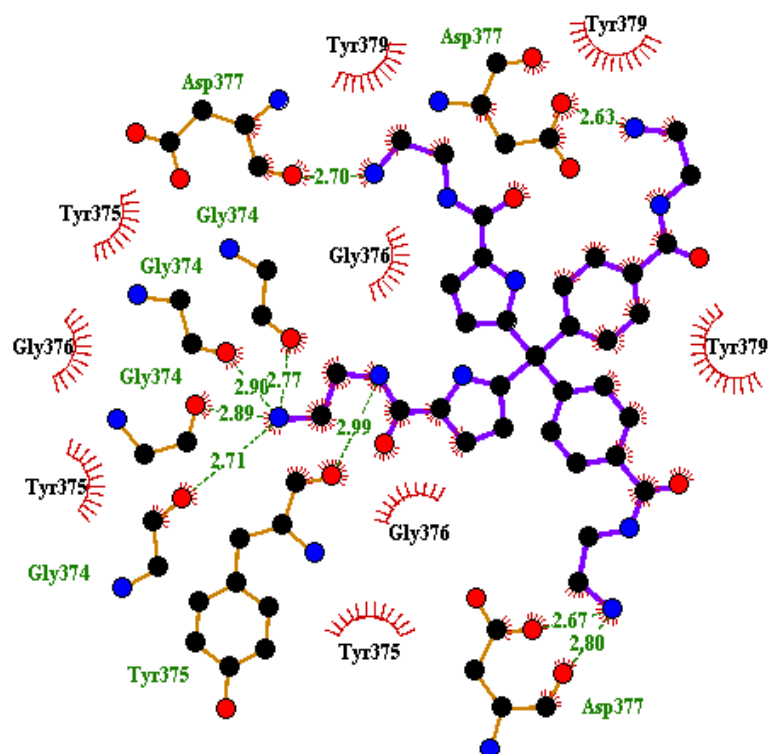Figure 4.24: 3D pose of **39** with the rat Kv1.1 model.

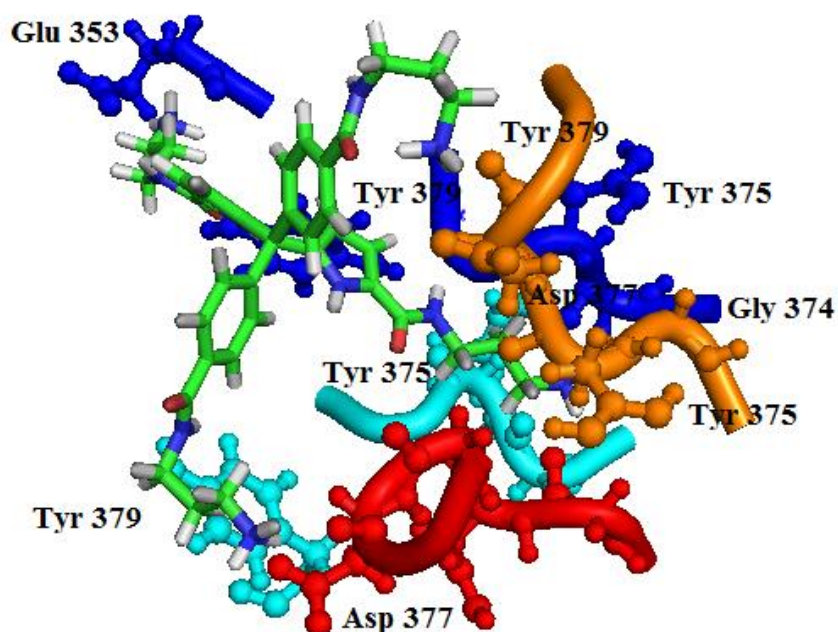Figure 4.25: Ligand-plot of **39** interacting with the rat Kv1.1 model.

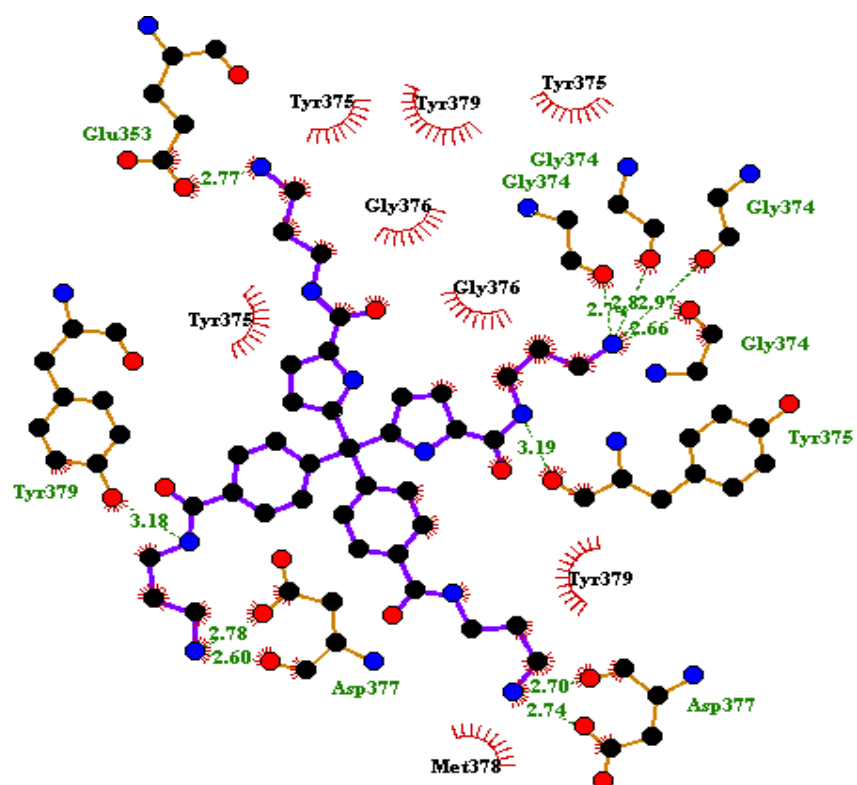Figure 4.26: 3D pose of **40** interacting with rat Kv1.1 model.

Figure 4.27: Ligand-plot of **40** interacting with rat Kv1.1 model
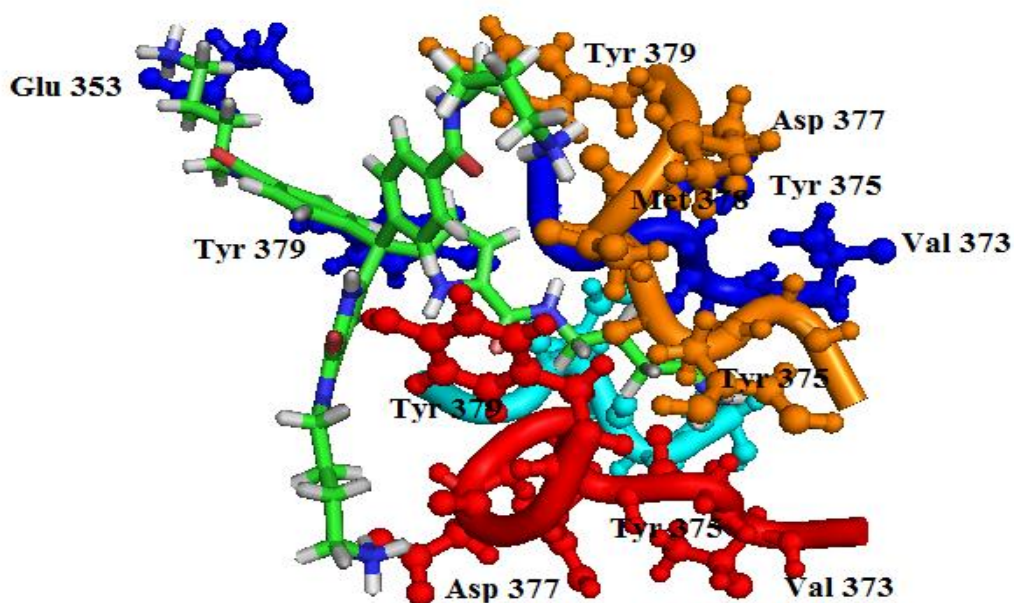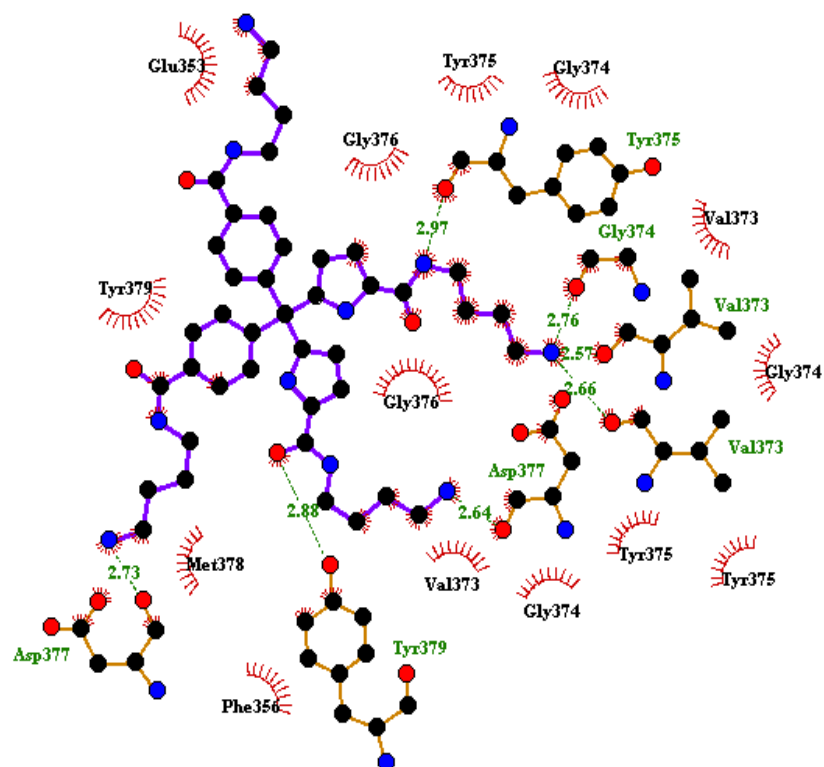

Figure 4.28: 3D pose of **41**.

Figure 4.29: Ligand-plot of **41** with the rat Kv1.1 model.

4.10 Experimental

Protein structures were downloaded from the protein databank (PDB: 2A79, 2.9Å[16] this was the crystal structure of Kv1.2. Accelrys Discovery Studio 3.5 was used to prepare the protein structures (add missing atoms, correct connectivity, correct names, etc.) For ligands, Accelrys Discovery Studio 3.0 was used to enumerate tautomers, stereoisomers and conformations.

The protein sequences (for Kv1.1, Kv1.3, Kv1.4, Kv1.5 and Kv1.6) obtained from uniplot were aligned to the template of known structure (PDB: 2A79) using Discovery Studio 3.0 and 100 protein structures were built for each alignment. The Modeller software implemented comparative protein structure modelling by satisfying spatial restraints[18, 21]. The alignment is used to construct a set of geometrical criteria that are converted into probability density functions (PDFs) for each restraint. A global optimization procedure refines the positions of all heavy atoms in the protein.

The PDFs include the following:

(1) Homology-derived restraints on distances and dihedral angles in the target sequence, taken from its alignment with the template structure(s)

(2) Stereochemical restraints such as bond length and bond angle preferences, obtained from the CHARMM-22 molecular mechanics force field

(3) Statistical preferences for dihedral angles and nonbonded interatomic distances, obtained from a representative set of known protein structures[21].

PDFs restrain Cα–Cα distances, main-chain N–O distances, and main-chain–side-chain dihedral angles. The three-dimensional model of a protein is obtained by optimization of molecular PDFs such that the model violates the input restraints as little as possible

The best model was selected using a combination of the Modeller discrete optimized protein energy (DOPE) score and a selection of protein assessment tools. Profiles 3D (Accelrys Discovery Studio 3.0) checks the validity of a protein structure by measuring the compatibility score of each residue in the given 3D environment[33]. PROCHECK[34] was employed to perform a stereochemical check, with every amino acid being classified as having a favoured, additionally allowed, generously allowed, or disallowed conformation. ERRAT[25] counts the number of nonbonded interactions between atoms (CC, CN, CO, NN,

NO, and OO) within a cutoff distance of 3.5 Å and yields an overall quality factor for each structure, which is expressed as the percentage of protein for which the calculated error value falls below a 95% rejection limit. Normally accepted model structures produce values above 50, with a higher score indicating that the model has a better ratio of nonbonded interactions. Procheck and ERRAT validation were accessed at (http://swift.cmbi.kun.nl/WIWWWI). The final model selected yielded the overall best performance across the validation tools, coupled with a structural analysis of the binding pocket.

Tetramer models were developed using Pymol[35] and the biological assembly of the Mammalian Shaker Kv1.2 potassium channel (PDB: 2A79[17]) structure

Table 4.5: Quality of the template and generated homology model as checked by Procheck and Errat. Ramachandran plot qualities show the percentage (%) of residues belonging to the core, allowed, generally allowed and disallowed region of the plot. The interaction energy per residue was also calculated by the PROSA2003 program. The Prosa z-score indicates overall model quality.

	Procheck – Ramachandran plot quality					Prosa3D	Errat Score
	Residue	Fully allowed %	Additionally Allowed %	Generously Allowed %	Disallowed %		
Template V1.2	658	75.91	20.45	2.08	1.56	-10.04	96.085
V1.1	636	88.69	8.60	2.23	0.48	-1.12	81.126

Validation of the models built was carried out using Ramachandran plot calculations computed with the PROCHECK program. Ramachandran plot qualities show the percentage (%) of residues belonging to the core, allowed, generally allowed and disallowed region of the plot. The φ and ψ distributions of the Ramachandran plots of non-glycine, non-proline residues are summarized in Figure 1 and Table 1. Altogether, for the Kv1.1, Kv1.4 and Kv1.6 models >98% of the (non Gly or Pro) residues were in favoured and allowed regions.

4.11 References

1. Umscheid CA, Margolis DJ, Grossman CE. Key concepts of clinical trials: A narrative review. Postgrad Med 2011;123(5):194-204.

2. [Internet]. Available from: http://www.rcsb.org/pdb/home/home.do.

3. Rubin EH, Gilliland DG. Drug development and clinical trials-the path to an approved cancer drug. Nature Reviews Clinical Oncology 2012;9(4):215-22.

4. Gane PJ, Dean PM. Recent advances in structure-based rational drug design. Curr Opin Struct Biol 2000;10(4):401-4.

5. Anderson AC. The process of structure-based drug design. Chem Biol 2003;10(9):787-97.

6. Sippl W. Receptor-based 3D QSAR analysis of estrogen receptor ligands - merging the accuracy of receptor-based alignments with the computational efficiency of ligand-based methods. J Comput Aided Mol Des 2000;14(6):559-72.

7. Lipinski CA, Lombardo F, Dominy BW, Feeney PJ. Experimental and computational approaches to estimate solubility and permeability in drug discovery and development settings. Adv Drug Deliv Rev 1997;23(1-3):3-25.

8. Lipinski CA. Drug-like properties and the causes of poor solubility and poor permeability. J Pharmacol Toxicol Methods 2000;44(1):235-49.

9. Judge S, Bever C. Potassium channel blockers in multiple sclerosis: Neuronal K-V channels and effects of symptomatic treatment. Pharmacol Ther 2006 JUL;111(1):224-59.

10. Leach AR, editor. Molecular modelling, principles and applications. Second edition ed. Prentice Hall; 2001. .

11. Zhou T, Huang D, Caflisch A. Quantum mechanical methods for drug design. Current Topics in Medicinal Chemistry 2010;10(1):33-45.

12. Wu GS, Robertson DH, Brooks CL, Vieth M. Detailed analysis of grid-based molecular docking: A case study of CDOCKER - A CHARMm-based MD docking algorithm. Journal of Computational Chemistry 2003;24(13):1549-62.

13. MacKerell AD, Bashford D, Bellott M, Dunbrack RL, Evanseck JD, Field MJ, Fischer S, Gao J, Guo H, Ha S, et al. All-atom empirical potential for molecular modeling and dynamics studies of proteins. J Phys Chem B 30 1998;102(18):3586-616.

14. Allinger NL. Conformational-analysis .130. Mm2 - hydrocarbon force-field utilizing V1 and V2 torsional terms. J Am Chem Soc 1977;99(25):8127-34.

15. Allinger NL, Burkert U, editors. Molecular mechanics. ACS; 1982.

16. Long S, Campbell E, MacKinnon R. Crystal structure of a mammalian voltage-dependent shaker family K+ channel. Science 2005;309(5736):897-903.

17. Long S, Campbell E, MacKinnon R. Voltage sensor of kv1.2: Structural basis of electromechanical coupling. Science 2005;309(5736):903-8.

18. Sali A, Blundell TL. Comparative protein modeling by satisfaction of spatial restraints. J Mol Biol 1993;234(3):779-815.

19. www.pymol.org [Internet]. Available from: www.pymol.org.

20. www.uniprot.org [Internet]. Available from: www.uniprot.org.

21. Sali A, Overington JP. Derivation of rules for comparative protein modeling from a database of protein-structure alignments. Protein Science 1994;3(9):1582-96.

22. Ramachandran GN, Ramakrishnan C, Sasisekharan V. Stereochemistry of polypeptide chain configurations. J Mol Biol 1963;7(1):95.

23. Ramachandran GN, Sasisekharan V. Conformation of polypeptides and proteins. Adv Protein Chem 1968;23:283-438.

24. Ramachandran GN, Ramakrishnan C, Sasisekharan V. Stereochemistry of polypeptide-chain configurations. Curr Sci 1990;59(17-18):813-7.

25. Colovos C, Yeates TO. Verification of protein structures - patterns of nonbonded atomic interactions. Protein Science 1993;2(9):1511-9.

26. Wiederstein M, Sippl MJ. ProSA-web: Interactive web service for the recognition of errors in three-dimensional structures of proteins. Nucleic Acids Res 2007;35:407-10.

27. Beusen DD, Shands EFB, Karasek SF, Marshall GR, Dammkoehler RA. Systematic search in conformational analysis. Theochem-Journal of Molecular Structure 1996;370(2-3):157-71.

28. Eliel E, editor. Conformational analysis. Interscience Publishers; 1965.

29. King GF. Venoms as a platform for human drugs: Translating toxins into therapeutics. Expert Opinion on Biological Therapy 2011;11(11):1469-84.

30. Lewis RJ, Garcia ML. Therapeutic potential of venom peptides. Nature Reviews Drug Discovery 2003;2(10)790-802.

31. Mirshafiey A. Venom therapy in multiple sclerosis. Neuropharmacology 2007;53(3):353-61.

32. Ader C, Schneider R, Hornig S, Velisetty P, Wilson EM, Lange A, Giller K, Ohmert I, Martin-Eauclaire M, Trauner D, et al. A structural link between inactivation and block of a K+ channel. Nature Structural & Molecular Biology 2008;15(6):605-12.

33. Bowie JU, Luthy R, Eisenberg D. A method to identify protein sequences that fold into a known 3-dimensional structure. Science 1991;253(5016):164-70.

34. Laskowski RA, MacArthur MW, Thornton JM. Validation of protein models derived from experiment. Curr Opin Struct Biol 1998;8(5):631-9.

35. DeLano WL. DS. The PyMOL Molecular Graphics System [computer program]. Palo Alto, CA, USA: 2002.

# Chapter 5: The synthesis and bioevaluation of dipyrromethanes

5.1 Objective of chapter

The interpretive data obtained from the molecular modelling in chapter 4 showed the specific binding affinities and the potential biological activity that the functionalised di-tolyldipyrromethane scaffold possesses. The interactions observed amongst known key amino acid residues in the selectivity filter and inner turret region make these compounds an extremely interesting series of molecules to probe the protein. This chapter involves the various synthetic strategies employed to reach the target molecules, the subsequent biological testing of the target compounds and the validation of the molecular modelling as a feasible tool to predict efficient inhibitors.

5.2 Results and Discussion

5.3 Synthesis of ditolyldipyrromethane target compounds

The synthesis of the dipyrromethane scaffold was prepared via the method by Turner *et al*[1] discussed in chapter 3 to give compound **29** in 50% yield (scheme 5.1). The variation to the method was 4,4 dimethylbenzophenone replaced benzophenone as the ketone. The reaction solvent was anhydrous MeOH rather than EtOH and the reaction period was 5 days rather than 7 days.
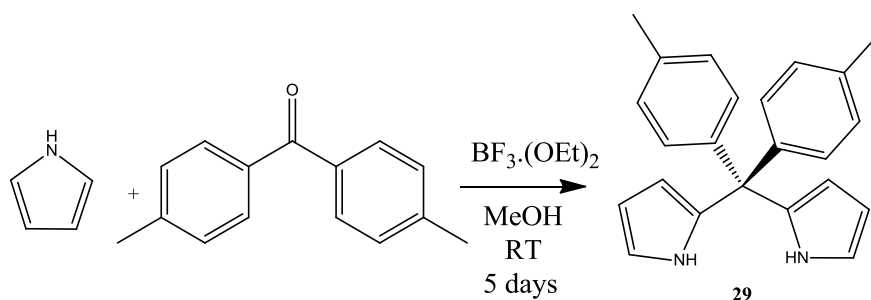
Scheme 5.1:Preparation of **29**.

There is another method to synthesize these dipyrromethane scaffolds that may offer the potential to derivatize the para position on the phenyl ring. The alternative method is a Grignard synthesis[2] shown in scheme 5.2.
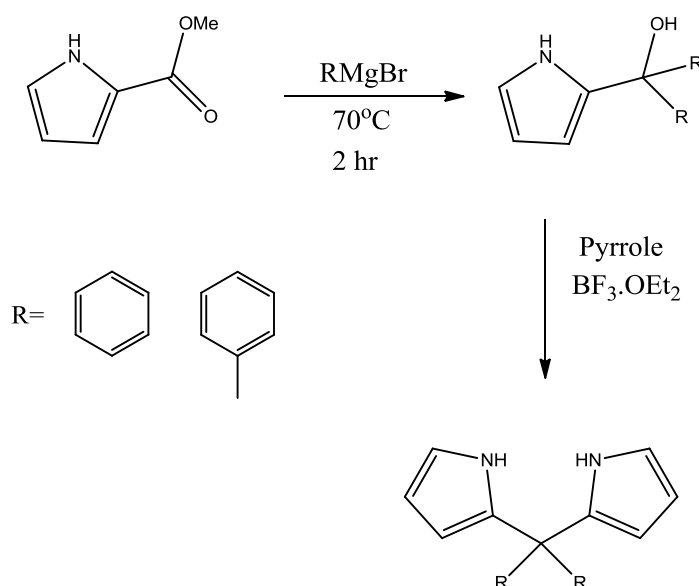

Scheme 5.2: Grignard synthesis of dipyrromethanes.

The synthesis of the dipyrromethane by the Grignard method uses the methyl ester derivative of the pyrrole molecule. To this freshly prepared tolyl magnesium bromide was added in high molar excess to ensure the conversion to the carbinol derivative was obtained. When isolated, the carbinol was further condensed with distilled excess pyrrole and catalytic $BF_3.(OEt)_2$ to form an instant precipitate which was isolated as the target scaffold.

The comparative dipyrromethanes synthesized from the Grignard method against the condensation method give higher yields and vastly superior reaction completion rates. The disadvantage is extremely dry conditions are required and the quantity of pyrrole required for the formation of the dipyrromethane from the carbinol is high, resulting in high quantities of pyrrole waste.

5.3.1 Functionalization of ditolyldipyrromethane scaffold with TFAA

The principle behind the attempted functionalization of the dipyrromethane is that the 2'
position of unmodified pyrrole has a high degree of electron density. The electron density is
vastly distributed in the 2' position vs. the 3' position. Because of this electrophilic
substitution is selectively favoured for the 2' position.
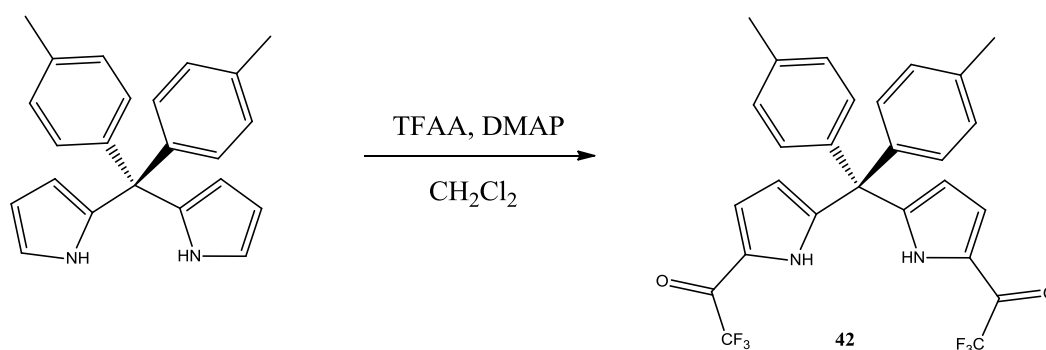
Scheme 5.3: Preparation of **42**.

The ditolyldipyrromethane scaffold (1 eq) was partially dissolved in anhydrous CH_2Cl_2 with
a catalytic quantity of DMAP. This solution was chilled to 0 ^{o}C and stirred under an argon
atmosphere. The dropwise addition of trifluoroacetic anhydride (2.5 eq) immediately
dissolves the partially dissolved dipyrromethane in solution. The reaction was allowed stir at
room temperature once all the TFAA was added. The rate of reaction was monitored by TLC
against the starting material using a solvent system of (95:5) hexane: ethyl acetate. The
reaction has a quick conversion rate in CH_2Cl_2 as full conversion is observed after 20
minutes. After sufficient aqueous washes with sodium bicarbonate, water and brine, the
organic solvent was removed *in vacco* and **42** was obtained in quantitative yield shown in
scheme 5.3. Compound **42** was fully analysed by ^{1}H, ^{19}F and ^{13}C.

The reaction was also attempted using diethyl ether and acetonitrile as solvents and the
results shown in table 5.1. Both of these methods were unsuccessful as a mix of mono and
disubstituted products were obtained after long reaction periods. Heating of the reaction did
not favour the formation of **42** as mono substituted product was still observed by TLC. The
efficiency of the reaction in CH_2Cl_2 was superior to both alternative solvents.

Table 5.1: Effects of solvent and temperature on the substitution of the ditolyldipyrromethane scaffold.

Solvent	Temperature	Mono/disubstitution mix after 24 hours	Exclusive 2,2 disubstitution (**42**)
Diethyl ether	0°C	Yes	No
Diethyl ether	RT	Yes	No
Diethyl ether	Reflux	Yes	No
Acetonitrile	0°C	Yes	No
Acetonitrile	RT	Yes	No
Acetonitrile	Reflux	Yes	No
Dichloromethane	**0°C-RT**	**No**	**Yes**

## 5.3.2 Direct coupling via the TFAA modified dipyrromethane

An attempt was made to prepare **43** by direct coupling of the side chain derivative N-Boc ethylenediamine with **42** as shown in scheme 5.4. The reaction was attempted in CH_2Cl_2 using TEA as a catalyst. The reaction did not proceed at room temperature nor upon heating with long reaction times. No starting material was converted to product nor by-product as shown by TLC. The trifluorocarbon appears to be a poor leaving group under the conditions used. The pKa of the CF_3^- species is ~28 (in H_2O). The pKa of the TEA catalyst is ~10.8 and the amine similar. The reaction conditions for amide formation with the CF_3 group would be difficult via this method as the pKa's are relatively close. As a result, the trifluorocarbonyl must be hydrolysed to the corresponding carboxylic acid to introduce the required side chain derivatives.
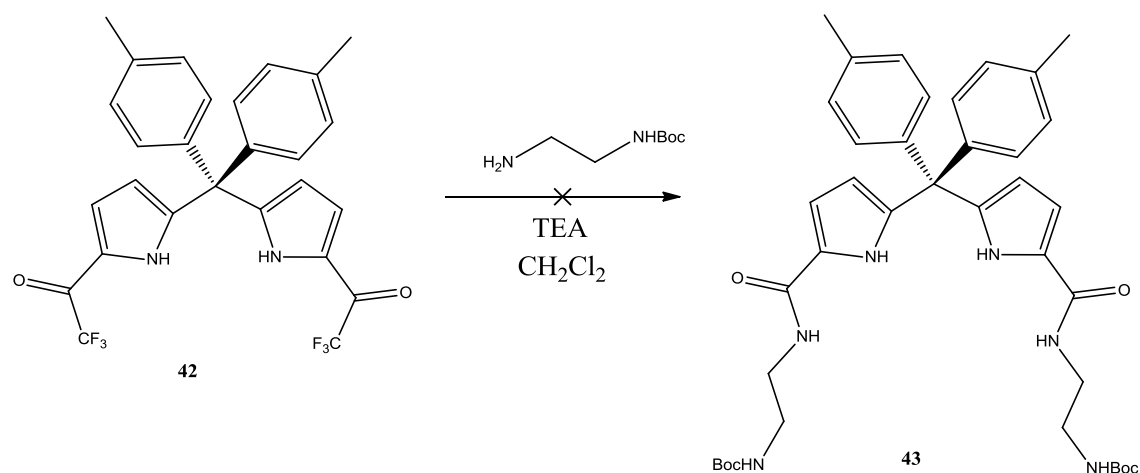
Scheme 5.4: Attempted preparation of **43**.

5.3.3 Hydrolysis of the functionalized dipyrromethane to 2,2 dicarboxyl-ditolyldipyrromethane

Dipyrromethane **42** (shown in scheme 5.5) was hydrolysed by refluxing the compound in a mix of aqueous NaOH and EtOH overnight. After the reaction had gone to completion the mother liquor was reduced to approximately a third of its volume. The pH was carefully acidified by the dropwise addition of concentrated HCl until full precipitation of the free acid **44** was observed. The precipitate that formed was a yellow/beige colour and was isolated by vacuum filtration and dried in the vacuum oven at 70 ^{o}C, 800 mbar to give **44** in quantitative yield. Selectively functionalizing these molecules from the initial ditolyldipyrromethane to 2,2-dicarboxyl-ditolyldipyrromethane was quantitative.
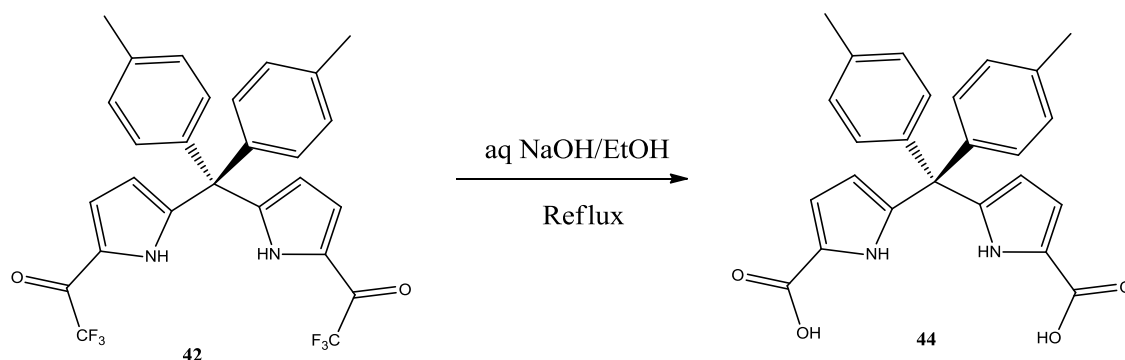
Scheme 5.5: Hydrolysis of **42** to the corresponding dicarboxylic acid **44.**

5.3.4 Synthesis of 43 via EDCI coupling

The target compounds **43** could now be synthesized using EDCI/NHS activation of the carboxylic acid followed by conversion to the amide, scheme 5.6. The solvents used for this coupling were CH_2Cl_2, CH_3Cl, ACN and DMF shown in table 5.2.
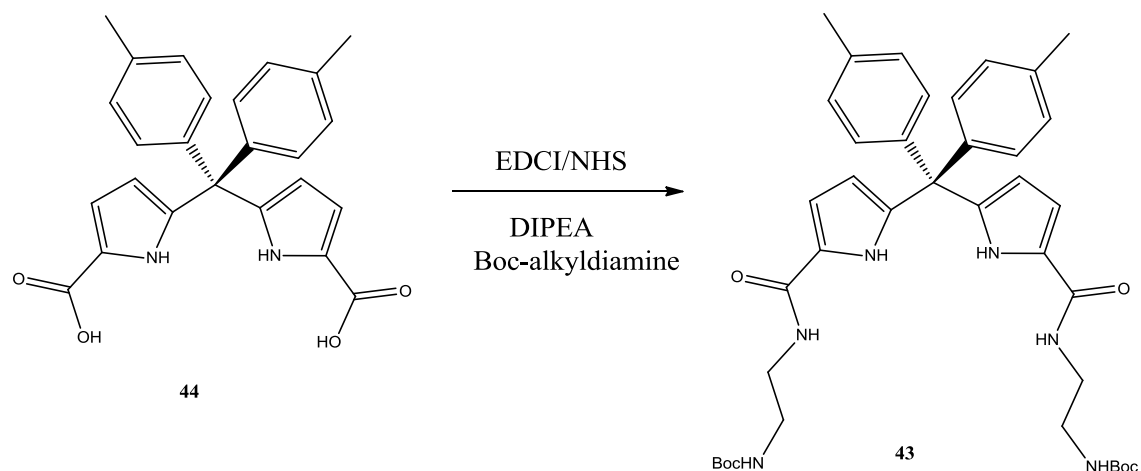
Scheme 5.6: Preparation of **43** by EDCI coupling.

Table 5.2 shows the reaction times for the conversions of **44** to **43**.

Solvent	Reaction time (hours)	Yield %
CH_2Cl_2	24,48,72	0
CH_3Cl	24,48,72	0
CAN	48	0
DMF	48	11
DMF	92	13

The coupling of the functionalized dipyrromethane was initially subjected to the same reaction conditions with different solvents. Compound **44**, was charged into a 2 neck reaction flask and placed under an argon atmosphere and stirred. The solvent was then added and the contents cooled to 0 $^{\circ}$C. The dipyrromethane was not fully soluble in any of the reaction solvents used. The coupling reagent (EDCI) and additive (NHS) was added quickly and

stirred at 0 $^{\circ}$C for an hour to activate the carboxylic acid. N-Boc ethylenediamine was added dropwise to the reaction flask with DIPEA. The reactions were monitored by TLC. For the chlorinated solvents CH_2Cl_2 and CH_3Cl no product was isolated. The TLC analysis for any of the reactions performed in these solvents showed a large number of unwanted impurities and that the starting material was fully consumed after 24 hours. The formation of the amide bond in the reaction was also monitored by FT-IR. Analysis after column chromatography 95:5 CH_2Cl_2:EtOH on silica gel showed the target compound **43** was not present. ^{1}H NMR of the isolated fractions gave an array of peaks which do not match with predicted spectra. FT-IR showed for all fractions isolated a mix of stretching vibrations for COOH, COOR and CO-NH. Acetonitrile was similar as no product was isolated from the reactions using this solvent.

However, the reaction did proceed in DMF giving yields for **43** of 11% after 48 hours and 13% after 92 hours. The reaction conditions were slightly modified to try to improve the yield of **43** in DMF. The modification made was to add the DIPEA base to the reaction before the EDCI/NHS was to be added. Dipyrromethane **44** was fully soluble in DIPEA, as the free acid is converted to the deprotonated conjugate base. The issue with this is that the coupling reagent requires **44** to be in the free acid form to initiate the coupling and this was reflected in the lack of any conversion to the target compound.

5.3.5 Introduction of the side chain derivatives alkyldiamines using TClAA.

The introduction of the required side chain N-boc alkyldiamines were introduced into the dipyrromethane scaffold with great difficulty, the coupling via EDCI was extremely solvent sensitive and very low yielding. Optimisation of the yield would require a different strategy of amide introduction rather than through the carboxylic acid. Taking adavantage of the knowledge that the Boc intermediate is highly insoluble in common bench organic solvents, no column chromatography would be required for purification. Eliminating additives such as coupling reagents reduces impurities such as N-acylurea by-products that could hinder the formation of the product.

The initial idea that the N-Boc alkyldiamine could be introduced via nucleophilic substitution of the trifluorocarbon to the amide was unsuccessful. The pKa of the CF_3 species appeared to be too unfavourable. The hydrolysis to the carboxylic acid proceeded at reflux and an excess of the hydroxide species to drive the reaction to completion. The introduction of the amide bond would be more favourable by replacing CF_3 with CCl_3. The CCl_3H, conjugate acid $^-CCl_3$ has a pKa of ~15.5 which would be theoretically more favourable for displacement. Pyrroles containing trichlorocarbonyls have been shown to convert to amide bonds under soft conditions[3].

5.3.5.1 Synthesis of 45

The preparation of **45** is outlined in scheme 5.7. Ditolyldipyrromethane (**29**) was partially dissolved in anhydrous CH_2Cl_2, a catalytic amount of DMAP was added. The solution was stirred under an argon atmosphere and chilled to 0 ^{o}C for 15 minutes. The dropwise addition of trichloroacetic anhydride to the solution turned the reaction a brownish colour. The reaction was monitored by TLC against **29** the dipyrromethane starting material. Full conversion to **45** was observed after two hours. The electrophilic substitution to the ditolyldipyrromethane is considerably less reactive when trichloroacetic anhydride replaces trifluoroacetic anhydride due to the higher electron withdrawning ability of fluorine compared to chlorine. The reaction, upon completion, was quenched using a saturated Na_2CO_3 solution and washed with brine. The organic solvent was removed *in vacco* and the resulting white solid was recovered in a quantitative yield.

TClAA, DMAP

CH_2Cl_2

29

45
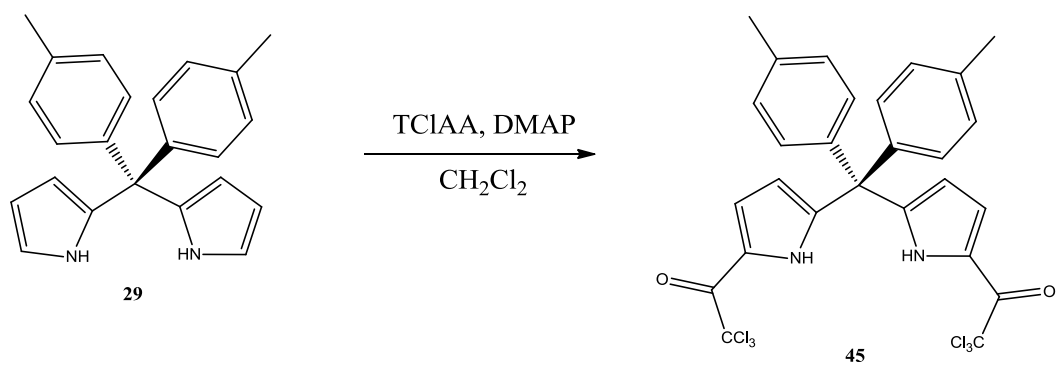
Scheme 5.7: Preparation of **45** from **29**.

5.3.5.2 The introduction of the amide bond into 45

To prepare **43** compound **45** was suspended in anhydrous CH_2Cl_2 and stirred under argon at room temperature. N-Boc ethylenediamine was added dropwise followed by the addition of TEA. The reaction was allowed stir for 24 hours to ensure reaction completion. The precipitate was filtered and washed with CH_2Cl_2 to yield a white solid **43** with a glasslike appearance similar to the isolated product from previous coupling by EDCI in DMF in quantitative yield. The benefit of the introduction of the amide via this route is the lack of impurities generated. The only by-product is chloroform from the nucleophilic displacement of the CCl_3 leaving group. No column chromatography was required as the insoluble nature of the compound allows any impurity to be washed into the filterate.

This method was then applied to prepare **46** and **47** using N-Boc-1,3-diaminopropane and N-Boc-1,4-diaminobutane as the source of amine. The isolated compounds **35** and **36** shown in scheme 5.8 were also yielded quantitatively.
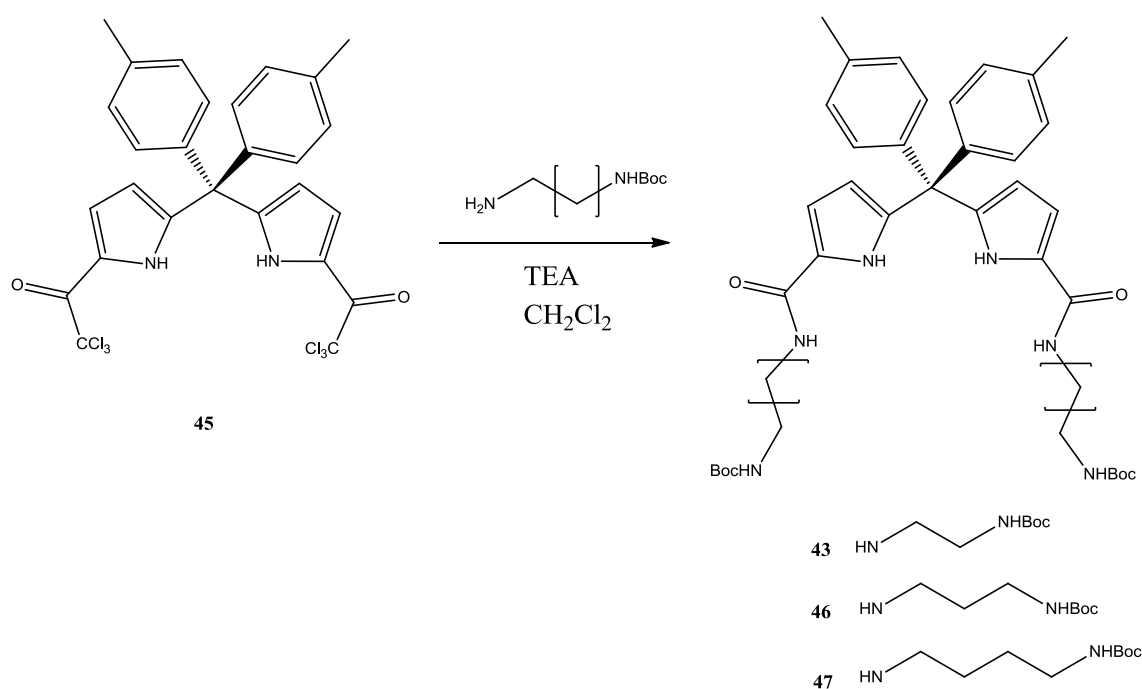
Scheme 5.8: Synthesis of **43**, **46** and **47**.

5.3.5.3 ¹H NMR of N-Boc diethylenediamine ditolyldipyrromethane

The ^{1}H NMR of **43** is shown in figure 5.1. The pyrrole NH protons are shown at 10.82 ppm as a broad singlet with an integration of two. The amide NH protons are observed at 8.04 ppm as a triplet with an integration of two. The phenyl protons are shown at 7.11 ppm and 6.80 ppm, these both have an integration of four and are observed as doublets due to the para disubstituted environment they are both experiencing. The NH protons from the carbamate are shown at 6.89 ppm as a triplet and also have an integration of two. The β-pyrrole hydrogen's are shown at 6.64 ppm and 5.69 ppm. Both multiplets have an integration of two. The two methylene groups on the alkyl chain are shown at 3.22 ppm and 3.06 ppm as broad quartets with both integrating to four. The methyl hydrogens at 2.29 ppm on the para phenyl region of the molecule have an integration of six and are seen as a singlet. The Boc protons are observed at 1.36 ppm and are also shown as a singlet with an integration of eighteen.
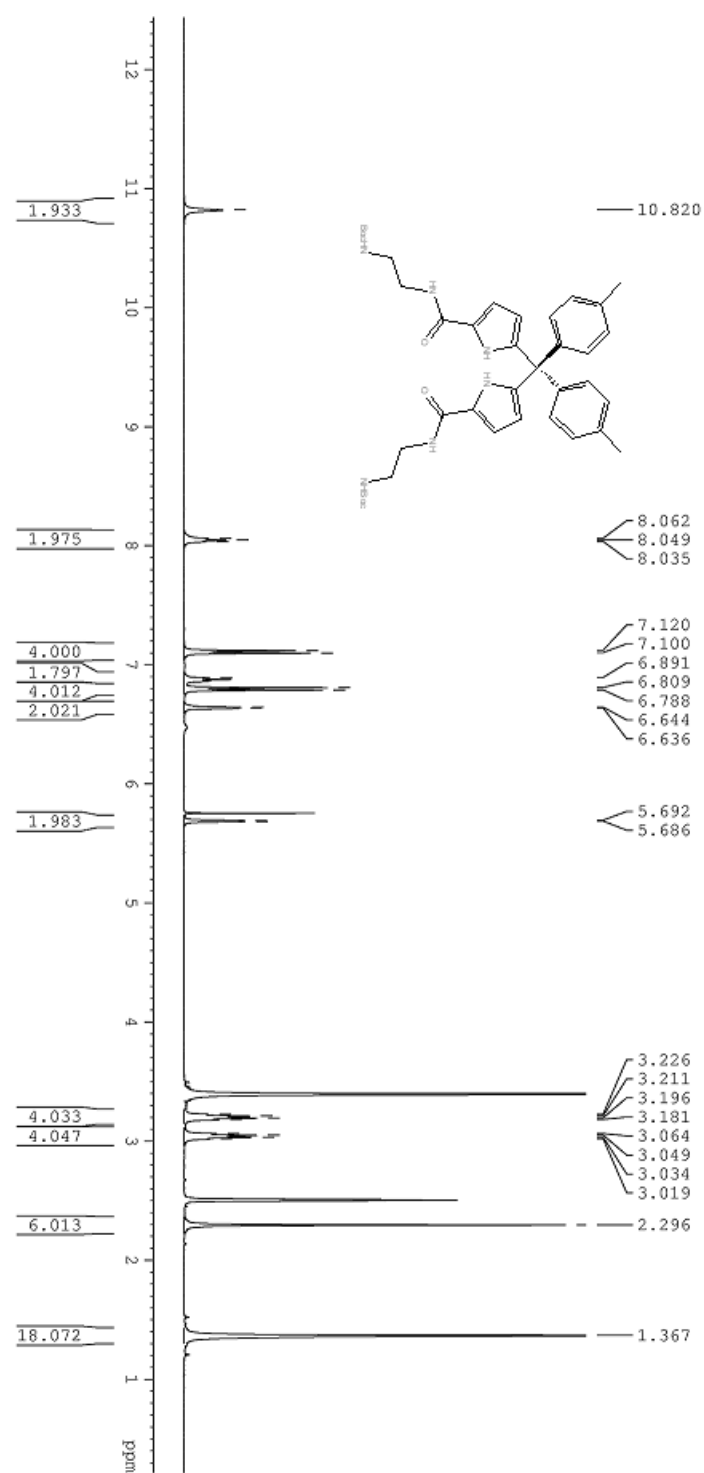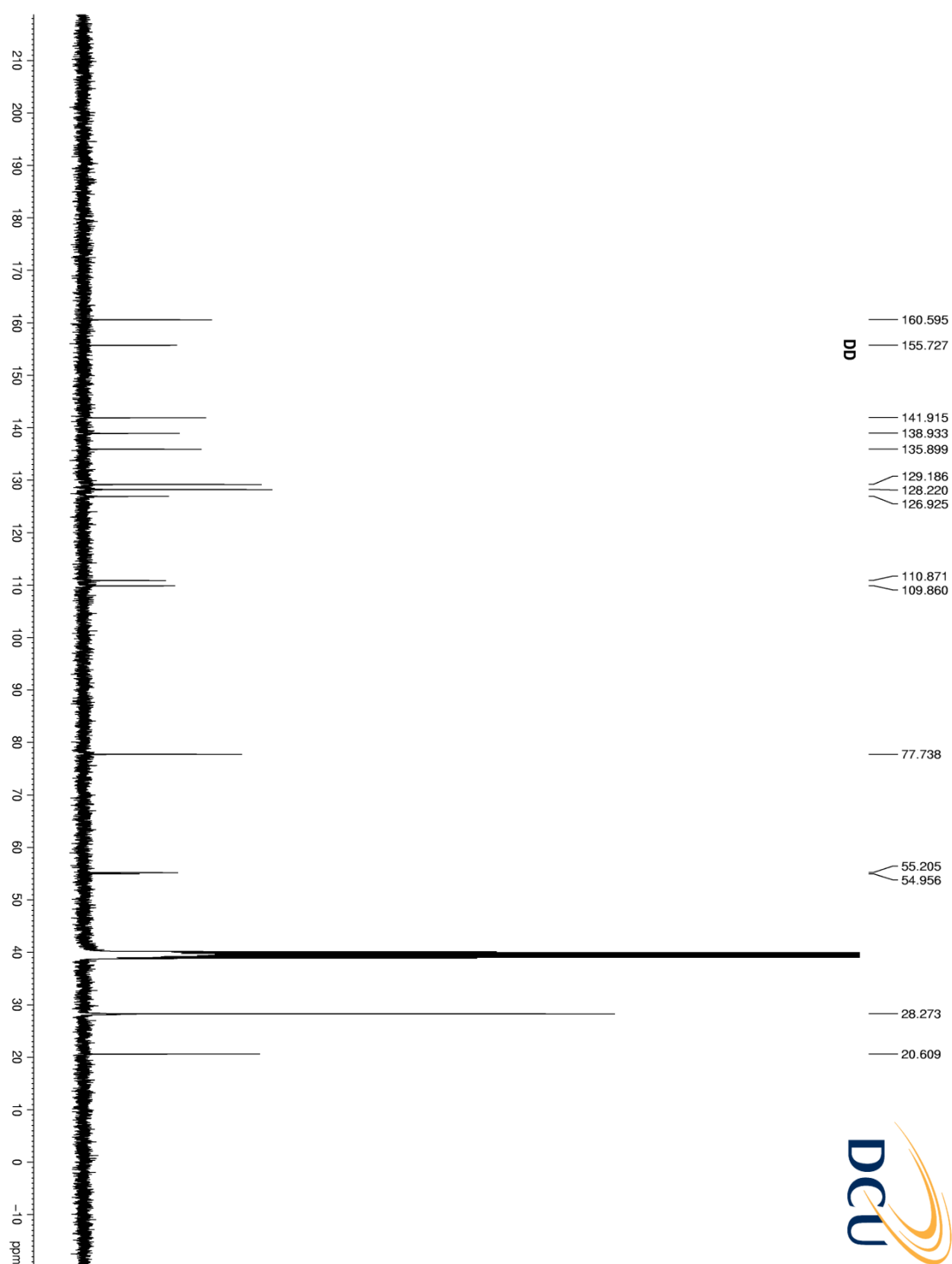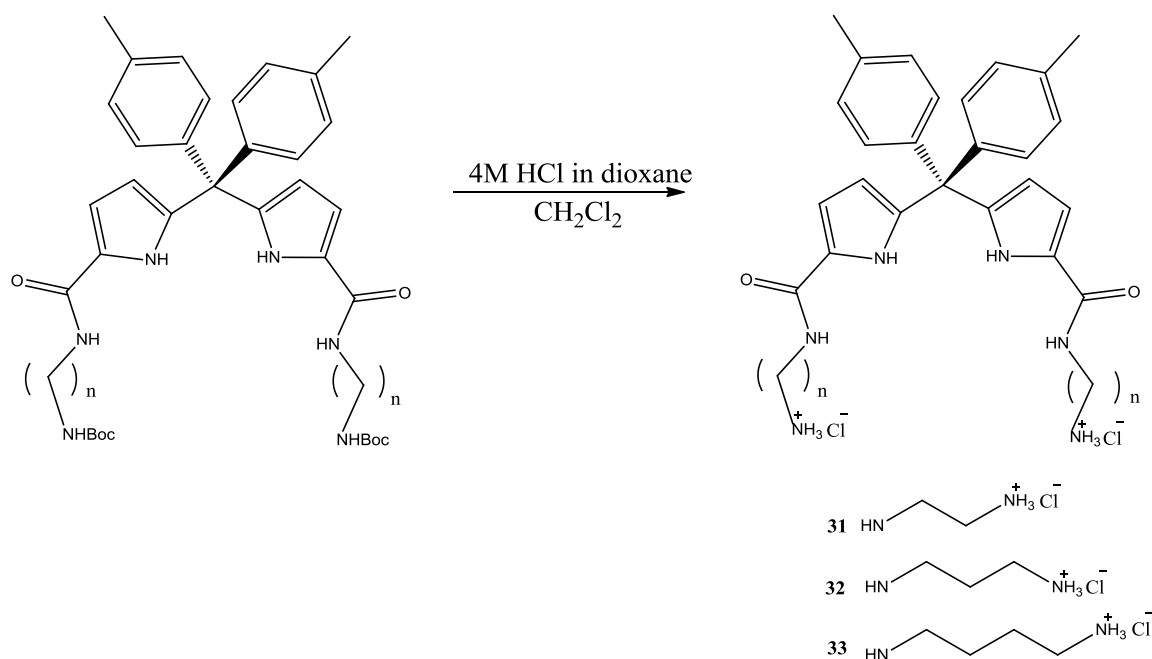
Figure 5.1a: ^{1}H NMR of **43** in DMSO-d$_6$.

Figure 5.1b: ^{13}C NMR of **43** in DMSO-d$_6$

5.3.5.4 Cleavage of N-Boc alkyldiamine ditolyldipyrromethanes.

Scheme 5.9: Deprotection of the Boc protecting groups to give **31-33**.

The cleavage of the N-Boc alkyl ditolyldipyrromethane derivatives **43,46** and **47** is outlined in scheme 5.9. The protected dipyrromethane derivatives were charged into a 25 mL round bottom flask and suspended in anhydrous CH_2Cl_2. The suspension was placed under an argon atmosphere and stirred at 0 °C. A volume of 4M HCl in dioxane solution was added dropwise to the suspension. The suspension slowly dissolved as the reaction was brought to room temperature. As the Boc groups cleave the HCl salt form of the dipyrromethane precipitates out of the CH_2Cl_2. The time required for this reaction was 24 hours to allow for complete cleavage of all the Boc groups. The products were isolated by filtration followed by washing with small aliquots of CH_2Cl_2 and Et_2O to give the products **31**, **32** and **33** as white solids in quantitative yields.

5.3.5.5 ¹H NMR and ¹³C NMR of 31

The ^{1}H NMR of **31** is shown in figure 5.2a. The pyrrole NH protons are shown at 10.95 ppm as a broad singlet with an integration of two. The amide NH protons are observed at 8.4 ppm as broad triplets with an integration of two. The NH_3^+ protons from the cleavage of the Boc groups appear as a broad singlet and an integration of six. The phenyl protons are shown at 7.1 ppm and 6.8 ppm, these both have an integration of four and are observed as doublets due to the para disubstitution. The β-pyrrole hydrogen's are shown at 6.7 ppm and 5.7 ppm. Both multiplets have an integration of two. The two methylene groups on the alkyl chain are shown at 3.5 ppm and 2.9 ppm with both having an integration of four. The multiplicity of the methylene group at 3.5 ppm is a quartet these represent the protons adjacent to the amide. The methylene group at 2.9 ppm is a triplet and these are the protons adjacent to the protonated amine. The methyl hydrogens at 2.3 ppm on the para phenyl region of the molecule have an integration of six and are seen as a singlet.

The ^{13}C NMR of **31** is shown in figure 5.2b. The amide carbonyl is found at 160.9 ppm. The quaternary pyrrole adjacent to the amide carbonyl is found at 141.8 ppm. The two quaternary carbons on the aryl ring is found at 139.2 ppm and 135.8 ppm. The two aryl C-H carbons are found at 129.1 ppm and 128.2 ppm. The last aromatic quaternary pyrrole carbon is found at 126.6 ppm. The two β-pyrrole carbons are found at 111.0 ppm and 110.3 ppm. The central quaternary carbon is found at 55.2 ppm. The aliphatic carbons on the alkyl chain are found at 40.1 ppm and 36.5 ppm. The peak at 40.1 ppm is underneath the solvent peak, however, DEPT-135 showed a negative peak indicating the presense of this peak. Lastly, the tolyl methyl carbon is found at 20.6 ppm.
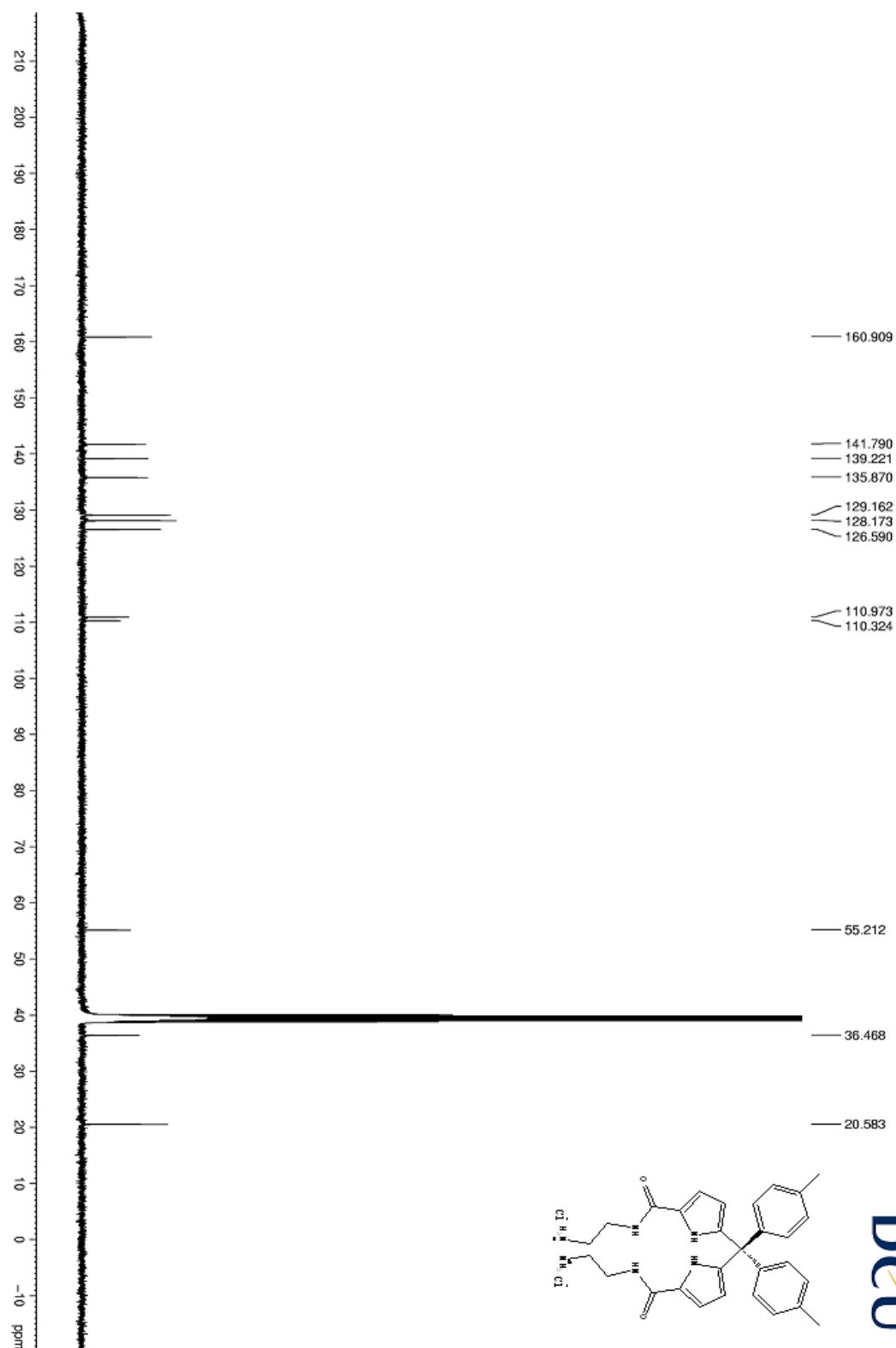
Figure 5.2a: ^{1}H NMR of **31**.

Figure 5.2b: ^{13}C NMR of **31**

### 5.3.5.6 Synthesis of diphenyldipyrromethane and modification with TClAA

The synthesis of diphenyldipyrromethane **22** from benzophenone and pyrrole was achieved by the same protocol used by Turner *et al*[1]. The modification of the 2' position with TClAA, shown in scheme 5.10, was performed to give the target compound **48** in quantitative yield. The purpose of the synthesis of this diphenyl derivative vs the ditolyl derivative was to identify whether or not the small modification on the phenyl group has drastic implications on the bioactivity of these molecules.
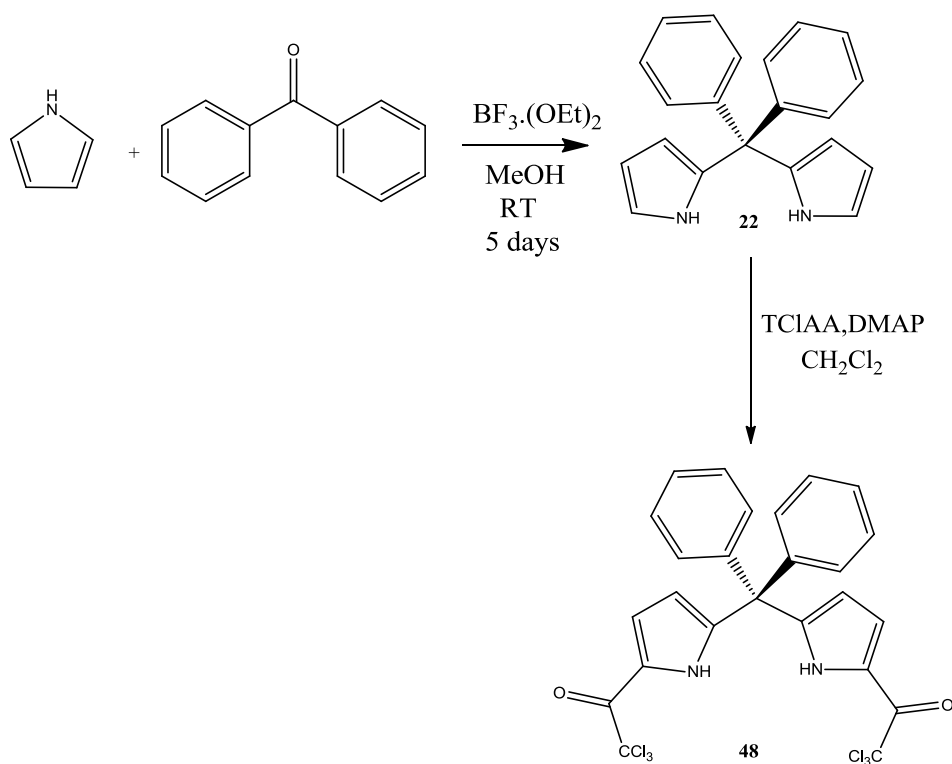
Scheme 5.10:Preparation of **48**.

5.3.5.7 Amide functionalization of the Diphenyldipyrromethane-COCCl₃ species.

Dipyrromethane **48** was converted to the N-Boc ethylene diamine derivative using the same procedure used for the preparation of **43** to give the product **49** in quantitative yield (shown in scheme 5.11). The ^{1}H NMR of **49** is shown in figure 5.3
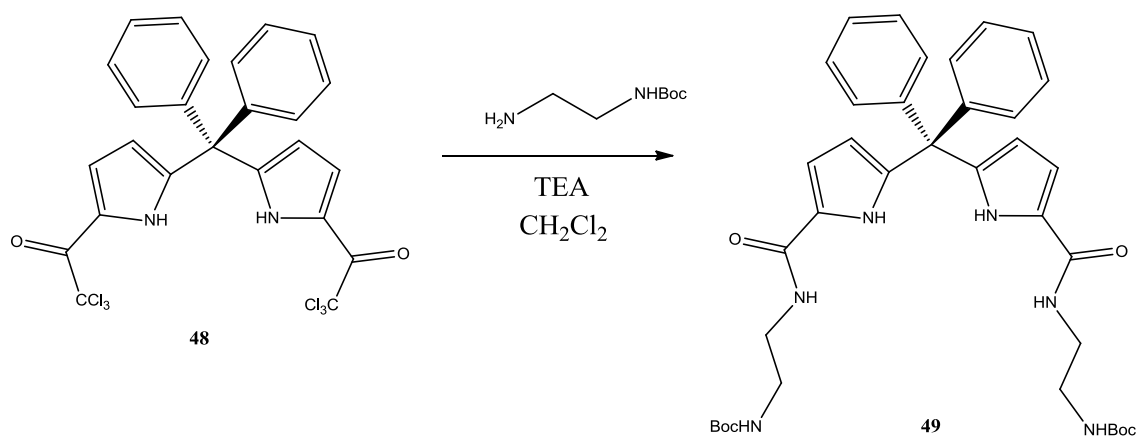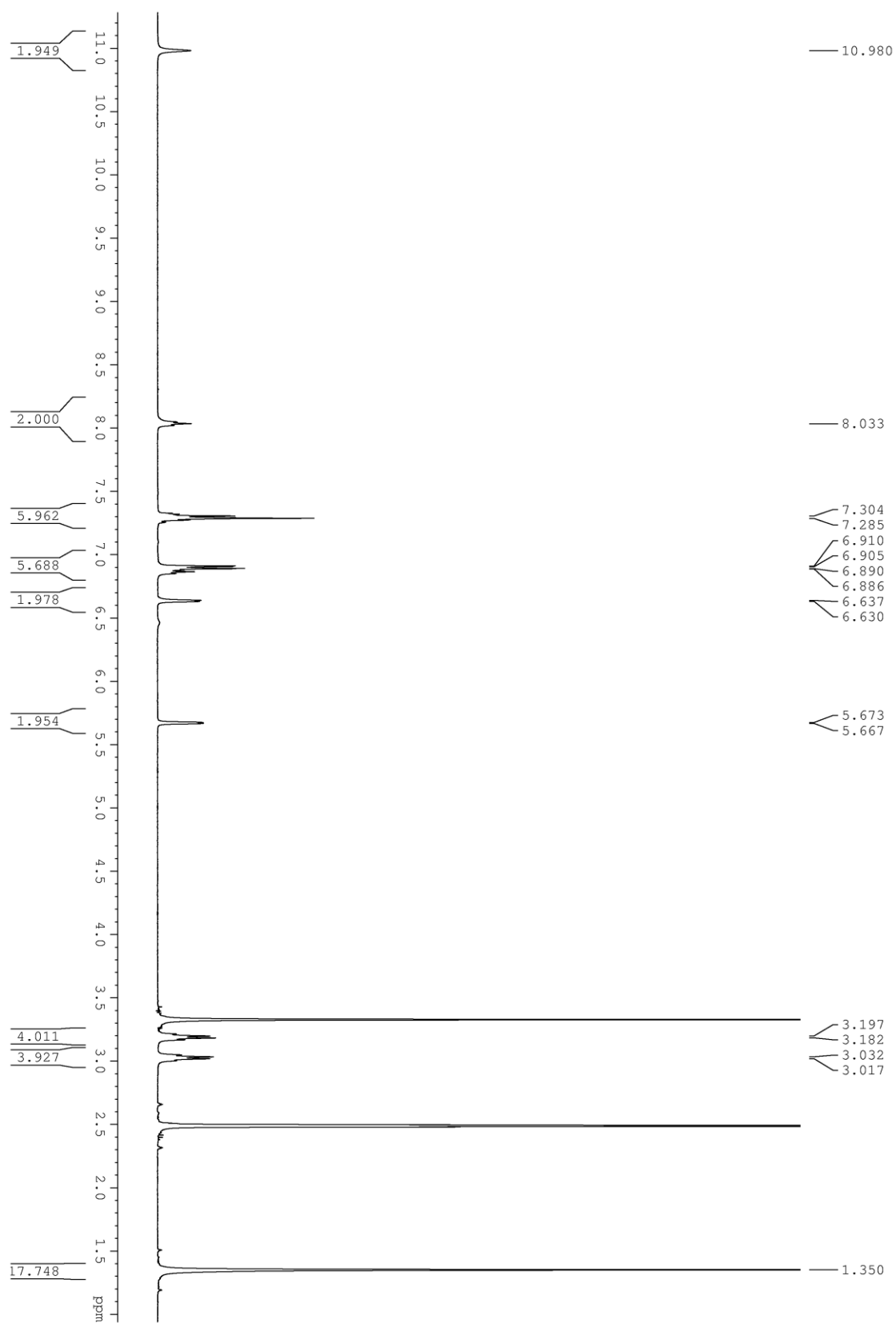

Scheme 5.11: Conversion of **48** to **49**.

Figure 5.3: ^{1}H NMR N-Boc ethylenediamine diphenyldipyrromethane **39**.

5.3.5.8 Cleavage of the N-Boc ethylenediamine diphenyldipyrromethane derivative

The N-Boc ethylenediamine diphenyldipyrromethane derivative **49**, shown in scheme 5.12 was deprotected using 4M HCl in dioxane solution to give the HCl salt product after filtration and CH_2Cl_2, Et_2O washing to give **50** in quantitative yield.
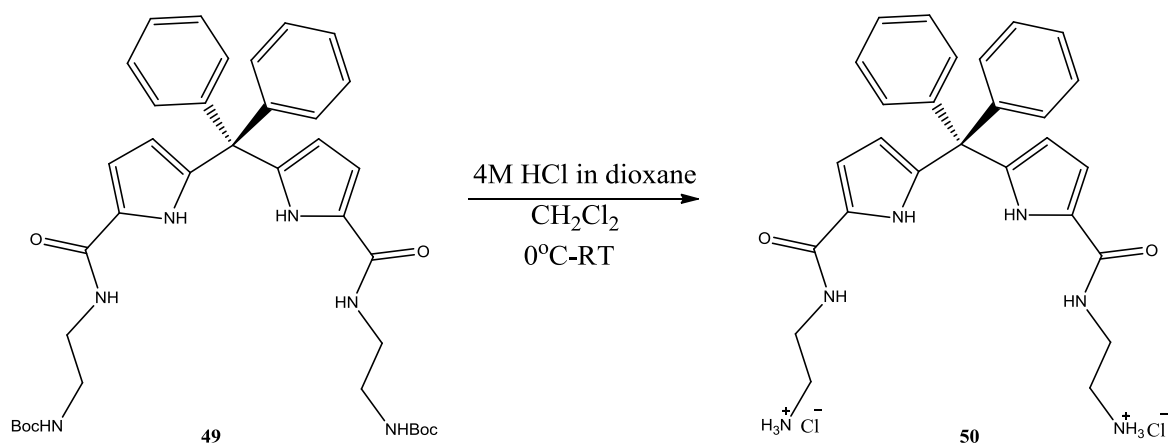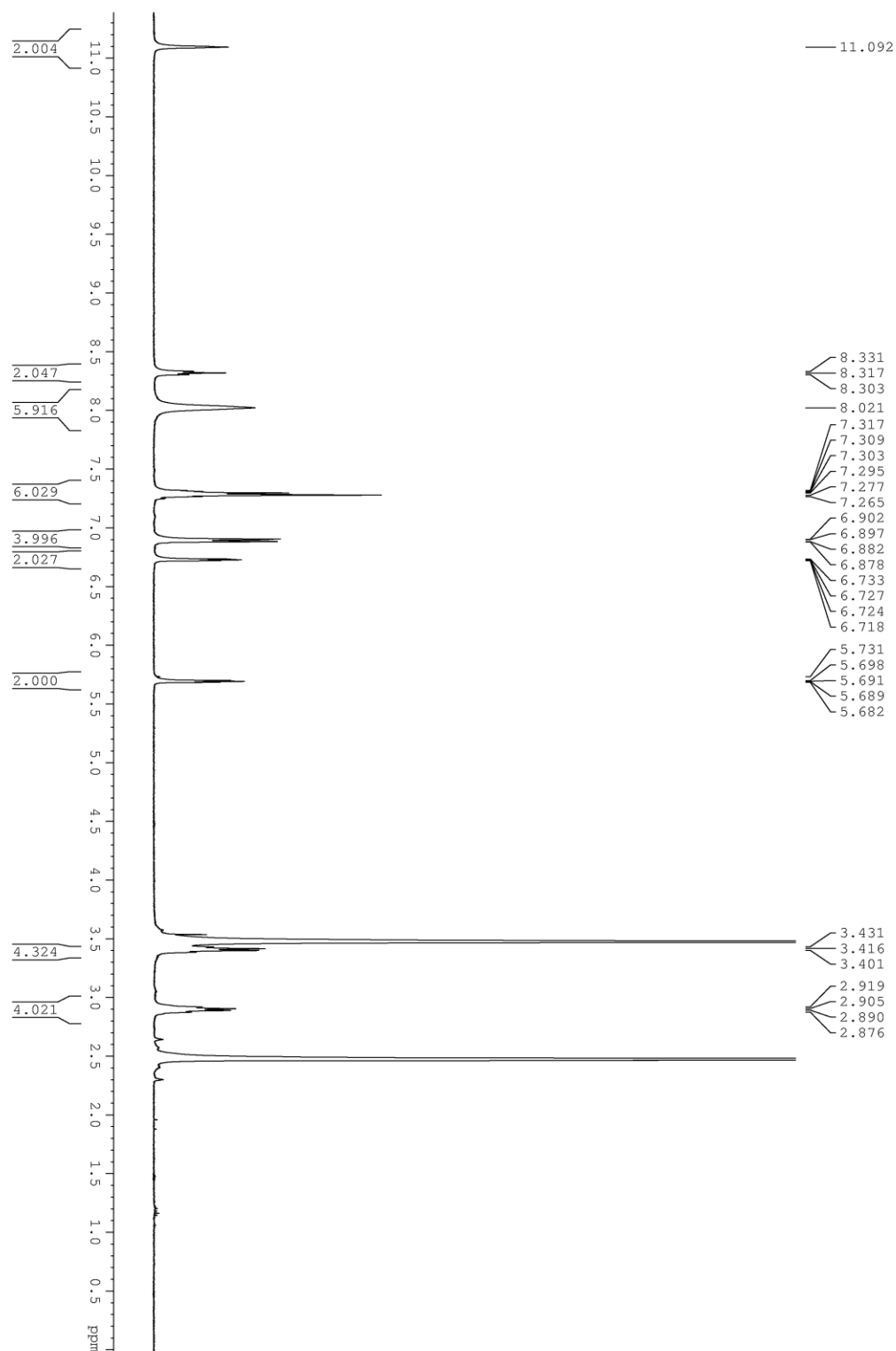

Scheme 5.12: Deprotection of **49** with 4M HCl in dioxane.

Figure 5.4: [^1]H NMR of **50**.

5.4 Synthesis of modified Ditolyl dipyrromethane at the para position

What was discovered from the calix[4]pyrrole chapter, particularly in the section that illustrated the point that aryl ketones bearing electron withdrawing/donating groups do not condense to the functionalised dipyrromethane. The molecular modelling simulations of theoretical molecules (Chapter 4 Figure 4.23 compounds **39**-**41**) that possess amide bonds and alkyl ammonium species in place of the tolyl group have shown a higher number of interactions with key amino acid residues that we believe to be important for inhibition. Thus, such compounds might be more potent Kv1 channel blockers, further investigation into preparing these derivatives was undertaken.
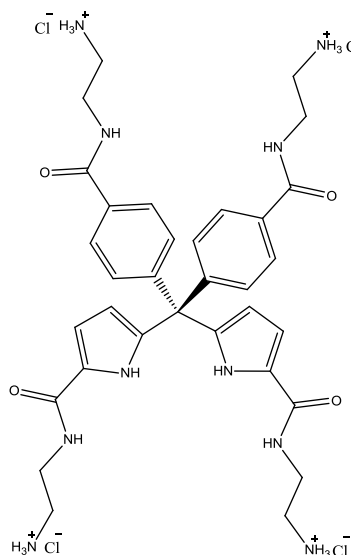

Figure 5.7: Plausible target, **39**, based upon molecular modelling simulations

5.4.1 Route 1: Condensation of dicarboxybenzophenone with pyrrole

An attempt to prepare the dipyrromethane starting precursor for **39** involved the condensation of pyrrole with 4,4-dicarboxybenzophenone in the ratio (1:2). Different acid catalysts were chosen along with different mono and duel solvent systems which are listed in table 5.3. The reactions were carried out at different temperatures ranging from room temperature to reflux over 5 days in a parallel carousel reaction apparatus. Subsequently, all reactions failed to produce any condensation product, for each reaction unreacted dicarboxyketone starting

material was recovered. The results of all of these reactions are shown in tables 5.3, 5.4 and scheme 5.13 .

Table 5.3: List of conditions for the condensation performed in carousel apparatus at room temperature.

Temperature	Solvent	Catalyst
Room temperature	MeOH	$BF_3.(OEt)_2$
Room temperature	MeOH	HCl
Room temperature	MeOH	$MeSO_3H$
Room temperature	MeOH	TFA
Room temperature	EtOH	$BF_3.(OEt)_2$
Room temperature	EtOH	HCl
Room temperature	EtOH	$MeSO_3H$
Room temperature	EtOH	TFA
Room temperature	TFA	TFA
Room temperature	DMF	$BF_3.(OEt)_2$
Room temperature	DMF	HCl
Room temperature	DMF	$MeSO_3H$
Room temperature	DMF	TFA
Room temperature	DMF	Acetic acid
Room temperature	$MeOH/CH_2Cl_2$	$BF_3.(OEt)_2$
Room temperature	$MeOH/CH_2Cl_2$	HCl
Room temperature	$MeOH/CH_2Cl_2$	$MeSO_3H$
Room temperature	$MeOH/CH_2Cl_2$	TFA

Table 5.4: List of conditions for condensation performed in carousel apparatus at elevated temperatures

Temperature	Solvent	Catalyst
Reflux	MeOH	$BF_3.(OEt)_2$
Reflux	MeOH	HCl
Reflux	MeOH	$MeSO_3H$

Reflux	MeOH	TFA
Reflux	EtOH	BF$_3$.(OEt)$_2$
Reflux	EtOH	HCl
Reflux	EtOH	MeSO$_3$H
Reflux	EtOH	TFA
Reflux	TFA	TFA
100°C	DMF	BF$_3$.(OEt)$_2$
100°C	DMF	HCl
100°C	DMF	MeSO$_3$H
100°C	DMF	Acetic acid
55°C	MeOH/CH$_2$Cl$_2$	BF$_3$.(OEt)$_2$
55°C	MeOH/CH$_2$Cl$_2$	HCl
55°C	MeOH/CH$_2$Cl$_2$	MeSO$_3$H
55°C	MeOH/CH$_2$Cl$_2$	TFA

The reactions were analysed by TLC and ^{1}H NMR. The main issue that was found with most of the reactions undertaken was related to the solubility of the ketone. The ketone was only fully soluble in DMF at room temperature. Duel solvent systems were also shown to be unsuccessful.
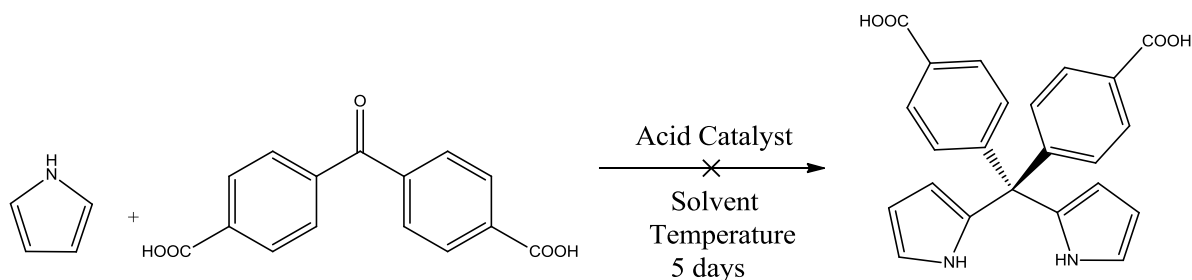
Scheme 5.13: Attempted condensations using various temperature and acid conditions.

To try to overcome these solubility problems the 4,4-dicarboxybenzophenone was subjected to esterification with methanol and dry HCl to form the methyl ester derivative shown in scheme 5.14. Condensation reactions between the 4,4- dimethylcarboxylate-benzophenone derivative and pyrrole were conducted to exactly the same conditions shown in table 5.3 and 5.4. The reactions followed the same fate as the previous reactions and no product was obtained.
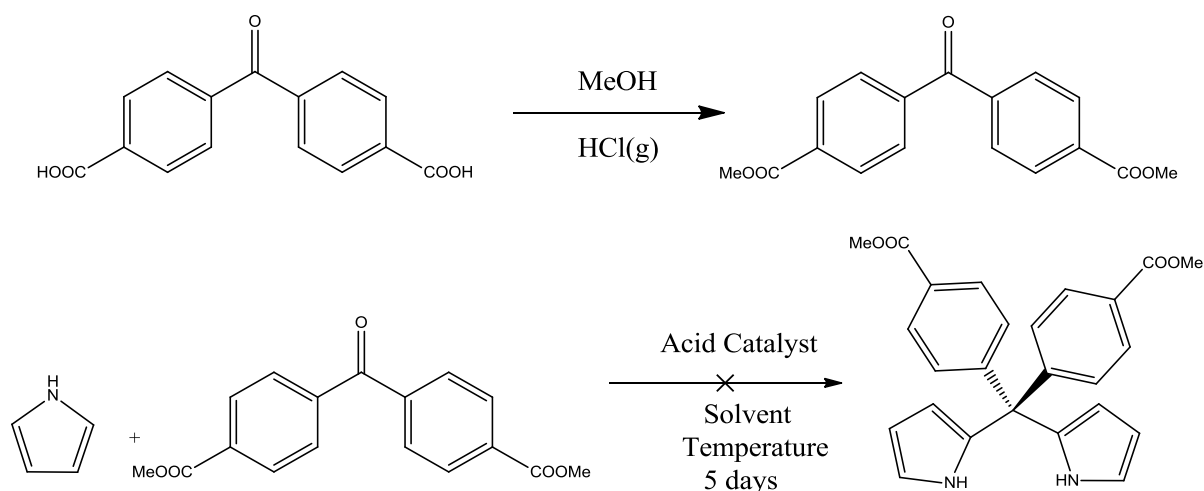
Scheme 5.14: Attempted condensation from the ester derivative.

These findings verify that condensation of the ketone is effected by the presence of electron withdrawing groups at the para position of the aryl phenyl ring. As a consequence a second approach to prepare the precursor for **39** was undertaken.
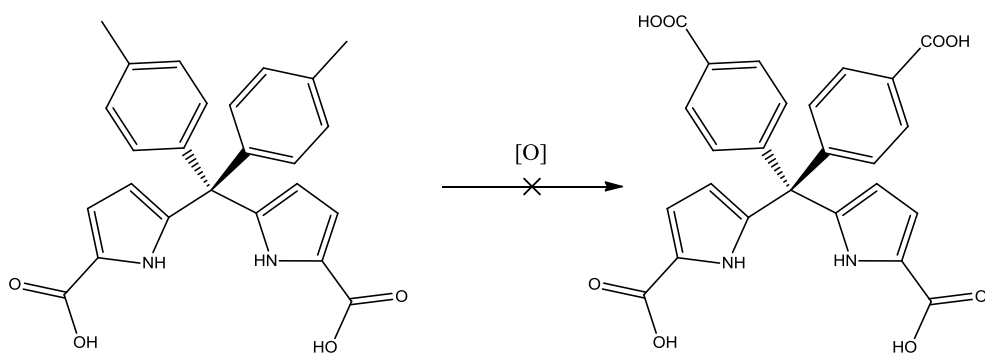
5.4.2 Oxidation

In chapter 3, post oxidative modification of the benzylic tolyl group of the calix[4]pyrrole ring was unsuccessful. The asymmetric calix[4]pyrrole was extremely unstable to oxidative conditions, this instability can be explained by the presence of four distorted sp^3 hybridised bridging carbons[4]. This distortion may have led to the oxidative destruction of the macrocycle. The oxidation of the dipyrromethanes would give definitive information as to whether the decomposition observed with the calix[4]pyrroles is a result of the distortion caused by the macrocycle ring or due to the oxidation of the pyrrole sub-unit.

The oxidation of dipyrromethane was performed on two substrates **29** shown in scheme 5.15 and **44** shown in figure 5.16. Both **29** and **44** decomposed under $KMnO_4$ conditions (same conditions as used in in chapter 3). The fact that both **29** and **44** decomposed illustrates the liability of the pyrrole ring to oxidation conditions. Precipitation of both reactions by acidifying the solutions subsequent filtration and analysis by ^1H NMR showed no pyrrole hydrogen's on the nitrogen nor the β-position.
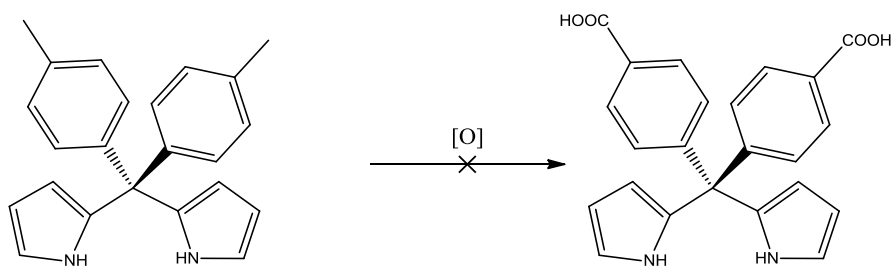
Scheme 5.15: Failed oxidation of ditolyldipyrromethane **29.**

Scheme 5.16: Failed oxidation of dicarboxy-ditolyldipyrromethane **44.**

5.5 Biological evaluation of dipyrromethanes.

In search of a small molecular weight blocker(s), a recently-designed expression platform[6,7] was utilized to express various Kv1 channels in a single open reading frame (ORF) after transfecting human embryonic kidney (HEK)-293 cells. Such a strategy allows predetermination of not just the combinations of α subunits in the Kv 1 channels but, also, their actual arrangements in the tetrameric channels on the plasmalemma. This is exemplified by the observed fast-inactivation of Kv1.4-containing channels only when Kv1.6 with its N-terminal inactivation prevention domain is placed adjacent to Kv1.4 [possesses an N-terminal inactivation ball].[6] In this way, the importance has been established of the stoichiometry and positioning of α subunits for determining the interaction of tetraethylammonium with Kv1.1- and 1.2-containing heteromers that mimic those in the brain[6,8]. Herein, these concatenated Kv1 channels were utilised as targets to evaluate the compounds **31**-**33** prepared in chapter 4.

5.5.1 Evaluation of the existing therapeutic 4-aminopyridine against the Kv channels.

As shown by *Judge and Bever*[5], the existing therapeutic 4-AP is not selective against the Kv1 channels. As already discussed in chapter one, all of the related side effects caused by 4-AP are directly related to non-selective inhibition. 4-AP was again tested against concatenated tetramers of Kv1.1 and Kv1.2. The results corresponded with the literature, there was no selectivity between the two channels, and both showed considerable inhibition. These experiments were important to act as a control. As shown in the review by *Judge and Bever*[5], there are considerably wide IC_{50} values reported for the inhibition of Kv1.1 (89-1100 μM) and Kv1.2 (200-800 μM) by 4-AP. It must be emphasised that these values are based upon homometric channels and don't mimic the Kv1 tetramers as they would appear in nature.

To verify any activity of the prepared dipyrromethanes, a direct comparison between the results found with 4-AP with **31**-**33** will be done in order to obtain a true evaluation of the potency and potential of **31**-**33** as Kv1 channel inhibitors.

Table 5.5: Concatenated Kv1.1 and 1.2 channels against 4-AP.

Channel	IC_{50} (µM)	Hill slope	Experiment no
Kv$(1.1)_4$	530 ± 56	0.8 ± 0.1	7
Kv$(1.2)_4$	850 ± 35	0.9 ± 0.1	10

The IC_{50} values shown in table 5.5 give the degree of inhibition 4-AP has for the Kv1 channels we have expressed. We only looked at Kv1.1 and Kv1.2 as these are channels are most prevalent in the brain. The 4-AP molecule only inhibits the Kv1.1 tetramer at 530 µM and the tetramer at 850 µM. For a therapeutic these IC_{50} values are not extremely attractive, as low µM-nM ranges are generally associated with most commonly marketed drugs. Even without the selectivity an increase in potency of ten-fold offers a viable alternative to 4-AP treatment. The hill slope obtained for 4-AP indicates that only one molecule of 4-AP is interacting with the inner pore region of the potassium channels. The dose response curve of 4-AP against Kv$(1.1)_4$ and Kv$(1.2)_4$ is shown in figure 5.8.
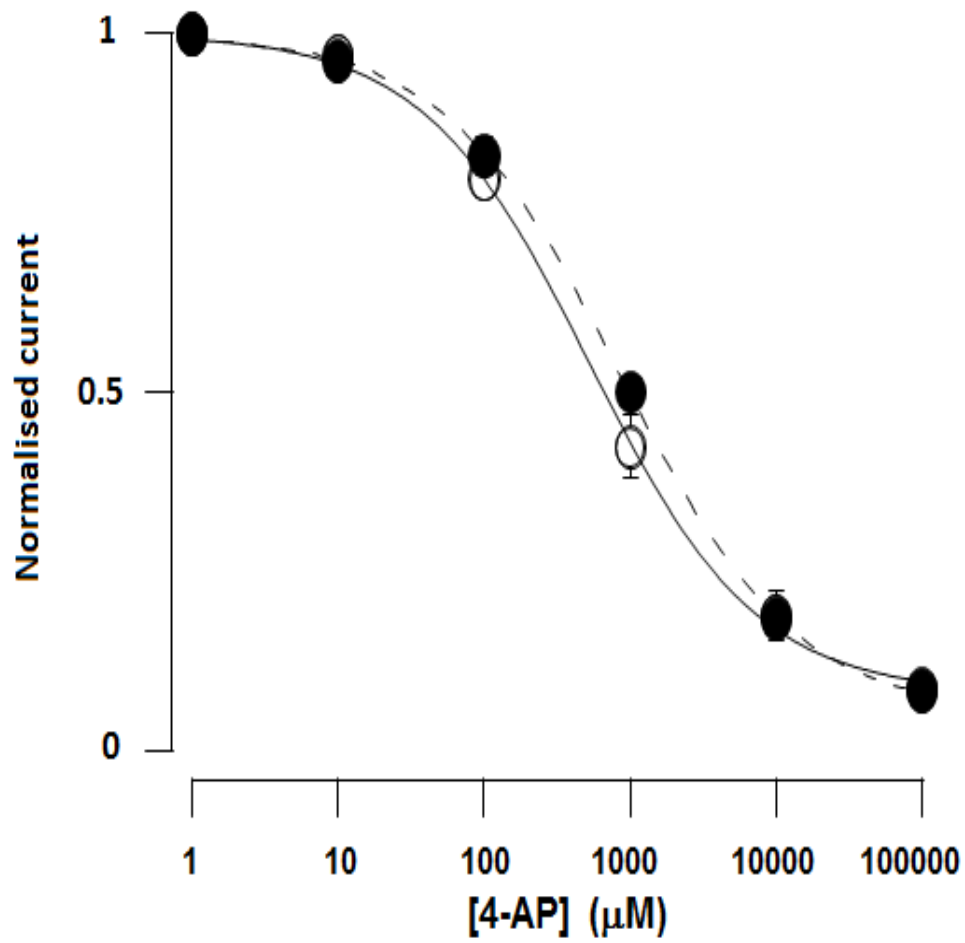
Figure 5.8: Dose response curve of 4-AP against the concatenated Kv1.1 and 1.2 channels.

5.5.2 Bio-evaluation of the prepared dipyrromethanes

The dipyrromethane compounds **31**-**33**, shown in figure 5.9, were tested on the Kv channels 1.1-1.6 as per the method by Al-Sabi *et al.*[6, 7] Each of the compounds were tested at 10 µM.
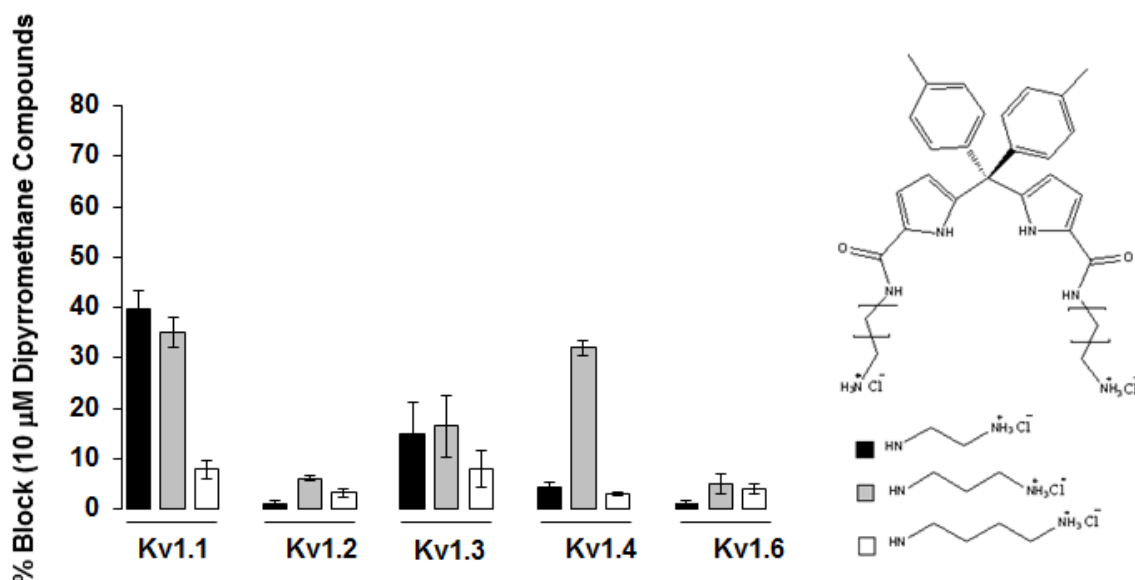

Figure 5.9: Preliminary screen of ditolyldipyrromethane derivatives **31**-**33**.

The graph shown in figure 5.9 represents the preliminary screen of the compounds derived from the molecular modelling of the ditolyldipyrromethane scaffold. The information obtained from the electrophysiology screening of the homometric channels Kv1.1-Kv1.6 showed that, similar to porphyrins, the channels are sensitive to alkyl chain length. Compound **31**, proved to be the most selective and the most potent amongst the compounds tested. Compound **31**, inhibits Kv1.1 at 40-43% and Kv1.3 at 15-17% at 10 µM, it was insensitive to Kv1.2, Kv1.4 and Kv1.6. The high similarities between the selectivity filter and inner turret regions of both Kv1.1 and Kv1.3 limit the preference of inhibition to (2:1) between the channels.

Compound **32**, has similar inhibition to that of **31** for Kv1.1 as it inhibits the channel at 36-38% at 10 µM. The extension of the carbon chain also increases the inhibition of Kv1.3 to 18-23%. The main difference in the activity between **31** and **32** was that **32** inhibited the channel Kv1.4 to the same extent as it inhibited Kv1.1 at 38%. This lack of observed selectivity of **32** between the Kv1.1 and Kv1.4 channel eliminated compound **32** as a

potential selective inhibitor. Lastly, compound **33**, was insensitive to all Kv1 channels as negligible inhibition was obtained when tested against the channels.

The molecular modelling of these compounds illustrated the number of interactions with key amino acid residues that aided in the prediction of their potential biological activity. From the ligand-plots of all three compounds shown in chapter four, both **31** and **32** demonstrated a number of significant interactions (H-bonding and π-π stacking) with the amino acid residues of the Kv1.1 channel. These interactions near the selectivity filter and in the inner turret region of Kv1.1 influence the conductance of the channel. Dipyrromethane **33** appeared not to have the same number of these interactions and this correlates with the observed biological activity. Figure 5.10 shows the corresponding currents as a function of time for **31**-**33** on the Kv1.1 channel. The line shape allow us to interpret the activation mechanism of how the compounds interact with the channel.
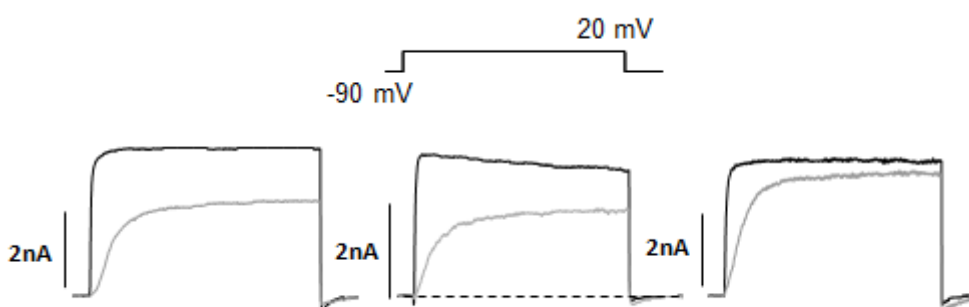

Figure 5.10: Respective current profiles of Kv1.1 treated with **31**, **32** and **33** plotted current against time.

5.5.3 Full cellular evaluation of 31(DDAAKN01)

Evaluation of the results from the preliminary studies of **31,32** and **33** have elucidated that the derivative **31** is the lead candidate from this series of compounds tested on the Kv1 channels. This finding is the first for this type of study using a small molecule inhibitor. The results obtained are only surpassed by extracted venom derived peptide toxins. To mark the exclusiveness of the lead candidate, it shall be renamed **DDAAKN01**.

The obtained IC_{50} value that **DDAAKN01** has is 14μM against Kv1.1. The significance of this potency is, it is approximately 40 times more potent than 4-AP against the Kv1.1 channel

from our testing. The captivating distinctness between **DDAAKN01** and 4-AP is the selectivity it possesses relative to the marketed therapeutic. **DDAAKN01** shows enhanced selectivity for Kv1.1 over the other channels such as Kv1.2, Kv1.4 and Kv1.6, unlike 4-AP which inhibits all of these channels. The measured LogP of **DDAAKN01** is -1.05, this characteristic value prevents it from passing the blood brain barrier (BBB) which is important for our studies as normalised Kv1.1/1.2 concatenated proteins reside in this region. 4-AP also possesses a negative LogP of -0.76
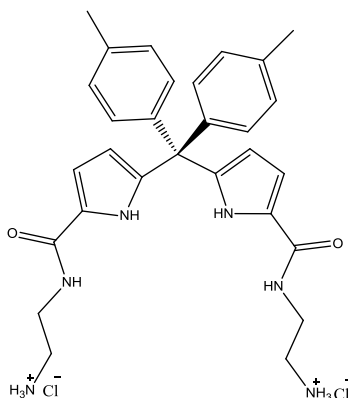
Figure 5.11: Lead dipyrromethane **DDAAKN01**.

The lead **DDAAKN01** was tested against the Kv1 channels and the concatenated tetramer of Kv(1.1)$_4$. These results are shown in figure 5.12. Interestingly the blockage of Kv1.1 improves when tested on the concatenated tetramer which is more common in nature rather than the artificial homometric species. Negligible inhibition was observed for the channels Kv1.2, Kv1.4 and Kv1.6. The result for Kv1.2 is the most interesting from this subset of channels as Kv1.2 propagates in the brain with Kv1.1 in MS patients, thus any potential therapeutic would have to inhibit Kv1.1 without interfering with Kv1.2. Our results show this.
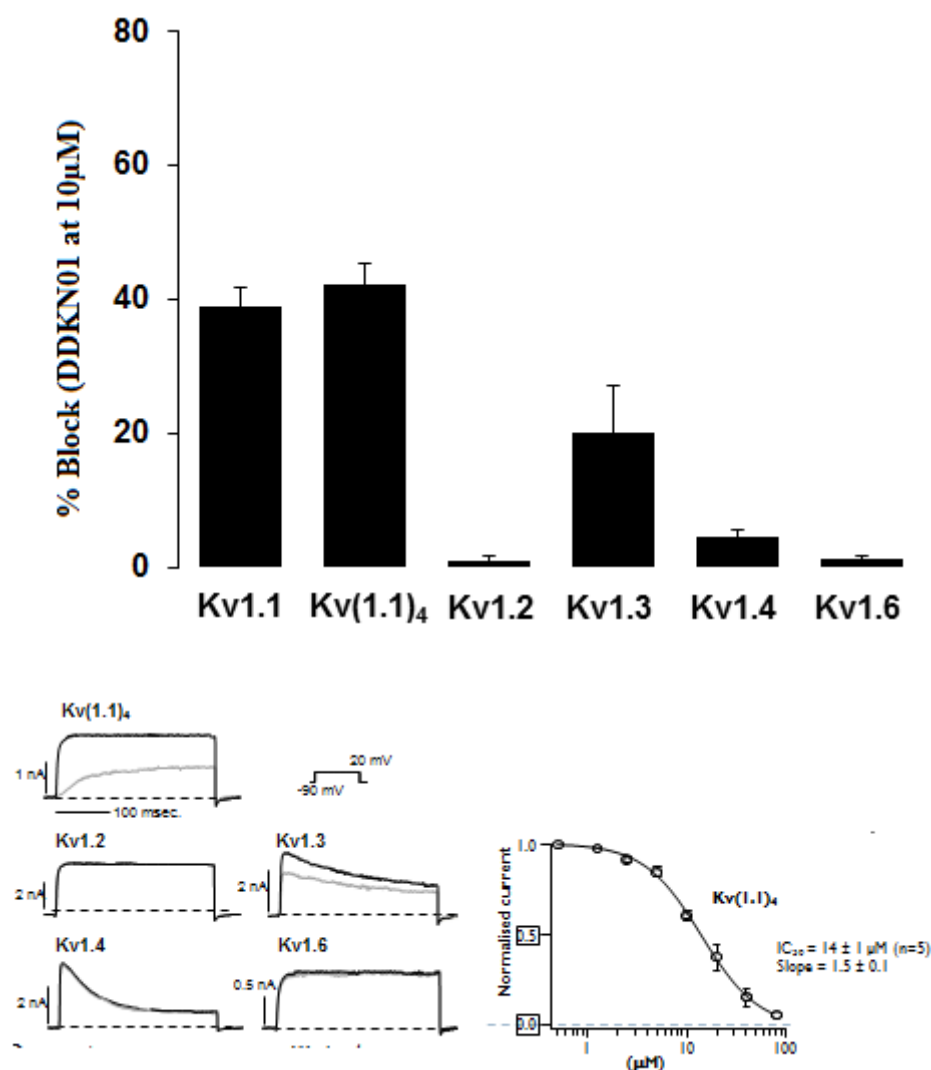
Figure 5.12: Overview of inhibition profile for **DDAAKN01** and the dose response curve.

The similarity in binding with the channels Kv1.1 and Kv1.3, shown in figure 5.13, may be a consequence that both channels are highly similar especially in the turret, selectivity filter and inner turret regions. Nature itself has great difficulty in distinguishing between these two channels. DTX_k is the only toxin found to date that has been found to selectively inhibit Kv1.1[9,10].

Kv1.1 (348-386): E A E E A E S H F S S I P D A F W W A V V S M T T V G Y G D M Y P V T I G G K

Kv1.3 (373-411): E A D D P S S G F N S I P D A F W W A V V T M T T V G Y G D M H P V T I G G K

Figure 5.13: Kv1.1 and Kv1.3 amino acid sequence adjacent to the inner turret.

Observing the residue sequence for both Kv1.1 and Kv1.2, in figure 5.13, the entire region highlighted yellow has the exact same amino acid sequence. The region surrounding the

selectivity filter is highly conserved for both channels and making minor changes to this region has an enormous effect on the biophysical properties of the channels. Highlighted in grey are the inner pore resides tyrosine (Kv1.1) and histidine (Kv1.3). We have already hypothesised that how the new lead compounds may be causing inhibition is by H-bonding interactions with surrounding amino acids in the selectivity filter region, furthermore the molecule can further interact by π-π with Tyr379 in the inner pore of Kv1.1. Histidine, the inner turret residue of Kv1.3, being aromatic itself, is also capable of π-π interactions, thus selectively distinguishing between the two channels is increasingly difficult. This hypothesis is plausible since on examining the inner pore residues of the other channels, Kv1.2 and Kv1.4, no observable π-π interaction is evident since valine is present as the inner pore residue in Kv1.2 and lysine is present as the inner pore residue in Kv1.4.

Kv1.6 does not fall under this hypothesis. Kv1.6 has a tyrosine residue as the selectivity filter residue and as discussed this could potentially π-π interact. The main difference between Kv1.1/1.3 and Kv1.6 is, Kv1.1/1.3 amino acid sequence is identical in the region surrounding the selectivity filter. Kv1.6 has a different sequence, Kv1.6 has two methionine residues in the vicinity of the selectivity filter. Methionine is capapble of forming disulphide bridges which subsequently changes the orientation of the protein in this region. What has been observed from both the porphyrin SAR study and the dipyrromethane screening is that small changes in alkyl chain length has significant implications on the inhibition of these channels.

Kv1.6 (398–436): E A D D V D S Q F P S I P D A F W W A V V T M T T V G Y G D M Y P M T V G G K

Figure 5.14: Amino acid sequence of Kv1.6, methionine residues are highlighted in yellow.

5.5.4 Effect of DDAAKN01 on conductance and τ activation

Inhibition of Kv1.1 homo-tetramer proved reversible as indicated by the time course of wash in/wash out of **DDAAKN01** (Figure 5.15).
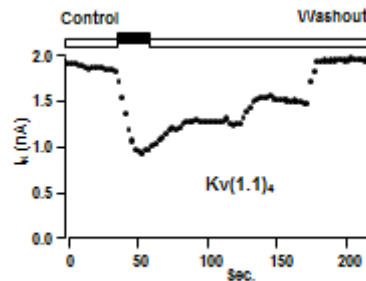

Figure 5.15: Reversible binding of **DDAAKN01** and its ability to wash out upon administration.

Interestingly, this effect of **DDAAKN01** on the $(Kv1.1)_4$ channel is associated with significant (~ 20 times; 3 ±0.3 ms before and 57 ±5 ms after 10 μM **10**, P<0.001 n=5 and 4, respectively) slowing of the activation kinetics, as indicated by the time course of activation (τ) shown in Figure 5.16a. Also, the gV relations of $Kv(1.1)_4$ (before, open circles) gave a typical half maximal of activation $(V_{1/2})$ value of -27 ±1 (n=7) [Figure 5.16b]. A significant shift of ~40 mV towards positive potentials was observed in the presence of 10 μM **DDAAKN01** [11 ±1 (n=4); Figure 5.16b (closed circles)]. These findings showed the promising inhibitory effect of **DDAAKN01** on the $(Kv1.1)_4$ channel. $Kv(1.1)_4$ only exists in diseased state channels as a result of demylination, the open circles shown in figure 5.16b mimic a diseased state. When **DDAAKN01** is applied the current shifts and thus mimics a normalised channel that does not undergo demylination.
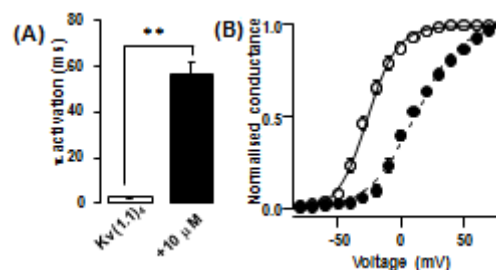

Figure 5.16 (a) the τ activation of the diseased state channel,(b) the regulation of the current due to administration of **DDAAKN01.**

5.5.5 Effect on bioactivity with minor modification to the scaffold

We have discussed the activity of **31**-**33** in detail, results have shown that if the chain length is extended it had a significant effect on both potency and selectivity. We predicted this using the porphyrin SAR study discussed in chapter 2, and used molecular modelling in chapter 4 to endorse these results. A second modification that is possible is the replacement of the methyl substituents of the tolulenes with hydrogen to give compound **50**. Such a modification could potentially give a substantial amount of information concerning the role of the methyl groups with respect to channel binding/inhibition.
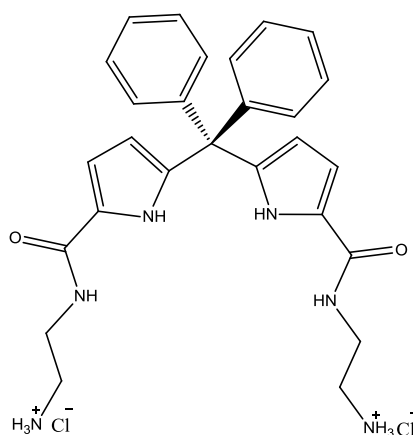
Figure 5.17: Structure of **50**.

As shown in figure 5.17, the modification to the scaffold in **50** is minor versus the active compound **DDAAKN01**. When this compound was tested against $Kv(1.1)_4$ the results were surprising, compound **50** showed no biological activity on the channels as shown in figure 5.18, removal of the methyl group eliminated all inhibition activity.
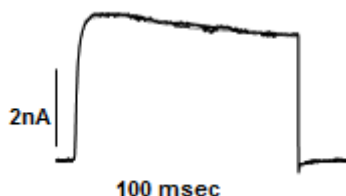

Figure 5.18: Current profile of **50**.

We can interpret this result in a number of ways; the first interpretation is that the methyl groups may be involved in hydrophobic interactions with the channel amino acid residues. Alternatively, the removal of the methy groups reduces the electron density of the aromatic ring affecting π-π interactions. Comparing Hammett parameters, substitution of the methyl group by a hydrogen the electron density on the ring changes and this would have a direct effect on the π interaction with tyrosine we discussed previously (figure 5.19). Another possible consequence of replacing the methy group with hydrogen on the phenyl ring is that the angle of the central tetrahedral quanternary carbon of **50** changes and as a result of this angle change the amide alkyl ammonium group which we know is essential for bioactivity changes. Making a minor variation on the scaffold has huge ramifications on the biological performance of this class of compound.
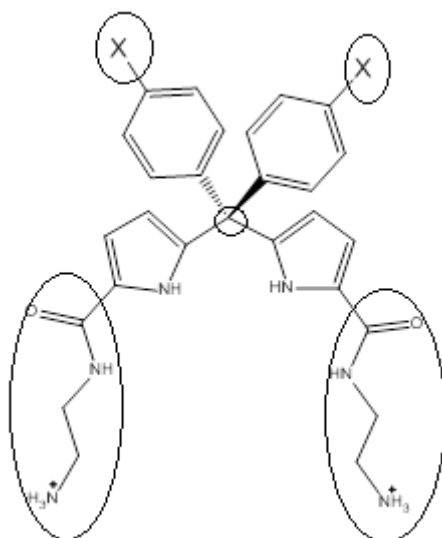

Figure 5.19: Potential change in bond angle of **50** on replacing methyl group.

5.5.6 Effect of DDAAKN01 on natural Kv1 channels in the brain.

The manner in which these concatenated Kv1 tetramer channels exist has not been discussed yet. These channels do not exist as simple tetramers Kv $(1.1)_4$ and Kv $(1.2)_4$, but rather as an amalgamation of both channels.

The effect of **DDAAKN01** was also tested on Kv1.1 with tetrameric channels containing Kv1.1 and/or Kv1.2 subunits in different combinations to mimic those that exist in the brain or associated with MS. Figure 5.20 summarizes a dose-response for the susceptibility of these combinations to **DDAAKN01**. Channels composed of Kv1.2 or 3 copies of Kv1.2 (Kv1.2-

1.2-1.1-1.1) were insensitive to this blocker. In contrast, these possessing two or three copies of Kv1.1 showed similar reactivity to **DDAAKN01**, with IC_{50} values between 40-60 μM. However, Kv1.1 or $Kv(1.1)_4$ channels showed similar sensitivity to this inhibitor with IC_{50}~15 μM. Table 5.7 summarizes these IC_{50} values.
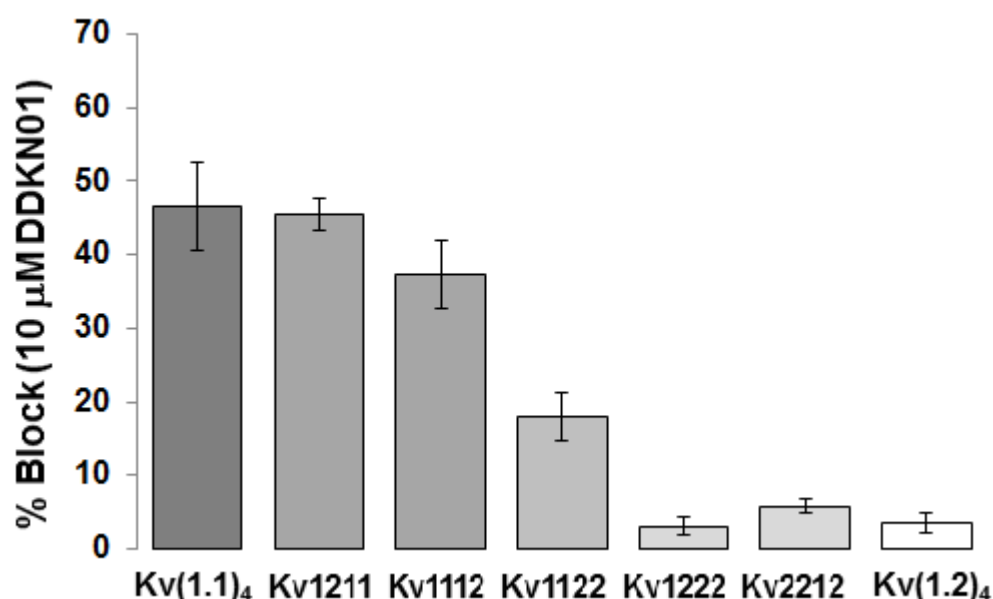

Figure 5.20: The percentage blockage of DDAAKN01 on the concatenated Kv1.1/1.2 channels as they exist in diseased state normally found in the brain.

Table 5.7: IC_{50} values for inhibition of **DDAAKN01** of Kv1 concatenated tetramers

Channel	IC_{50} (μM)	Hill Slope	No of experiments
Kv 1.1	17 ± 1	1.4 ± 0.2	6
$Kv(1.1)_4$	14 ± 1	1.5 ± 0.1	7
Kv 1.1-1.2-1.1-1.1	43 ± 4	1.8 ± 0.2	5
Kv 1.1-1.1-1.1-1.2	57 ± 2	1.3 ± 0.3	4
Kv 1.1-1.1-1.2-1.2	18 ± 3	-------------	5
Kv 1.2-1.2-1.1-1.2	>100	-------------	6
$Kv(1.2)_4$	>100	-------------	4

Interestingly, Hill's slope values deviated from unity when 3 or 4 copies of Kv1.1 subunits were present in the concatamer, indicating that one or more molecules of **DDAAKN01** might

be binding to the same channel. However, **DDAAKN01** inhibits currents from tetramers with 2 or 3 copies of Kv1.1, in a similar manner independently of the positioning of these subunits. These results indicate that **DDAAKN01** inhibits channels enriched with Kv1.1, in a similar manner as extracellular blockers, such as DTX_K[9].

5.6 Conclusion

The target ditolyldipyrromethane derivatives that were docked into rat Kv1.1 comparative model and detailed in chapter 4 were prepared. **DDAAKN01**, showed high selectivity for the potassium channel Kv(1.1)$_4$ which is believed to be highly associated with MS. Minimal variations to the molecule, as shown with **50**, has drastic implications to both the selectivity and potency of these molecules. The hill-slope for **DDAAKN01** indicated that more than one molecule is interacting with the tetrameric protein **DDAAKN01** was also observed to be highly selective for Kv channels that only possess Kv1.1, with Kv1.2 incorporated into tetrameric sub-unit, the inhibition profile reduces proportionately.
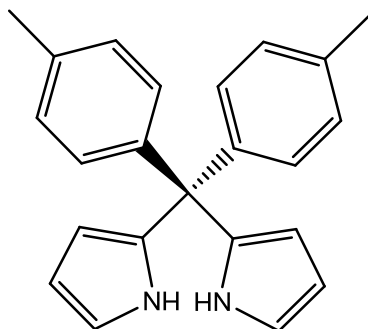
5.7 Experimental

Materials

All operations were carried out under an atmosphere of argon or nitrogen using standard Schlenk techniques. All solvents were supplied by the Aldrich Chemical Company and TCI. Dichloromethane was dried over $MgSO_4$ prior to use. Methanol was distilled over magnesium turnings and iodine before use. All organic reagents were purchased from the Aldrich Chemical Company and TCI. Pyrrole was freshly distilled over potassium hydroxide before use. Anhydrous triethylamine, borontrifluoride diethyletherate and were all used without further purification.

Column chromatography was carried out using neutral silica gel (Merck, used as received). All mobile phases for column chromatography were dried over $MgSO_4$ prior to use.. All solvents were deoxygenated by purging withargon or nitrogen for ~10 minutes

Equipment

All syntheses involving air- and moisture-sensitive reagents were performed in oven or flame dried glassware. NMR spectra were recorded on a Bruker model AC 400 MHz spectrometer and Bruker model ANC 600 MHz spectrometer using $CDCl_3$ as solvent. All NMR spectra were calibrated according to the residual solvent peak, i.e. $CHCl_3$ at 7.26 ppm, DMSO-d_6 2.50 ppm for all ^1H spectra and 77.16 ppm and 39.52 ppm for all ^{13}C spectra. Chemical shifts are given in parts per million (ppm).

29

Synthesis of di-p-tolyldipyrromethane

To a 250 mL 2-necked round bottom flask, 1.31 g (6.18 mmol) of 4,4-dimethylbenzophenone was charged. To this 50 mL of anhydrous methanol was added and magnetically stirred under a argon atmosphere. When the 4,4-dimethylbenzophenone was fully dissolved 1.07 mL (15.5 mmol) of freshly distilled pyrrole was added dropwise. After 5 minutes, 1.07 mL (8.6 mmol) of $BF_3.(OEt)_2$ was added and the reaction was allowed stir for 5 days. The precipitate formed was filtered and washed with cold methanol to give a white solid **30**. (1.007 g, 50%)

^{1}H NMR (400 MHz) δ (DMSO- d_6) 10.22 (2H, s, pyrrole-NH) 7.12 (2H, d, aryl-H) 6.88 (2H, d, aryl-H) 6.76 (2H, m, pyrrole-H) 5.94 (2H, m, pyrrole-H) 5.65 (2H, m, pyrrole-H) 2.29 (6H, s, Tolyl-CH₃) ^{13}C NMR (100 MHz, DMSO- d_6) δ 143.6, 135.7, 135.1, 129.0, 127.8, 117.9, 108.7, 105.9, 54.7, 20.3
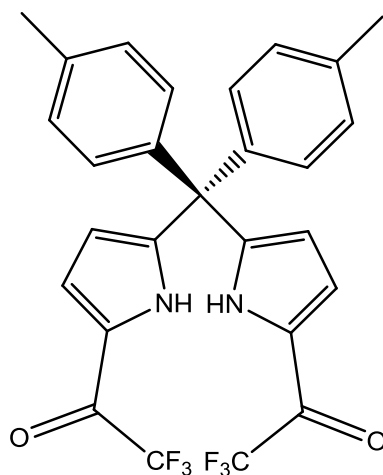
42

5,5'-(di-p-tolyldipyrromethane)bis(2-trifluorocarbonyl)

To a 25 mL 2-neck round bottom flask, 336 mg (1 mmol) of **29** and 24 mg (0.2 mmol) of DMAP was charged with a small magnetic stirring bar and placed over was cooled to 0 $^{\circ}$C. To the stirring solution 350 μL (2.5 mmol) of trifluoroacetic anhydride was added dropwise and the reaction was allowed stir for 10 minutes at room temperature. The reaction was transferred to a small separating funnel and the organic phase was washed with 2x10 mL water, 2x10 mL NaHCO$_3$ and dried with MgSO$_4$. The CH$_2$Cl$_2$ was removed to give a white solid in quantitative yield to give compound **31**.

^{1}H NMR (400 MHz) δ (DMSO- d$_6$) 12.58 (2H, s, pyrrole-NH) 7.28 (6H, d, aryl-H + pyrrole-H) 6.93 (4H, d, aryl-H) 6.11 (2H, m, pyrrole-H) 2.29 (6H, s, tolyl-CH$_3$)^{13}C NMR (100 MHz, DMSO- d$_6$) δ (168.1,167.9,167.7,167.5) 147.7, 140.0, 136.3, 128.9, 128.5, 125.5, 121.32, (119.7, 117.8, 115.8,113.9), 114.6, 55.8, 20.3
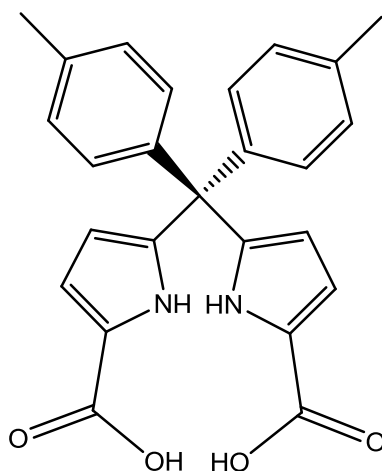
44

5,5'-(di-p-tolyldipyrromethane)bis(2-carboxylic acid)

To a 50 mL round bottom flask 500 mg of compound **42** was charged. To this 4 g of NaOH dissolved in 20 mL of water was added along with 10 mL of ethanol. The reaction was allowed to reflux for 6 hours. The reaction mixture was then concentrated to approximately half of its original volume and to this 1M HCl was added dropwise to reach a pH of 2. The yellow precipitate formed was filtered and dried to obtain the carboxylic acid dipyrromethane derivative **32** in quantitative yield.

^{1}H NMR (400 MHz) δ (DMSO- d_6) 12.24 (2H, s, COOH) 11.47 (2H, s, pyrrole-NH) 7.13 (4H, d, aryl-H) 6.77 (4H, d, aryl-H) 6.63 (2H, m, pyrrole-H) 5.73 (2H, m, pyrrole-H) 2.29 (6H, s, tolyl-CH$_3$)^{13}C NMR (100 MHz, DMSO- d_6) δ 161.8, 141.6, 140.9, 135.9, 129.2 128.1, 123.7, 113.8, 111.9, 55.4, 20.5
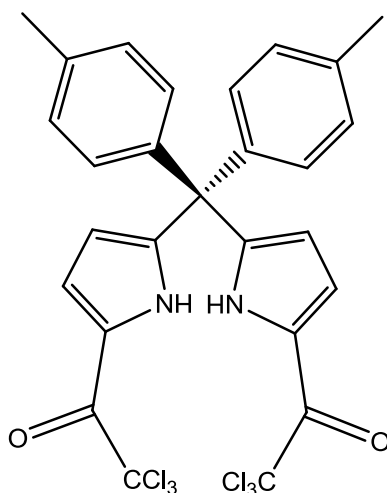
45

5,5'-(di-p-tolyldipyrromethane)bis(2-trichlorocarbonyl)

To a 25 mL 2-neck round bottom flask, 336 mg (1 mmol) of - **29** and 24 mg (0.2 mmol) of DMAP was charged with a small magnetic stirring bar and placed over an argon atmosphere. To this 10 mL of anhydrous DCM was added and the reaction mixture was cooled to 0 ^{o}C. To the stirring solution 457 μL (2.5 mmol) of trichloroacetic anhydride was added dropwise and the reaction was allowed stir for 2 hours at room temperature. The reaction was transferred to a small separating funnel and the organic phase was washed with 2x10 mL water, 2x10 mL NaHCO$_3$ and dried with MgSO$_4$. The CH$_2$Cl$_2$ was removed to give **33** as a white solid in quantitative yield.

^{1}H NMR (400 MHz) δ (DMSO- d$_6$) 12.20 (2H, s, pyrrole-NH) 7.29 (2H, d, pyrrole-H) 7.28 (2H, d, aryl-H) 6.94 (2H, d, aryl-H) 6.06 (2H, m, pyrrole-H) 2.29 (6H, s, tolyl-CH$_3$) ^{13}C NMR (100 MHz, DMSO- d$_6$) δ 171.8, 145.8, 140.4, 136.4, 129.0, 128.5, 122.5, 120.8, 113.9, 95.2, 55.9, 20.3

General procedure 4 for the preparation of N-Boc protected dipyrromethanes from 33

To a 50 mL round bottom flask (400 mg; 0.648 mmol) of the **45** were added with 5 mL of CH$_2$Cl$_2$. This mixture was allowed stir for 5 mins at room temperature under an argon atmosphere. N-boc ethylenediamine (250 µL; 1.6 mmol) was then added to the mixture followed by the dropwise addition of anhydrous triethylamine (360 µL; 2.6 mmol). The reaction was stirred at room temperature overnight. The precipitate that formed was collected by suction filteration and the precipitate was washed twice with 25mL aliquots of CH$_2$Cl$_2$ and was then vacuum dried to give the N-Boc derivatives in quantitative yield.
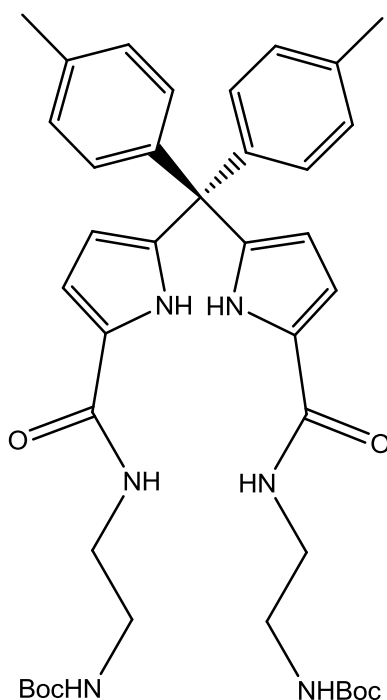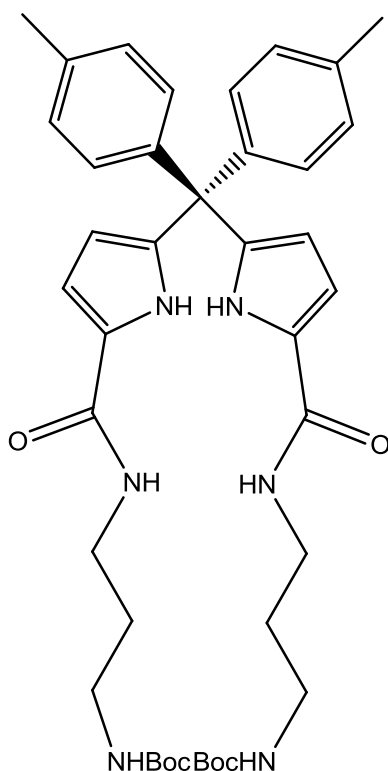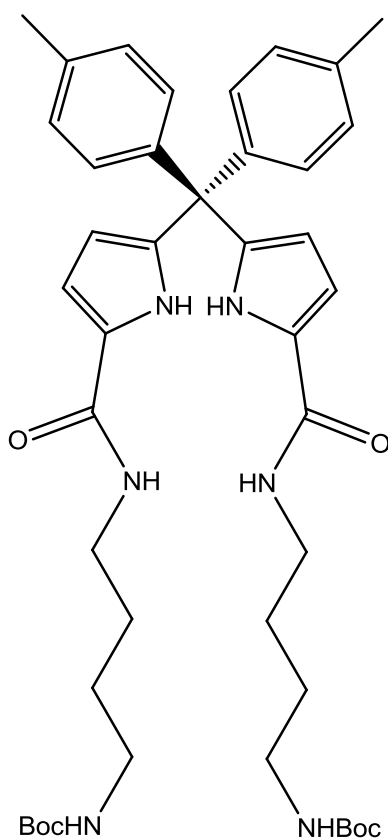

43

Di-tert-butyl (((5,5'-(di-p-tolyldipyrromethane)bis(2,2'-carbonyl)) bis (azanediyl)) bis(ethane-2,1-diyl))dicarbamate

General procedure 4 was followed using **45** (400 mg; 0.648mmol) and N-boc 1,2 ethanediamine (250 µL; 1.6mmol) to give **43** in quantitative yield.

^{1}H NMR (400 MHz) δ (DMSO- d$_6$) 10.82 (2H, s, pyrrole NH) 8.06 (2H, t, amide NH) 7.12 (4H, d, aryl-H) 6.89 (2H, t, amide-NH) 6.78 (4H, d, aryl-H) 6.64 (2H, d, pyrrole-H) 5.69 (2H, d, pyrrole-H) 3.22 (4H, q, CH$_2$) 3.06 (4H, q, CH$_2$) 2.29 (6H, s, tol-CH$_3$) 1.37 (18H, s, Boc-CH$_3$). ^{13}C NMR (100 MHz, DMSO- d$_6$) δ 160.6, 155.7, 141.9, 138.9, 135.9, 129.2, 128.2, 126.9, 110.9, 109.9, 77.7, 55.2, 54.9, 39.5, 38.7, 28.3, 20.6.

46

Di-tert-butyl (((5,5'-(di-p-tolyldipyrromethane)bis(2,2'-carbonyl)) bis (azanediyl)) bis(propane-3,1-diyl))dicarbamate

General procedure 4 was followed using **45** (400 mg; 0.648mmol) and N-boc-1,3-propanediamine (270 µL; 1.6mmol) to give di-tert-butyl **46** in quantitative yield.

^{1}H NMR (400 MHz) δ (DMSO- d_6) 10.77 (2H, s, pyrrole NH) 7.98 (2H, t, amide NH) 7.11 (4H, d, aryl-H) 6.79 (4H, t, aryl-H + (2H) amide-NH) 6.62 (2H, d, pyrrole-H) 5.66 (2H, d, pyrrole-H) 3.18 (4H, q, CH$_2$) 2.91 (4H, q, CH$_2$) 2.28 (6H, s, tol-CH$_3$) 1.56 (4H, p, CH$_2$) 1.35 (18H, s, Boc-CH$_3$). ^{13}C NMR (100 MHz, DMSO- d_6) δ 160.4, 155.6, 141.9, 138.7, 135.9, 129.2, 128.2, 126.9, 110.8, 109.7, 77.5, 55.2, 54.9, 37.7, 36.2, 29.9, 28.3, 20.6.

47

Di-tert-butyl (((5,5'-(di-p-tolyldipyrromethane)bis(2,2'-carbonyl)) bis(azanediyl))bis (butane-4,1-diyl))dicarbamate

General procedure 4 was followed using **45** (400 mg; 0.648mmol) and N-boc-1,4-butanediamine (290 μL; 1.6mmol) to give **47** in quantitative yield.

^{1}H NMR (400 MHz) δ (DMSO- d_6) 10.72 (2H, s, pyrrole NH) 7.99 (2H, t, amide NH) 7.12 (4H, d, aryl-H) 6.81 (4H, t, aryl-H + 2H amide-NH) 6.64 (2H, d, pyrrole-H) 5.67 (2H, d, pyrrole-H) 3.16 (4H, q, CH$_2$) 2.93 (4H, q, CH$_2$) 2.29 (6H, s, tol-CH$_3$) 1.41 (8H, m, CH$_2$) 1.36 (18H, s, Boc-CH$_3$). ^{13}C NMR (100 MHz, DMSO- d_6) δ 160.3, 155.7, 142.0, 138.7, 135.9, 129.2, 128.2, 127.1, 110.8, 109.7, 77.4, 55.2, 55.0, 39.4, 38.3, 28.3, 27.2, 26.9, 20.6.

General Procedure 5 for deprotection of compounds 43, 46-47

To a 25 mL round bottom flask 100 mg of the boc protected dipyrromethanes and a stirring bar were added. The flask was then placed under an argon atmosphere and 10 mL of anhydrous CH_2Cl_2 was added with stirring. The reaction mixture cooled to 0 °C and 1 mL of 4M HCl in dioxane was added dropwise to the reaction mixture at 0 °C. After addition was completed the reaction mixture was allowed stir overnight at room temperature. The formed precipitate was then collected by suction filtration and washed with CH_2Cl_2 to give a white solid.
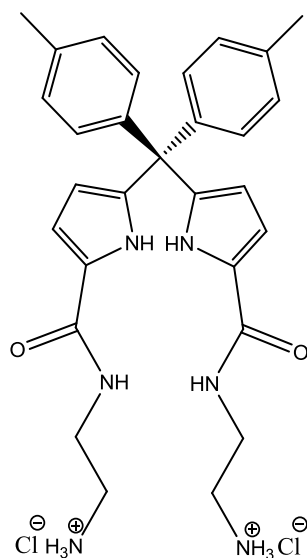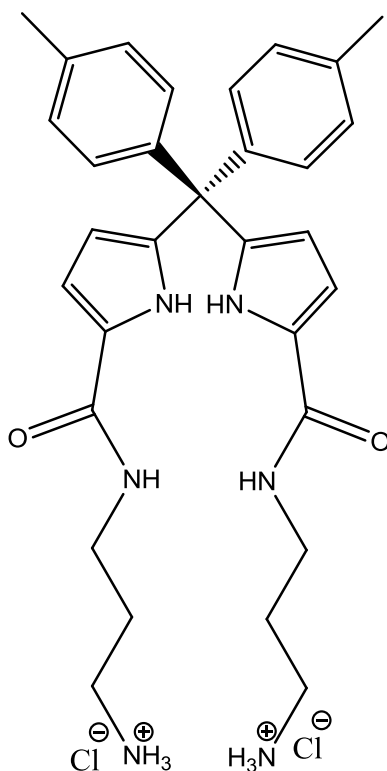

31

2,2'-((5,5'-(di-p-tolyldipyrromethane)bis(2,2'carbonyl))bis(azanediyl))-diethaneamine.2HCl

General procedure 5 was followed using 100 mg of **43** to yield **31** as a white solid in quantitative yield.

^{1}H NMR (400 MHz) δ (DMSO- d_6) 10.96 (2H, s, pyrrole-NH) 8.30 (2H, t, amide-NH) 7.95 (6H, s, NH3) 7.13 (4H, d, aryl-H) 6.79 (4H, d, aryl-H) 6.72 (2H, m, pyrrole-H) 5.73 (2H, m, pyrrole-H) 3.40 (4H, q, CH$_2$) 2.95 (4H, q, CH$_2$) 2.29 (6H, s, CH$_3$)^{13}C NMR (100 MHz, DMSO- d_6) δ 160.9, 141.7, 139.2, 135.9, 129.1, 128.1, 126.5, 110.94, 110.2, 55.2, 38.8, 36.5, 20.5.

MALDI-HRMS: Calculated C$_{29}$H$_{36}$Cl$_2$N$_6$O$_2$ (M+1-4HCl) 499.2777 Observed (M+1-4HCl) 499.3296 m/z; (M+Na) 521.3234
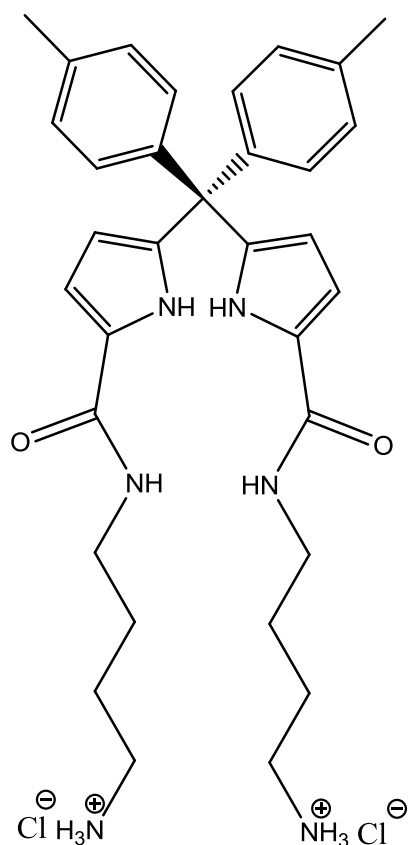
32

3,3'-((5,5'-(di-p-tolyldipyrromethane)bis(2,2'-carbonyl))bis(azanediyl))-dipropaneamine.2HCl

General procedure 5 was followed using 100 mg of **46** to yield **32** as a white solid in quantitative yield.

^{1}H NMR (400 MHz) δ (DMSO- d$_6$) 10.87 (2H, s, pyrrole-NH) 8.24 (2H, t, amide-NH) 7.88 (6H, s, NH$_3$) 7.11 (4H, d, phenyl-H) 6.78 (4H, d, phenyl-H) 6.67 (2H, m, pyrrole-H) 5.68 (2H, m, pyrrole-H) 3.25 (4H, q, CH$_2$) 2.80 (4H, q, CH$_2$) 2.28 (6H, s, CH$_3$), 1.77 (4H, p, CH$_2$)^{13}C NMR (100 MHz, DMSO- d$_6$) δ 160.7, 141.9, 139.0, 135.9, 129.2, 128.2, 126.8, 111.0, 110.0, 55.2, 36.8, 35.5, 27.6, 20.6.

MALDI-HRMS- Calculated C$_{31}$H$_{40}$Cl$_2$N$_6$O$_2$ (M-4HCl) 527.3190 Observed (M+1-4HCl):527.3686; (M+Na):549.3571

33

4,'-((5,5'-(di-p-tolyldipyrromethane)bis(2,2'-carbonyl))bis(azanediyl))-dibutaneamine.2HCl

General procedure 5 was followed using 100 mg of **47**, to yield **33** as a white solid in quantitative yield.

^{1}H NMR (400 MHz) δ (DMSO- d$_6$) 10.83 (2H, s, pyrrole-NH) 8.14 (2H, t, amide-NH) 7.91 (6H, s, NH$_3$) 7.12 (4H, d, phenyl-H) 6.76 (4H, d, phenyl-H) 6.67 (2H, m, pyrrole-H) 5.68 (2H, m, pyrrole-H) 3.19 (4H, q, CH$_2$) 2.77 (4H, q, CH$_2$) 2.29 (6H, s, CH$_3$), 1.55 (8H, p, CH$_2$)^{13}C NMR (100 MHz, DMSO- d$_6$) δ 160.3, 141.9, 138.8, 135.9, 129.2, 128.2, 127.0, 110.9, 109.8, 55.2, 38.5, 37.8, 26.4, 24.6, 20.6.

MALDI-HRMS Calculated C$_{33}$H$_{44}$Cl$_2$N$_6$O$_2$ (M-4HCl): 555.4103: Observed:(M+1-4HCl): 555.4175
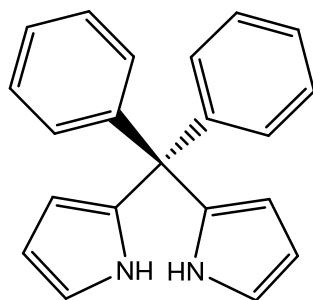
22

Synthesis of di-phenyldipyrromethane

To a 250 mL 2-necked round bottom flask, 1.13 g (6.18 mmol) of benzophenone was charged. To this 50 mL of anhydrous methanol was added and magnetically stirred under a argon atmosphere. When the benzophenone was fully dissolved 1.07 mL (15.5 mmol) of freshly distilled pyrrole was added dropwise. After 5 minutes, 1.07 mL (8.6 mmol) of $BF_3.(OEt)_2$ was added and the reaction was allowed stir for 5 days. The precipitate formed was filtered and washed with cold methanol to give a white solid **37**. (0.615 g, 50%)

[1]H and ^{13}C match with literature values *Turner et al*[1]
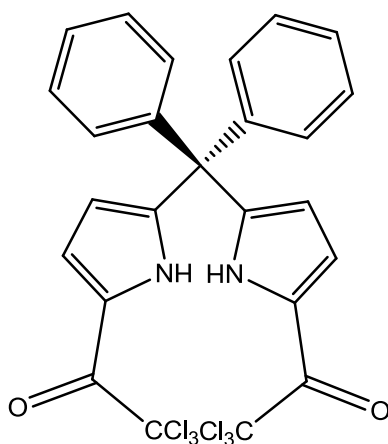
48

To a 25 mL 2-neck round bottom flask, 298 mg (1 mmol) of **22** and 24 mg (0.2 mmol) of DMAP was charged with a small magnetic stirring bar and placed over an argon atmosphere. To this 10 mL of anhydrous CH_2Cl_2 was added and the reaction mixture was cooled to 0 °C. To the stirring solution 457 μL (2.5 mmol) of trichloroacetic anhydride was added dropwise and the reaction was allowed stir for 2 hours at room temperature. The reaction was transferred to a small separating funnel and the organic phase was washed with 2*10 mL water, 2*10 mL NaHCO$_3$ and dried with MgSO$_4$. The DCM was removed to give **48** as a white solid in quantitative yield.

^{1}H NMR (400 MHz) δ (DMSO- d$_6$) 12.25 (2H, s, pyrrole-NH) 7.29 (6H, m, aryl-H) 7.31 (2H, d, pyrrole-H) 7.04 (4H, m, aryl-H) 6.08 (2H, d, pyrrole-H)^{13}C NMR (100 MHz, DMSO- d$_6$) δ 171.8, 145.4, 143.2, 129.1, 128.0, 127.3, 122.6, 120.8, 113.9, 85.1, 56.4.
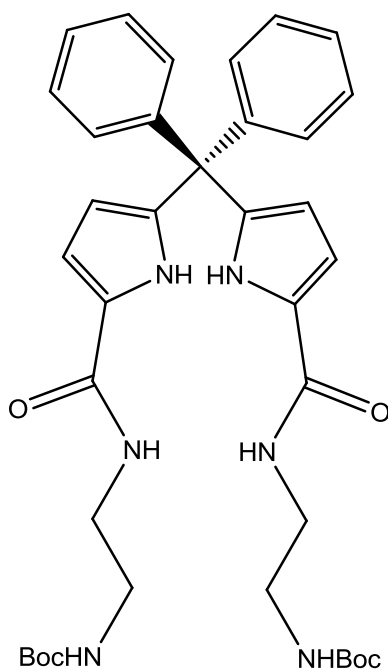
49

To a 50 mL round bottom flask 350 mg (0.594 mmol) of compound **48** was charged. To this 5mL of CH_2Cl_2 was added and allowed stir for 5 minutes under an argon atmosphere. 225 μL (1.4 mmol) of N-boc ethylenediamine was added. To this 330 μL (2.4mmol) anhydrous triethylamine was added dropwise and the reaction was allowed stir at room temperature overnight. The precipitate that was formed was filtered and washed with 2*25 mL aliquots of CH_2Cl_2. The resulting precipitate was dried to form compound **49** in quantitative yield.

^{1}H NMR (400 MHz) δ (DMSO- d_6) 10.98 (2H, s, pyrrole-H) 8.03 (2H, t, amide-NH) 7.30 (6H, m, aryl-H) 6.91 (6H, m, aryl-H + amide-NH) 6.7 (2H, d, pyrrole-H) 5.7 (2H, d, pyrrole-H) 3.2 (4H, q, CH_2) 3.0 (4H, q, CH_2) 1.4 (18H, s, Boc-H)^{13}C NMR (100 MHz, DMSO- d_6) δ 160.5, 155.6, 144.6, 138.5, 129.3, 127.6, 127.1, 126.8, 111.0, 109.6, 77.6, 55.8, 39.4, 38.7, 28.1
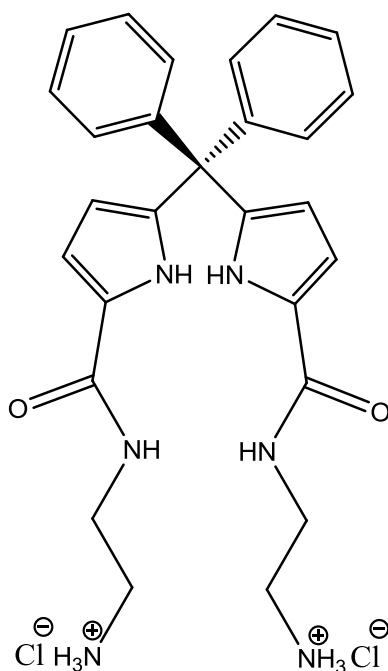
50

2,2'-((5,5'-(diphenyldipyrromethane)bis(2,2'-carbonyl))bis(azanediyl))diethanamine 2HCl

To a 25 mL round bottom flask 100 mg of **49** and stirring bar was added. The flask was then placed under an argon atmosphere. To this 10 mL of anhydrous CH_2Cl_2 was added. The reaction was cooled to 0 ^{o}C and stirred. To this 1 mL of 4M HCl in dioxane was added and the reaction was allowed stir overnight. The precipitated material was filtered and washed with CH_2Cl_2 to yield **50** as a white solid in quantitative yield.

^{1}H NMR (400 MHz) δ (DMSO- d_6) 11.09 (2H, s, pyrrole-NH) 8.33 (2H, t, amide-H) 8.02 (6H, s, NH_3) 7.32 (6H, m, phenyl-H) 6.90 (4H, m, phenyl-H) 6.73 (2H, m, pyrrole-H) 5.70 (2H, m, pyrrole-H) 3.43 (4H, q, CH_2) 2.91 (4H, q, CH_2)^{13}C NMR (100 MHz, DMSO- d_6) δ 160.8, 144.5, 138.8, 129.2, 127.5, 126.8, 126.7, 111.1, 110.1, 55.8, 38.7, 36.4

5.8 References

1. Turner B, Botoshansky M, Eichen Y. Extended calixpyrroles: Meso-substituted calix[6]pyrroles. Angewandte Chemie-International Edition 1998;37(18):2475-8.

2. Sreedevi KCG, Thomas AP, Salini PS, Ramakrishnan S, Anju KS, Holaday MGD, Reddy MLP, Suresh CH, Srinivasan A. 5,5-diaryldipyrromethanes: Syntheses and anion binding properties. Tetrahedron Lett 2011;52(45):5995-9.

3. Folleas B, Marek I, Normant JF, Saint-Jalmes L. Fluoroform: An efficient precursor for the trifluoromethylation of aldehydes. Tetrahedron 2000;56(2):275-83.

4. Song MY, Na HK, Kim EY, Lee SJ, Kim KI, Baek EM, Kim HS, An DK, Lee CH. Hetero-calix[4]pyrroles: Incorporation of furans, thiophenes, thiazoles or fluorenes as a part of the macrocycle. Tetrahedron Lett 2004;45(2):299-301.

5. Judge S, Bever C. Potassium channel blockers in multiple sclerosis: Neuronal K-V channels and effects of symptomatic treatment. Pharmacol Ther 2006;111(1):224-59.

6. Al-Sabi A, Kaza S, Le Berre M, O'Hara L, Bodeker M, Wang J, Dolly JO. Position-dependent attenuation by Kv1.6 of N-type inactivation of Kv1.4-containing channels. Biochem J 2011;438:389-96.

7. Al-Sabi A, Shamotienko O, Dhochartaigh SN, Muniyappa N, Le Berre M, Shaban H, Wang J, Sack JT, Dolly JO. Arrangement of Kv1 alpha subunits dictates sensitivity to tetraethylammonium. J Gen Physiol 2010;136(3):273-82.

8. Al-Sabi, Ahmed; Kaza, Seshu Kumar; Dolly, J. Oliver; et al. Biochemical Journal, 2013 Volume: 454 Pages: 101-108

9. Wang FC, Bell N, Reid P, Smith LA, McIntosh P, Robertson B, and Dolly JO. Identification of residues in dendrotoxin K responsible for its discrimination between neuronal K$^+$ channels containing K$_V$1.1 and 1.2 alpha subunits. *Eur J Biochem* 1999 263:222-229

10. Imredy JP, and MacKinnon R. Energetic and Structural Interactions between delta-Dendrotoxin and a Voltage-gated Potassium Channel. *J. Mol. Biol.* 2000 296:1283-1294

Chapter 6: The synthesis and bioevaluation of a bridged dipyrromethane system

6.1 Bridged dipyrromethane systems

In the previous chapter four, the theoretical binding of small dipyrromethane molecules were modelled against the homology model of Kv1.1. These results showed a high number of localised interactions between DDAAKN01, the selectivity filter and inner turret region residues. In chapter 5, the synthesis of these compounds was undertaken with subsequent biological evaluation. As selective and potent the inhibitor DDAAKN01 was, the modelling highlighted the issue that these small dipyrromethanes do not take full advantage of all important residue interactions due to size constraints. The Hill slope for DDAAKN01 was found to be between 1.5-1.8, indicating that two molecules are interacting with the Kv1.1 channel. The concept of linking two dipyrromethanes can offer a route to maximising fourfold interaction. A plausible scaffold to test this hypothesis is shown in figure 6.1.
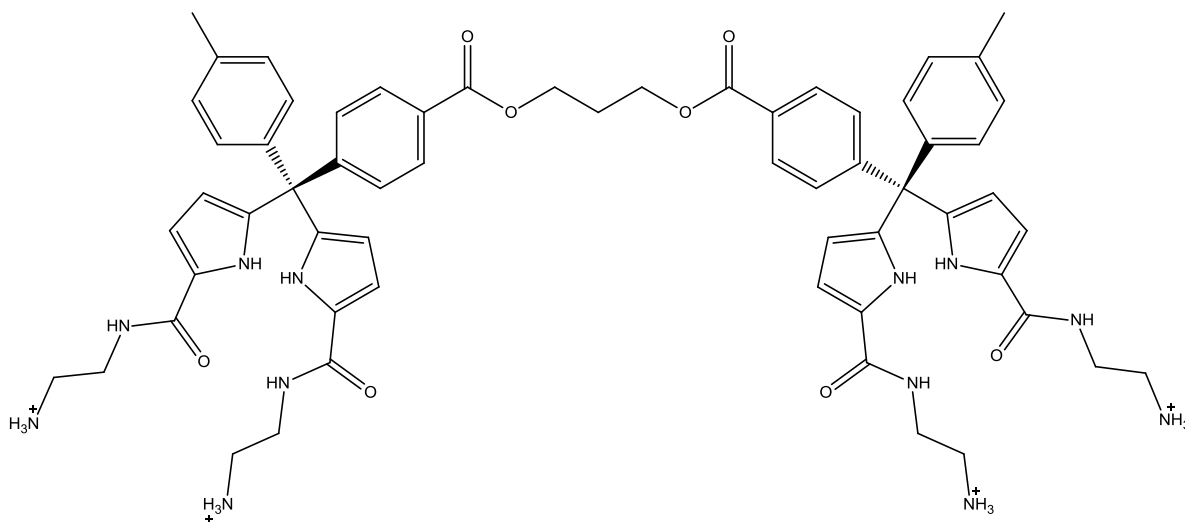

Figure 6.1: Proposed 'dimer' of DDAAKN01

The issue with making a dimer of DDAAKN01 is that functionalization of the scaffold in the para positions of the ditolyldipyrromethanes can not be performed, as illustrated in chapter five, with the attempts to oxidise at the para position of the scaffold proving to be unsuccessful.

A potential solution to this problem is outlined in scheme 6.1. This approach is a viable alternative for the dimer shown in figure 6.1. Outlined in scheme 6.1 is a plausible synthetic route for the preparation of a new dimeric dipyrromethane **54**. The key difference between **54** and the proposed dimer shown in figure 6.1 is that one of the phenyl groups of the dipyrromethane are replaced with a methyl group and in the second phenyl ring the para

methyl group is replaced with an amide. The original homology models of **DDAAKN01**, showed that only one of the tolyl groups had direct π-π interactions with Tyr 379 whilst the other tolyl remained on the peripheral region of the pore. As a result of this finding, removal of one of these substituents in theory, if the model is accurate, should not disrupt the molecule-protein interaction therefore **54** should indeed interact with the target Kv1 channels (molecular modelling discussed later). Thus the preparation of **54** was undertaken.
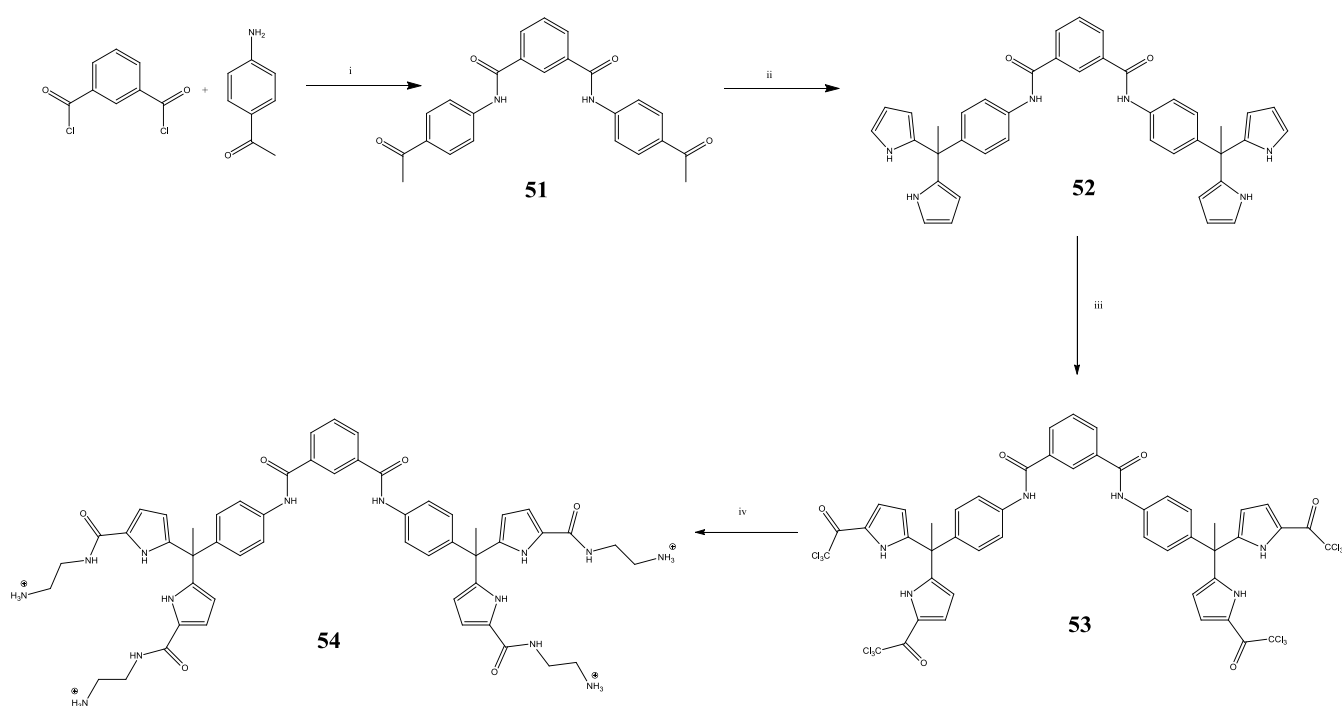
Scheme 6.1: Full schematic of the [2+2] synthesis of the dipyrromethane **54**. (i, TEA, THF, RT, 24hr, ii pyrrole, TFA, reflux, 4 hr, iii TClAA, DMAP, CH_2Cl_2, iv N-Boc ethylenediamine, TEA, CH_2Cl_2, v 4M HCl in dioxane CH_2Cl_2)

220

6.2 Results and discussion

The modelling performed on compound **54** is shown in figure 6.2. This molecule was docked into the rat Kv1.1 homology model constructed in chapter 4. The key interactions that were observed were π- π and HB interactions with the inner turret amino acid Tyr 379 on all chains (A-D). There was also strong interaction between the terminal amines and the Asp 377 residues on two of the chains (A and B) and hydrogen bonding between **54** and Tyr 375 on one of the chains (C). The phenyl linker holds the two dipyrromethane molecules covalently together via an amide bond, positioning the molecule in the centre of the pore region and spatially aligns the active sites of the molecule against the corresponding residues in the protein matrix. The most interesting aspect of modelling this candidate is the sole molecule thus far that has shown that it interacts with Tyr 379 on all residues. This type of selective interaction was identified as an initial objective; the Tyr 379 residue is unique to this Kv1.1 channel over the other Kv1 channels.
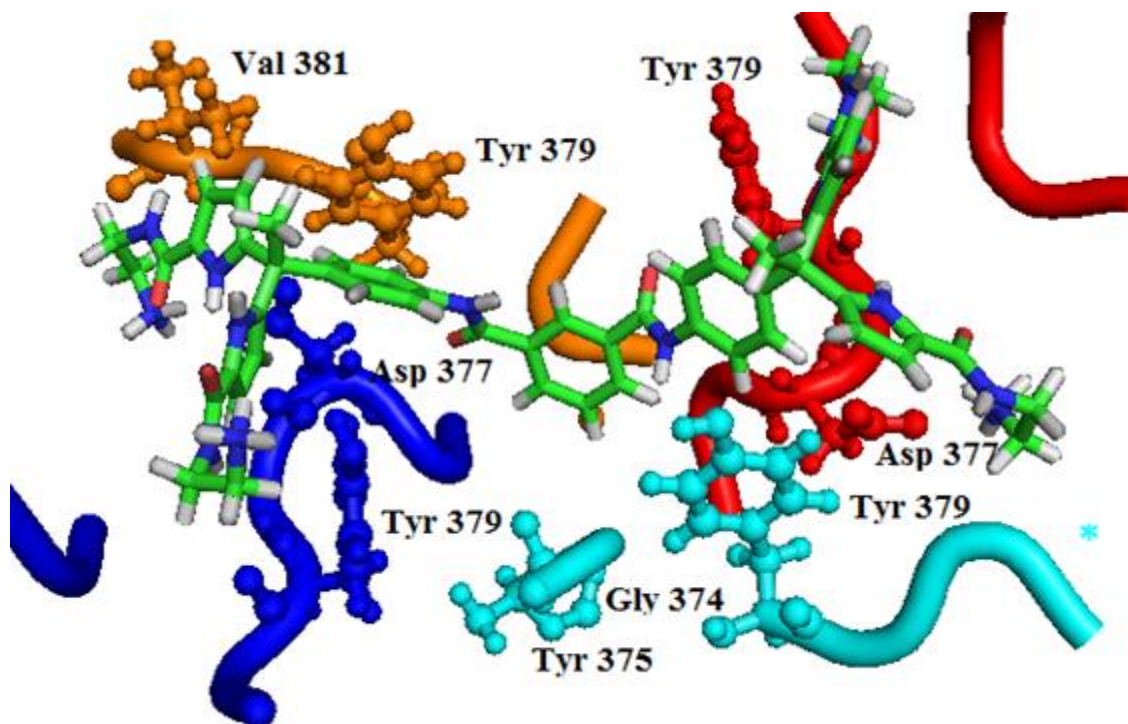

Figure 6.2: The linked dipyrromethane **54** docked into the rat Kv1.1 homology model. Red illustrates chain A, Blue relates to chain B, Cyan indicates chain C and orange is chain D.
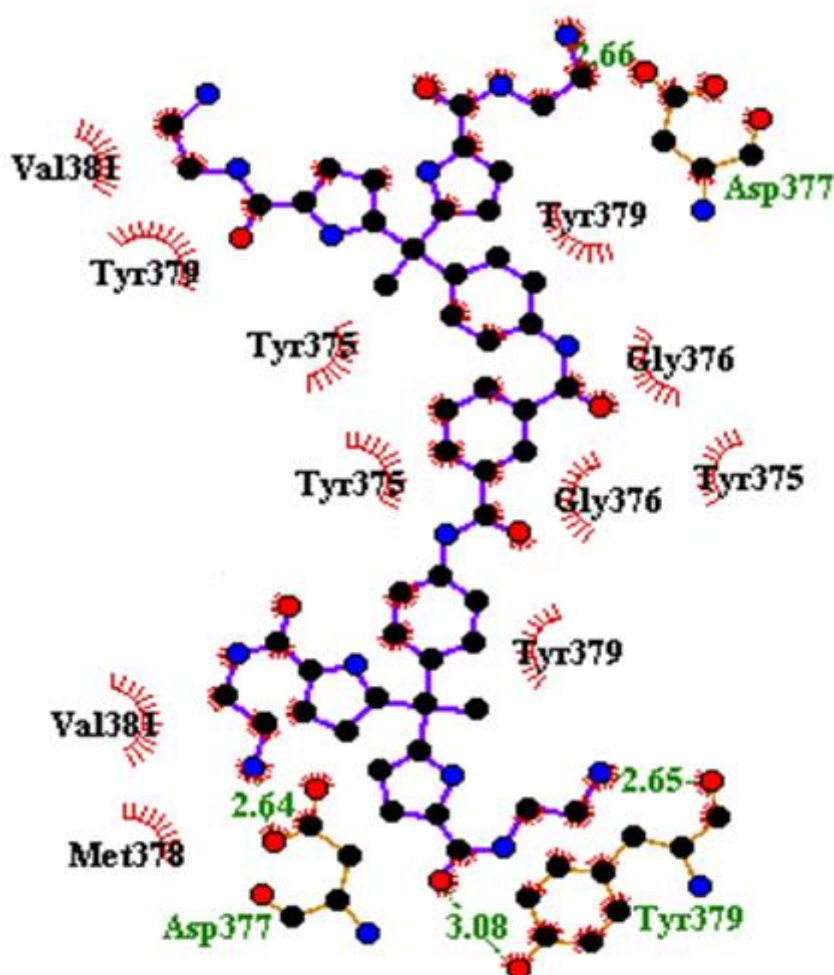
Figure 6.3: 2D ligand-plot of the linked dipyrromethane **54** docked into the rat Kv1.1 homology model.

The ligand plot indicates the full molecule-protein interaction. This 2D image shows the high degree of potential distortion between all of the residues mentioned above and shown in figure 6.2. The major observation from the ligand plot in figure 6.3 is the optimum HB interaction between the Tyr379 residue and both the amide and terminal amine moiety of the side group of **54**. As discussed earlier in chapter 4 and 5, this type of interaction, with this particular inner turret residue is believed to be essential in causing selective inhibition.
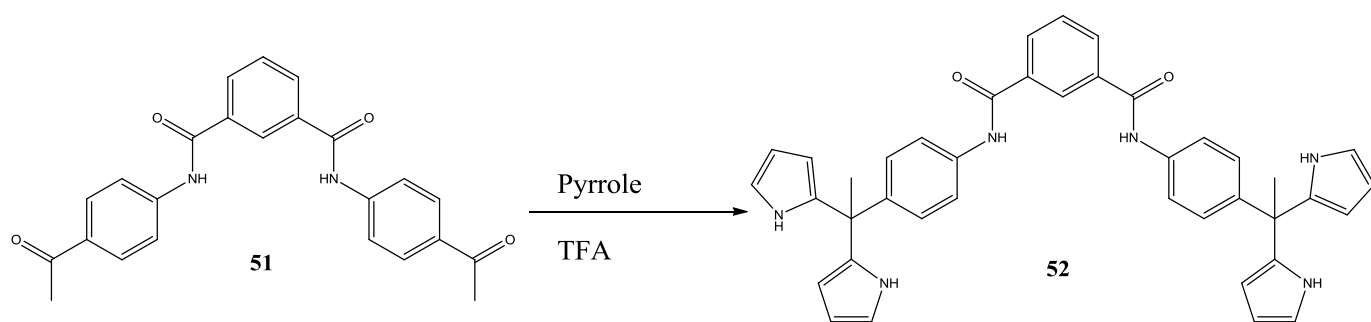
6.2.1 Synthesis of 54

The initial step in the synthesis of **54** consisted of a coupling between isophthaloyl chloride and 4-aminoacetophenone using TEA as a base. The 4-aminoacetophenone (2.2 eq) was dissolved in anhydrous THF with anhydrous TEA (2.2 eq) and chilled to 0 $^{\circ}$C. The isophthaloyl chloride dissolved in anhydrous THF was added dropwise. Upon addition of the acid chloride to the reaction flask a white precipitate is observed. The reaction was stirred at room temperature for 2 hours and the precipitate was filtered and thoroughly washed with water and CH_2Cl_2 to remove the triethylamine hydrochloride side product from the precipitate. The precipitate was then dried overnight in the vacuum oven at 70 $^{\circ}$C, 800 mbar to obtain **50** as a white solid in 85% yield. Analysed by ^{1}H and ^{13}C NMR.
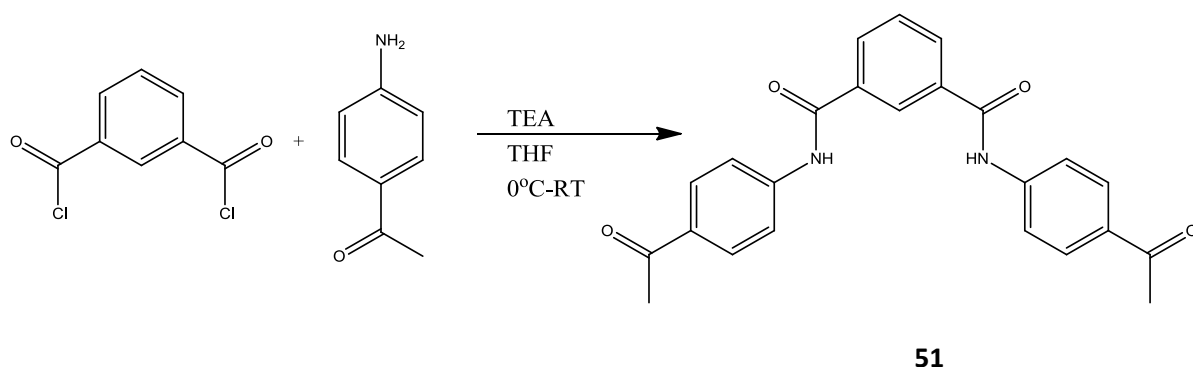
Scheme 6.2: Synthesis of compound **51**.

Condensation of **51** was performed using neat distilled pyrrole and excess TFA. The reaction solution was heated to 70 °C and stirred for 4 hours. The reaction was quenched with 5 ml of triethylamine and the residual pyrrole was removed by evaporation *in vacuo*. To the resulting black sticky oil, silica was added until a fine powder was obtained. The crude product was purified by column chromatography over silica gel (eluent: ethyl acetate/hexane (2:3). Column chromatography of the crude mixture of compound **52** is challenging and required tediously long columns to isolate the target compound. Synthesis of this compound provides a basic, similar scaffold to that shown in figure 6.1 in 28% yield.
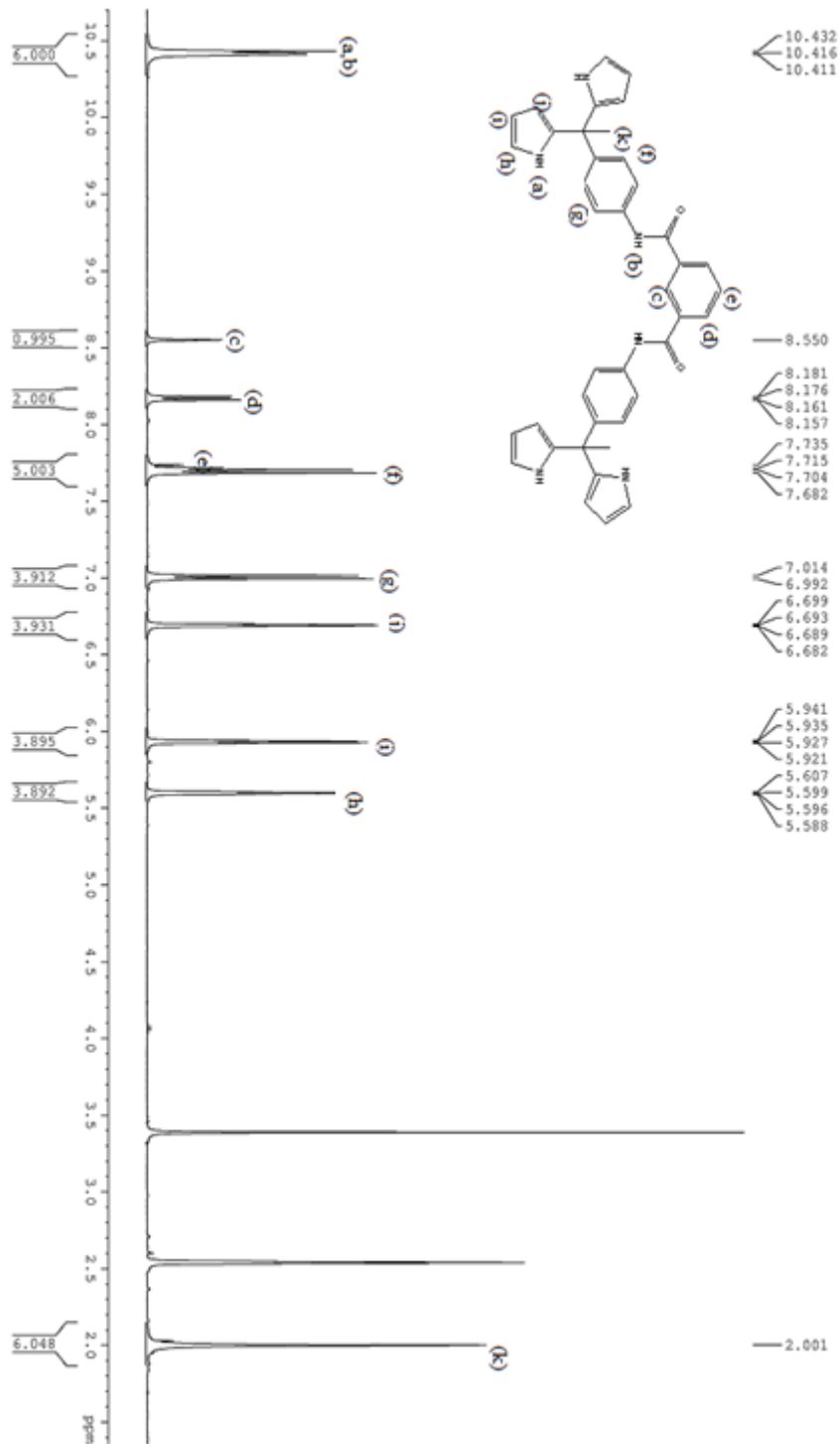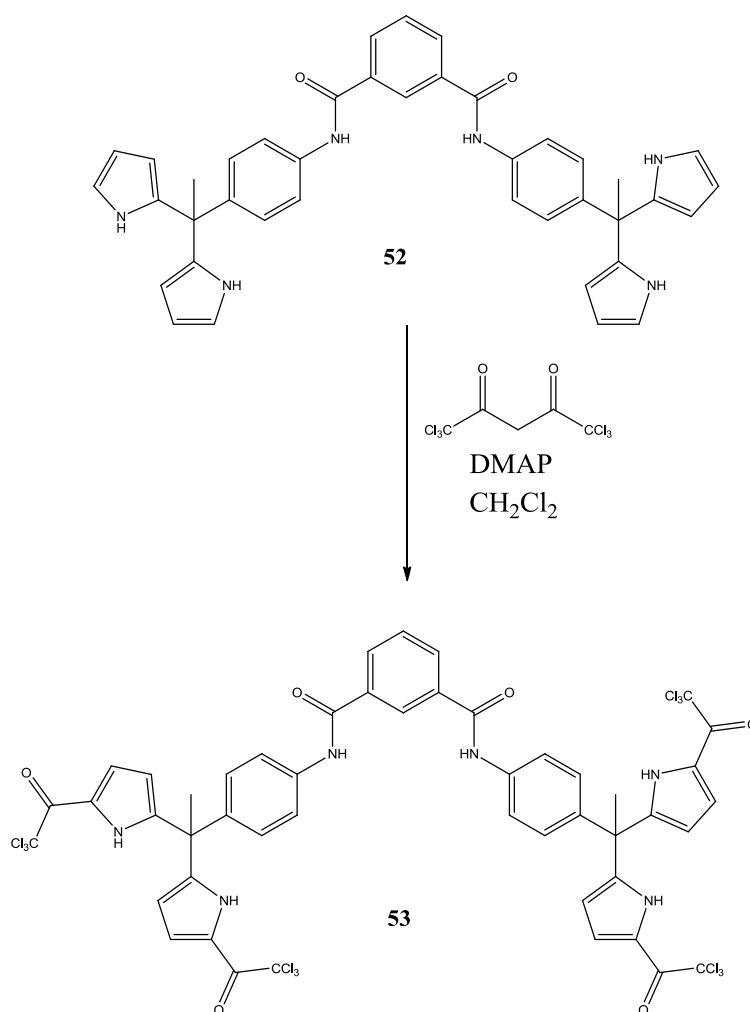

Scheme 6.3: Synthesis of compound **52**.

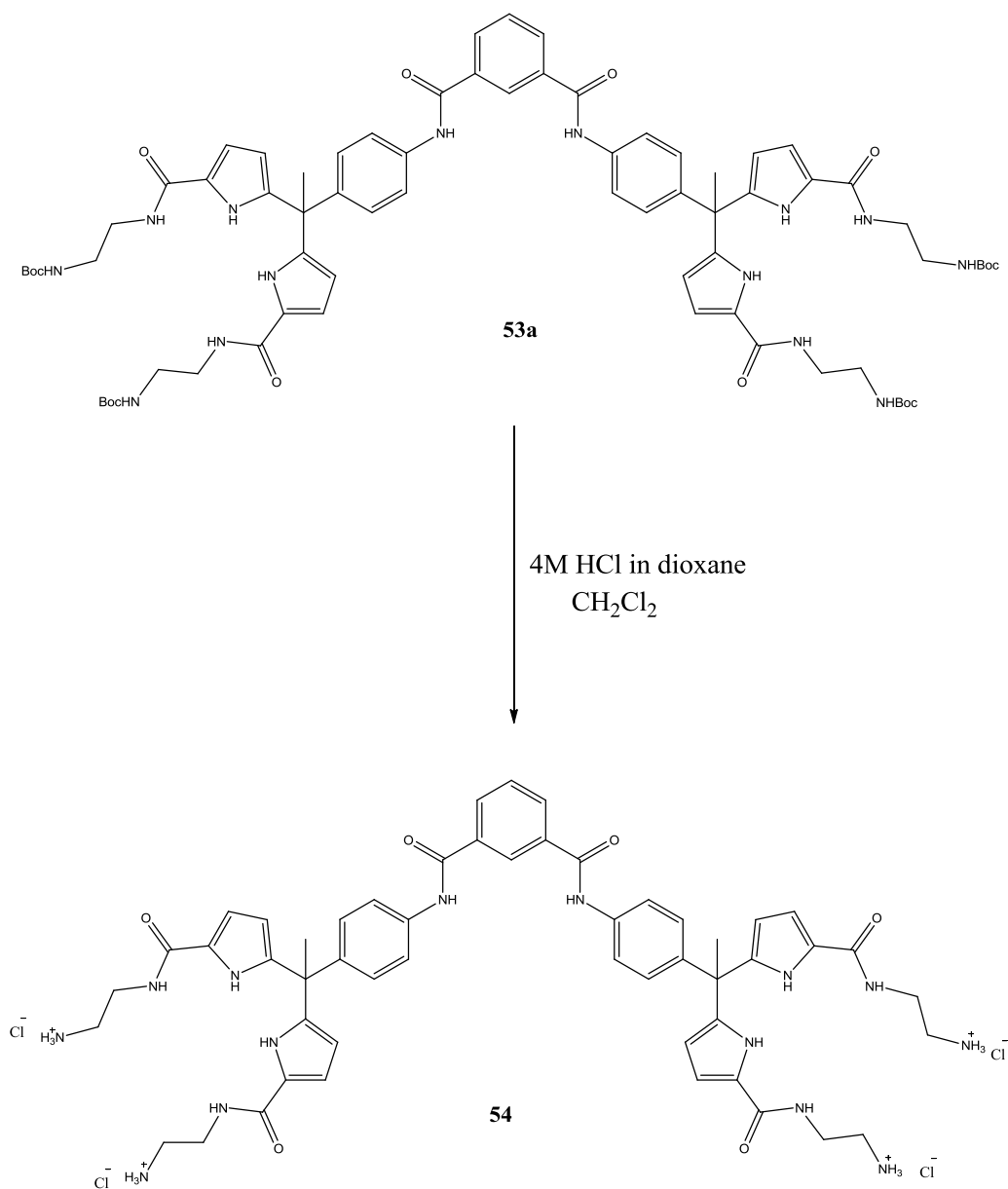Figure 6.4: ^{1}H NMR of compound **52**

The modification of compound **52** was performed using the same methods described in chapter 5, TClAA and DMAP was successfully used to modify the pyrrole scaffold in compound 51, selectively in the 2' position to give **53** in 68% yield. Unlike the ditolyldipyrromethanes, compound **53** required column chromatography ethyl acetate:hexane (3:1) to remove trace trifunctionalised impurities. The removal of these impurities is extremely important at this step, neglecting them introduces amino trifunctionalised species in later steps making purification difficult.

Scheme 6.4: Synthesis of compound **53**

The coupling between the N-Boc ethylenediamine species and **53** was performed under the same conditions used in chapter 5. Compound **53** was suspended in anhydrous CH_2Cl_2 at 0 ^{o}C and stirred with N-Boc ethylenediamine (4.8 eq). To this mixture anhydrous TEA (4.8 eq) was added dropwise, when finished the solution was allowed heat to room temperature and stir overnight. The precipitate was filtered, and washed thoroughly with both Et_2O and CH_2Cl_2.

Scheme 6.5: Synthesis of the Boc protected linked dipyrromethane **53a**

The final step required the cleavage of the carbamate protecting group. Compound **53a** was suspended in anhydrous CH_2Cl_2. The reaction was cooled to 0 ^{o}C and stirred. To this 1 mL of 4M HCl in dioxane was added and the reaction was allowed stir overnight. The precipitate was isolated and washed with diethyl ether.

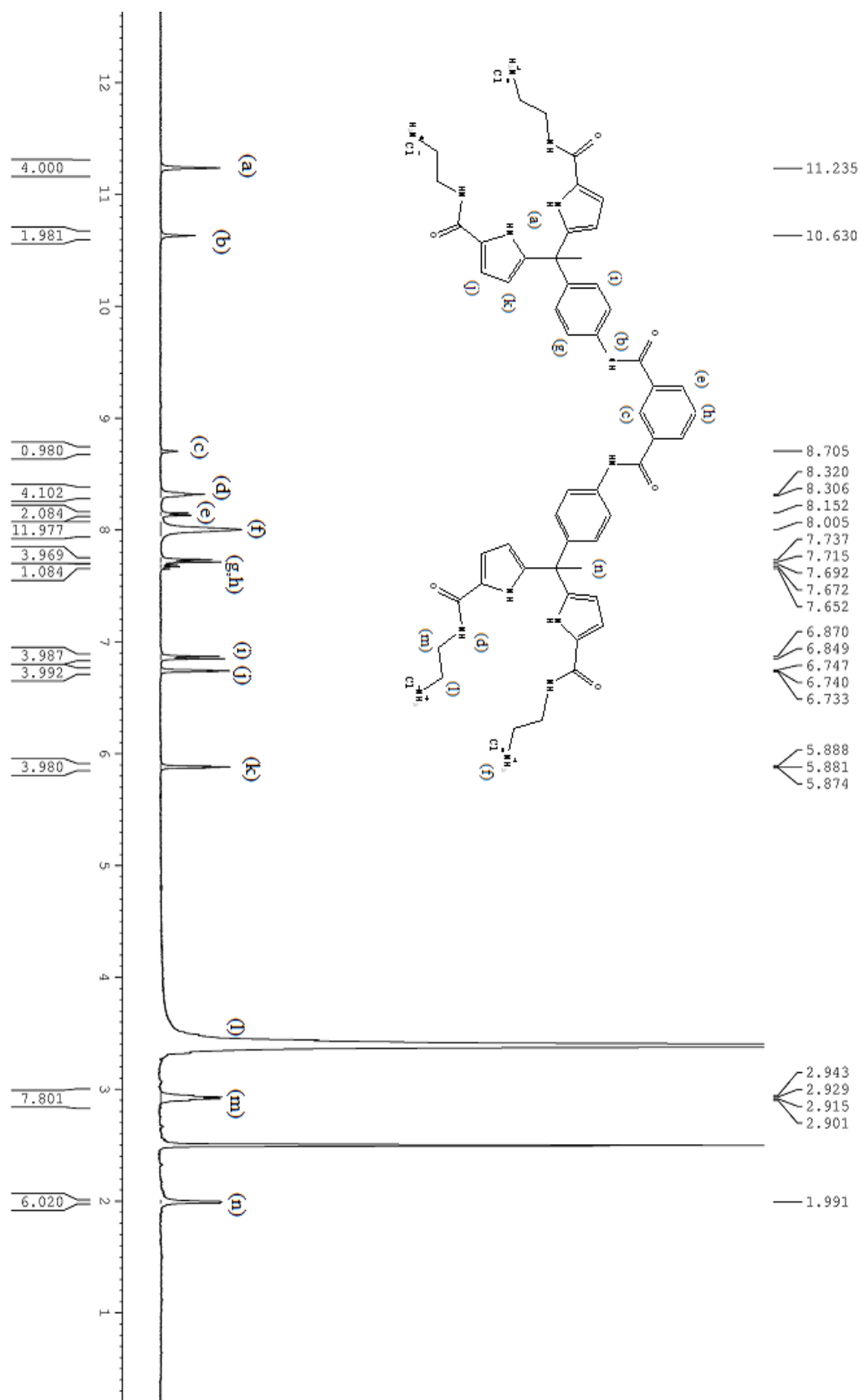Scheme 6.6: Final deprotected linked dipyrromethane **54**

Figure 6.5: ^{1}H NMR of compound **54**

6.3 Biological evaluation of DDAAKN02 vs DDAAKN01

The results discussed concerning **DDAAKN01** showed excellent potency and selectivity in the inhibition of the diseased state channel $Kv(1.1)_4$. The Hill's slopes indicate that more than one molecule of **DDAAKN01** was interacting with the channel, presumably through a H-bonding mechanism. Based on these results compound **54** (**DDAAKN02**) was prepared in the hope that the presence of two dipyrromethanes in the same compound would optimise all possible interactions leading to a more potent and selective inhibitor.

When the linked dipyrromethane **54** (**DDAAKN02**) was screened it was observed that this molecule gave a Hill's slope of 1, this results illustrates that only one molecule of **DDAAKN02** is solely interacting with the tetramer channel.

Bio-evaluation of **DDAAKN02** vs **DDAAKN01** was performed and the results are shown in figure 6.7. The comparative results between the compounds are highly interesting as DDAAKN02 is almost twice as potent for the diseased state $Kv(1.1)_4$ channels against the smaller molecule **DDAAKN01** and follows the same inhibition pattern. Results have also shown that the linked molecule **DDAAKN02** inhibits the Kv1.3 slightly less than **DDAAKN01**. The most interesting discovery on comparing these results is that the ratio of inhibition for the Kv1.1 channel against Kv1.3 was 2:1 with **DDAAKN01** however with **DDAAKN02** this ratio increased to almost 4:1. The modifications made in the design of DDAAKN02 could hold the key to the discovery of a molecule that is 100% exclusive to $Kv(1.1)_4$. The calculated IC_{50} value for **DDAAKN02** was 8±0.4 µM.
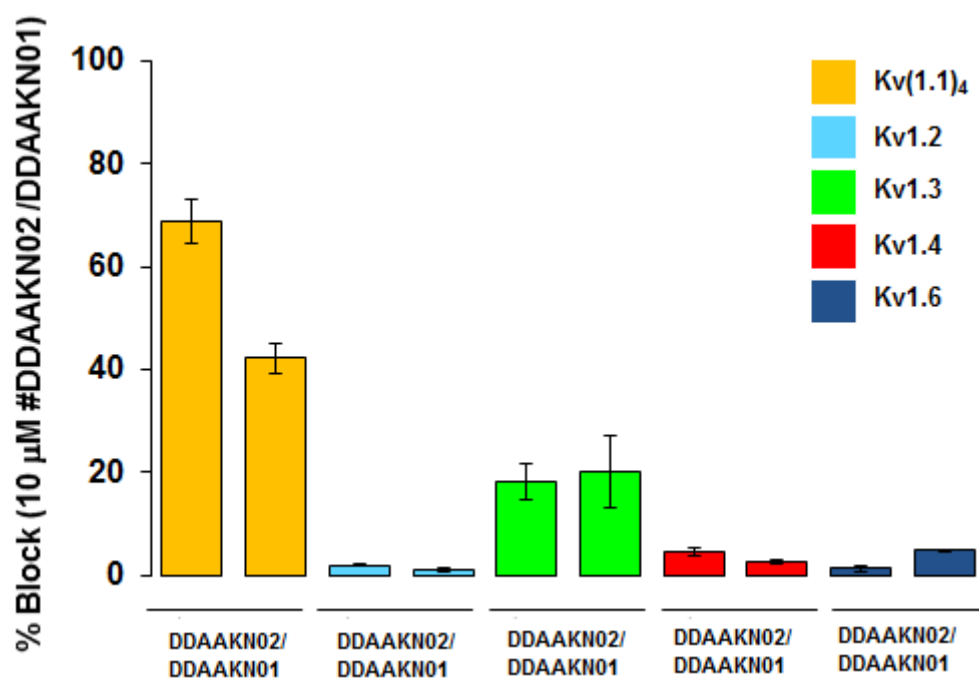
Figure 6.7: Linked dipyrromethane **DDAAKN02** against **DDAAKN01** tested upon the rat Kv1 channels.

6.3.1 Comparisment of concatenated tetramers Kv(1.1/1.2)$_4$ with DDAAKN02 and DDAAKN01

The real 'acid test' of the efficiency of **DDAAKN01** is to test it against the diseased state channel Kv(1.1)$_4$ and the normal channels Kv(1.1)$_3$-(1.2), Kv(1.1)$_2$-(1.2)$_2$ and Kv(1.2)$_4$ shown in figure 6.8. The screening results revealed that **DDAAKN02** inhibited only the diseased state concatenated tetramer at about 70%. When we introduced one copy of Kv(1.2) into the tetramer we only inhibit at 10%, the addition of another copy of Kv(1.2) totally stops the channel from undergoing inhibition.

The main distinction between **DDAAKN02** and **DDAAKN01** is, that **DDAAKN01** will inhibit the normal channels very marginally whereas **DDAAKN02** eliminates the inhibition of the normal channels to a negligible effect.

This selectivity over the two channels Kv(1.1)/Kv(1.2) is fundamentally important to the potential development of any possible therapeutic because inhibiting Kv1.2 results in serious side-effects a good example of this is 4-AP which lacks this selectivity and causes major side-effects. Thus DDAAKN02 can be considered a viable new lead for the treatment of MS.
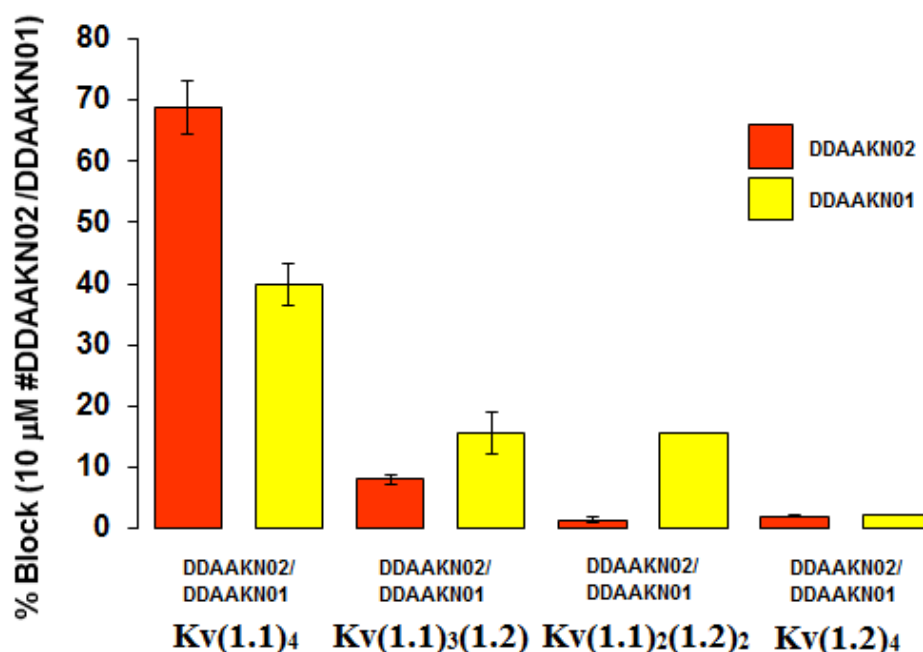

Figure 6.8: **DDAAKN02** against **DDAAKN01** upon the concatenated channels Kv1.1/1.2 expressed in the brain and diseased state.

6.3.2 Ca²⁺ and Na⁺ blockage with DDAAKN01 and DDAAKN02

As detailed in the literature review in chapter one the other classes of ion channels, that also have biological importance, were discussed. Both **DDAAKN01** and **DDAAKN02** were screened against both Na⁺(figure 6.09) and Ca²⁺(figure 6.10) channels for possible associated side effects with these channels. Both compounds were tested on TTX-sensitive Na⁺ channels from - F-11 DRG neuroblastoma mouse cell line.
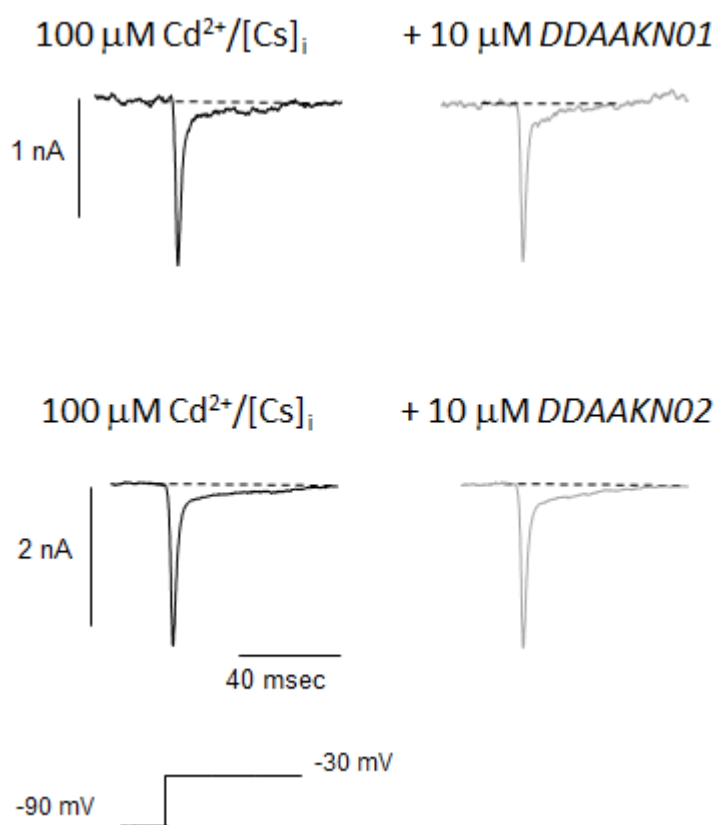

Figure 6.9: **DDAAKN01** and **DDAAKN01** tested on TTX-sensitive Na⁺ channels.

Both compounds showed to be insensitive to Na⁺ channels. There was no observed change in the inward current as a result of administration of the two inhibitors to the cell lines. This is an extremely important finding as similar to Kv channels, Na⁺ channels are directly associated to the action potential within the cell, and inhibiting them would cause unwanted side-effects. The selectivity towards Kv1 provides a suitable platform for these compounds to be further investigated as a plausible therapeutic.
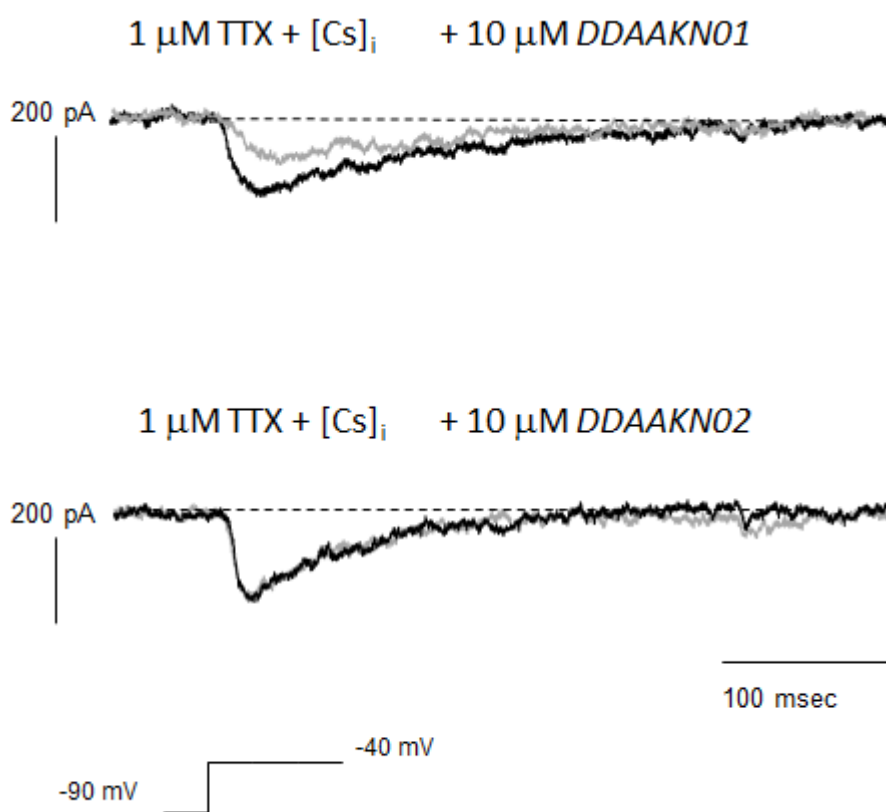
Figure 6.10: **DDAAKN01** and **DDAAKN02** screened against the native Kca channels.

Shown in figure 6.10, only **DDAAKN01** inhibits the native calcium channel. The rate of inhibition is ~30%. **DDAAKN02** is totally insensitive to the channel.

6.4 Conclusion

Improvements on the selectivity and potency were achieved by modifying the previous lead candidate **DDAAKN01** detailed in chapter 5. The modified inhibitor **DDAAKN02** has vastly improved potency believed to be due to the higher percentage of key interactions between the inhibitor and the key amino acid residues in the channel. As a result of the designed and strategic incorporation of more key moieties **DDAAKN02** has proved to be a superior
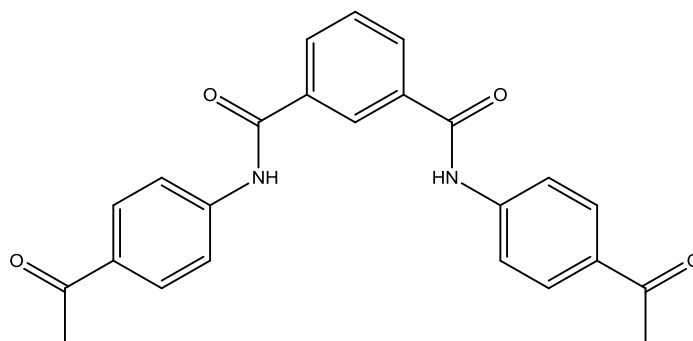
candidate to selectively inhibit Kv1.1. **DDAAKN02** showed that it was more selective to the diseased channel $Kv(1.1)_4$ and that normalised channels with incorperated Kv1.2 sub-units had negligible inhibition potential. Both Na^+ and Ca^{2+} were unaffected when treated with **DDAAKN02** whereas **DDAAKN01** showed some sensitivity to the native calcium channel. These results demonstrate both the selectivity and potency of **DDAAKN02** as a feasible therapeutic for Kv1.1 related diseases such as MS.

6.5 Experimental

All operations were carried out under an atmosphere of argon or nitrogen using standard Schlenk techniques. All solvents were supplied by the Aldrich Chemical Company and TCI. Dichloromethane was dried over $MgSO_4$ prior to use. All organic reagents were purchased from the Aldrich Chemical Company and TCI. Pyrrole was freshly distilled over potassium hydroxide before use. Anhydrous triethylamine, borontrifluoride diethyletherate and were all used without further purification. Column chromatography was carried out using neutral silica gel (Merck, used as received). All mobile phases for column chromatography were dried over $MgSO_4$ prior to use.. All solvents were deoxygenated by purging withargon or nitrogen for ~10 minutes

Equipment

All syntheses involving air- and moisture-sensitive reagents were performed in oven or flame dried glassware. NMR spectra were recorded on a Bruker model AC 400 MHz spectrometer and Bruker model ANC 600 MHz spectrometer using $CDCl_3$ as solvent. All NMR spectra were calibrated according to the residual solvent peak, i.e. $CHCl_3$ at 7.26 ppm, DMSO-d$_6$ 2.50 ppm for all ^1H spectra and 77.16 ppm and 39.52 ppm for all ^{13}C spectra. Chemical shifts are given in parts per million (ppm).

51

To a 250 mL round bottom flask, 4.3 g (32.5 mmol) of 4-aminoacetophenone was added. This was dissolved in 45 mL of anhydrous THF. A volume of 2.5mL of anhydrous TEA was added and the reaction mixture was chilled to 0 °C and stirred. A weight of 3.0 g (14.8mmol of isophthaloyl chloride was dissolved in 30mL of anhydrous THF and added dropwise to the stirring solution. The reaction was stirred for 4 hours and the precipitate was filtered. The precipitate was washed with 5x50 mL H_2O and 5x50 mL washings of CH_2Cl_2. The precipitate was dried to yield a white solid 5.02 g, 85% yield.

^{1}H NMR (400 MHz) δ (DMSO- d$_6$) 10.72 (2H, s, NH) 8.53 (1H, s, CH) 8.11 (2H, m, CH) 7.89 (8H, dd, p-aryl-H) 7.72 (1H, t, CH) 2.41 (6H, s, CH$_3$)^{13}C NMR (100 MHz, DMSO- d$_6$) 196.6, 165.4, 143.4, 134.8, 132.1, 131.1, 129.3, 128.8, 127.2, 119.5, 26.5.
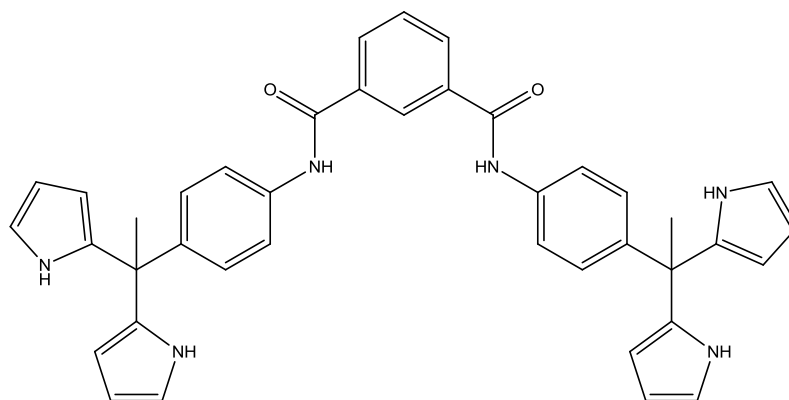
52

To a 100 mL round bottom flask, 1 g (2.49 mmol) of **51** was added. To this 15 mL (216 mmol) of freshly distilled pyrrole was added. A volume of 2 mL TFA was added dropwise and the reaction was stirred at 70 $^{\circ}$C for 4 hours. The reaction was quenched with 5 mL of TEA and stirred at room temperature for 20 mins. The unreacted pyrrole was removed under high vaccum at 50 $^{\circ}$C to leave a black tar-like oil. The crude reaction mixture was purified by silica gel chromatography eluting with hexane: ethyl acetate (3:2) and the solvent removed in vacco to give a beige solid 450 mg; 28% yield.

^{1}H NMR (400 MHz) δ (DMSO- d_6) 10.43 (6H ,m, NH pyrrole + NH amide) 8.55 (1H, s, CH) 8.18 (2H, m, CH) 7.73 (5H, d, aryl-H + CH) 7.01 (4H, d, aryl-H) 6.69 (4H, m, pyrrole-H) 5.94 (4H, s, pyrrole-H) 5.60 (4H, m, pyrrole-H) 2.00 (6H, s, CH$_3$)^{13}C NMR (100 MHz, DMSO- d_6) 165.8, 145.2, 138.7, 137.9, 136.1, 131.5, 129.5, 128.3, 127.9, 120.4, 118.1, 107.2, 106.8, 44.8, 28.9
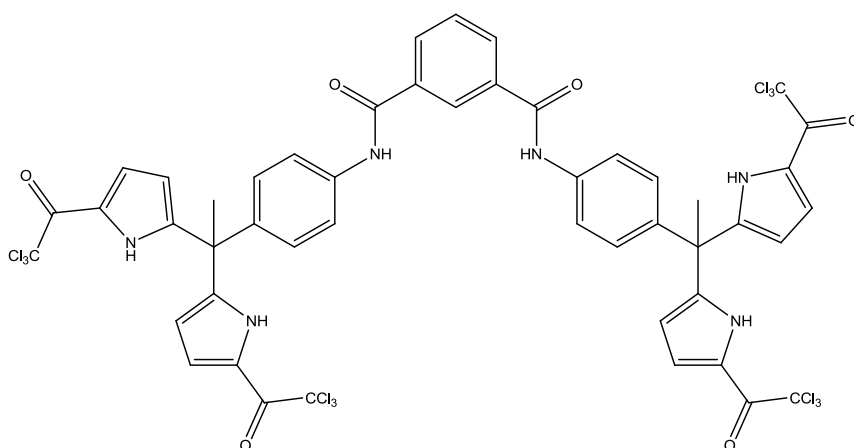
53

To a 50 mL round bottom flask 200 mg (0.316 mmol) of compound **52** was added with 18 mg (0.158 mmol) of DMAP. These were suspended in 10 mL anhydrous CH_2Cl_2 and the reaction mixture chilled to 0 ^{o}C and placed under an argon atmosphere. 0.288 mL (1.58 mmol) of trichloroacetic anhydride was added dropwise and the reaction was stirred at room temperature for 2 hours. The reaction was quenched with aq $NaHCO_3$ and washed with brine 2x10 mL. The crude product was purified by silica gel column chromatography, eluting with ethyl acetate and hexane (1:3) to give **52** as a white solid 0.2614 g, 68% yield.

^{1}H NMR (400 MHz) δ (DMSO- d_6) 12.22 (4H, s, NH-pyrrole) 10.51 (2H, s, NH-amide) 8.58 (1H, s, CH) 8.11 (2H, m, CH) 7.80-7.78 (5H, d, aryl-H + CH) 7.31 (4H, m, pyrrole-H) 7.02 (4H, d, aryl-H) 6.15 (4H, m, pyrrole-H) 2.13 (6H, s, CH_3) ^{13}C NMR (100 MHz, DMSO- d_6) 171.8, 165.0, 147.8, 141.0, 137.7, 135.0, 130.7, 128.6, 127.3, 127.0, 122.3, 121.2, 120.4, 111.3, 95.3, 45.2, 27.5.
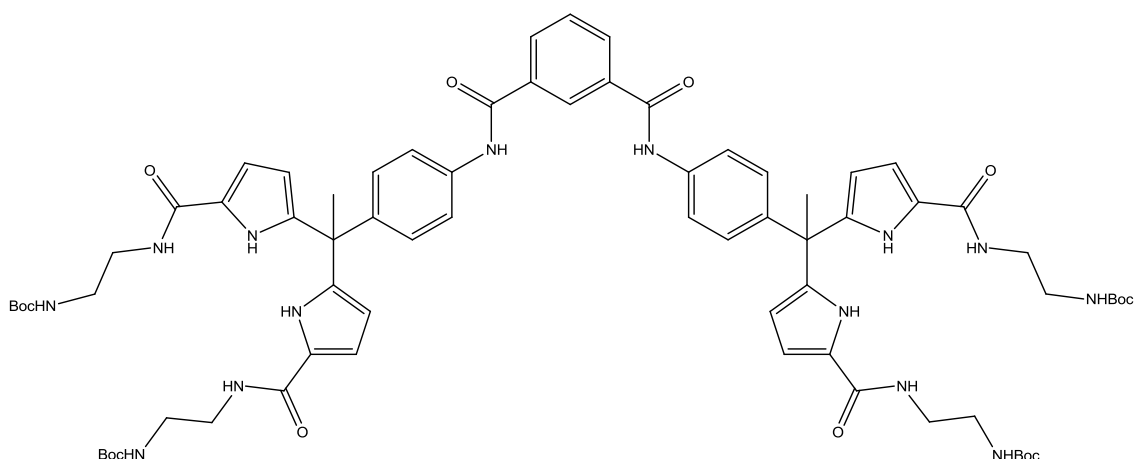
53a

To a 25 ml round bottom flask 150 mg (0.125 mmol) of compound **53** and 5 mL of anhydrous CH$_2$Cl$_2$ was added and placed over an argon atmosphere. 0.094 mL (0.592 mmol) of N-Boc ethylenediamine was added dropwise and the reaction mixture was allowed to stir for 10 mins. To this 0.082 mL (0.592mmol) of anhydrous TEA was added and the reaction was allowed stir for 24hours at room temperature. The precipitate was filtered and washed thoroughly with CH$_2$Cl$_2$ to leave a white/beige solid 0.144 g, 84% yield.
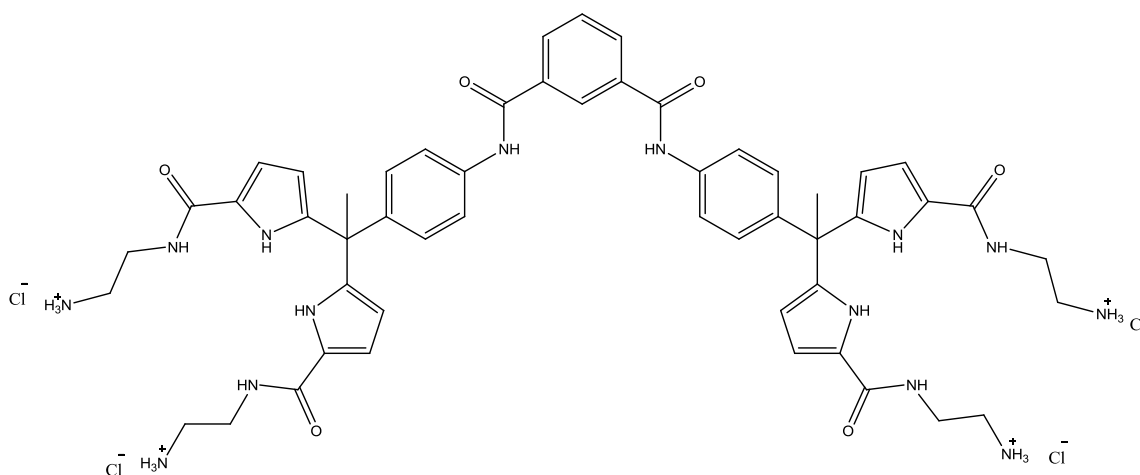
54

To a 25 mL round bottom flask, 100mg of compound **53a** was charged. A volume of 5 mL anhydrous CH_2Cl_2 was added, placed under an argon atmosphere and chilled to 0 ^{o}C. To this 1mL of 4M HCl in dioxane was added and the reaction was stirred for 24 hours at room temperature. The precipitate was filtered and washed with CH_2Cl_2 to give compound **54** in quantitative yield.

^{1}H NMR (400 MHz) δ (DMSO- d_6) 11.2 (4H, s, NH-pyrrole) 10.6 (2H, s, NH-amide) 8.7 (1H, s, CH) 8.3 (4H, t, NH-amide) 8.1 (2H, m, CH) 8.0 (12H, s, NH_3^+) 7.7 (5H, d, phenyl-H+ CH) 6.9 (4H, d, phenyl-H) 6.7 (4H, m, pyrrole-H) 5.9 (4H, m, pyrrole-H) 3.3 (8H, m, CH_2) 2.9 (8H, m, CH_2) 2.0 (6H, s, CH_3) HR-MALDI MS: Calculated $C_{52}H_{64}Cl_4N_{14}O_6$ (M+1-4HCl: 977.4854) Observed (M+1-4HCl: 977.4899)

Thesis Conclusion

The overall objective of the thesis was a success, the initial SAR work performed on the porphyrin scaffold provided enough information to design two new, selective and potent inhibitors for Kv1.1 channels associated with MS. Although the porphyrins that were prepared did not possess high selectivity to any particular Kv1 channel, (except for compound **18**, which gave sole selectivity for Kv1.2) essential information was obtained to aid in the creation of a simple pharmacaphore model. An attempt was then made to translation the porphyrin pharmacaphore to a non photoactive calix[4]pyrrole scaffold. Unfortunately this approach was unsuccessful due to the inability to prepare the target calix[4]pyrroles.

However, by applying comparative modelling of the porphyrin results with Kv1.1 allowed for the visual interactions between the key amino acids of the channel and the active porphyrins. From the comparative modelling study three new lead dipyrromethanes were synthesised and evaluated against the Kv1 channels. From this study a new lead was discovered, **DDAAKN01** (**31**) , which exhibited excellent selectivity and potency for the target Kv1 channels that are associated with MS. It was also discovered that two molecules of **DDAAKN01** are involved in the channel blockage based on the Hill slope study. Further modelling was then undertaken on **DDAAKN01** to better understand the key interactions between the new lead and the target channels. From the modelling work a new improved lead , **DDAAKN02** (**54**), was designed and synthesised. The subsequent bioevaluation of this new compound revealed that **DDAAKN02** possesses both far superior binding and selectivity than **DDAAKN01**.

It should be note that both **DDAAKN01** and **DDAAKN02** are the first examples of small molecules that demonstrate such high selectivity and potency toward the target Kv1.1 channels. Furthermore, both compounds outperform the MS marketed drug 4-AP with respect to both selectivity and potency making them excellent lead structure candidates for the treatment of MS.